



University
of Glasgow

Foote, Kirsty K. (2012) *Characterisation of cardiac function and RUNX expression in two separate models of heart disease*. PhD thesis.

<http://theses.gla.ac.uk/3746/>

Copyright and moral rights for this thesis are retained by the author

A copy can be downloaded for personal non-commercial research or study

This thesis cannot be reproduced or quoted extensively from without first obtaining permission in writing from the Author

The content must not be changed in any way or sold commercially in any format or medium without the formal permission of the Author

When referring to this work, full bibliographic details including the author, title, awarding institution and date of the thesis must be given



Characterisation of cardiac function and RUNX expression in two separate models of heart disease

Kirsty K. Foote, BSc (Hons)

A thesis submitted in fulfilment of the degree of Doctor of Philosophy to the
College of Medical, Veterinary and Life Sciences,
University of Glasgow, U.K.

Research completed within the Glasgow Cardiovascular Research Centre,
Institute of Cardiovascular and Medical Sciences,
University of Glasgow, U.K.

Abstract

Heart disease is the leading cause of death worldwide. Despite considerable progress in the prevention and treatment of heart disease it remains a highly prevalent source of patient morbidity and mortality. The heart has the ability to change in shape, size, structure and function in response to adverse stimuli in a process known as cardiac remodelling which is intended to be an adaptive response initially but can become detrimental leading to eventual heart failure (HF). The mechanisms underlying the progression from remodelling to HF remain poorly understood. Remodelling in the heart is known to be associated with alterations in cardiac gene expression for which transcription factors play a significant role. It has been reported that the RUNX family of transcription factors which play important roles in developmental pathways, have been increasingly implicated in disease and in tissue injury. One member of this family of transcription factors, RUNX1, has been shown to be up-regulated in heart tissue taken from human patients with MI. Despite this knowledge, a precise quantitative measure of the altered expression of *Runx* in the heart in terms of regional and temporal changes using an animal model has not been previously explored. Therefore the aim of the work presented in this thesis was to investigate the altered expression of the *Runx* genes in two different experimental animal models of heart disease: a mouse model of myocardial infarction (MI) and a rat model of hypertension and altered left ventricular (LV) mass to assess the changes in *Runx* expression in response to the different cardiac disease types.

For this study a mouse model of MI was developed using the well-established coronary artery ligation (CAL) method and the phenotype of this model was characterised at different time points by assessing survival trends, performing *in vivo* functional measurements (pressure-volume (PV) loop methodology and electrocardiograms) with assessment of structural alterations of remodelling using histological and morphometric measurements. The model was found to exhibit many of the clinical features consistent not only with other published murine model data but also those of human MI. The mouse MI model was then used to measure *Runx* gene expression in the hearts using real time quantitative reverse transcription PCR (qRT-PCR) and immunohistochemistry (IHC) methods. This was to assess whole heart and regional expression differences, how expression levels change over time as the MI develops, assessment of expression patterns of the different *Runx* gene members and exploration of potential links with *Runx* expression and possible functional relevance to the heart. In the mouse model, *Runx* genes

were found to be up-regulated in response to MI with highest levels confined to the areas within and around the infarct and peri-infarct region by 4 weeks post-MI extending into the remote regions by 8 weeks. *Runx* levels were found to be highest in the hearts with the greatest dysfunction.

The second model of heart disease for assessing changes in *Runx* was a rat model of hypertension, with congenic sub-strains of this model showing altered LV mass also tested. The congenic rat strains were specifically bred models of rat with a chromosome 14 substitution. This contained a quantitative trait locus (QTL) from either normotensive or hypertensive strains for genes associated with LV mass. These models were analysed using *in vivo* PV methodology to assess function without influence from blood pressure (BP) loading conditions (to assess whether the QTL is BP-dependent) and structural remodelling in the form of cardiac fibrosis was measured histologically. The data revealed enhanced systolic function with diastolic dysfunction and cardiac fibrosis in hypertensive animals consistent with other published models. The chromosome 14 congenic rat strains showed a BP-independent diastolic dysfunction or improved function linked to cardiac fibrosis. Furthermore, in contrast to the MI model, the levels of *Runx1* were significantly down-regulated in the rat models of hypertension and altered LV mass indicating potential differences in the triggers for altered expression between volume-overload versus pressure-overload models of heart disease.

Overall this thesis has shown the altered expression of *Runx* genes in two different animal models of heart disease which has not been previously explored and indicates potential for future investigation into the functional significance of *Runx* in the heart during disease.

Table of Contents

Abstract	2
List of Tables	8
List of Figures	9
Acknowledgements	11
Author's Declaration	12
Abbreviations	13
Introduction	18
1.1 Cardiac EC coupling.....	19
1.1.1 Initiation and Ca ²⁺ influx	19
1.1.2 Calcium-induced calcium release.....	20
1.1.3 Ca ²⁺ -mediated cross-linking and contraction	21
1.1.4 Relaxation and Ca ²⁺ extrusion	21
1.2 Cardiovascular disease (CVD)	23
1.2.1 Myocardial Infarction	23
1.2.2 Hypertension	30
1.3 Mechanisms contributing to progression to HF in both MI and hypertension	34
1.3.1 Abnormal Ca ²⁺ handling	35
1.3.2 Contractile elements.....	36
1.3.3 ECM alterations	37
1.4 Altered gene expression in cardiac disease	38
1.4.1 Differential gene expression in different cardiac diseases	38
1.4.2 Transcription factors.....	39
1.5 RUNX transcription factors	45
1.5.1 Identification and structure	45
1.5.2 Function of RUNX proteins.....	51
1.5.3 Tissue-specific expression of RUNX.....	53
1.5.4 Regulatory mechanisms of <i>RUNX</i> gene and RUNX protein expression	54
1.5.5 RUNX in human disease	55
1.5.6 RUNX in damaged muscle.....	56
1.5.7 RUNX in the heart	57
1.6 Animal models of cardiac disease	60
1.6.1 Need for animal models of disease	60
1.6.2 Criteria for use of animal models.....	61
1.6.3 Use of animal models to investigate RUNX expression in the heart during disease ..	61
1.6.4 Mouse model of MI.....	61
1.6.5 Rat model of hypertension and congenic models of altered LV mass	62
1.7 Characterisation of cardiac function in the two models	63
1.7.1 Use of PV catheters to assess cardiac function.....	63
1.8 Measurement of gene expression	64
1.9 Aims	64
General Methods	66
2.1 Experimental mouse model of MI	67
2.1.1 Animals	67
2.1.2 Anaesthesia and pre-surgical preparation	67
2.1.3 Surgical procedure	70
2.2 Congenic rat model of altered LV mass	79
2.2.1 Generation of congenic strains.....	79
2.2.2 Genotyping of congenic strains	79
2.3 PV measurements	79
2.3.1 The PV loop.....	79
2.3.2 Principle of operation.....	81
2.3.3 Volume signal correction	81
2.3.4 Calibration of PV catheters.....	84
2.3.5 Surgical procedure for insertion of PV catheter into the LV <i>in vivo</i>	88
2.3.6 Data acquisition	92
2.3.7 Calculation of volume	92
2.3.8 Calculation of alpha (α)	93
2.3.9 Calculation of V _P	98

2.3.10	Calculation of load-independent indices	98
2.3.11	Baseline haemodynamic data from control animals	98
2.4	ECG	102
2.4.1	ECG as a method of assessing cardiac function <i>in vivo</i>	102
2.4.2	Protocol for measuring ECG	102
2.4.3	Data analysis	103
2.5	Organ harvest and weighing	103
2.5.1	Heart	103
2.5.2	Lungs and liver	104
2.5.3	Thymus	104
2.5.4	Tibial length for normalisation of organ weights	104
2.6	Preparation of histological sections of the heart	104
2.6.1	Mouse heart sections	104
2.6.2	Rat heart sections	105
2.7	Staining of heart sections	105
2.7.1	Mouse heart sections	105
2.7.2	Rat heart sections	106
2.8	Histological morphometry of the mouse heart	107
2.8.1	Infarct thickness	107
2.8.2	LV chamber size	107
2.8.3	Infarct size measurements	108
2.9	Collagen quantification	109
2.9.1	Collagen quantification in rat hearts (perivascular vs. interstitial fibrosis)	109
2.9.2	Collagen quantification in mouse hearts	110
2.10	Mouse cardiomyocyte isolation	111
2.10.1	Mouse cardiomyocyte isolation protocol	111
2.10.2	Measurements of cardiomyocyte length, width and cross-sectional area	112
2.10.3	Filtration of cardiomyocytes to remove other cell types	113
2.11	Immunohistochemistry	114
2.11.1	Staining protocol	114
2.11.2	Quantification of IHC staining	116
2.12	RNA extraction, cDNA synthesis and qRT-PCR	116
2.12.1	Gene expression based on quantification of messenger RNA levels	116
2.12.2	RNA extraction	117
2.12.3	Synthesis of cDNA	121
2.12.4	Verification of cDNA synthesis	123
2.12.5	qRT-PCR	125
2.12.6	Interpretation of qRT-PCR data	132
2.12.7	Limitations of the technique	139
	Characterisation of a mouse model of myocardial infarction.....	145
3.1	Introduction	146
3.1.1	MI is a serious public health problem	146
3.1.2	Need for an animal model of MI	146
3.1.3	Surgical methods of inducing MI in an animal model	146
3.1.4	How well does CAL-induced experimental MI resemble human MI?	149
3.1.5	Aims	152
3.2	Methods	152
3.2.1	Induction of MI	152
3.2.2	Experimental timeline	152
3.2.3	Haemodynamic assessment of LV function	153
3.2.4	Assessment of electrical cardiac function	153
3.2.5	Harvesting of hearts	153
3.2.6	Preparation of heart sections	154
3.2.7	Morphometry and infarct measurements	154
3.2.8	Lung and liver weights	155
3.2.9	Cardiomyocyte isolation and measurements of cell length, width and estimated cross-sectional area	155
3.2.10	Data recording and statistical analysis	156
3.3	Results	156
3.3.1	Survival following MI	156
3.3.2	Effect of MI on haemodynamic LV function	159
3.3.3	Effect of MI on the electrical properties of the heart	165
3.3.4	Effect of MI on the structural properties of the heart	167
3.3.5	Effect of MI on lung and liver weight	171

3.4	Discussion.....	172
3.4.1	Inducing MI leads to reduced survival.....	172
3.4.2	MI alters the structural properties of the heart	175
3.4.3	Early onset of structural remodelling can have adverse effects.....	178
3.4.4	MI leads to impairment of cardiac function.....	179
3.4.5	MI alters electrical activity and increases the frequency of cardiac arrhythmia	180
3.4.6	Summary	181
Expression of <i>Runx</i> in the heart in a mouse model of myocardial infarction		182
4.1	Introduction	183
4.1.1	Altered gene expression in MI.....	183
4.1.2	Transcription factors in MI.....	185
4.1.3	RUNX transcription factors.....	186
4.1.4	Aims.....	187
4.2	Methods	187
4.2.1	Induction of MI	187
4.2.2	Tissue harvest	187
4.2.3	Cardiomyocyte isolation and purification.....	189
4.2.4	IHC and quantitative imaging	189
4.2.5	RNA extraction	190
4.2.6	cDNA synthesis	191
4.2.7	Verification of cDNA synthesis	191
4.2.8	qRT-PCR	191
4.2.9	Interpretation of qRT-PCR data.....	192
4.3	Results	193
4.3.1	Expression of <i>Runx1</i> in the whole heart post-MI.....	193
4.3.2	Expression of <i>Runx1</i> in different regions of the heart post-MI	195
4.3.3	Expression of <i>Runx1</i> at different time points post-MI.....	197
4.3.4	Comparison of regional expression of different <i>Runx</i> genes post-MI	201
4.3.5	Links with <i>Runx</i> expression and LV function.....	205
4.3.6	IHC localisation of RUNX1 and quantification of expression	210
4.3.7	Verification of RUNX1 expression in cardiomyocytes	215
4.4	Discussion.....	218
4.4.1	<i>Runx1</i> expression is increased post-MI	218
4.4.2	Elevated <i>Runx1</i> expression is localised to areas within and adjacent to the injury ..	219
4.4.3	RUNX1 may be mislocalised in injured cardiomyocytes	222
4.4.4	Localised regional expression of other genes in MI	224
4.4.5	Temporal alterations in <i>Runx1</i> expression post-MI.....	225
4.4.6	Other <i>RUNX</i> genes show similar altered expression but to varying extents	226
4.4.7	Functional role of RUNX1 in cardiomyocytes.....	227
4.4.8	Summary	232
Characterisation of cardiac function and <i>Runx1</i> expression in a congenic rat model of altered left ventricular mass.....		233
5.1	Introduction	234
5.1.1	Altered <i>RUNX</i> gene expression in cardiac disease	234
5.1.2	LV mass and hypertension.....	234
5.1.3	Rat model of hypertension	235
5.1.4	Functional assessment of the models using PV methodology.....	238
5.1.5	Cardiac fibrosis can alter normal functioning in these models.....	238
5.1.6	Aims.....	239
5.2	Methods	239
5.2.1	Blood pressure determination	239
5.2.2	LV mass measurements.....	240
5.2.3	LV PV Measurements	240
5.2.4	Harvesting of hearts	240
5.2.5	Preparation of heart sections for Sirius red staining	241
5.2.6	Measurement of cardiac fibrosis	241
5.2.7	qRT-PCR	241
5.2.8	Data recording and statistical analysis.....	242
5.3	Results	242
5.3.1	LV mass and systolic blood pressure.....	242
5.3.2	Haemodynamic LV function	243
5.3.3	Collagen content.....	248
5.3.4	<i>Runx1</i> gene expression.....	249

5.3.5	Links with <i>Runx1</i> expression and LV function.....	250
5.4	Discussion.....	251
5.4.1	Congenetic strains demonstrate a separation between LV mass and BP	252
5.4.2	Congenetic strains with altered LV mass show BP-independent diastolic dysfunction	253
5.4.3	Altered diastolic dysfunction may be linked to altered cardiac fibrosis	256
5.4.4	<i>Runx1</i> expression is altered in the congenic strain of increased LV mass	258
5.4.5	Potential links with <i>Runx1</i> and degree of LV dysfunction	259
	General Discussion	261
6.1	Rationale for the study.....	262
6.2	Major aims and findings.....	262
6.2.1	Suitability of animal models.....	262
6.2.2	Development and characterisation of a mouse model of MI.....	263
6.2.3	Characterisation of congenic rat strains of altered LV mass.....	263
6.2.4	<i>Runx</i> and MI	264
6.2.5	<i>Runx</i> and hypertension/altered LV mass	266
6.2.6	Differences in <i>Runx</i> expression between the different models	266
6.3	Future directions	267
6.4	Final conclusion	268
	Appendix	270
	References	272

List of Tables

Table 1.1	Functional roles of the regulatory regions of <i>RUNX</i> genes.	47
Table 1.2	Summary of <i>RUNX</i> expression sites.	54
Table 2.1	Baseline haemodynamic parameters of LV function in stock mice compared to published values.	99
Table 2.2	Haemodynamic PV indices of LV function in three different groups of rats. ...	100
Table 2.3	Reverse transcription reaction components.	123
Table 2.4	qRT-PCR mastermix reaction components.	131
Table 3.1	Characteristics of murine models of MI using the permanent CAL method. ...	151
Table 3.2	Effect of myocardial infarction on haemodynamic indices of LV function in mice.	163
Table 5.1	LVMI and SBP in the congenic and background strains.	243
Table 5.2	Haemodynamic PV data from the congenic and background strains.	247

List of Figures

Figure 1.1	Ca ²⁺ transport in the ventricular cardiomyocyte.	22
Figure 1.2	Representation of the pathways of LV remodelling post-MI.	27
Figure 1.3	Timeline of LV remodelling after MI.	29
Figure 1.4	Summary process from transcription to translation.	40
Figure 1.5	Assembly of the transcription initiation complex in eukaryotes.	42
Figure 1.6	RUNX genes structure and elements involved in expression regulation.	47
Figure 1.7	Schematic representation of the functional domains of the RUNX proteins.	50
Figure 1.8	Schematic representation of RUNX transcriptional regulatory complexes for activation and repression of gene expression.	51
Figure 2.1	Development of a method for endotracheal intubation of mice.	69
Figure 2.2	Positioning of the mouse for CAL surgery.	71
Figure 2.3	Location of the mouse LAD coronary artery using Evan's Blue dye.	73
Figure 2.4	Photographs of various stages of the surgical method used for inducing MI in mice.	78
Figure 2.5	LV pressure and volume and the PV loop.	80
Figure 2.6	Scisense PV catheter.	81
Figure 2.7	Example of parallel volume estimation.	83
Figure 2.8	Calibration curves using different calibration combinations from the in-built system and a cuvette calibration.	86
Figure 2.9	Transonic flow probe and mechanism of operation.	94
Figure 2.10	Comparison of CO measurements obtained with a PV catheter and an aortic flow probe in mice.	96
Figure 2.11	Comparison of CO measurements obtained with a PV catheter and an aortic flow probe in rats.	96
Figure 2.12	Comparison of haemodynamic parameters using different surgical approaches for PV catheterisation in rats.	101
Figure 2.13	Diagram showing how measurements of infarct thickness and LV area were measured.	108
Figure 2.14	Measurement of infarct size using Sirius red sections of the heart.	109
Figure 2.15	Diagram showing how perivascular and interstitial fibrosis was measured in the rat hearts using <i>ImageProPlus</i> .	110
Figure 2.16	Apparatus for mouse ventricular cardiomyocyte isolation.	112
Figure 2.17	Diagram showing how cardiomyocyte width and length were measured.	112
Figure 2.18	Schematic representation of the principle of IHC staining.	115
Figure 2.19	Example electrophoresis output traces from the <i>Agilent Bioanalyzer</i> showing analysis of RNA integrity.	121
Figure 2.20	cDNA synthesis by reverse transcription.	122
Figure 2.21	Example gels from DNA gel electrophoresis to verify reverse transcription and appropriate size products.	125
Figure 2.22	Schematic representation of the PCR process.	128
Figure 2.23	Phases of a conventional PCR reaction.	129
Figure 2.24	SYBR green binding during PCR amplification.	130
Figure 2.25	Graphical representation of qRT-PCR data.	133
Figure 2.26	Example melting curves from the qRT-PCR dissociation stage.	134
Figure 2.27	Example outputs of statistical analysis of qRT-PCR data using SPSS software.	136
Figure 2.28	Sample qRT-PCR data analysis of mouse MI tissue using the 2 ^{-ΔCt} method.	137
Figure 2.29	Sample qRT-PCR data analysis of mouse MI tissue using the 2 ^{-ΔΔCt} method.	138

Figure 2.30 Sample qRT-PCR data analysis of congenic rat tissue using the $2^{-\Delta Ct}$ method.	138
Figure 2.31 Comparison of different housekeeping genes for qRT-PCR between sham and MI hearts.	143
Figure 2.32 Validation of <i>Gapdh</i> as a suitable housekeeping gene between four different rat strains.	144
Figure 3.1 CAL model experimental time line.	153
Figure 3.2 Survival following MI.	158
Figure 3.3 Effects of MI on pressure, volume and heart rate.	160
Figure 3.4 Effects of MI on haemodynamic indices of LV function in mice.	164
Figure 3.5 Effect of MI on the electric properties of the heart.	166
Figure 3.6 Effect of MI on heart weight and cardiomyocyte size.	168
Figure 3.7 Altered LV dimensions after MI.	169
Figure 3.8 Infarct size and collagen content after MI.	171
Figure 3.9 Lung and liver weights after MI.	172
Figure 4.1 Location of mouse thymus in the upper thorax above the base of the heart.	188
Figure 4.2 <i>Runx1</i> expression and <i>Gapdh</i> stability in the whole heart 4 weeks post-MI.	194
Figure 4.3 Regional expression of <i>Runx1</i> 4 weeks post-MI.	196
Figure 4.4 Regional <i>Runx1</i> expression at different time points post-MI.	200
Figure 4.5 Expression of different <i>Runx</i> genes post-MI.	204
Figure 4.6 Correlations with <i>Runx</i> gene expression and LV function.	207
Figure 4.7 Correlations with <i>Runx</i> gene expression and LV function (excluding the infarct)	208
Figure 4.8 Correlation between infarct size and <i>Runx1</i> expression.	209
Figure 4.9 IHC expression of RUNX1 at 4-wk and 8-wk post-MI.	213
Figure 4.10 Cytoplasmic staining of RUNX1.	214
Figure 4.11 Verification of RUNX1 expression in cardiomyocytes.	217
Figure 4.12 Diagram showing possible mechanism for how the CBF β partner unit enters the nucleus to permit formation of the heterodimer complex required for transcription.	224
Figure 5.1 Traditional and speed congenic breeding.	237
Figure 5.2 Representative LV pressures and PV loops.	245
Figure 5.3 Haemodynamic PV indices of LV function.	246
Figure 5.4 Collagen levels in the congenic and background strains.	249
Figure 5.5 <i>Runx1</i> expression in the congenic and background strains.	250
Figure 5.6 Relationship between Tau (τ) and <i>Runx1</i> expression in the WKY, SHRSP and SHRSP-congenic strains.	251

Acknowledgements

First and foremost, I would like to express my gratitude to my supervisor, Dr Chris Loughrey, for all his support and guidance throughout the course of my PhD. I could not have achieved nearly as much as I have without his help, patience and excellent supervision and I am very grateful to all that he has done for me. I would also like to acknowledge my second supervisor, Prof. Ewan Cameron, for his assistance and expertise in the field of RUNX and for his help in reading my thesis.

I'd like to say a big thank you to Elspeth for all her help and advice throughout the project, and for always looking out for me. I'd like to thank other members of staff at the University who have helped me with various aspects of my work, to Dr Martin McBride and Dr Delyth Graham for all their help with the congenic project, and to Dr Liam Morrison for teaching me qRT-PCR and helping me troubleshoot with these experiments.

I'd like to thank all the technical staff who helped make a lot of my experimental work possible. I am grateful to Mrs Lynn Stevenson and the staff at the Histopathology Unit for performing the immunohistochemistry work so well and I extend my thanks also to all the staff at the Biological Services animal unit for all their assistance and care for the animals. Special thanks to our technician Mrs Caron Hawksby, for her friendly and helpful nature, and for being such a great help around the lab.

I have been extremely lucky to have made some really special friends during my PhD who have made these last few years much more fun and been there for me through all the tough times. To Doug, who has helped me so much with things both in and outside of work, and for all the wine and curry nights, board games and cups of tea! And a very special thank you goes to Allen, who has been there for me through everything and his support has meant the world to me. I'm so grateful to him for all the times he listened to my endless worries and kept me going – and for all the laughs and fun we've had!!

A special mention to Ann, my close friend outside of the lab, who has also been a great support and always knew how to cheer me up with cocktails and girly days out!

Finally, a special thanks to my family for their continued love and support. My parents have always supported me throughout all my education and I'm so grateful to all the help they have given me, particularly during my write-up. I'd like to dedicate this thesis to my parents.

Author's Declaration

The work presented within this thesis was performed by myself except where otherwise acknowledged in the text and has not been presented as part of any other degree. Some of the results during the period of research have been presented in abstract form and are detailed below:

K.K. Foote & C.M. Loughrey. A comparison of left ventricular pressure-volume measurements in adult rats using three different techniques. Abstract – Physiological Society annual meeting Manchester, *J Physiol* 2010; Proc Physiol Soc 19: PC22.

K.K. Foote, M.W. McBride, D. Graham, K. Douglas, S. Kettlewell, G.L. Smith, A.F. Dominiczak and C.M. Loughrey. Assessment of cardiac function in chromosome 14 congenic strains using pressure-volume measurements. Abstract – Biophysical Society annual meeting Baltimore, USA. *Biophysical Journal* 2011; 100 (3): 299a-299a.

Abbreviations

α	Alpha gain coefficient
$^{\circ}\text{C}$	Degrees celcius
μl	Microlitre
AGM	Aorta-gonad-mesonephros
AML	Acute myeloid leukemia
AMP	Adenosine monophosphate
Ang II	Angiotensin II
ANOVA	Analysis of variance
ANP	Atrial natriuretic peptide
ATP	Adenosine triphosphate
AV node	Atrioventricular node
AVP	Arginine(8)-vasopressin
BNP	Brain natriuretic peptide
BP	Blood pressure
Bp	Base pairs
Bpm	Beats per minute
BSA	Bovine serum albumin
Ca^{2+}	Calcium ion
CAL	Coronary artery ligation
CaM kinase	Ca^{2+} /calmodulin-dependent protein kinase
CARP	Cardiac-restricted ankyrin repeat protein
CBF	Core-binding factor
CCD	Cleidocranial dysplasia
cDNA	Complementary deoxyribonucleic acid
CF	Coronary flow
CHD	Coronary heart disease
CICR	Calcium-induced calcium release
CNS	Central nervous system
CO	Cardiac output
CoCl_2	Cobalt(II) Chloride
CpG	Cytosine-phosphate-guanidine
Ct	Threshold cycle
CVD	Cardiovascular disease
DAB	Diaminobenzidine tetrahydrochloride
DCM	Dilated cardiomyopathy
dNTP	Deoxyribonucleotide triphosphate

dP/dt_{\max}	Maximum rate of rise of pressure
dP/dt_{\min}	Minimum rate of fall of pressure
DPX	Dibutyl phthalate xylene
EC coupling	Excitation-contraction coupling
ECG	Electrocardiogram
ECM	Extracellular matrix
EDP	End-diastolic pressure
EDPVR	End-diastolic pressure-volume relationship
EDV	End-diastolic volume
EF	Ejection fraction
ESP	End-systolic pressure
ESV	End-systolic volume
EtBr	Ethidium Bromide
FOX	Forkhead box
GAPDH	Glyceraldehyde-3-phosphate dehydrogenase
γ -interferon	Gamma interferon
H&E	Haematoxylin and eosin
HBSS	Hank's Buffered Saline Solution
HCM	Hypertrophic cardiomyopathy
HEKC	Human embryonic kidney cells
HF	Heart failure
HIF1 α	Hypoxia-inducible factor 1 alpha
HPRT	Hypoxanthine-guanine phosphoriboyltransferase
HR	Heart rate
HRP	Horseradish peroxidase
HSC	Haematopoietic stem cells
HTH	Helix-turn-helix
I/R	Ischaemia-reperfusion
ID	Inhibitory domain
Ig	Immuoglobulin
IHC	Immunohistochemistry
IL	Interleukin
IRES	Internal ribosome entry site
IV	Intravenous
IVC	Inferior vena cava
JAK/STAT	Janus kinase/signal transducer and activator of transcription
K ⁺	Potassium ion
KATP	ATP-dependent potassium channel
KH	Krebs-Henseleit

L	Length between electrodes
LAD	Left anterior descending
LCA	Left coronary artery
LV	Left ventricle
LVH	Left ventricular hypertrophy
LVMi	LV mass index
MAP	Mean arterial pressure
MAPK	Mitogen-activated protein kinase
MHC	Myosin heavy chain
MI	Myocardial infarction
MLC	Myosin light chain
mM	Millimolar
MMP	Matrix metalloproteinases
MRI	Magnetic resonance imaging
mRNA	Messenger ribonucleic acid
MW	Molecular weight
Na ⁺	Sodium ion
NaCl	Sodium chloride
NCAM	Neural cellular adhesion molecule
NCX	Sodium-calcium exchanger
NLS	Nuclear localisation signal
NMTS	Nuclear matrix targeting signal
NTC	No template control
OD	Outer diameter
PCR	Polymerase chain reaction
PE	Polyethylene
PEBP2 α	Polyoma enhancer-binding protein-2 α
PEEP	Positive end-expiratory pressure
PIC	Pre-iniation complex
PLN (or PLB)	Phospholamban
Pol II	RNA polymerase II
PV	Pressure-volume
qRT-PCR	Quantitative reverse transcription PCR
QTL	Quantitative trait loci
ρ	Resistivity of blood
RAAS	Renin-angiotensin-aldosterone system
RHD	Runt homology domain
RIN	RNA integrity number
Rn	Normalised reporter fluorescence

RNA	Ribonucleic acid
RPLP0	Ribosomal protein P0
RQ	Relative quantitation
RR	Respiration rate
rRNA	Ribosomal ribonucleic acid
RT	Reverse transcription
RUNX	Runt-related box
RV	Right ventricle
RWT	Relative wall thickness
RyR	Ryanodine receptor
SA node	Sinoatrial node
SAPK	Stress activated protein kinase
SBP	Systolic blood pressure
SD	Standard deviation
SEM	Standard error of the mean
SERCA	Sarcoplasmic reticulum calcium ATPase
SHR	Spontaneously hypertensive rat
SHRSP	Stroke-prone spontaneously hypertensive rat
SNP	Short nucleotide polymorphisms
SR	Sarcoplasmic reticulum
STWS	Scott's Tap Water Substitute
SV	Stroke volume
τ	Relaxation time constant Tau
TAC	Transverse aortic constriction
TAF	TATA binding protein associated factors
TBE	Tris/Borate/EDTA
TBP	TATA binding protein
TBS	Tris-buffered saline
TF	Transcription factor
TGF- β 1	Transforming growth factor beta 1
T_i/T_t	Inspiratory to total time of the respiratory cycle
TL	Tibial length
TLE	Transducin-like enhancer of split
T_m	Melting temperature
TPR	Total peripheral resistance
tRNA	Transfer ribonucleic acid
TSC	Transforming growth factor- β -stimulated clone
T-tubule	Transverse tubule
UTR	Untranslated region

V_C	Volume measured by catheter
V_P	Parallel volume
VPC	Ventricular premature complex
WT-1	Wilms' tumour protein

CHAPTER 1

Introduction

The primary function of the heart is to maintain circulation of blood to the organs and tissues of the body. The inability to supply the oxygen and nutrients necessary to support the needs of the body is the major consequence of heart disease and constitutes the basis of heart failure (HF). Heart disease is currently the leading cause of morbidity and mortality worldwide (WHO, 2011). In order to understand the complex nature of heart disease for the research of novel treatments it is important to understand the basic functioning of the heart and its adaptive capabilities as an organ during normal and pathological conditions.

1.1 Cardiac EC coupling

The mammalian heart is divided into a right and left side and has four chambers; two atria and two ventricles. The right and left ventricles (which receive blood from the right and left atrium respectively) represent two synchronous muscular pumps contracting in a timed fashion. Contraction occurs at the level of the individual contractile cells of the heart, the cardiomyocytes, by a process known as excitation-contraction (EC) coupling which is the sequence of events from electrical excitation of the cardiomyocyte to mechanical contraction of the heart. During this process, calcium ions (Ca^{2+}) play a pivotal role. The main stages of EC coupling are described below and depicted in Figure 1.1.

1.1.1 Initiation and Ca^{2+} influx

The process of EC coupling is initiated by the cardiac action potential which is an electrical impulse that rapidly alters cell membrane potential. The action potential originates from the pacemaker cells of the sinoatrial (SA) node located in the right atrium and is quickly transmitted to the atrioventricular (AV) node (a small mass of cells located in the lower atrial septum) and through fast-conduction muscle fibres known as the Bundle of His to the Purkinje fibres which supply the signal to the ventricular cardiomyocytes. This occurs rapidly from one cardiomyocyte to the next *via* gap junctions as a wave propagation system. The action potential creates a wave of depolarisation along the surface cell membrane (the sarcolemma) of the cardiomyocytes along distinct invagination structures that extend into the cell called transverse tubules (T-tubules). This triggers the opening of voltage-gated L-type Ca^{2+} channels located along the T-tubules (Bers & Perez-Reyes, 1999). This allows Ca^{2+} to enter the cell which contributes to the plateau phase of the action potential. Both extracellular and intracellular Ca^{2+} is absolutely essential for EC coupling as was first discovered by the physiologist Sydney Ringer in the early 1880s when he found that an isolated frog heart ceased to beat when Ca^{2+} was accidentally

removed from the solution that perfused the heart (Ringer, 1882a;Ringer, 1882b;Ringer, 1883a;Ringer, 1883b).

1.1.2 Calcium-induced calcium release

1.1.2.1 Background to calcium-induced calcium release

Ca^{2+} entry into the cell triggers a release of Ca^{2+} from the intracellular Ca^{2+} store organelle, the sarcoplasmic reticulum (SR); this is known as calcium-induced calcium release (CICR). CICR was demonstrated in the 1970s and 1980s through a series of experiments performed by Fabiato and Fabiato who demonstrated that in skinned canine cardiomyocytes where the sarcolemmal membrane was removed (therefore lacked T-tubules allowing intracellular Ca^{2+} to be equilibrated with a known Ca^{2+} concentration in the bathing fluid), the skinned cells were found to relax at 0.02-0.03 μM Ca^{2+} , contract moderately at 0.1 μM Ca^{2+} and contract maximally at 0.3 μM Ca^{2+} (Fabiato & Fabiato, 1975). This revealed that contractions were induced by Ca^{2+} -triggered release of Ca^{2+} from the SR and that the amount of Ca^{2+} released is a function of the amount of trigger Ca^{2+} (Ca^{2+} entering the cell through the L-type channel). They later revealed that at high trigger Ca^{2+} concentrations (10 μM for 150 ms) CICR could be inhibited (Fabiato, 1985).

1.1.2.2 Ca^{2+} release from the SR

There are two distinct domains of the SR; the junctional domain which contains the channels for Ca^{2+} release from the SR and the longitudinal domain which contains the channel for Ca^{2+} uptake into the SR (Franzini-Armstrong, 1970; Winegrad, 1965). Ca^{2+} is released from the SR during CICR *via* release channels on the junctional SR known as ryanodine receptors (RyR). RyR are proteins (~ 2.3 million Dalton with the functional tetramer visible at the electron microscope level; (Saito *et al.*, 1988)) and are located within nanometers of the sarcolemma of a T-tubule placing them in extremely close proximity with L-type Ca^{2+} channels. The ratio for number of RyR per L-type Ca^{2+} channel ranges from 8:1 in rat, 6:1 in humans and 4:1 in guinea pig (Bers & Stiffel, 1993). Inward flux of Ca^{2+} across the entire cell leads to release of Ca^{2+} from the SR (typically no greater than 50% of the SR Ca^{2+} content however this is dependent on available SR Ca^{2+} (Shannon *et al.*, 2000)) but a substantial fraction is released into the cytosol. The intracellular free Ca^{2+} concentration ($[\text{Ca}^{2+}]_i$) rises from 0.1 μM to ~ 0.5-2.0 μM of which 75-90% comes from the SR release and the remaining 10-25% comes from the inward current through the L-type Ca^{2+} channel (Eisner *et al.*, 1998). The total cytosolic Ca^{2+}

($[\text{Ca}^{2+}]_{\text{total}} = [\text{Ca}^{2+}]_i$ plus bound Ca^{2+}) required for half-maximal activation of contraction is approximately $70 \mu\text{mol l}^{-1}$ cytosol (Bers, 2002).

1.1.3 Ca^{2+} -mediated cross-linking and contraction

The intracellular rise in $[\text{Ca}^{2+}]_i$ allows Ca^{2+} ions to bind to the myofilament protein troponin C which is bound to another myofilament protein called tropomyosin as part of the tropomyosin-troponin complex. At rest (Ca^{2+} unbound to troponin C) this complex is bound to the actin (thin) filament of the contractile sarcomere apparatus and in doing so obscures the myosin-binding sites on the actin. When Ca^{2+} binds to troponin C it causes a shift in the tropomyosin-troponin complex shifting it deeper into the actin groove thereby exposing the myosin-binding sites. Myosin can then subsequently bind to actin forming a cross-bridge and *via* adenosine triphosphate (ATP) hydrolysis the myosin head pulls the actin filament to the centre of the sarcomere causing it to shorten and contract the cell (Layland *et al.*, 2005).

1.1.4 Relaxation and Ca^{2+} extrusion

In order for the cardiomyocyte to relax (which is important to allow the heart to fill with blood again) $[\text{Ca}^{2+}]_i$ must be restored back to resting levels. This is necessary to allow Ca^{2+} to dissociate from troponin and allow the tropomyosin-troponin complex to return to its position where it obscures the actin binding sites and prevents myosin binding. The majority of Ca^{2+} is transported out of the cytosol by four different pathways:

- (i) The **SR Ca^{2+} ATPase (SERCA)** pump located on the surface membrane of the SR which transports Ca^{2+} back into the SR. SERCA is regulated by an inhibitory protein called phospholamban (PLN) which in its basal unphosphorylated state inhibits SERCA by decreasing the affinity of SERCA to Ca^{2+} (James *et al.*, 1989; Voss *et al.*, 1994). In its phosphorylated state, PLN enhances the activity of SERCA by increasing the pump's affinity for Ca^{2+} (James *et al.*, 1989) and permits resequestration of Ca^{2+} back into the SR.
- (ii) The **sodium-calcium exchanger (NCX)** is a sarcolemmal pump which moves 1 Ca^{2+} ion out of the cell in exchange for 3 Na^+ ions into the cell; this mechanism is driven by both transmembrane voltage and by Na^+ and Ca^{2+} concentration gradients (Blaustein & Lederer, 1999).

(iii) The **sarcolemmal Ca^{2+} ATPase** is also a sarcolemmal pump which hydrolyses ATP to transport Ca^{2+} out of the cell. This contributes to a sarcolemmal current which is small in comparison to that of the NCX (Caroni & Carafoli, 1981).

(iv) The **mitochondrial uniporter** is a pore in the inner membrane of mitochondria which moves cytosolic Ca^{2+} into the mitochondria down an electrochemical gradient (Kirichok *et al.*, 2004).

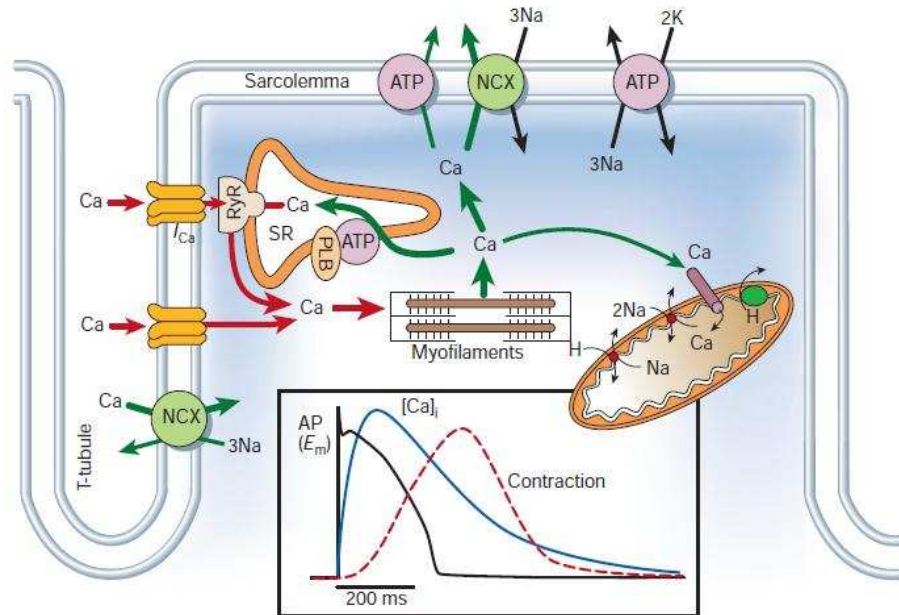


Figure 1.1 Ca^{2+} transport in the ventricular cardiomyocyte.

Schematic representation of Ca^{2+} transport within the cardiomyocytes with inset showing the time course of the rabbit ventricular cardiomyocytes action potential (black line), intracellular Ca^{2+} transient (blue line) and contraction (red dashed line). Red arrows indicate means of Ca^{2+} entry into the cell and green arrows indicate means of Ca^{2+} extrusion from the cell. ATP (ATPase); NCX ($\text{Na}^+/\text{Ca}^{2+}$ exchanger); PLB (phospholamban); SR (sarcoplasmic reticulum); RyR (ryanodine receptor). Taken from (Bers, 2002).

1.1.4.1 Proportions of Ca^{2+} extrusion by each mechanism

The proportion of Ca^{2+} extruded by each mechanism is different and varies between species; in rabbit cardiomyocytes the proportions of Ca^{2+} extruded are approximately as follows: 70% by SERCA, 28% by the NCX and 2% by the Ca^{2+} ATPase and the mitochondrial uniporter (Bassani *et al.*, 1994). In rat cardiomyocytes, approximately 92% is through SERCA, 7% through NCX and 1% through the Ca^{2+} ATPase and mitochondrial uniporter (Bassani *et al.*, 1994). The proportions in the mouse are very similar to the rat (Li *et al.*, 1998). These differences are largely due to a greater activity of SERCA in rodents (due to greater number of SERCA molecules) (Hove-Madsen & Bers, 1993). The

entire process from Ca^{2+} influx to contraction and Ca^{2+} extrusion is then repeated for further contraction and relaxation of cardiomyocytes which forms the basic pumping mechanism of the heart.

1.2 Cardiovascular disease (CVD)

Disease of the cardiovascular system occurs when the normal structure and functioning of the heart becomes compromised which can eventually lead to HF. The heart is an adaptive organ and is capable of adapting to disease or injury through alterations to its structural properties and functional ability in order to maintain normal cardiac output (CO) within physiological limits. This process is known as cardiac remodelling and refers to changes in the size, shape and function of the heart in response to cardiac load or injury (Cohn *et al.*, 2000). This tends to be beneficial initially but in the longer term it often becomes maladaptive and results in further deterioration of function (Colucci, 1997). As a result, cardiac remodelling is a central feature in the development of HF. Remodelling is a progressive process characterised by a complex array of cellular and molecular changes which are largely dependent on the underlying stimuli (Kehat & Molkentin, 2010). The main features of remodelling involve changes in the size of the individual cardiomyocytes, cellular apoptosis of cardiomyocytes, changes in the molecular phenotype of the cardiomyocytes (e.g. altered gene expression) and alterations in the quantity and composition of the extracellular matrix (ECM) (Colucci, 1997). Remodelling occurs differently in response to different cardiac disease types and details of each remodelling process for two common cardiac diseases relevant to this thesis; **MI** and **hypertension with hypertrophy**, will be discussed in the sections that follow.

1.2.1 Myocardial Infarction

1.2.1.1 Definition and prevalence

MI (also known as a heart attack) is defined as the death of a region of myocardium in the heart due to an obstruction of a coronary artery (Thygesen *et al.*, 2007). MI is one of the main forms of coronary heart disease (CHD) (Thygesen *et al.*, 2007) which is the collective term for cardiac diseases characterised by narrowing of the coronary blood vessels leading to disruption in the supply of adequate circulation to the heart (Cohen & Hasselbring, 2007). CHD in the form of MI is the leading cause of HF and represents the largest cause of mortality in the U.K. (Scarborough *et al.*, 2011). Although CHD mortality has fallen in recent years (by 32% between 2001 and 2009) it continues to be a serious

public health problem with death rates reaching 88,000 each year in the UK (Scarborough *et al.*, 2011).

1.2.1.2 Main cause of MI

MI is caused by an accumulation of fatty and fibrous deposits along the interior of a coronary artery which over time can progress to considerable thickening and hardening of the arterial wall (Cohen & Hasselbring, 2007). While usually asymptomatic for decades, it may eventually become a serious problem if the plaque inside the artery suddenly ruptures causing a thrombus formation that can partially or completely obstruct coronary blood flow.

1.2.1.3 Post-MI remodelling

MI is a complex disease which progresses through a number of distinct stages.

(i) Ischaemia and cell death

A blockage or occlusion of the coronary blood flow results in oxygen deprivation to a region of the myocardium (defined as ischaemia). The consequences of ischaemia can vary depending on the extent and duration of the ischaemia. During ischaemia, the oxygen and nutrient deprivation disrupts normal oxidative phosphorylation leading to a reduction in ATP necessary for normal function. If the ischaemic episode is brief (<30 min in rodent models) (Ferdinandy *et al.*, 2007) and reperfusion of blood is restored it is possible for the injured cardiomyocytes to regain normal structure and function but with time (i.e. not immediate) - in this case the myocardium is said to be stunned (Kloner & Jennings, 2001). Hibernating myocardium refers to an adaptive reduction of contractile function in response to a reduction of blood flow which is not regarded as a consequence to the energy deficit but rather an adaptive mechanism to maintain cardiomyocyte integrity and viability (Heusch & Schulz, 2002). Prolonged ischaemia can lead to irreversible cell death (infarction). This usually occurs within hours of the insult as a result of oxygen deprivation and depletion of ATP. For continuous functioning, the myocardium is absolutely dependent on aerobic metabolism for the production of energy in the form of ATP. During normoxia, ATP is produced in the mitochondria by oxidative phosphorylation; however during oxygen and substrate deprivation (ischaemia) this leads to a rapid decline in the production of ATP without which the cell cannot survive. This leads to a multitude of subsequent processes that can lead to cell death by three main

methods: necrosis, apoptosis and autophagy (although autophagy is less understood in the context of MI) (Marambio *et al.*, 2010; Olivetti *et al.*, 1997; Wencker *et al.*, 2003).

Necrosis is a form of cell death characterised by loss of ATP, cell swelling, organelle swelling and membrane damage. Depletion of ATP leads to an accumulation of AMP which triggers the activation of glycolytic enzymes and a switch to anaerobic metabolism and lactate production. Increased lactate in the cell leads to accumulation of water and resultant osmotic stress to the cell eventually leading to organelle and cell swelling with resultant sarcolemmal membrane damage (damage to phospholipids and ion channels) (de Zwaan *et al.*, 2001).

Apoptosis is a form of 'programmed cell death' during which the cell instructs its own death. This is different to necrosis which is considered a passive or accidental process. Apoptosis is rare in normal myocardium, occurring in 0.01-0.001% of normal human cardiomyocytes (Soonpaa & Field, 1998) increasing to 0.12-0.70% in human HF (van Empel *et al.*, 2005). It is triggered by neurohormonal factors, cytokines and extracellular factors which can activate apoptosis *via* the Janus kinase/signal transducer and activator of transcription (JAK/STAT) signalling pathway or *via* the stress activated protein kinase (SAPK) pathway (Mani & Kitsis, 2003; Negoro *et al.*, 2001).

Autophagy is a highly-conserved process in which intracellular membrane-bound organelles called lysosomes that contain enzymes can break down the cell's own structures through activation of these enzymes. During ischaemia, lysosomes are activated and can hydrolyse the organelle/cell membranes which can lead to osmotic stress and further sarcolemmal disruption (de Zwaan *et al.*, 2001).

The process of LV remodelling following cardiomyocyte death is summarised in the flow-diagram in Figure 1.2 below.

(ii) Inflammation

Cardiomyocyte necrosis triggers the recruitment of various inflammatory cells to the infarcted area such as macrophages, monocytes and neutrophils to repair the damaged myocardium. The localised area of dead myocardium is referred to as the infarct. Necrotic cardiomyocytes activate the complement system and leads to free-radical generation causing a cascade of signalling molecules known as cytokines to be released by the dying

cells. Examples of cytokines involved include interleukin-8 and C5a which recruit neutrophils to the infarcted region that release potent protease enzymes and phagocytose necrotic cardiomyocytes and cellular debris. Transforming growth factor-beta 1 (TGF- β 1) and gamma-interferon (γ -interferon) then recruit monocytes to the area which differentiate into macrophages, important for scavenging (phagocytosing) the dead cells (Frangogiannis *et al.*, 2002; Nian *et al.*, 2004). As part of the cell clean-up process (neutrophils and macrophages engulfing dead cardiomyocytes), neutrophils release enzymes called serine proteases and matrix metalloproteinases (MMP) which break down the collagen fibres holding the cardiomyocytes together (Siwik & Colucci, 2004). This leads to infarct expansion.

(iii) Infarct expansion

Infarct expansion (infarct thinning and LV chamber dilation) can occur within hours of the infarction. There are several mechanisms responsible for infarct expansion including (i) cell stretching due to increased sarcomere length, (ii) reduction in inter-cellular space such as the capillary beds which causes cells to be closer together in the infarcted region, but is predominantly due to (iii) the sliding movement of the cardiomyocytes also known as 'slippage' (Rohde *et al.*, 1999). Side-slippage of cardiomyocytes occurs because of the loss of collagen holding the cells together therefore allowing them to slip (Whittaker *et al.*, 1991). Cardiomyocyte cell death also contributes to the process allowing the neighbouring viable cells to slip (Gajarsa & Kloner, 2011).

(iv) Cardiac fibrosis

Cardiac fibrosis is the deposition of collagen in the heart in response to stimuli and can be one of two main types: reactive or reparative. Reactive fibrosis refers to the collagen of abnormal thickness and density which occupies the perivascular or interstitial space which was previously devoid of collagen whereas reparative fibrosis refers to the replacement of lost/dead cardiomyocytes ('scarring') and is often seen as a patchy distribution and serves to preserve the structural integrity of the myocardium. Infarct expansion during MI can trigger myofibroblasts to proliferate and deposit collagen into the thinned tissue continually to form a scar (where dead tissue is replaced by collagen) which resists further expansion (Sun & Weber, 2000). Therefore cardiac fibrosis in MI is largely a reparative fibrosis. The collagen deposition is a compensatory response to stabilise the distending forces and support the thinned myocardium (French & Kramer, 2007).

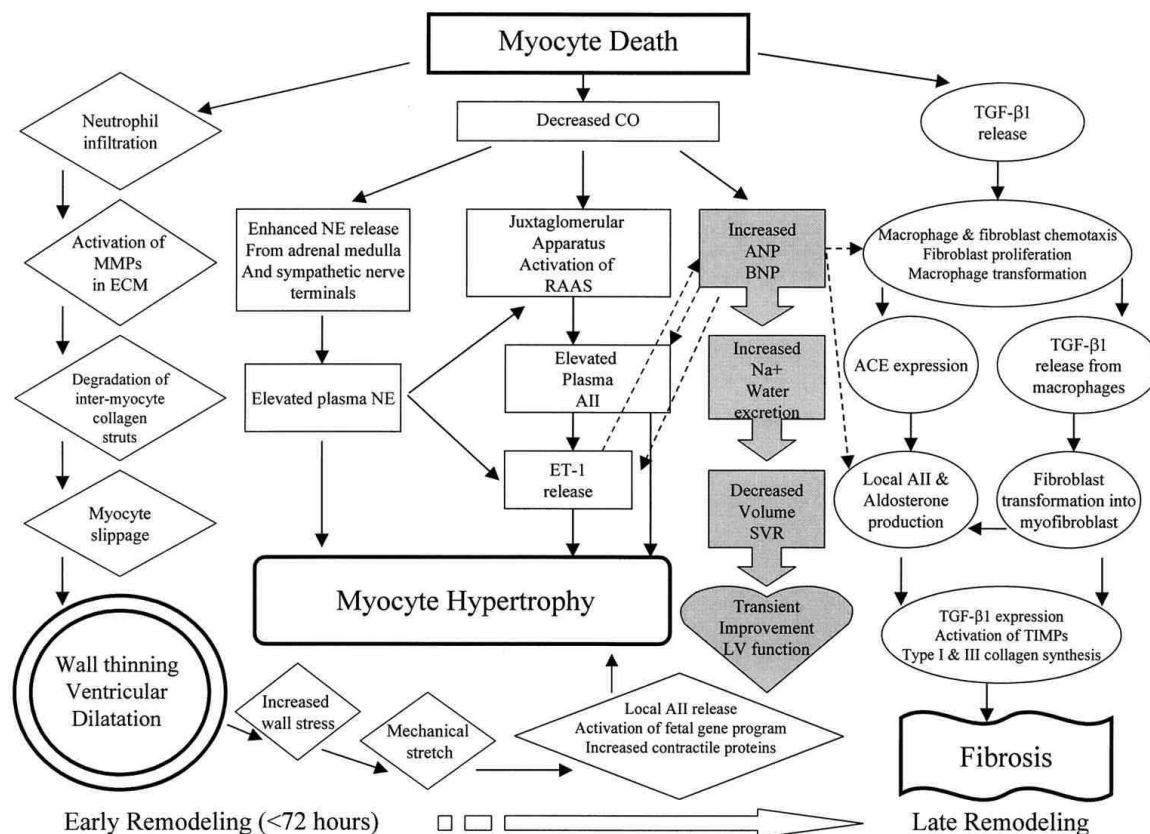


Figure 1.2 Representation of the pathways of LV remodelling post-MI.

ECM, extracellular matrix; RAAS, renin-angiotensin-aldosterone system; CO, cardiac output; SVR, systemic vascular resistance; LV, left-ventricular and AII, angiotensin II. Figure taken from (Sutton & Sharpe, 2000)

(v) Cardiac hypertrophy

Cardiac hypertrophy is the enlargement of cardiomyocytes in response to external stimuli and there are two main forms: eccentric and concentric.

Eccentric hypertrophy refers to the in-series addition of sarcomeres (increase in cardiomyocyte length) and occurs under conditions of volume-overload (e.g. MI) causing a decrease in the ventricular wall thickness. Chamber dilatation leads to an increase in systolic and diastolic wall stress; this occurs because the increase in LV radius increases the wall stress and oxygen demand by Laplace's law (Pfeffer *et al.*, 1991a). Elevated wall stress triggers eccentric hypertrophy (end-to-end lengthwise cell enlargement) in the non-infarcted myocardium by causing altered expression of genes which encode contractile proteins (e.g. β myosin heavy chain) for assembly of new sarcomeres (Sadoshima *et al.*, 1992).

Concentric hypertrophy is the in-parallel addition of sarcomeres (increase in cardiomyocyte width) and typically occurs under conditions of pressure-overload causing an increase in ventricular wall thickness although this can also occur in volume overload.

Hypertrophy in MI is mainly eccentric: Hypertrophy is an adaptive response aimed to compensate for the functional loss of the infarcted myocardium (Pfeffer & Braunwald, 1990). Therefore, early acute chamber dilation is largely due to infarct expansion (in the infarct region) whereas late dilation is the result of eccentric hypertrophy of the non-infarcted regions. Eccentric hypertrophy is therefore *secondary* to infarct expansion and while they both contribute to dilation of the chamber, they differ in the mechanism by which their dilatory effect comes about: infarct expansion leads to dilation through slippage and loss of cardiomyocytes in the infarcted region whereas eccentric hypertrophy contributes to dilation through elongation of surviving cardiomyocytes in the non-infarcted regions by addition of sarcomeres (infarct expansion can result in stretching of existing sarcomeres which is different to the addition of more) (Weisman *et al.*, 1988). Eccentric hypertrophy is considered beneficial initially as it can maintain or in some cases improve contractility in the non-infarcted region; this has been demonstrated in isolated cardiomyocytes from the non-infarcted septum in mice 10-wk post-MI with eccentric hypertrophy (22.5% increase in cell length but no change in cell width versus sham) which showed improved contractility with a 24.6% increase in the Ca^{2+} amplitude compared to sham (Mork *et al.*, 2009). Over time however the LV chamber becomes so dilated that it begins to severely impair contractile function which is the most common cause of HF. A summary of the time course of events of post-MI remodelling is summarised below in Figure 1.3 showing an example from a murine experimental model of MI.

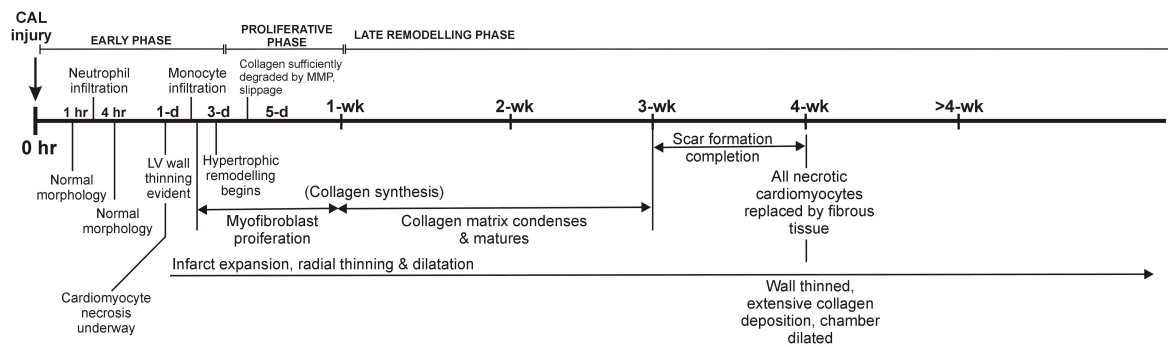


Figure 1.3 Timeline of LV remodelling after MI.

Example LV remodelling timeline showing major events which occur post-MI. This is an example from a mouse MI model showing the three main phases of remodelling; early phase (<72h), proliferative phase (3-7 days) and late phase (>1-wk). Times may vary depending on the extent of the injury. Figure generated from studies by (Wang *et al.*, 2006; Yang *et al.*, 2002).

1.2.1.4 Progression to HF

LV remodelling and HF have both been extensively studied but the mechanisms underlying the transition from one to the other remain unclear. One of the main mechanisms is chamber dilation as described above; it is however also believed to be linked to characteristics of the peri-infarct myocardium (Jackson *et al.*, 2002; Jackson *et al.*, 2003). This refers to the region of myocardium found at the immediate periphery of a developing infarct (also termed border zone) where an interface exists between ischaemic and viable tissue. The peri-infarct myocardium consists of viable surviving cardiomyocytes intermingled with dead necrotic cells and are potential substrates for life-threatening ventricular arrhythmias (Pinto & Boyden, 1999). Fibroblasts and inflammatory monocytes may also be present in the peri-infarct zone although they are predominantly found within the infarct region. Furthermore, close contact between thin-walled infarct and viable myocardium results in an abnormally increased radius of curvature of the myocardium at the infarct margin, leading to elevated wall stress and associated energy demands in the peri-infarct (Buda *et al.*, 1986; Guccione *et al.*, 2001). Energetic insufficiency in the peri-infarct can expand to the rest of the LV and lead to global LV dysfunction and potentially HF. The peri-infarct is believed to play a major role in the development from compensated LV remodelling to HF. Understanding altered function in the peri-infarct myocardium at the cellular level is important for gaining a better insight into the mechanisms underlying the progression of heart failure. Studies have shown that cardiomyocytes isolated from this region demonstrate: (i) altered calcium handling, including decreased SR Ca^{2+} accumulation (Licata *et al.*, 1997), (ii) altered ionic currents

(Pu *et al.*, 2000) and (iii) limited cell shortening due to impaired contractile elements (Licata *et al.*, 1997).

1.2.2 Hypertension

1.2.2.1 Definition and prevalence of hypertension

Human hypertension is considered the largest cause of CVD worldwide (Hajjar *et al.*, 2006). It has been estimated that between 1999-2002, 28.6% of the US population had hypertension (Hajjar *et al.*, 2006). The Health Survey of England in 2010 revealed that the incidence of hypertension was 31.5% in men and 29.0% in women living in England, U.K. (NHS Information Centre, 2010). Hypertension is a chronic, progressive disease characterised by an elevation in arterial BP sufficient to increase the incidence of stroke (4-6 fold), HF (2-3 fold) and renal failure (Schocken *et al.*, 2008). Although hypertension is a major risk factor for MI, the two diseases can occur independently of one another and exhibit very different phenotypes, therefore for the purpose of this thesis they will be referred to separately. Clinically, hypertension is diagnosed when repeated measurements of resting brachial artery pressure exceed 140/90 mmHg in patients under 50 years of age, or 160/95 mmHg in patients older than 50 years (Levick, 2010). However hypertension is emerging as a complex disease and some believe that it cannot be defined by BP limits alone and should incorporate the cardiac and vasculature abnormalities associated with the disease (Giles *et al.*, 2005).

1.2.2.2 Classification of hypertension

Hypertension can be classified as either primary (essential) which means high BP with no underlying medical cause which is the most common form affecting the majority of cases (90-95%) (Carretero & Oparil, 2000), or secondary (remaining 5-10%) which means it is secondary to another medical condition affecting the arteries, kidneys, heart or endocrine system (O'Brien *et al.*, 2007). Despite the debates on the exact definition it is generally accepted that the hallmark of hypertension is the narrowing and stiffening of the arteries which supply blood to the body's tissues (Izzo, Jr. & Shykoff, 2001). At an early stage this is characterised by an increase in vascular tone (ability to constrict) and is reversible with the administration of vasodilator drugs. However as the disease progresses the structure of the arterial tunica media (middle) layer changes; in mild hypertension rearrangement of the vascular smooth muscle myocytes occurs with a modest increase in the ECM which narrows the lumen by ~10% with little change in wall area, this is known as inward

eutrophic remodelling (Intengan & Schiffrin, 2001). At this stage vasodilator drugs are ineffective to rectify the abnormal resistance. In severe hypertension remodelling of the tunica media continues with hypertrophy (increased cell size) and hyperplasia (increased cell numbers) of the smooth muscle myocytes in addition to their rearrangement previously undergone (Amann *et al.*, 1995). The overall consequence is the narrowing of the artery with reduced compliance (stiffer) leading to an increase in the total peripheral resistance (TPR) and increased mean arterial pressure (MAP).

1.2.2.3 Main causes of hypertension

The causes of hypertension have not been fully elucidated but are linked to both genetic and environmental factors:

Genetic factors have been shown to be important factors as it is estimated that 30-60% of BP phenotypic variation among individuals is genetically determined (Shih & O'Connor, 2008). Genetic links are also reflected by the familial and racial tendencies observed in the disease: i.e. hypertension is highly heritable (Doris & Fornage, 2005) and hypertension is more common among patients of Afro-Caribbean or African descent compared to Caucasians (Primates *et al.*, 2000). Studies using identical twins further support a genetic link as monozygotic twins have substantially greater similarities in LV mass than dizygotic twins (Adams *et al.*, 1985). It is very rare that just a single gene is involved and is usually multiple genes linked at distinct chromosomal regions known as quantitative trait loci (QTL) which will be covered in more detail in Chapter 5.

Environmental factors that have been linked to hypertension include high dietary salt (Na^+) intake, low dietary potassium (K^+) intake, obesity, stress and alcohol consumption (Dickinson *et al.*, 2006). High dietary Na^+ is considered one of the highest risk factors as plasma $[\text{Na}^+]$ is known to be elevated by ~2-3 mM in hypertensive patients (normal plasma $[\text{Na}^+]$ is 136-145 mM, abnormal plasma $[\text{Na}^+]$ in hypertension ≥ 147 mM) (Herrera & Garvin, 2005). The mechanism by which high Na^+ leads to hypertension is believed to occur by the following: high plasma $[\text{Na}^+]$ stimulates the adrenal cortex and the brain causing release of a substance called ouabain, an endogenous hormone and potent inhibitor of the Na^+/K^+ pump of the vascular smooth muscle cells. Inhibition of the Na^+/K^+ pump causes partial depolarisation which increases the open probability of the L-type Ca^{2+} channels. The rise in intracellular $[\text{Na}^+]$ reduces Ca^{2+} excretion from the cell by the NCX leading to increased $[\text{Ca}^{2+}]$ and resulting increased vascular tone (Blaustein *et al.*, 2007).

Ouabain has the same effect on cardiomyocytes exerting a positive inotropic effect by the same mechanism - inhibition of the Na^+/K^+ pump (Muller-Ehmsen *et al.*, 2003). Other factors which link Na^+ to hypertension are reduced expression of the α_2 Na^+ pump subunits and reduced expression of NCX1 which have also been shown to cause hypertension (Blaustein *et al.*, 2006).

Impaired Na^+ renal handling is also believed to play a pivotal role in causing hypertension although it is not clear if this is genetically linked (Liu *et al.*, 2011). Under normal conditions, high $[\text{Na}^+]$ triggers a drop in circulating renin-angiotensin II-aldosterone (RAA) levels which reduces distal tubular Na^+ reabsorption to maintain the Na^+ balance. A large amount of Na^+ is filtered into the nephron (25,000 mmol/day) and 99% of this is reabsorbed. Approximately ~65% of the reabsorption occurs in the proximal tubule, ~25% through the thick ascending Loop of Henle, ~5% through the distal tubule and ~5% through the principal cells of the collecting duct (Zhao *et al.*, 2009). There are two hypotheses which have been proposed to explain the imbalance. Firstly, RAA levels are higher in hypertensive patients which would explain the inappropriate retention of Na^+ , however not all hypertensive patients demonstrate elevated RAA levels (Williams, 1982). The second hypothesis is that there is a defect in the gene(s) encoding essential renal ion channels or transporter proteins – this hypothesis is substantiated by the observation that normal rats develop hypertension when transplanted with kidneys from SHR with narrow afferent renal arterioles (Rettig, 1993).

Other factors which can be risk factors for the cause of hypertension include stress as this can lead to temporary periods of increased BP which can heighten an individual's susceptibility to developing hypertension (Dickinson *et al.*, 2006).

Overall hypertension has become regarded as a multifactorial disease and is likely to be caused as a result of complex interactions between dietary, neural, hormonal and renal mechanisms.

1.2.2.4 Structural remodelling in the heart during hypertension

Hypertension affects a number of systems of the body including the vasculature, the heart, the kidneys and the brain. The structural impact on the heart is largely in response to pressure overload. The narrowed, stiffened arteries raise MAP creating an elevated load on the ventricles; this basically means the ventricles have to work to greater extents to

ensure adequate delivery of blood to all of the body's tissues. In response to elevated BP, the heart undergoes structural remodelling in three main ways:

(i) LV hypertrophy (LVH): Due to the increased pressure load on the heart the major response is cardiomyocyte hypertrophy i.e. individual cardiomyocytes of the heart become enlarged through parallel addition of sarcomeres (Frey & Olson, 2003) in attempts to enhance contractile function and cope with the persistent afterload. Cardiomyocyte hypertrophy is driven by local growth factors (such as angiotensin II (AngII) and endothelin (Sadoshima *et al.*, 1993; Shubeita *et al.*, 1990), inflammatory cytokines (e.g. interleukin-1 β) (Thaik *et al.*, 1995) and mechanical stretch (Sadoshima & Izumo, 1993). These trigger the MAP kinase cascade causing an activation of cardiac nuclear transcription factors (e.g. GATA4) which in turn activate genes involved in the hypertrophy process of the cell (e.g. β myosin heavy chain), further details on cardiac transcription factors involved in this process are covered in Section 1.4.2.4. Hypertensive-induced hypertrophy affects the cardiomyocytes of the LV only causing an overall increase in LV mass (RV cardiomyocytes remain normal in size until a pressure overload caused by pulmonary venous hypertension and LV failure is present). LVH is considered an important feature of hypertensive heart disease: firstly, it is one of the earliest responses to hypertension, present in children and adolescents with borderline elevation in BP (Daniels *et al.*, 1990) and secondly, most importantly LVH is a major risk factor for adverse heart disease (see below).

(ii) Coronary artery remodelling. Similar to the narrowing and hardening of arteries of the systemic circulation, the same can also occur in the coronary arteries of the heart during hypertension (Jalil *et al.*, 1991). As described previously, the coronary arteries can also undergo medial thickening caused by hypertrophy and (in some cases) hyperplasia of the vascular smooth muscle cells (Amann *et al.*, 1995).

(iii) Perivascular and interstitial fibrosis. Vascular smooth muscle cells can also undergo structural realignment with enhanced accumulation of ECM proteins such as collagen and elastin which is evident as a perivascular fibrosis (Jalil *et al.*, 1991). This occurs in response to the pressure-overload on the heart triggering the activation of neurohormonal factors including catecholamines, the RAA system and endothelin (Kai *et al.*, 2005) leading to production of collagen by fibroblasts and vascular smooth muscle cells. The accumulation of collagen can spread progressively from the perivascular space into the adjacent interstitial areas (reactive fibrosis) (Silver *et al.*, 1990). The reactive

fibrosis occurs when individual cardiomyocytes are encircled by collagen fibres which impair their ability to contract and relax causing increased myocardial stiffness (which is different to reparative fibrosis which replaces dead cardiomyocytes). Cardiac fibrosis is not present in all types of LVH, for example it does not tend to occur with infrarenal aortic banding or volume-overload uninephrectomy and high Na⁺ diet (Brilla *et al.*, 1990), compensated arteriovenous fistula (Salzmann *et al.*, 1986), atrial septal defects (Marino *et al.*, 1985) or chronic thyroxine administration (Bartosova *et al.*, 1969).

1.2.2.5 Progression to HF

Persistent hypertensive heart disease can push the structural remodelling to a level where it become detrimental and can eventually lead to HF. It has been estimated that hypertension is responsible for causing HF in 39% of men and 59% of women (Levy *et al.*, 1996). The structural adaptations outlined above which occur during hypertension can lead to cardiac dysfunction in several ways. Both LVH and increased interstitial fibrosis lead to increased LV stiffness resulting in diastolic dysfunction (Kahan & Bergfeldt, 2005; Kai *et al.*, 2005). Cardiomyocytes begin to die by necrosis and apoptosis which is believed to occur because of the increased diffusion distance into thickened myocardium causing local intracellular hypoxia (Kahan & Bergfeldt, 2005). This is supported by the observations that discrete foci of reparative fibrosis (replacing necrotic myocytes) become evident throughout the myocardium (Lopez *et al.*, 2001). Loss of cardiomyocytes can lead to a dilated cardiomyopathy and according to Laplace's Law, as radius increases, wall stress increases which further exacerbates cardiomyocyte death rate. Hypertension-related LVH also increases a patient's risk of MI which can also be the cause of dilated cardiomyopathy (Scarborough, 2010). Dilated cardiomyopathy is a serious problem for patients as once this stage is reached it is very difficult to reverse. About 1 in 3 cases of congestive HF are due to a dilated cardiomyopathy (Jameson *et al.*, 2005).

1.3 Mechanisms contributing to progression to HF in both MI and hypertension

As described in the preceding sections the heart has the capability to adapt structurally and functionally as a protective mechanism in response to pathological conditions. While remodelling is initially protective, over time persistent remodelling eventually begins to exacerbate rather than maintain normal function and this leads to eventual HF in the majority of CVD. HF is defined by the chronic inability of the heart to maintain a sufficient CO to adequately perfuse the body's tissues. Researchers have devoted many

years to the study of remodelling and the precise mechanisms by which this leads to HF. Although this still remains an area of intense investigation there are a number of cellular and molecular changes which occur during remodelling that are known to contribute to the functional decline associated with HF. While HF can have distinctly different causes (e.g. MI or hypertension/hypertrophy) the functional characteristics of failing myocardium is very similar as detailed below.

1.3.1 Abnormal Ca^{2+} handling

Morgan *et al.* (1991) were the first to observe altered Ca^{2+} handling in failing human ventricular tissue (trabeculae carneae); they demonstrated prolonged time to peak (93.6% greater than control) and prolonged relaxation (60.6% longer time to reach 50% relaxation from peak than control) (Gwathmey *et al.*, 1987; Morgan, 1991). It has been well-established that the dysfunction in contractility and generation of life-threatening arrhythmias observed in HF is largely due to abnormal Ca^{2+} handling (Pogwizd *et al.*, 2001). Failing human cardiomyocytes demonstrate prolongation of action potential duration (Gwathmey *et al.*, 1990; Nabauer & Kaab, 1998; Ohler & Ravens, 1994), reduced amplitude of the intracellular $[\text{Ca}^{2+}]_i$ transient (Beuckelmann *et al.*, 1992; Gwathmey *et al.*, 1991; Morgan, 1991), impaired force development (Gwathmey *et al.*, 1990; Mulieri *et al.*, 1992) and slowed relaxation (Beuckelmann *et al.*, 1992; Schwinger *et al.*, 1992).

1.3.1.1 Alterations in Ca^{2+} handling proteins

Many of these changes occur due to alterations in the expression and/or interactions between the Ca^{2+} regulatory proteins. The reduced contractility of failing cardiomyocytes, as stated above, is primarily due to a reduced systolic Ca^{2+} transient amplitude arising from ineffective CICR. CICR is reduced in HF often because of a decrease in SR Ca^{2+} content, the cause of which is believed to be for two reasons: (i) there is a reduced expression and activity of **SERCA2** in human failing cardiomyocytes (Arai *et al.*, 1993; Meyer *et al.*, 1995), although some studies have shown no change in SERCA2 expression but reduced Ca^{2+} uptake activity (Movsesian *et al.*, 1989; Schwinger *et al.*, 1995). The second reason (ii) is due to diastolic leak of Ca^{2+} as a result of altered function and/or abundance of the Ca^{2+} release channel, **RyR**. There is also evidence that the abundance of **L-type Ca^{2+} channels** is reduced in HF which would also play a role in reduced CICR (Chen *et al.*, 2002). Ca^{2+} 'leak' is generally defined as loss of Ca^{2+} from the SR during resting or quiescent conditions and is believed to occur from abnormalities in RyR phosphorylation which increase the open probability of the channel (Shannon *et al.*, 2000). Together the

diastolic Ca^{2+} leak and slow Ca^{2+} uptake by SERCA2 impair diastolic relaxation which may be a contributory mechanism for diastolic dysfunction. HF also induces abnormal alterations in the SERCA regulatory protein, **PLN**: for example alterations have been shown in the abundance of PLN (Kiss *et al.*, 1995; Linck *et al.*, 1996), the PLN/SERCA2 stoichiometry (Koss *et al.*, 1997), basal level of PLN phosphorylation (Schmidt *et al.*, 1999) and the ability of β -adrenergic signalling to mediate PLN phosphorylation (Huang *et al.*, 1999). Reduced phosphorylation of PLN and increase in PLN/SERCA2a ratio both contribute to contractile dysfunction in HF (Schmidt *et al.*, 1999). Each of these abnormalities in PLN has been demonstrated in HF however the observations are not always consistent suggesting there are other factors involved. Finally, the **NCX** has also been shown to be misregulated in HF with increased abundance and activity reported (Hasenfuss *et al.*, 1999). The functional significance of this is believed to be that increased NCX activity may compensate for reduced SERCA2 function – this has been demonstrated through use of transgenic mice overexpressing NCX whereby a 2.4 fold increase in NCX activity compensated for reduced SERCA function by 28% allowing maintenance of the duration of the Ca^{2+} transient (Terracciano *et al.*, 2001). Furthermore these changes in the NCX are not always consistently observed in HF, particularly in animal models – in a review by Sipido *et al.*, of the 29 different studies investigating hypertrophy-induced HF, 14 showed an increase in NCX expression and/or function, 10 showed a decrease and 5 showed no change (Sipido *et al.*, 2002).

Relevant to this thesis, in a mouse model isolated cardiomyocytes from viable septum 10-wk post-MI showed prolongation of the Ca^{2+} transient time to peak (15% greater than sham) indicative of slowed Ca^{2+} release (Mork *et al.*, 2009). In another study, mouse cardiomyocytes isolated from the whole LV post-MI showed a 14.7% reduction in the Ca^{2+} transient amplitude compared to sham (Zhang *et al.*, 2010).

Collectively these findings demonstrate that the abnormalities in Ca^{2+} handling are predominantly due to altered Ca^{2+} handling proteins but due to the conflicting evidence it is unlikely to be due to a change in any single protein but rather a disturbance in the balance and/or regulatory interactions between them that is responsible.

1.3.2 Contractile elements

The contractile apparatus of the cardiomyocytes is another potential site of functional abnormality that is believed to contribute to the functional decline during HF. The

contractile mechanism consists of two major structural proteins (actin and myosin) and a complex of regulatory proteins consisting of tropomyosin, troponin C, troponin I and troponin T for the regulation of normal contraction and relaxation of the cell. Troponin T, a regulator of the actin-myosin interaction, is an example of a contractile element found to be altered in human HF: in the normal heart the troponin T isoform T1 predominates, however in patients with HF there is an increased abundance of the T2 isoform which normally only accounts for ~2% of the total troponin (Anderson *et al.*, 1992) although the significance of this shift is unknown.

1.3.3 ECM alterations

The ECM is a mesh of connective tissue which interconnects cardiomyocytes and other cell types of the heart. It is composed of collagens, proteoglycans, glycoproteins, peptide growth factors and proteases and its primary functions are to maintain alignment of cardiac muscle fibres and neighbouring vasculature, and provide an orderly transmission of force to the entire ventricle during systole. The ECM is an important determinant of the structural integrity of the heart and is a very important central feature in structural remodelling during heart disease – disproportionate deposition of ECM proteins or loss of ECM proteins are the major causes of stiffened myocardium (diastolic dysfunction) and dilation, respectively which are two major causes of decompensatory HF. During HF, the release of endothelin influences the synthesis or degradation of collagen in the myocardium (Guarda *et al.*, 1993). The most commonly observed ECM remodelling during disease is the adverse accumulation of fibrillar collagen, expressed as cardiac fibrosis (both reactive and reparative) which has been demonstrated in diseased post-mortem human hearts (Beltrami *et al.*, 1994; Pearlman *et al.*, 1982). This is largely controlled by effector hormones of the RAA system (Weber *et al.*, 1991b) e.g. AngII increases collagen synthesis in a dose-dependent manner by (i) induction of fibroblast hyperplasia, (ii) activation of collagen synthesis pathways, and (iii) inhibition of collagen degradation pathways (Gonzalez *et al.*, 2004). Fibrosis can provide structural support to thinned myocardial infarcts however it can also exacerbate normal functioning as it can limit normal diastolic ‘suction’ (recoil), impair myocardial compliance and compromise the length-dependent muscle fibre shortening during contraction (Moreo *et al.*, 2009).

1.4 Altered gene expression in cardiac disease

Many of the changes above which contribute to functional decline during pathological remodelling with regard to Ca^{2+} handling proteins, the contractile proteins and the ECM proteins occur due to alterations in the gene messenger RNA (mRNA) levels that encode these proteins. An important pattern of altered gene expression during cardiac disease involves the re-expression of foetal genes not normally expressed in adult myocardium, for example up-regulation of atrionatriuretic peptide receptor C (Takahashi *et al.*, 1992). As well as re-induction of foetal genes, cardiac disease can elicit alterations in a diverse range of adult cardiac genes. These genes are extremely important in cardiac research as they could represent potential therapeutic targets for disease treatment.

1.4.1 Differential gene expression in different cardiac diseases

As detailed earlier, different cardiac diseases lead to different morphological forms of structural remodelling (MI *vs.* hypertensive heart disease and LVH) and each are also associated with distinct patterns of gene expression. Genes can therefore be altered differently in different cardiac diseases, and by examining changes in a single gene in different diseases represents a powerful means of elucidating the functional significance of target genes which could represent potential therapeutic targets in CVD. This is important because different forms of cardiac disease are characterised by different pathophysiology, prognosis and response to therapy. For example it has been shown that the same gene can be altered differently in ischaemic *versus* non-ischaemic human cardiomyopathy – e.g. the gene for the leptin receptor which is involved in the regulation of adipose tissue mass was shown to be down-regulated (~1.8-fold) in ischaemic cardiomyopathy but up-regulated (~2-fold) in non-ischaemic cardiomyopathy compared to control healthy hearts (Kittleson *et al.*, 2005). The gene encoding lumican, a regulator of fibrillogenesis, followed a very similar pattern with down-regulation in ischaemic (~1.8-fold) but up-regulation in non-ischaemic cardiomyopathy (~2.5-fold) (Kittleson *et al.*, 2005). Altered gene patterns have been well characterised in animal models of MI which show altered expression of genes encoding proteins involved in calcium-handling (Swynghedauw, 1999), contractile function (Yue *et al.*, 1998), ECM (Weber, 1997) and the RAA system (Holtz, 1998).

Microarray techniques have emerged as a large-scale approach for the identification of target genes altered during cardiac disease (Kaab *et al.*, 2004); however, this may involve large numbers of genes and targets still require validation using qRT-PCR. Gene

expression profiles are complex and require detailed understanding of the precise regulatory mechanisms underlying the control of their expression patterns. It is for this reason that transcription factors have emerged as important targets in elucidating the intricate mechanisms of altered gene expression during the pathophysiology of HF (Buermans *et al.*, 2005).

1.4.2 Transcription factors

A transcription factor is a protein which regulates the precise location, timing and rate of the process of transcription which is the transfer of genetic information from DNA by the synthesis of an RNA molecule copied from a DNA template. Transcription factors are essential to life as they directly control the expression of genes in response to specific physiological stimuli and developmental signals (Latchman, 1997). Transcription factors therefore lie at the core of regulatory and developmental processes (Lee & Young, 2000; Mitchell & Tjian, 1989). They are also extremely important in disease as they respond to pathophysiological stimuli and are often recruited to direct gene expression for protective mechanisms against the disease (Semenza, 1999). In addition they represent important therapeutic targets - approximately 10% of currently prescribed drugs directly target the nuclear receptor class of transcription factors (Overington *et al.*, 2006) an example of this is tamoxifen for the treatment of breast cancer (Gronemeyer *et al.*, 2004).

1.4.2.1 Transcriptional regulation of gene expression

Every cell in the body, with a few exceptions, has identical DNA but there are very distinct cell types and tissue types which vary in structure and function, this is because of transcriptional control (selective gene expression) by transcription factors. Transcription factors initiate the transcription process for subsequent translation into proteins. The process is discussed briefly and summarised in Figure 1.4. Transcription factors bind to a specific region of DNA and recruit an enzyme known as RNA polymerase to synthesise a complementary mRNA strand based on the gene sequence from the DNA template. Once the mRNA strand is synthesised, it leaves the nucleus and enters the cytoplasm where it attaches to a ribosome to begin translation (the process of protein synthesis from the mRNA template). A different RNA molecule called transfer RNA (tRNA) bearing a three-base (anti-codon) sequence joined to an amino acid binds to the complementary anti-codon sequence of the mRNA strand. The ribosome continues along the mRNA strand adding more tRNA-amino acid sequences to form a growing polypeptide chain that forms the protein for which the original gene sequence encodes.

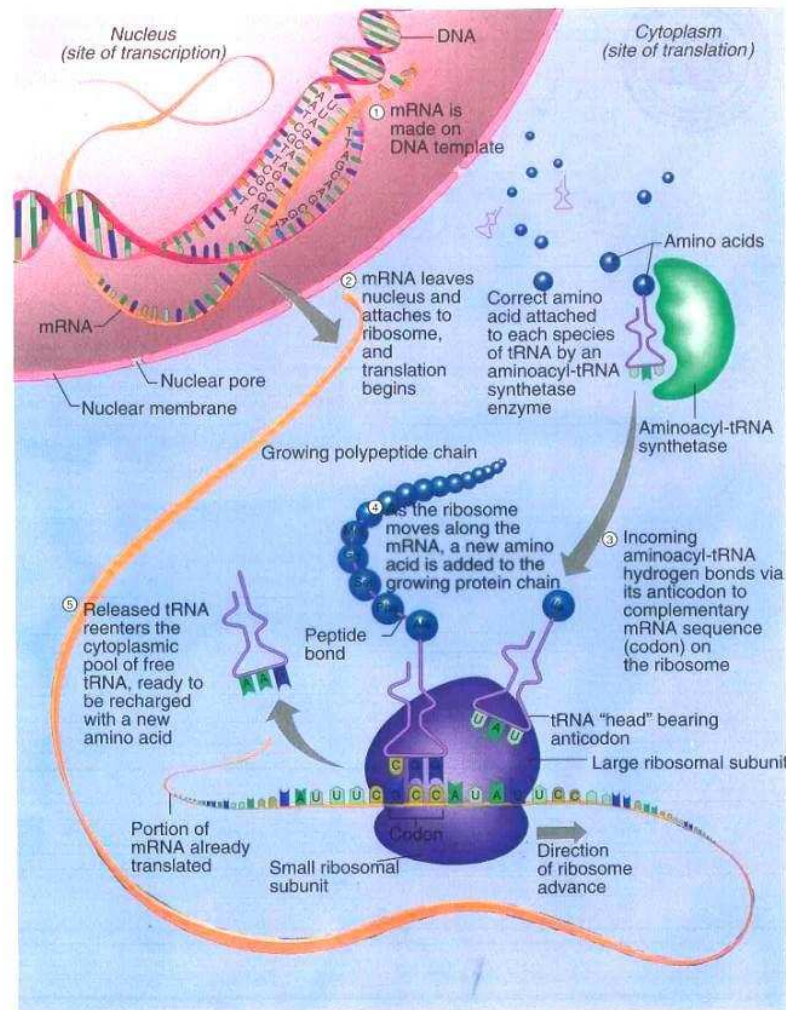


Figure 1.4 Summary process from transcription to translation.

Transcription occurs in the nucleus with the synthesis of an mRNA strand from a DNA template containing the gene sequence. The mRNA strand leaves the nucleus into the cytoplasm for the synthesis of the protein (translation). Steps 1-5 summarise the process. mRNA; messenger RNA. tRNA; transfer RNA. Amino acids are illustrated by the blue circular shapes. Figure taken from Benjamin-Cummings, *Addison Wesley Longman Inc.*

1.4.2.2 Transcription factors bind to DNA

Transcription factors bind to specific DNA sequences located in regulatory regions (usually promoters or enhancers) found near the transcription initiation site of a gene which is the first nucleotide of the DNA that will be transcribed into RNA. These regulatory regions can include elements such as the TATA box (a core promoter DNA sequence) and CpG islands (high frequency linear cytosine and guanidine DNA sequences). These regulatory sequences are generally located 30 bp upstream of the

initiation site and serve to direct binding of RNA polymerase II (Pol II) (Figure 1.5). Transcription factors contain functional domains which are clusters of amino acids which allow the protein to carry out a specific function, namely a DNA-binding domain for binding to DNA and a transactivation domain which activates transcription *via* interaction with other proteins. The DNA binding domain usually takes one of three structures which allow it to bind to DNA; (i) helix-turn-helix (HTH) which consists of two adjacent α -helices separated by a turn of several amino acids; (ii) zinc finger which co-ordinates zinc ions with a combination of cysteine and histidine residues or (iii) basic leucine zipper consisting of four leucine residues at 7-residue intervals which form an α -helix with protruding leucine residues such that when two leucine residues dimerize the motif's 'zip' together (Klug & Cummings, 2005).

1.4.2.3 Transcription initiation complex

In eukaryotes, transcription is initiated by a group of general transcription factors that form an initiation complex (Figure 1.5). A sequence-specific transcriptional activator protein (TATA binding protein; TBP) is a protein that binds to the TATA sequence of a promoter on the DNA to activate the assembly of a well-known group of general transcription factors (TFII). These transcription factors are responsible for the positioning and activation of the Pol II enzyme which catalyses the transcription process. The complex is assembled in the following order. Once TBP is bound to the promoter, TBP-associated factors (TAF) bind and this recruits the binding of TFIIB and TFIIA first which are responsible for positioning Pol II in the correct place. Next, Pol II complexed with TFIIF are positioned in place. Finally a multi-subunit complex containing TFIIH binds and through helicase activity facilitates the separation of the DNA strands and phosphorylates Pol II *via* its C-terminal domain which activates Pol II for transcription at the start site. Collectively this forms the transcription pre-initiation complex (PIC) that accompanies all eukaryotic transcription but is sufficient only for a low basal level of transcription. The final stage involves the *induced* level of transcription which represents the higher, stimulated stage – this involves other areas of the promoter region, enhancers and the binding of other transcription factors.

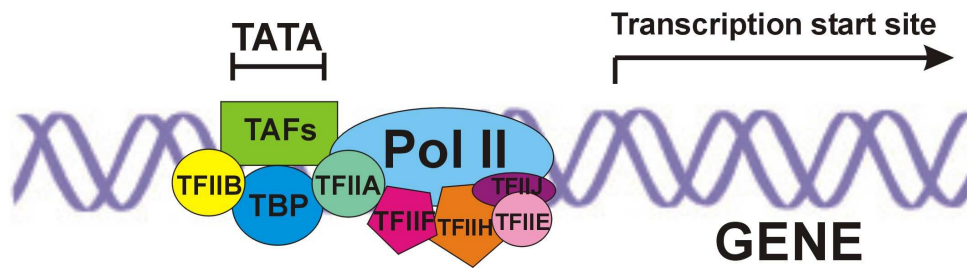


Figure 1.5 Assembly of the transcription initiation complex in eukaryotes.

TBP binds to the TATA box which initiates the binding of a combination of general transcription factors (TF) to assemble the initiation complex required for mRNA synthesis. Following TBP binding, the next to bind are TFIIB and TFIIA (which position Pol II), followed by TFIIF which is complexed with Pol II. TFIIE is then added followed by TFIIH, which separates the two DNA strands and phosphorylates the Pol II C-terminus for initiation of transcription at the start site. TBP = TATA-binding protein; TAFs = TBP-associated factors; TFIIA,B,E,F,H,J = transcription factors required to direct RNA polymerase II binding; Pol II = RNA polymerase II.

1.4.2.4 Role of transcription factors in the heart

Much of the alterations in the structural properties of the heart during remodelling (both physiological and pathophysiological) are due to altered gene expression by the action of transcription factors. One clear example of this is during cardiac hypertrophy. In response to specific stimuli, transcription factors such as GATA, MEF2, Gx/Nkx2-5 and HAND direct the expression of various genes necessary for enlargement of the cardiomyocytes, including the transcription of genes responsible for the production and assembly of contractile proteins to increase sarcomeric unit number (Glennon *et al.*, 1995). These cardiac transcription factors are known to play a crucial role in the heart during embryogenesis; however in recent years they have received increasing interest in the post-natal heart particularly during disease of the heart. Their role is crucial during hypertrophy as cardiomyocytes are terminally differentiated and do not have the ability to proliferate. Therefore transcription factors control the cellular alterations necessary for cardiomyocytes to adapt under various conditions. Transcription factors integrate a wide range of stress signals (e.g. mechanical load, neurohormones and cytokines) and therefore represent a point of convergence in the pathway from cardiac stress to cardiac remodelling and failure (Frey & Olson, 2003). Further details on the transcription factors which have been implicated in the regulation of myocardial gene expression during the pathogenesis of cardiac disease are detailed below:

The **GATA** transcription factor family bind to the specific consensus DNA sequence (A/T)GATA(A/G) *via* a highly conserved domain containing double zinc fingers (Patient & McGhee, 2002). There are three members of the GATA family which are known to be

expressed in the heart: GATA4, GATA5 and GATA6. GATA4 and GATA6 are expressed in the nuclei of cardiomyocytes (Koutsourakis *et al.*, 1999; Perrino & Rockman, 2006) while GATA5 is restricted to endothelial cells (Morrissey *et al.*, 1997). Of the three, GATA4 plays the more prominent role as it directly regulates the expression of a range of cardiac-specific genes including: α -myosin heavy chain (α -MHC), myosin light chain 1/3 (MLC1/3), atrial natriuretic peptide (ANP), brain natriuretic peptide (BNP), cardiac troponin C, cardiac troponin I, cardiac sodium-calcium exchanger (NCX1) and cardiac-restricted ankyrin repeat protein (CARP) (Liang & Molkenin, 2002; Molkenin, 2000). GATA4 is also critically involved in inducing gene expression in the heart in response to various hypertrophic stimulations (Herzig *et al.*, 1997). For example GATA4 is essential for the up-regulation of β -MHC and the AngII type 1 α receptor in response to transverse aortic constriction (TAC) (Hasegawa *et al.*, 1997) and GATA4 DNA-binding activity is significantly enhanced in response to pressure-overload by intravenous infusion of arginine(8)-vasopressin (AVP) in conscious rats (Hautala *et al.*, 2001). GATA1 has been reported to be up-regulated 2-3 fold in the remote LV 24-48 h post-MI in a rat model (LaFramboise *et al.*, 2005).

MEF2 transcription factors bind to specific A/T rich consensus DNA sequences to regulate a number of cardiac genes including α -MHC, SERCA, cardiac troponin T, cardiac troponin C, cardiac troponin I and desmin (Bhavsar *et al.*, 2000; Black & Olson, 1998). MEF2 is expressed in cardiomyocyte nuclei (Wang *et al.*, 2011) and is also critically involved in the regulation of genes during cardiac hypertrophy (Zhu *et al.*, 1991). The regulatory DNA-binding of MEF2 increases in the cardiomyocytes of rat hearts exposed to pressure or volume overload (Molkenin & Markham, 1993). MEF2 also functions as an important effector of intracellular Ca^{2+} signalling pathways as its activity is stimulated by Ca^{2+} /calmodulin-dependent protein kinase (CaM kinase) (Passier *et al.*, 2000).

Csx/Nkx2-5 are homeobox transcription factors with a helix-turn-helix DNA-binding motif which binds to a specific consensus DNA sequence T(C/T)AAGTG (Chen & Schwartz, 1996). Homeobox refers to a sequence of DNA ~180bp long which encodes a 60 amino acid DNA-binding protein domain (homeodomain) for transcriptional regulation. Csx/Nkx2-5 are expressed in cardiomyocyte nuclei (Zhu *et al.*, 2000) and directly regulate a number of cardiac-specific genes such as ANP (Shiojima *et al.*, 1999), cardiac α -actin (Chen & Schwartz, 1996), connexin40 (Bruneau *et al.*, 2001) and NCX1 (Muller *et al.*, 2002). Csx/Nkx2-3 has been shown to be essential during embryogenesis as the Csx/Nkx2-3-null phenotype results in embryonic lethality due to arrested looping

morphogenesis of the heart tube (Lyons *et al.*, 1995). *Csx/Nkx2-3* is also expressed in the adult mammalian heart (Kasahara *et al.*, 1998) but its roles post-natal are less understood. It has been shown that *Csx/Nkx2-3* expression is up-regulated in hypertrophic hearts (Saadane *et al.*, 1999) and protects against cytotoxic damage in the heart (Toko *et al.*, 2002).

HAND transcription factors (eHAND and dHAND) bind DNA *via* basic helix-loop-helix motifs to regulate genes specific to cardiac development (Srivastava, 1999). eHAND and dHAND are expressed in human hearts but the eHAND isoform is significantly down-regulated in hearts from patients with cardiomyopathies (Natarajan *et al.*, 2001). eHAND has been shown to be expressed in the nucleus of cardiomyocytes (Togi *et al.*, 2004) and dHAND has been shown to be expressed in the endocardium and myocardium by RT-PCR (although cell types were not specified) (Yamagishi *et al.*, 2000). In a mouse model of hypertrophy, eHAND expression is down-regulated in the LV only and dHAND expression is down-regulated in the RV only (Thattaliyath *et al.*, 2002). Knowledge of the direct downstream genes regulated by HAND is at present limited.

Forkhead box (FOX) transcription factors are present in other tissue types as well as the heart such as skeletal muscle, lung, liver, thymus and nervous system (Hoekman *et al.*, 2006;Maiese *et al.*, 2008) and have recently been implicated as having a major role during cardiac disease. FOX transcription factors are up-regulated in early (1-wk) post-MI rat hearts by ~5.5 fold (*FoxO1*) and in advanced human HF by 4-8 fold (Hannenhalli *et al.*, 2006;Philip-Couderc *et al.*, 2008). Abundant expression of FOXP1 protein has been localised to nuclei of failing human cardiomyocytes by IHC (Hannenhalli *et al.*, 2006). FOX transcription factors activate the expression of genes encoding ATP-dependent potassium (KATP) channels (e.g. *KIR6.1*) in the peri-infarct region in a rat model of MI (Philip-Couderc *et al.*, 2008) and promote autophagy in cardiomyocytes by activating autophagy pathway genes *Gabarapl1* and *Atg12* (Sengupta *et al.*, 2009). Therefore, even small changes in the expression of transcription factors in the heart can have important phenotypic and functional consequences.

Other: In another study by Hannenhalli *et al.* (2006), the investigators used a combination of microarrays and a computational approach to identify particular transcription factors which were responsible for the changes in gene expression between failing and non-failing hearts and their study revealed that the following transcription factor-binding sites were responsible for many of the altered gene expression patterns involved in HF: GATA, MEF-

2, Nkx, NF-AT, polyA, TATA, FOX, Octamer, IRF, CDP, AIRE, C/EBP, AFP1 and Msx-1 (Hannenhalli *et al.*, 2006). The regulation of cardiac gene expression is known to be a complex process mediated by interactions between transcription factors, coactivators, corepressors and epigenetic modifications (e.g. histone acetylation); however transcriptional genomics – assessing single transcription factors - (as opposed to a microarray-based identification of a large number of genes) may provide a more integrative analysis to identify therapeutic targets against transcription factors through targeting of a number of genes rather than just a single target gene.

1.5 RUNX transcription factors

The RUNX family are a group of transcription factors which represent a novel group of proteins in the context of myocardial injury. This section will provide background information on the RUNX family followed by their recent interest in cardiac disease.

1.5.1 Identification and structure

1.5.1.1 Nomenclature

The RUNX proteins are a family of transcription factors which regulate gene expression for normal metazoan development (Coffman, 2003). RUNX proteins are encoded by the *RUNX* genes and are defined by the ‘runt box’ which is a highly conserved protein domain important for DNA binding and protein-protein interactions and represents a unique characteristic of all members of the RUNX family (Kagoshima *et al.*, 1993). The runt box derives its name from the first member of the family to be discovered, the *Drosophila melanogaster* gene *Runt* which is responsible for segmentation of the *Drosophila* fly embryo during development (Gergen & Butler, 1988). Over the years alternative names have been assigned to RUNX proteins which have been derived from their roles in disease such as acute myeloid leukemia (AML), core-binding factor α (CBF α) and polyoma enhancer-binding protein-2 α (PEBP2 α). In this thesis they will be referred throughout as the RUNX family. Where the description refers to the protein (human, rat and mouse) this will be written in uppercase (RUNX) and for references to the gene this will be written in italics either with all letters uppercase, *RUNX* (human) or only the first letter in uppercase, *Runx* (rat or mouse) according to standard genetic nomenclature (Elsevier, 1998).

1.5.1.2 Chromosomal location of *RUNX* genes

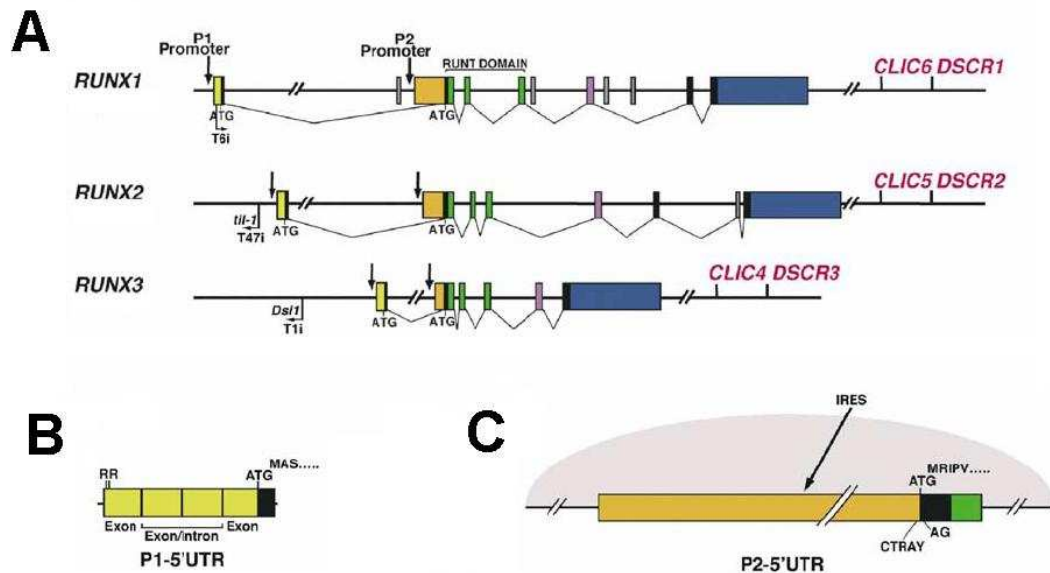
Runx genes are present in a diverse range of organisms (Rennert *et al.*, 2003) and the number of *RUNX* genes can vary depending on phylogenetic background; for example mammals have three, *Drosophila* have four and lower invertebrates such as the eukaryotic nematode *C. elegans* and the sea urchin *S. purpuratus* have only a single *Runx* gene (Nam *et al.*, 2002; Robertson *et al.*, 2002). Relevant to this thesis, the three mammalian *RUNX* genes, *RUNX1*, *RUNX2* and *RUNX3* are located on human chromosome 21, 6 and 1; mouse chromosome 16, 17 and 4; and rat chromosome 11, 9 and 5 respectively (*GenBank*, National Centre for Biotechnology Information; NCBI).

1.5.1.3 Structure of *RUNX* genes

A summary diagram of the structure of the *RUNX* genes is depicted in Figure 1.6. Each *RUNX* gene (*RUNX1*, *RUNX2* and *RUNX3*) encodes the respective named protein (*RUNX1*, *RUNX2* and *RUNX3*). The *RUNX* genes are very closely related and share extensive regulatory elements and functional coding regions known as exons (Levanon & Groner, 2004). Firstly, each of the three genes is transcriptionally regulated from two promoters; P1 (distal) and P2 (proximal) (Bangsow *et al.*, 2001; Levanon *et al.*, 2001b; Park *et al.*, 2001). Both promoters direct transcription of adjacent 5'-untranslated regions (5'UTR) which are regions transcribed but not translated. The P1-5'UTR (452 bp long) contains four exons and two *RUNX*-binding sites (which allow the *RUNX* protein to bind to the *RUNX* gene) within a highly conserved 18 bp sequence found at the beginning of the P1 5'-CAACCACAGAACCACAAG-3' (the underlined bases represent the two *RUNX*-binding sites) (Drissi *et al.*, 2000; Bangsow *et al.*, 2001). The fourth exon encodes the initiator ATG and the highly conserved P1 N-terminal peptide (MAS) (Pozner *et al.*, 2000). The P2-5'UTR contains a single exon which directs translation of the P2 N-terminal peptide (MRIPV), contains an internal ribosome entry site (IRES) and terminates with an in-exon splice site (Pozner *et al.*, 2000). The P2-5'UTR is the larger of the two 5'UTRs (1631 bp) and is distinctly nested within a very large CpG island (high frequency of linear cytosine and guanidine sequences) not found in the P1-5'UTR (Levanon *et al.*, 2001a). The *RUNX* genes also contain exons which encode different functional domains of the *RUNX* proteins including the Runt domain and the transactivation domain (Levanon & Groner, 2004). In addition they also share similarities outwith the *RUNX* locus itself with highly conserved neighbouring genes such as the *CLIC6* and *DSCR1* genes (Levanon & Groner, 2004). The *RUNX3* gene is the smallest of the three with the fewest exons (Bangsow *et al.*, 2001). Major features of the *RUNX* genes are summarised in Table 1.1.

Table 1.1 Functional roles of the regulatory regions of *RUNX* genes.

Gene Region	Function
ATG initiator	First codon (start codon) of mRNA transcript which is translated into the amino acid methionine.
Exons 2-4 6	Functional coding region. Encodes Runt domain. Encodes transactivation domain.
UTR	Regions of DNA which can influence translation but are themselves not translated.
MAS	N-terminal sequence encoded by the P1-5'UTR.
MRIPV	N-terminal sequence encoded by the P2-5'UTR.

**Figure 1.6 *RUNX* genes structure and elements involved in expression regulation.**

(A) Structure of the three mammalian *RUNX* genes; *RUNX1*, *RUNX2* and *RUNX3*. All *RUNX* genes have similar genomic organisation with two promoters (P1 and P2) and a very large first intron. Common exons are shown in the same colour. 5' untranslated regions (UTRs) are shown in yellow and orange, and 3' UTRs shown in blue. The highly conserved Runt domain is encoded by three exons (green boxes). The exons comprising the transactivation domain are shown in black and grey. The conserved neighbouring genes are also shown (CLIC6 & DSCR1). *RUNX3* is the smallest of the three *RUNX* genes with the fewest exons. (B) Schematic showing the common structure of the P1-5'UTR (yellow in diagram A) which contains four exons; the two *RUNX* binding sites are indicated by RR (for binding by the *RUNX* protein to the *RUNX* gene); and the fourth exon encodes the initiator ATG and the highly conserved P1 N-terminal peptide (MAS). (C) Schematic showing the P2-5'UTR (orange in diagram A) which has a single exon which terminates with an in-exon splice site (AG) which is preceded by a branch point signal CTRAY. The P2-5'UTR contains an internal ribosome entry site (IRES) and is nested within a very large CpG island depicted by the grey cloud. Figure taken from (Levanon & Groner, 2004).

1.5.1.4 Structure of RUNX proteins

Runt homology domain

A schematic representation of the domain structures of each mammalian RUNX protein is shown in Figure 1.7. The most important and defining feature of the RUNX proteins is a highly conserved region known as the Runt homology domain (RHD) (Ito, 1999). The RHD is located in the N-terminus of the protein and is necessary for DNA binding and protein-protein interactions (Kagoshima *et al.*, 1993; Crute *et al.*, 1996). The RHD is an s-type immunoglobulin (Ig) fold domain similar to the DNA-binding domains found in other transcription factors such as NF κ B, p53, NFAT and STAT, but differs in that the RHD loops at both ends of the Ig-fold rather than just the end which contacts the DNA. This is believed to give the RHD the ability to substantially bend the DNA more (Berardi *et al.*, 1999).

Other functional domains

Another highly conserved region among all three proteins is the nuclear localisation signal (NLS) domain which is immediately adjacent to the RHD and is responsible for the sub-cellular nuclear localisation of the RUNX proteins (Choi *et al.*, 2001). Together the RHD and the NLS comprise the very highly conserved 128 amino acid sequence of the RUNX proteins (Choi *et al.*, 2001). Other functional domains common to all three RUNX proteins are the transactivation domain which is required for transcriptional activity, the inhibitory domain (ID) which is necessary for repressing transcriptional activity (Coffman, 2003), the nuclear matrix targeting signal (NMTS) which is important for attachment to the nuclear matrix once directed into the nucleus by the NLS (Tang *et al.*, 1999) and the VWRPY motif which mediates transcriptional repression by recruiting the transcription co-repressor, Groucho and its mammalian homologue transducin-like enhancer of split (TLE) and directing them to the target promoter regions (Levanon *et al.*, 1998). The NLS, transactivation domain, ID, NMTS and VWRPY are all located in the C-terminus of the protein (Coffman, 2003). RUNX2 has an additional two domains within the N-terminus which are not present in RUNX1 or RUNX3 which is the polyglutamine and polyalanine (23Q/17A) domains (Thirunavukkarasu *et al.*, 1998).

Amino acid composition

Beyond their common functional domains, the RUNX proteins are similar in the composition of amino acids but the sequences can vary between each. In all three RUNX proteins, the C-terminus is rich in proline, serine and threonine residues (PST) (Coffman, 2003). Given that the two promoters (P1 and P2) generate different 5'UTRs and therefore different N-terminal regions of the protein this can lead to multiple gene products with variable N-terminal peptide sequences. The different UTRs can lead to differences in peptide amino acid sequences at the N-terminal due to the difference in translational-regulatory mechanisms of each: for example, for RUNX1 the P1-5'UTR directs cap-dependent translational control while the P2-5'UTR regulates translation by the IRES mechanism. All eukaryotic mRNA have a cap structure (a 5' terminal nuclear modification) which affects RNA splicing, stabilisation, transport and translation which acts as a 'molecular tag' to direct the 40S ribosomal subunit in place. IRES is a mechanism which allows a ribosome to bind in the middle of the mRNA strand rather than at the cap-end (Levanon & Groner, 2004). The RUNX1 sequence derived from P1 begins with a MASDS amino acid sequence at the N-terminal, and from P2 begins with a MRIPV amino acid sequence. Transcription from the two alternative promoters can give rise to splice variants of the RUNX protein which differ in their N-termini sequences and as a result, have alterations in the functioning of the protein. The use of multiple promoters in gene expression confers versatility to the final protein where it may be required to be expressed in different tissue types or at different developmental stages for which a single promoter may not be sufficient (Ayoubi & Van De Ven, 1996). In particular this can have significant effects for RUNX1 in that it can cause the protein to have reverse roles in selected cell types. For example, the short isoform of RUNX1 (RUNX1/p26 or RUNX1A) lacks much of the C-terminus including the transactivation domain which can therefore affect transcriptional activity, but also lacks some of the domains which inhibit DNA binding *via* the Runt domain (Kim *et al.*, 1999; Gu *et al.*, 2000) and therefore has the ability to bind DNA more effectively in some cases. RUNX1A has been shown to block differentiation and promote proliferation in a murine myeloid cell line whereas the normal RUNX1/p46 protein (p46 refers to the isoform) does the opposite (blocks proliferation and promotes differentiation). Therefore it is possible that alternatively spliced RUNX proteins can play opposing roles.

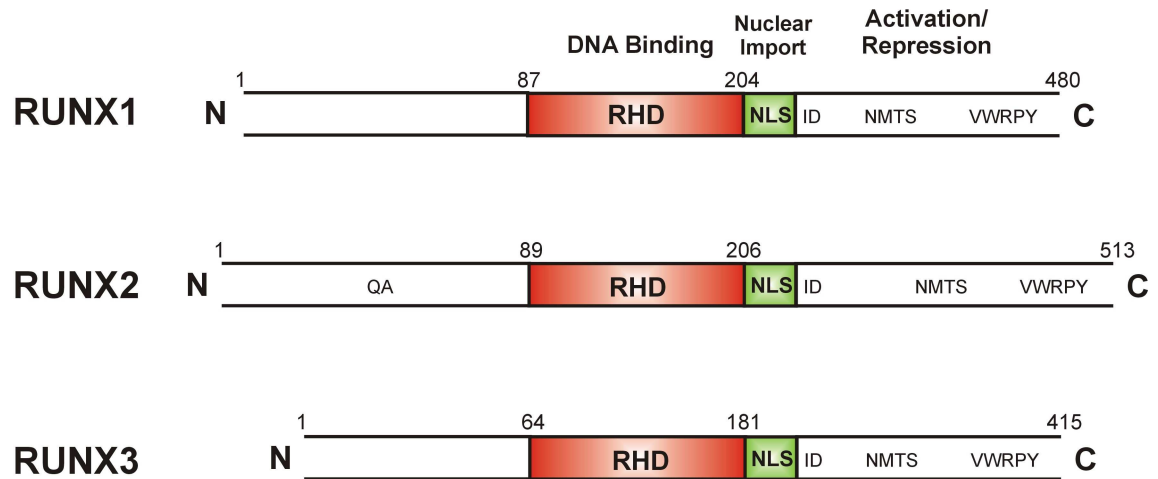


Figure 1.7 Schematic representation of the functional domains of the RUNX proteins.

Schematic representation of the structure of RUNX1, RUNX2 and RUNX3 proteins. The numbers refer to amino acids. The N-terminus (N) and C-terminus (C) are shown. The functional domains conserved across each RUNX protein are shown in colour; the Runt Homology Domain (RHD) in red which mediates DNA-binding and protein-protein interactions and the Nuclear Localisation Signal (NLS) domain shown in green which is responsible for nuclear localisation. The C-terminus contains motifs common to all RUNX proteins including the inhibitory domain (ID) which represses transcriptional activity, the nuclear matrix targeting signal (NMTS) important for nuclear targeting and the VWRPY motif which mediates transcriptional repression through its association with a transcription co-repressor, Groucho/transducin-like enhancer of split (TLE). The letters Q and A on RUNX2 designate homopolymeric stretches of glutamine and alanine residues present at the N-terminus which are unique to RUNX2 as was referred to in the text above.

Multimeric complex formation

All RUNX proteins bind *via* the RHD to the same specific DNA consensus sequence (TGTTGGT) in the promoter region of a target gene through recruitment of common transcriptional modulators (Bae & Ito, 1999). Additionally they all bind to DNA as part of a multimeric complex containing a number of different proteins (Kamachi *et al.*, 1990). These include a partner protein known as the core binding factor beta subunit (CBF β) as well as other transcription factors and co-activators/co-repressors (Durst & Hiebert, 2004). CBF β binds to RUNX *via* the RHD and helps stabilize the complex and increase the affinity for DNA-binding but does not itself bind to DNA (Ogawa *et al.*, 1993). The mechanism by which CBF β stabilizes the complex is understood to be that it maintains the RHD in an open conformation serving as a kind of ‘molecular clamp’ (Habtemariam *et al.*, 2005). Once bound to CBF β , RUNX recruits other DNA binding transcription factors to build a multi-protein complex for regulated transcription. For example, RUNX binding sites are often located adjacent to DNA-binding sites for other transcription factors such as members of the Ets family, Myb and C/EBP (Lund & van, 2002;Durst & Hiebert, 2004).

RUNX can also interact with a number of co-activators (HAT, p300, CBP) or co-repressors (mSin3A, TLE and HDACs) which can activate or repress transcription respectively (Pelletier *et al.*, 2002) as shown in Figure 1.8.

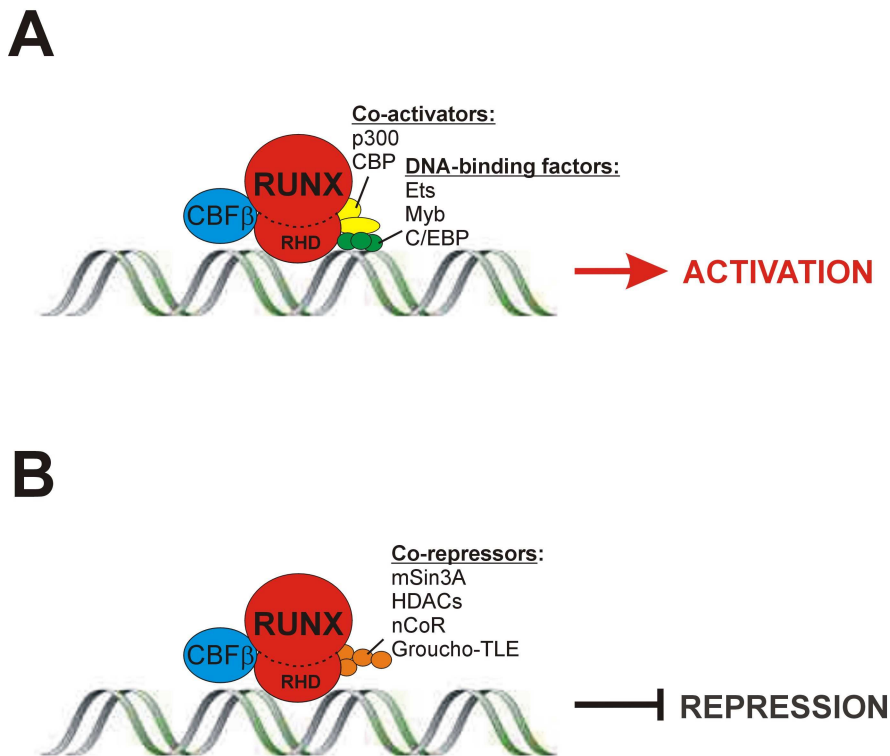


Figure 1.8 Schematic representation of RUNX transcriptional regulatory complexes for activation and repression of gene expression.

(A) Schematic representation of a RUNX **activation** complex. The Runt Homology Domain (RHD) of the RUNX protein (red) binds DNA and facilitates binding of CBF β (blue) and various DNA-binding factors such as Ets, Myb and C/EBP (green) which recruit co-activating factors such as p300 and CBP (yellow) - together results in activation of the target gene of interest. (B) Schematic representation of a RUNX **repression** complex. The RHD of the RUNX protein (red) binds DNA and facilitates binding of CBF β (blue) and various co-repressors such as mSin3A, TLE and HDACs which together results in repression of the target gene of interest.

1.5.2 Function of RUNX proteins

All RUNX proteins function as transcription factors which regulate specific gene expression in developmental pathways. It is well-established that RUNX transcription factors have opposing functioning as both activators and repressors of transcriptional regulation depending on the context of the regulatory region (Coffman, 2003; Blyth *et al.*, 2005). There are sequences in the C-terminus that control this through recruitment of associative activators or repressor proteins to the complex. For example, RUNX can activate transcription through interactions with histone acetyl-transferases (e.g. MOZ and MORF) (Kitabayashi *et al.*, 2001; Pelletier *et al.*, 2002) or they can also inhibit

transcription by interacting with the dominant co-repressor Groucho/TLE (Aronson *et al.*, 1997) or the mSin3A co-repressor (Lutterbach *et al.*, 2000). However, despite the highly conserved structural similarities between the RUNX proteins and their shared properties in binding to the same DNA consensus sequence through pairing with CBF β , each of the RUNX proteins have distinct functional roles in different lineage-specific development. This is reflected in the different phenotypes which have been elucidated from the respective genetic knockouts.

1.5.2.1 RUNX1 functions as a regulator of haematopoiesis

Haematopoiesis is the formation and development of blood cells. In the embryo two waves of haematopoiesis occur; primitive and definitive haematopoiesis, which give rise to the embryonic precursor cells and the adult HSCs that form specific blood cells capable of self-renewal, respectively (Lensch & Daley, 2004). RUNX1 is absolutely critical for definitive haematopoiesis by controlling haematopoietic stem cell development and differentiation (initiation phase only) (Okuda *et al.*, 1996; Okuda *et al.*, 2001; Hoogenkamp *et al.*, 2009). This has been clearly demonstrated by *Runx1*^{-/-} mice which die at an early embryonic stage (E11.5-E13.5) from an early block in blood development (Okuda *et al.*, 1996). These mice exhibit normal primitive haematopoiesis but a complete lack of definitive haematopoiesis (Okuda *et al.*, 1996; North *et al.*, 1999).

1.5.2.2 RUNX2 is required for bone development

RUNX2 is involved in the regulation of osteogenesis which is the development of bones; this has been verified in *Runx2*^{-/-} mice which die shortly after birth from a complete lack of bone formation although they do form the cartilage of an ossified skeleton (Otto *et al.*, 1997; Komori *et al.*, 1997).

1.5.2.3 RUNX3 is involved in neurogenesis

RUNX3 regulates the development and survival of proprioceptive neurons in dorsal root ganglia (Inoue *et al.*, 2002), this has been confirmed by *Runx3*^{-/-} mice which demonstrate severe limb ataxia due to defective development of proprioceptive neurons (Levanon *et al.*, 2002). However there are discrepancies between the *Runx3*^{-/-} phenotype as others have shown a hyperproliferation of epithelial cells in the gastric mucosa which led to death of the *Runx3*-deficient animals shortly after birth from starvation (Li *et al.*, 2002); an observation not seen by Levanon *et al.* (2002). RUNX3 is also known to be a putative

gastric tumour repressor as it controls cell proliferation and apoptosis of gastric epithelium (Li *et al.*, 2002).

1.5.3 Tissue-specific expression of RUNX

In addition to their distinct roles, each RUNX protein also shows a very specific spatio/temporal expression pattern in different tissue types. It is believed that the RUNX1 protein can promote its own expression by binding to the *Runx1* gene promoters or enhancers and down-regulate its own expression by recruiting the repressor Smad6 (Pimanda *et al.*, 2007). The RUNX protein binds to distinct RUNX-binding sites located within the P1 promoter which is indicated by the yellow box in Figure 1.6A and by RR in Figure 1.6B. It has been proposed that the highly conserved CpG islands present at both ends of *RUNX* genes may be involved in the tissue-specific expression (Ehrlich, 2003) although the precise role by which this occurs remains unclear. Tissue sites for RUNX expression are detailed below and summarised in Table 1.2.

RUNX1 is first detected in mouse embryos within definitive haematopoietic stem cells (HSC) and in endothelial cells at HSC emergence sites, for example the yolk sac, umbilical arteries, aorta-gonad-mesonephros (AGM) and liver (North *et al.*, 1999;Cai *et al.*, 2000). RUNX1 is also expressed in the bronchi, mucosa of the oesophagus and stomach, epithelia of palatal ridges, in ectodermal invaginations (e.g. salivary and mammary glands) and epidermal appendages (e.g. whiskers and teeth; epithelia only) of the embryo. RUNX1 is also expressed in the mesenchyme of the heart (see later) and central nervous system (CNS) of the embryo.

RUNX2 is expressed predominantly in chondrocytes (prehypertrophic and hypertrophic) and osteoblasts which is not surprising given its role in the developing skeleton. RUNX2 is also expressed in fibroblasts of periodontal ligament fibroblast cell lines (Saito *et al.*, 2002) and in primary murine fibroblasts (Kilbey *et al.*, 2007). RUNX2 has also been shown to be expressed in the epidermal appendages (whiskers and teeth) but confined to the papilla regions (Levanon & Groner, 2004).

Table 1.2 Summary of RUNX expression sites.

Tissue/Cell Type	RUNX1	RUNX2	RUNX3	References
<u>Haematopoietic System</u>				
(Embryonic)				
Aorta-gonad-mesonephros	+			North <i>et al.</i> 1999
Liver (haematopoietic precursors)	+		+	Levanon <i>et al.</i> 2001
Thymus	+	+	+	Woolf <i>et al.</i> 2003
Spleen	+		+	Levanon <i>et al.</i> 2004
(Adult)				
Thymus	+	+	+	Woolf <i>et al.</i> 2003
Myeloid, B and T lymphoid cells	+			Lorsbach <i>et al.</i> 2003
<u>Skeleton</u>				
Immature and permanent cartilage	+			
Prehypertrophic cartilage			+	
Hypertrophic cartilage		+	+	Levanon <i>et al.</i> 2001
Osteoblasts	+	+		
Membranous bone	+	+		
<u>Dorsal Root Ganglia</u>				
(Embryonic)				
TrkA neurons	+			
TrkC neurons			+	Levanon <i>et al.</i> 2001
(Adult)				
Mature dendritic cells			+	Fainaru <i>et al.</i> , 2004
<u>Epidermal appendages</u>				
Epithelial	+			
Mesenchymal		+	+	Levanon <i>et al.</i> 2001

+ indicates positive expression at the respective sites.

RUNX3 is also expressed in prehypertrophic and hypertrophic chondrocytes (however in the latter, RUNX2 predominates). RUNX3 is not detected in osteoblasts. RUNX3 is also expressed in the salivary and mammary glands, and the whiskers and teeth (although confined to the mesenchyme) (Levanon *et al.*, 2001).

Collectively, it can be seen that there are overlap of the RUNX proteins in the tissue in which they are expressed but there are differences in the regional distribution within the shared tissues.

1.5.4 Regulatory mechanisms of *RUNX* gene and RUNX protein expression

1.5.4.1 Transcriptional control

RUNX genes can be regulated by SMAD5 signalling pathways; the up-regulation of *Runx2* mRNA for osteoblastic differentiation is preceded by an increase in Smad5 expression

(Lee *et al.*, 2000). A number of cytokines can also regulate *RUNX* expression; TGF- β is known to regulate *RUNX2* and *RUNX3* expression. However depending on the tissue type or cell line, TGF- β can either induce or repress *RUNX2* and *RUNX3* expression. Inhibition by TGF- β is believed to occur through inhibition of the *RUNX* P1 promoter (Alliston *et al.*, 2001). The Notch signalling pathway has also been implicated as a regulatory mechanism of *RUNX* expression as the Notch-*RUNX* pathway has been shown to be critical for the developmental specification of HSCs (Burns *et al.*, 2005). The FGF pathway can also activate or repress *RUNX* expression depending on the cell type - for example FGF activates *Runx2* in the mesenchymal pluripotent cell line C3H10T1/2 but represses *Runx2* in the rat osteosarcoma cell line ROS17/2.8 (Zhou *et al.*, 2000). *RUNX* can also be regulated by signalling pathways *via* GATA, FOG and FOXP3 (Levanon & Groner, 2004).

1.5.4.2 Translational control

In addition to transcriptional control, *RUNX* expression can also be controlled through transcription-coupled translational control mechanisms (e.g. cap- and IRES-mediated translational control as described previously in Section 1.5.1.3) (Pozner *et al.*, 2000). The two 5'UTRs are the key players in the translational regulation of *RUNX* directing cap-dependent (P1-5'UTR) and IRES-dependent (P2-5'UTR) as described previously. The functional significance of cap and IRES-mediated translation is that IRES is believed to control translation when the cap system is impaired (e.g. during mitosis, differentiation or stress conditions). The presence of both cap- and IRES-mediated control indicates the complexity of how *RUNX* genes are regulated.

1.5.5 *RUNX* in human disease

Due to their essential roles in cell proliferation and differentiation, it is not surprising that *RUNX* genes have been implicated in human disease. *RUNX* genes are best known for their altered expression levels in human cancers (Look, 1997; Planaguma *et al.*, 2004; Sakakura *et al.*, 2005). The most notable is the link with *RUNX1* and human leukaemia, caused by chromosomal translocations of *RUNX1* – the most frequently observed (seen in 10-20% of acute myeloid leukaemia cases) is the t(8;21) translocation which results in fusion of the N-terminal half of *RUNX1* (containing the entire Runt domain) with the C-terminus of the ETO (for eight-twenty one translocation) partner protein (Miyoshi *et al.*, 1991). *RUNX1* is also over-expressed in endometrioid carcinoma tumours (Planaguma *et al.*, 2004) and down-regulated in gastric cancer tumours (Sakakura

et al., 2005). Mutations of *RUNX2* can cause cleidocranial dysplasia (CCD), a congenital bone malformation disease caused by haploinsufficiency (Otto *et al.*, 1997) consistent with its roles in osteogenesis. Deletion or inactivation of the *RUNX3* gene has also been shown to be involved in gastric cancers (Li *et al.*, 2002). The role of RUNX in cancer development however is very complex in that they have dualistic roles as both dominant oncogenes as well as tumour repressors in a highly context-dependent manner (Blyth *et al.*, 2005). It is clear that precise regulation of RUNX is critical for normal function. The same may be true in the heart.

1.5.6 RUNX in damaged muscle

Recently it has been increasingly documented that *RUNX* genes may also be linked to conditions of metabolic stress following tissue injury (Wang *et al.*, 2005; Ghosh *et al.*, 2010; Custodio *et al.*, 2012). This has been found to be the case in injured skeletal muscle; in the healthy muscle *Runx1* levels were measured using a labelled RNA probe and were found to be barely detectable (0.0001% mRNA) in the nuclei of skeletal myocytes; however, following denervation of the muscle *Runx1* mRNA expression was increased 50-100 fold (Zhu *et al.*, 1995; Wang *et al.*, 2005). Interestingly, under these conditions the muscle retained much of its structural features intact. However when these experiments were repeated in animals with genetic ablation of *Runx1* in the muscle, this led to severe distortion of the muscle's structure during denervation including (i) misaligned and irregularly spaced Z-discs, (ii) a lack of thick filaments, (iii) a severely dilated SR and (iv) presence of autophagic vacuoles (Wang *et al.*, 2005). *Runx1* is therefore necessary for the prevention of muscle atrophy in denervated skeletal muscle. Skeletal muscle shares many structural similarities with cardiac muscle in that they are both part of the striated muscle group with sarcomeres and the primary structural proteins in each are actin and myosin, therefore the role of *Runx1* in protecting the structural malformations of the muscle may be applicable to cardiac muscle. Furthermore, the disrupted electrical activity that triggers *Runx1* expression in denervated skeletal muscle could also be possible under conditions of altered electrical activity in the heart during MI. In the heart under normal conditions, electrical signals propagate freely between cardiomyocytes *via* gap junctions; however following an MI, disruptions in electrical activity in the remodelled peri-infarct arise due to marked changes in gap junction organisation and connexin43 distribution in addition to the physical loss of communication between viable and dying cardiomyocytes (Peters, 1995).

1.5.7 RUNX in the heart

Despite knowledge of its expression and protective role in other striated muscle tissue, very little is known about the expression and functional role of RUNX1 and the other RUNX proteins in the heart.

1.5.7.1 RUNX1

Normal tissue

The presence of RUNX1 in the heart under healthy conditions is not clear; one study revealed that RUNX1 was present in all adult human tissues except the heart and brain (Miyoshi *et al.*, 1995). However RUNX1 has been shown to be present in the mammalian heart during mouse embryogenesis (Levanon *et al.*, 2001a). Telfer and colleagues (2001) have also confirmed expression of RUNX1 in the murine whole heart homogenates, although it was not clear from their study whether this was embryonic or adult tissue (Telfer & Rothenberg, 2001). RUNX1 has been shown to be present within the nucleus of mesenchymal cells in the valvular regions of the heart at E16.5 during mouse embryogenesis (Levanon *et al.*, 2003).

Diseased tissue

Gattenlohner *et al.* (2003) found that RUNX1 was detectable in healthy human hearts by Western Blot but shows elevated expression in the heart after ischaemic cardiomyopathy, although it was also not clear from which region of the heart the samples were taken (Gattenlohner *et al.*, 2003). In the same study, it was found that over-expression of RUNX1 in the human heart during ischaemic cardiomyopathy occurred in parallel with increased expression of a Neural Cellular Adhesion Molecule (NCAM) (Gattenlohner *et al.*, 2003). NCAM is a glycoprotein present on select cell type surfaces that mediates adhesive interactions between cells (Edelman, 1986). NCAM levels are low in the healthy adult human heart relative to neonatal tissue with expression confined to the intercalated discs as detected by IHC (Gordon *et al.*, 1990b; Gattenlohner *et al.*, 2003). In addition to cardiomyocytes NCAM is also expressed in endothelial cells (Gerety & Watanabe, 1997), mesothelial cells (Lackie *et al.*, 1991) and neuronal cells that innervate the heart (Watanabe *et al.*, 1992). NCAM has been reported to be up-regulated after human MI, preferentially in the infarct and peri-infarct regions (Gattenlohner *et al.*, 2003). This has also been found to be the case in animal models of MI, both in rat (Gattenlohner *et al.*,

2003) and mouse (Nagao *et al.*, 2010) which both show up-regulation of NCAM post-MI in areas within or around the infarcted myocardium. RUNX1 has been identified to have a binding site within the NCAM promoter (Gattenlohner *et al.*, 2003) and therefore promotes NCAM expression. Furthermore NCAM is shown to be specific for ischaemic damage, compared to other forms of cardiac disease (e.g. myocarditis and sarcoidosis) and its expression is believed to be as a result of a loss of cell-cell communication (Gattenlohner *et al.*, 2004). Ischaemia-specific damage as a trigger for NCAM expression is further supported by the evidence that NCAM is also up-regulated in hypoxia-induced rat model of hypertrophy relative to control animals (Gordon *et al.*, 1990) and increased in human transplanted hearts where there is extrinsic denervation relative to non-transplanted hearts (both shown by immunofluorescence and western blots but not quantified) (Gordon *et al.*, 1990b). Furthermore, another cause of NCAM up-regulation has been reported to be metabolic stress (reduced intracellular ATP) *via* the p38 mitogen-activated protein kinase (MAPK) dependent pathway which has been demonstrated in isolated rat neonatal cardiomyocytes (Nagao *et al.*, 2010). It may be that the loss of communication between cells (i.e. loss of the ability for molecules/ions to cross one from cell to the next) or stress stimuli across the remodelled peri-infarct zone may also be an important stimulus in the up-regulation of RUNX1.

Knockout studies in skeletal muscle identified 29 genes which were selectively regulated by RUNX1 and are responsible for the expression of various structural and signalling proteins, many of which are also present in cardiac muscle e.g. phospholamban, osteopontin, sodium channel type V and thrombospondin (Wang *et al.*, 2005). These proteins are critical proteins in the heart which highlights the potential importance of RUNX1 in the heart during disease. RUNX proteins may therefore be prime candidates in understanding the mechanisms underlying the pathophysiology of adverse remodelling as their regulation may be important for post-infarction healing and modified SR-mediated Ca²⁺ handling.

1.5.7.2 RUNX2

RUNX2 expression in the heart is relatively unknown; a recent study has shown that it is undetectable in the rat heart – negative with IHC but is up-regulated in the nuclei of cardiomyocytes under conditions of uremia-induced myocardial hypertrophy and fibrosis during high phosphorous conditions or parathyroid hormone infusion (Custodio *et al.*, 2012). Inhibition of the Notch receptor protein involved in cell signalling has been found

to cause a ~2-fold increase in the expression of *RUNX2* in aortic valve interstitial cells and under these circumstances *RUNX2* can contribute to aortic valve calcification in humans (Garg *et al.*, 2005) and mice (Nigam & Srivastava, 2009). Notch signalling has been reported to inhibit *RUNX2* transcriptional activity through stimulated expression of the *Hey1* gene (a direct Notch target gene) which represses *RUNX2* during osteogenesis (Zamurovic *et al.*, 2004). Notch signalling has been shown to be increased in a mouse MI model (Gude *et al.*, 2008) which may have implications for reduced expression or activity for *RUNX2*. It also been reported that *RUNX2* is crucial for vascular remodelling observed in atherosclerosis and *RUNX2* expression is increased in calcifying human atherosclerotic plaques and artery lesions obtained from human patients with ischaemic heart disease (Tyson *et al.*, 2003) therefore *RUNX2* may play an important role in coronary artery disease (including MI for which the main cause is atherosclerotic plaque disruption in coronary vessels) (Hansson, 2005) through activation of chondrocytic and osteoblastic proteins that contribute to the calcification process (Tyson *et al.*, 2003). Recently, a preliminary report revealed that increased *RUNX2* in the heart may promote cardiac fibrosis and further deteriorate function (Nakahara *et al.*, 2008). Another study revealed similar findings in which transgenic mice with cardiomyocyte-specific double genetic ablation of dystrophin (a protein which links the cytoskeleton to the ECM in muscle) and $\beta 1$ -integrin (a cellular adhesion molecule) showed increased myocardial dysfunction, cardiac fibrosis and calcification which was concurrent with a ≈ 10 -fold increase in *Runx2* mRNA (measured by qRT-PCR) in whole heart homogenates (Elsherif *et al.*, 2008). A review by Sanoudou *et al.* (2005) into the genes altered in human end-stage HF as analysed by microarray revealed that *RUNX2* was significantly up-regulated in human cardiomyopathies such as dilated cardiomyopathy (DCM) and hypertrophic cardiomyopathy (HCM) although exact quantification was not specified (Sanoudou *et al.*, 2005).

1.5.7.3 *RUNX3*

RUNX3 has also been shown to be expressed in the mouse embryonic heart (Levanon *et al.*, 2001a). *RUNX3* has also been located in the endocardial cushion in mouse embryonic hearts which is a specialised region that gives rise to the septum and valves at E10.5 during heart development (Fu *et al.*, 2011). Similar to *RUNX2*, *RUNX3* is a direct target of Notch signalling in endocardial cells however in the case of *RUNX3*, Notch activation significantly increases *RUNX3* mRNA rather than inhibit as it does for *RUNX2* (Fu *et al.*,

2011). As above, Notch signalling is activated in mice post-MI and this may have implications for potential increased expression of *RUNX3* post-MI.

Despite the information detailed above, *RUNX* expression in the heart remains somewhat unclear and information is lacking in the following areas: (i) *RUNX* has been shown to be expressed in embryonic murine tissue however there are discrepancies in the expression of *RUNX* in the adult mammalian heart, with limited knowledge on its expression in cardiomyocytes, (ii) the altered expression patterns of *RUNX* have not been assessed in animal models of MI or hypertension; (iii) at present, there is no quantitative data for the altered expression of *RUNX* in the heart during disease and (iv) no evidence exists on the expression of *Runx* genes in different regions of the heart, or (v) over different time-points post-MI or any links with the cardiac expression in relation to the functioning of the heart. These areas were the main focus of this thesis.

1.6 Animal models of cardiac disease

1.6.1 Need for animal models of disease

As mentioned above although *RUNX* expression has been reported to be altered in human cardiac disease, very little is known about the quantifiable levels of altered expression in the diseased heart nor the potential functional significance of this altered expression. Unfortunately performing such measurements on human heart samples to investigate this further is associated with a number of problems. Firstly, it can be very difficult to acquire a sufficient number of human cardiac samples for medical research as tissue is often in short supply or needed for other uses such as transplantation. Secondly, human heart samples may be highly variable in terms of disease stage or from patients being on different treatments and tend to come from an end-stage (therefore usually severe stage) only rather than during the transition phase from compensated remodelling to HF. Thirdly, it is difficult to obtain healthy hearts for control tissue. Despite these limitations human heart tissue is extremely valuable to medical research. However it is for the reasons named above that animal models of cardiac disease have become invaluable as an alternative for the study of cardiac disease progression (Patten & Hall-Porter, 2009). The most common pathophysiological changes in human cardiovascular disease including MI, hypertension and cardiac hypertrophy have been successfully reproduced in animal models.

1.6.2 Criteria for use of animal models

An ideal model for any human cardiovascular disease must satisfy the following criteria: (i) mimic the human disease as closely as possible, (ii) produce symptoms and characteristics which are predictable and controllable, (iii) allow studies in a stable, chronic condition (iv) conform to appropriate ethical and animal welfare considerations and appropriate legislation and (v) allow measurement of relevant cardiac, haemodynamic and biochemical parameters (Doggrell & Brown, 1998; Houser *et al.*, 2012). Animal models provide a means of studying a specific disease condition in a controlled way. These experimental models can provide vital information on the structural and functional alterations which occur during different cardiac diseases as well as cellular and molecular alterations associated with the disease (Hasenfuss, 1998). The use of mice as animal models is particularly useful due to the ability to manipulate their genome and generate transgenic strains (Fox, 2007). Through over-expression or targeted disruption of a particular gene, mouse models provide a unique approach to studying specific genes which is of great benefit in understanding the pathophysiology of HF (Rockman *et al.*, 1994; Lin *et al.*, 1995).

1.6.3 Use of animal models to investigate *RUNX* expression in the heart during disease

The investigation of altered *RUNX* gene expression in cardiac disease is possible through use of clinically-relevant animal models of cardiac disease. For this thesis, the two animal models of interest include: (a) **a mouse model of MI** and (b) **a rat model of hypertension and congenic rat model of altered LV mass (LVH)**. A very brief description of each model is described below but more details on each model will be provided in the respective later chapters (Chapter 3 and Chapter 5).

1.6.4 Mouse model of MI

Human MI is caused by chronic narrowing or acute occlusion of coronary arteries by atherosclerotic plaques and thrombosis respectively (Libby, 2001). The most common approach for inducing MI experimentally in an animal model is by surgical coronary artery ligation (CAL). This involves placing the animal under anaesthesia with mechanical ventilation and the heart is accessed from between two ribs in a thoracotomy procedure; a fine thread or suture is then placed around the left coronary artery and tied to induce permanent MI. Animals are permitted to recover and researchers can then study

myocardial changes such as remodelling and dysfunction over different time periods and under different conditions according to the nature of the study. Animal models of MI have been widely used in different species such as dog (Kass *et al.*, 1988), pig (Eising, 1994), rabbit (Masaki *et al.*, 1993) and rat (Flaim *et al.*, 1981). CAL-induced MI in a mouse model was first described in 1978 by Zolotareva and Kogan (Zolotareva & Kogan, 1978). With the advent of genetic modifications possible in the mouse, this species has gained popularity for the use of models of cardiac disease such as MI (Patten, 1998; Michael *et al.*, 1999; Gao *et al.*, 2010).

1.6.5 Rat model of hypertension and congenic models of altered LV mass

The spontaneously hypertensive rat (SHR) is an animal model of human essential hypertension and represents the most commonly used model of cardiovascular disease (Doggrell & Brown, 1998). The strain originates from a colony of male Wistar rats in Kyoto, Japan in the 1960s which were bred by Okamoto *et al.* (1963) for high blood pressure (Okamoto & Aoki, 1963). The SHR is normotensive for the first 6-8 weeks of its life with systolic blood pressures (SBP) of 100-120 mmHg and then hypertension develops over the next 12-14 weeks with SBP >150 mmHg reaching 180-200 mmHg in its adult life. Like the human condition, the SHR develops characteristic symptoms of the disease such as cardiac hypertrophy and renal disease (Doggrell & Brown, 1998). A second strain of rat has been developed from the SHR known as the stroke-prone spontaneously hypertensive rat (SHRSP) as having a higher incidence of stroke by selective mating of offspring with at least one parent with spontaneous stroke (Okamoto *et al.*, 1974). Like SHR, the SHRSP strain develops hypertension from 5 weeks of age but the SBP can increase to 250 mmHg in males (compared to 200 mmHg in SHR males) with a higher incidence of stroke. There is a significant positive correlation between BP and the incidence of stroke. Additionally, salt loading accelerates the onset of hypertension and the occurrence of stroke (Okamoto *et al.*, 1974; Vacher *et al.*, 1996). Post-mortem examination of the brains of SHRSP rats show lesions in the cortex or subcortex of frontal, medial or occipital areas (Okamoto *et al.*, 1974) similar to those observed in humans (Bogousslavsky, 2003).

1.6.5.1 Use of congenic sub-strains for particular genes of interest

Inbred animal models offer the advantage of genetic homogeneity and complete control of environmental factors but most importantly they allow for specific inter-crosses to generate sub-strains which can provide insights into genetic determinants of hypertension which are

beyond the scope of human studies. These sub-strains are useful for the study of specific genetic regions important for hypertension such as altered LV mass. This approach involves the identification of quantitative trait loci (QTL), which are regions of a chromosome containing genes for a particular trait. This then makes it possible to narrow down the genes contained within the QTL interval. This novel congenic rat model permits exploration of possible triggers for RUNX expression.

1.7 Characterisation of cardiac function in the two models

1.7.1 Use of PV catheters to assess cardiac function

PV measurements are regarded as the gold standard for measuring cardiac function, particularly *in vivo* (Kass *et al.*, 1986;Burkhoff *et al.*, 2005). The simultaneous measurement of LV pressure and volume, both during steady-state conditions and during varying load on the heart have established a very comprehensive means of understanding cardiac mechanics. The ability to assess both load-dependent and load-independent measures of cardiac function is an important feature of the PV technique which is not possible using alternative measures of LV function such as echocardiography. This however has recently become possible using magnetic resonance imaging (MRI) in combination with a pressure catheter with MRI-based volume measurements to create the PV loop (Lederman, 2005). The PV catheter technique uses a single impedance (conductance) catheter which is designed to lie along the long axis of the LV and contains sensors that measure both pressure and volume simultaneously. PV methodology has been applied to humans (Kass *et al.*, 1988b) and large animals (Little & Cheng, 1993); however with recent technological advances in miniature sensors this technique can now be applied to smaller animals, including rats and mice (Georgakopoulos *et al.*, 1998). The PV technique offers many advantages over other techniques such as the ability to assess more accurate load-independent indices of function; it does not rely on geometric assumptions, and can easily be applied to small rodents. However the procedure is invasive and can normally only be performed once in the animal prior to termination meaning that longitudinal or repeated measurements in the same animal are not easily achievable (unlike echo and MRI). However, it has recently become possible to do the PV technique in conscious mice (Joho *et al.*, 2007). The technique also relies on appropriate volume calibration methods such as the hypertonic saline dilution method and independent assessments of SV (details on this can be found in the General Methods chapter). Despite

these limitations, the PV technique is considered to be one of the most accurate methods of assessing cardiac function and was therefore selected as the method of choice for functional measurements in this thesis.

1.8 Measurement of gene expression

The expression level (mRNA levels) of a particular gene in a tissue sample may be measured using a technique known as the polymerase chain reaction (PCR). The PCR technique was developed in 1983 by Kary Mullis and it completely revolutionised the detection of nucleic acids; Mullis was later awarded the Nobel Prize for Chemistry together with Michael Smith in 1993 for his work in developing the PCR method (Bartlett & Stirling, 2003). The technique is based upon the amplification of a specific target sequence of DNA (specific to gene of interest) by repeated cycles of heating and cooling to permit melting and subsequent replication of specific regions of double-stranded DNA by the enzyme DNA polymerase directed by short oligonucleotide sequences known as primers. The DNA generated by each cycle serves as the template for further replication and therefore sets in motion a “chain reaction” during which the target DNA sequence is exponentially amplified. By measuring the amount of cellular mRNA this provides information on the extent a particular gene is expressed. Full details on the technique are covered in the General Methods (Chapter 2).

1.9 Aims

The RUNX family of transcription factors have been shown to have a protective role in skeletal muscle and have been recently shown to have altered expression in cardiac disease. However, quantitative data on the degree to which *Runx* expression in the heart is altered during cardiac disease is limited. The major aim of this thesis was to characterise the changes in expression of *Runx* mRNA levels in two separate animal models of cardiac disease; a mouse model of MI and a rat model of hypertension and altered LV mass. *RUNX* expression has not been measured in the cardiac tissue of either of these animal models previously.

1. The first aim (i) was to establish and characterise a mouse model of MI which would later be used as an experimental model for measuring altered *Runx* expression during MI. This was a new model in the laboratory therefore this involved developing a technique to perform CAL-induced MI in mice which was reproducible with low mortality. It was then further aimed to (ii) perform a detailed characterisation of the

mouse MI model in terms of assessing structural alterations of the heart through histological and morphological measurements, and changes in cardiac function using *in vivo* electrocardiograms and PV methodology. The associated survival characteristics of the model were also investigated. These measurements were performed at two separate time points (4 or 8 weeks after the procedure) to assess whether the model demonstrated cardiac remodelling and dysfunction associated with MI. It was hypothesised that performing CAL in mice would produce a model with characteristics of MI comparable to other published murine MI models and mimic human MI.

2. The second set of aims was to assess alterations in the expression of the three *Runx* genes (*Runx1*, *Runx2* and *Runx3*) in cardiac tissue from the mouse MI model using qRT-PCR methodology. This was to investigate whether there were differences in *Runx* mRNA levels after MI, and whether there were (i) changes in different regions of the infarcted heart, (ii) temporal alterations as the MI developed, and (iii) whether the different *Runx* genes showed different patterns of expression. It was also aimed to perform immunohistochemical experiments of heart tissue sections to visualise the localisation of RUNX within the cells of the heart. Given the data on RUNX1 up-regulation in human MI, it was hypothesised that a similar pattern of increased *Runx* expression would occur in response to MI in the mouse model.
3. The final set of aims were to characterise the structural and functional changes in two different but related animal models of cardiac disease – a rat model of hypertensive heart disease and novel congenic sub-strains of the hypertensive rat model for altered LV mass. It was therefore aimed to characterise each model in terms of structural alterations through assessment of cardiac fibrosis and hypertrophy and assess LV function using PV methodology. *Runx1* mRNA levels were also quantified in these two models using qRT-PCR permitting: (i) investigation of altered patterns of *Runx1* expression and (ii) comparison with the MI model to further dissect the role of RUNX in the heart during cardiac disease and therefore assess its potential as a future therapeutic target. It was hypothesised that the different congenic sub-strains would demonstrate different patterns of cardiac mechanical dysfunction and fibrosis patterns, and altered *Runx* gene expression levels in response to CVD similar to MI.

CHAPTER 2

General Methods

All surgical procedures were performed in accordance with the Animals (Scientific Procedures) Act 1986 and were approved by the University of Glasgow's ethics committee. All animal experiments conformed to the Guide for the Care and Use of Laboratory Animals published by the US National Institutes of Health (NIH Publication No. 85-23, revised 1996).

2.1 Experimental mouse model of MI

After a period of approximately 1 year of microsurgical training by Dr Christopher Loughrey, MI was independently induced in mice using the CAL method. This was a new model in our laboratory, therefore it was important to develop a method which was reproducible and efficient with low mortality; but most importantly that would demonstrate features of dysfunction and remodelling as described in human MI (Chapter 3).

Development of this model therefore required rigorous optimisation and refinement. Due to their small size, the use of mice presented additional challenges in the need for precise microsurgical skills and meticulous intra-operative technique. A detailed description of the development of the mouse MI model is found in the sections that follow.

2.1.1 Animals

The strain of mice used was the C57Bl/6 strain. All mice were obtained from a licensed commercial breeder in the U.K. (*Harlan Laboratories, U.K.*) and were housed 5-10 animals per cage (or singly post-procedure) in the Biological Services facility at the University of Glasgow with 12/12 hour light and dark cycles and free access to water and food pellets. Adult males were used (8-10 weeks of age; 18-25 g); at this age the developmental growth of the heart is complete (Tarnavski *et al.*, 2004).

2.1.2 Anaesthesia and pre-surgical preparation

The surgical set-up and surgical instruments used for this procedure are shown in Figure 2.4A and B, respectively. As this was recovery surgery, the operations were performed under aseptic conditions as much as possible. The surgical instruments were autoclaved once (at the beginning of the day prior to surgery) and decontaminated between surgeries using a hot-bead steriliser (*Germinator 500, SouthPointe Surgical Supply Inc, USA*). The surgical operating area was disinfected with a chlorhexidine gluconate spray (*Ecolab, U.K.*) and sterile towels were laid down on the surgical table. A sterile drape was used for the animal and a new pair of sterile gloves was used for each animal. The mouse was

collected and weighed. The type of anaesthesia used was isofluorane (*Isoflo*, *Abbott Laboratories, USA*) mixed with 100% oxygen. Inhalable anaesthetics were preferred because these offer more precise control over depth of anaesthesia and have the least depressive effects on the cardiovascular and respiratory systems compared to other forms of anaesthetics (e.g. injectables) (Richardson & Flecknell, 2005). Anaesthesia was induced by placing the mouse in a pre-filled closed induction box (Figure 2.4C). Following loss of the righting reflex, animals were moved to a face mask (4% isofluorane; 1.5 L.min⁻¹). The fur was clipped from the entire chest area using an electric shaver and the skin was thoroughly cleansed with clean gauze swabs using a warm surgical skin disinfectant (*Hibiscrub*, *Ecolab Ltd, U.K.*) (Figure 2.4D). To minimise body heat loss, the solution was prepared warm with very minimal wetting of the skin. Pre-operative analgesia of 5 mg/kg carprofen (*Rimadyl*, *Pfizer Animal Health, U.K.*; injected 20 µl of the 5 mg/ml stock concentration) and 0.1 mg/kg buprenorphine (*Vetergesic*, *Reckitt Benckiser Healthcare Ltd, U.K.*; injected 30 µl of the 0.03 mg/ml stock concentration) along with sterile saline (0.9% sodium chloride; 500 ml bag) were administered at this stage as a single intraperitoneal injection - final combined volume of all three components was 0.4 ml (Figure 2.4E). Pre-operative administration allowed sufficient time for the drugs to take effect in time for the animal awakening from surgery. A sterile ocular lubricant (*Lacri-lube ointment*, *Allergen Inc, USA*) was then applied to both eyes to protect corneal drying during the procedure (Figure 2.4F).

2.1.2.1 Endotracheal intubation

There are numerous methods for the intubation of mice described in the literature ranging from non-invasive oral intubation (Spoelstra *et al.*, 2007; Hamacher *et al.*, 2008) to more invasive tracheostomy (Moldestad *et al.*, 2009). The ability to intubate mice quickly, reproducibly and with as little damage as possible is imperative for a survival model. For our model, we preferred not to use the tracheostomy approach as the animal would be subjected to further surgical intervention which could also lead to serious complications post-operatively such as bleeding, infection and incomplete tracheal seal (Spoelstra *et al.*, 2007). In cases where the trachea was exposed through a cervical incision to guide intubation, this also led to fatal respiratory complications after the operation and it was for this reason that this method was no longer used. The best success in our model with endotracheal intubation has been with direct visualisation of the glottis and vocal cords using a method which was quick, efficient and as minimally invasive as possible. A number of different methods were adopted to achieve this. The earliest method tried was

placing the mouse on a polystyrene board at a 45° angle and using a fibre optic light source shone on to the neck to illuminate the trachea. However this did not provide sufficient visualisation of the structures of the throat and led to potential tissue trauma and incorrect placement of the tracheal cannula into the oesophagus. The next step was to find a way to position the mouse under the microscope (at the appropriate height for x 25 magnification) to allow for improved visualisation of the vocal cords and tracheal opening. This approach required the mouse to be held vertically so that the microscope could be used to look directly down into the oral cavity. For this, an L-shaped stand made of acrylic plastic with a ring of thick silk suture (3-0) was utilised (Figure 2.1). The (anaesthetised) mouse was suspended from a suture loop by its front incisors on the vertical side of the L-shaped support. The tongue was held aside with the thumb and forefinger and the animal's body was supported with the rest of this hand, freeing the other hand to insert the cannula (Figure 2.1B; Figure 2.4G). Using this manoeuvre the opening of the oral cavity was parallel to the microscope lens and therefore provided a very clear view of the tracheal opening which ensured accurate placement of the cannula into the trachea and markedly reduced any tissue trauma or accidental placement into the oesophagus. The cannula (0.8 mm O.D.) was then gently inserted into the trachea until the Y-piece connector just entered the mouth. By doing it this way, endotracheal intubation of the mouse took < 20s and therefore it was not necessary to maintain the supply of isoflurane to the animal during this time (mouse remained unconscious throughout intubation). This method therefore proved to be a quick, non-invasive and reproducible approach to endotracheal intubation of the mice.

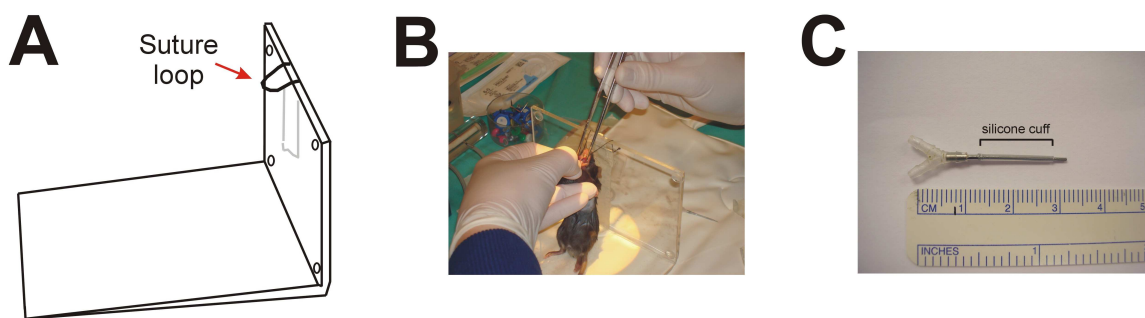


Figure 2.1 Development of a method for endotracheal intubation of mice.

(A) Schematic illustration of the L-shaped plastic stand used to support the mouse during endotracheal intubation. This consists of an acrylic plastic stand with a loop of thick suture fixed in place with tape. (B) Positioning of the mouse and retraction of the tongue for cannula insertion (all performed under a surgical microscope). (C) Tracheal cannula used with silicone tubing placed around the cannula (indicated) with connector Y-piece attached.

Tracheal cannula and ventilator settings

The tracheal cannula was a stainless steel tube custom-designed (25 mm long; 0.8 mm O.D.) (*Harvard Apparatus, U.K.*) as shown in Figure 2.1C. A number of different cannulae were tried previously including intravenous catheters and polyethylene (PE) tubing; however these were found to lack rigidity and resulted in greater dead space. Metal cannulae manufactured for mice (*Harvard Apparatus, U.K.*) were found to be more suitable as their rigidity meant they remained in position within the trachea better. A range of sizes of metal cannulae ranging in length and diameter were tested including (i) 1.0 mm O.D & 28 mm long; (ii) 1.2 mm O.D & 30 mm long but these were found to be too large in diameter that they caused too much trauma to the vocal cords and surrounding throat structures, and their long lengths were not suitable for the size of mice in our studies and risked damage to the bronchial bifurcation. A 0.8 mm O.D cannula was manufactured courtesy of *Harvard Apparatus, U.K.* and the smaller O.D and shorter length were safer and minimised the risks of damage. In order to increase the O.D of the shaft of the cannula (to improve fit within the trachea but minimise damage during insertion) a piece of thin silicone tubing was used over the cannula which served as a cuff-like design which also improved the ‘grip’ within the trachea. Once inserted, the tube was connected (*via* the Y-piece) to a mouse ventilator (*Hugo-Sachs, Harvard Apparatus, Germany*) and the animals were ventilated at 120 breaths per min with a tidal volume of 120 μ l as recommended by the supplier (*Harvard Apparatus, Germany*) for mice of BW 20-25g by the equations below. Chest movements in synchrony with the ventilator confirmed successful intubation and mechanical ventilation. The connection tubes were taped down securely to prevent accidental extubation during the procedure.

$$\text{Respiration Rate (breaths per min)} = 53.5 \times BW^{-0.26} \quad \text{Eq. 1}$$

$$\text{Tidal Volume } (\mu\text{l}) = 6.2 \times BW^{1.04} \quad \text{Eq. 2}$$

Where BW is the body weight of the animal in g.

2.1.3 Surgical procedure

2.1.3.1 Positioning of the animal

The mouse was then positioned for surgery on a warm heat mat (to maintain body heat throughout) in a supine position slightly turned towards its right side and left forearm

retracted with soft tubing (Figure 2.2; Figure 2.4H,I). The remaining limbs on the right side were taped down (leaving the left leg free for toe-pinch checks to assess depth of anaesthesia). The positioning of the animal was a key part of the procedure as it can largely influence the access to the heart and how much the left lung permits or impedes the window of access. Where the animals were positioned supine or fully on their right side proved to be problematic as the sternum or left lung would restrict access to the heart, respectively. Thus it was found that a positioning of the animal between supine and right lateral was the most suitable. The orientation of the animal with respect to the surgeon was also found to be important, with lateral positioning proving to create problems with the lung collapse, requiring physical movement of the lung with a swab or tissue. This was found to lead to problems with respiration post-operatively likely as a result of damage to the lung. A longitudinal positioning of the mouse (with the head furthest away and the caudal end closest to the operator) meant that the manipulation and ligation of the coronary artery was at a more favourable angle and the lung would collapse away naturally without the need for swabs that could cause damage.

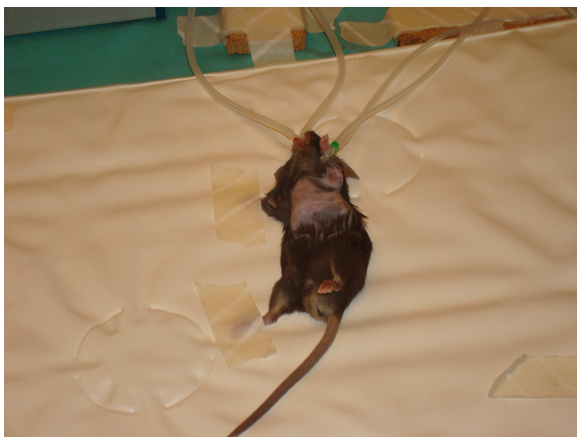


Figure 2.2 Positioning of the mouse for CAL surgery.

Photograph shows the view from operator's point of view in which the animal is placed supine and turned slightly on its right side with right limbs taped down, the left arm retracted with tubing and the left leg left free for toe-pinch withdrawal reflex (anaesthesia depth) checks.

2.1.3.2 Lateral left thoracotomy

The surgical procedure was performed with the aid of a microsurgical microscope which was set up at the beginning of the surgical procedure by performing the following in this order: (1) the dioptr e eyepieces were set to zero, (2) a small object (usually a pin tack) was placed in the centre of the field of view on a flat surface, (3) the highest magnification (x40) was selected and the object was focused using the coarse focus dial, (4) the lowest

magnification was then selected (x10) and the right eyepiece dioptre was adjusted until sharp focus of the object was achieved without altering the coarse focus dial, (5) the highest magnification was selected to ensure the object still remained in sharp focus, (6) if this was the case, the lowest magnification was selected and this time the left eyepiece dioptre was adjusted until sharp focus of the object, (7) it was then verified that the microscope was parfocal at each magnification by switching through each magnification ensuring the object remained in sharp focus at each. Prior to incision, a final check for sufficient depth of anaesthesia was confirmed by lack of response to toe-pinch reflex (isoflurane was reduced to ~3.5% by this point gradually from 4% at induction; anaesthesia was continually reduced by 0.25% gradually to a minimum of 1.5% thereafter). A 1 cm-long incision was then made laterally across the left side of the chest perpendicular to the sternum in line with the ribs (approximately 5 mm above the xiphoid) (Figure 2.4J-L). The skin and thoracic muscles overlaying the rib cage were retracted using elastic blunt-hook retractors (*Harvard Apparatus, U.K.*) (Figure 2.4M,N). The position of the left lung prior to opening the chest was noted by marking with a line either side of the incision using a surgical marker pen. This was to ensure that the lungs were reinflated back to this point during close-up to limit complications due to insufficient lung reinflation. The muscle between the ribs of the fourth intercostal space was perforated using angled forceps and incised using a battery-operated cauteriser (*Harvard Apparatus, U.K.*) taking care not to damage the heart or left lung. This was achieved by gripping the rib above gently and pulling upwards to create distance between the cauteriser and major organs beneath (Figure 2.4O). The ribs were then retracted using a further two blunt-hook retractors to fully expose the heart (Figure 2.4P). Due to the positioning of the animal, opening the thoracic cavity caused the left lung to fall away naturally and negated the need for any swabs and/or touching of the lung as described previously.

2.1.3.3 Left anterior descending (LAD) coronary artery ligation

Experiments to improve visualisation of the LAD coronary artery

Visualisation of the LAD coronary artery in mice is more difficult than in other species due to its very small size and deep embedment within the myocardium. Intense lighting and high magnification were found to be essential for this. Generally, the anatomy of the left coronary artery (LCA) in mice is believed to be comparable with other mammals; however it has also been known to be highly variable in mice even within inbred strains (Michael *et al.*, 1995). There are also discrepancies in the origin, course and branching

structures of the LCA in mice. Through use of plastic casts, groups have found that the LCA does not branch into a septal portion (Kumar *et al.*, 2005) whereas others have found it does (Fernandez *et al.*, 2008) but what seems to be consistent is that whether there is a septal branch or not, ligation of the LCA tends to produce infarction of the LV only while the septum is still perfused (Salto-Tellez *et al.*, 2004). Although investigation into the anatomy of the LCA in mice was beyond the scope of this thesis, some experiments were performed on a cohort of isolated mouse hearts ($n=6$) in which a coloured dye was used to facilitate identification of the LAD coronary artery. Briefly, hearts were excised and following an initial perfusion with saline to remove the blood, hearts were then perfused very gradually with a small amount of blue dye (Evan's Blue) to highlight the location of the LAD, taking care only to perfuse as far as the arteries (not veins). The hearts were then photographed and an example is shown in Figure 2.3. This method was effective in identifying anatomical landmarks, reduce blind ligating, and improve reproducibility.

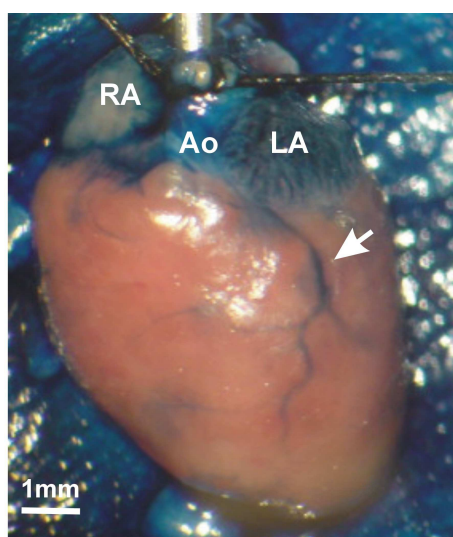


Figure 2.3 Location of the mouse LAD coronary artery using Evan's Blue dye.

LCA indicated by arrow. RA = right atrium, LA = left atrium and Ao = aorta.

LAD ligation *in vivo*

In vivo the LAD was visible as a bright orange tortuous-shaped vessel running through the LV from under the left atrium. The pericardium was gently removed and tucked behind the heart and a 9-0 nylon non-absorbable suture (*W2829 Ethilon, Johnson & Johnson, U.K.*) was passed around the LAD coronary artery approximately 1.5 mm below the left atrium and tied to produce permanent occlusion (Figure 2.4Q). Ligating any closer to the left atrium than this (<1.5 mm) was found to markedly affect survival and was often fatal,

most likely as a result of too severe an infarction (based on observation only). This is in agreement with what others have found (Salto-Tellez *et al.*, 2004). Ligating at the 1.5 mm mark produced statistically reproducible infarct sizes (Chapter 3, Figure 3.8) within the threshold required for survival and produced adequate dysfunction and structural remodelling associated with MI (Chapter 3). Ligation was deemed successful when the LV became pale in colour and in some animals by the ST-elevation on the ECG.

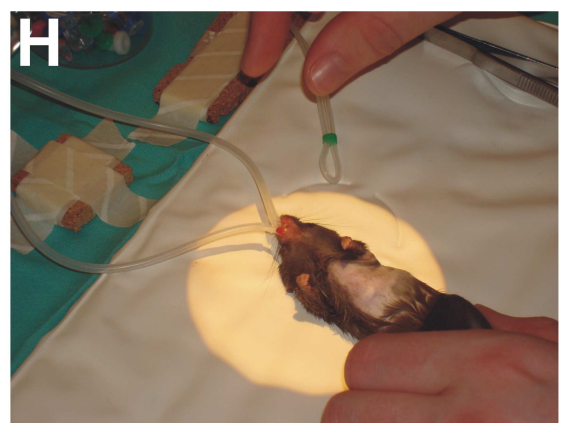
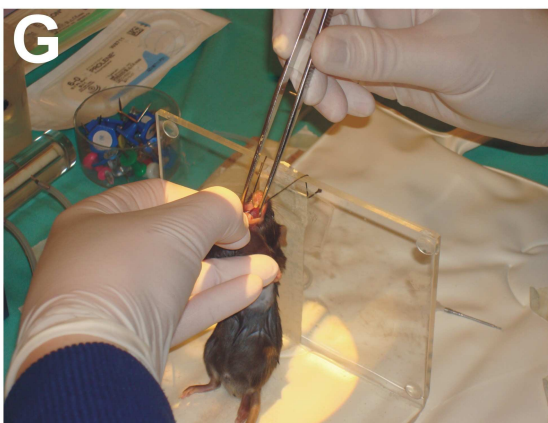
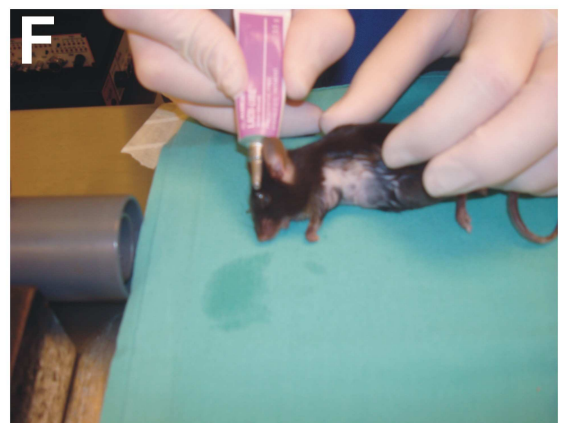
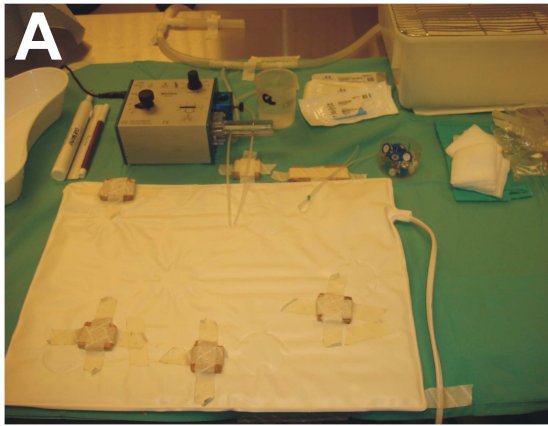
2.1.3.4 Closing up

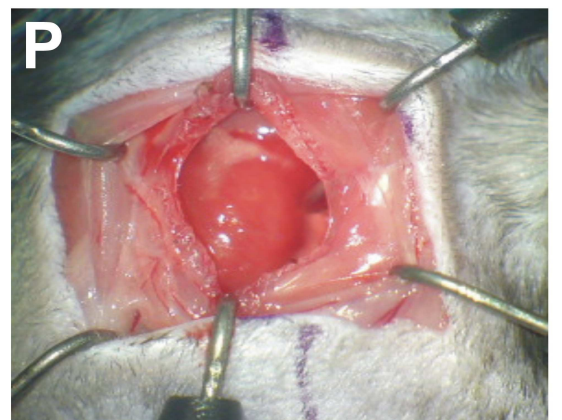
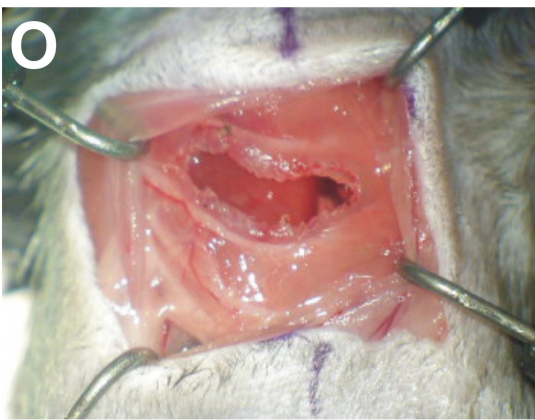
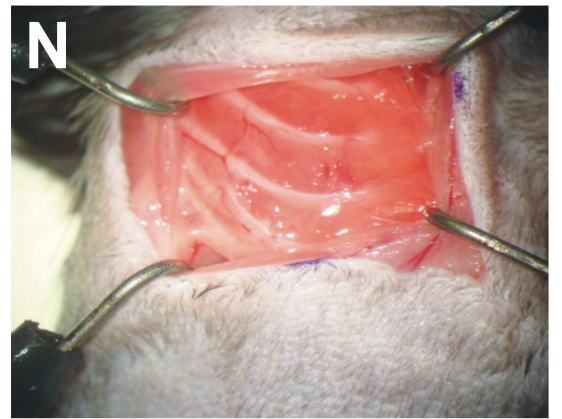
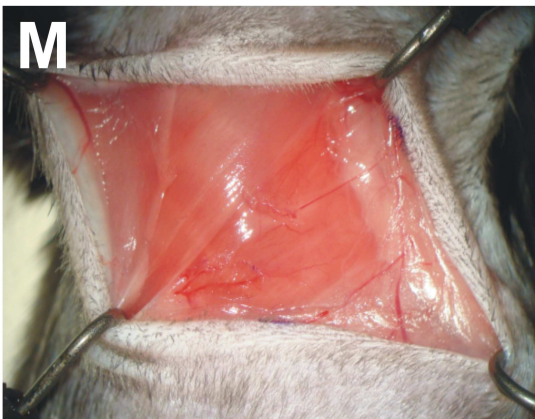
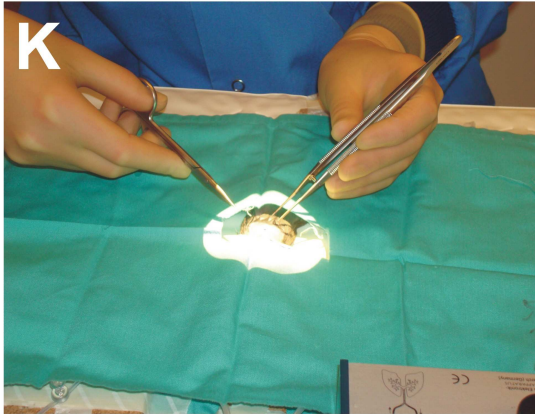
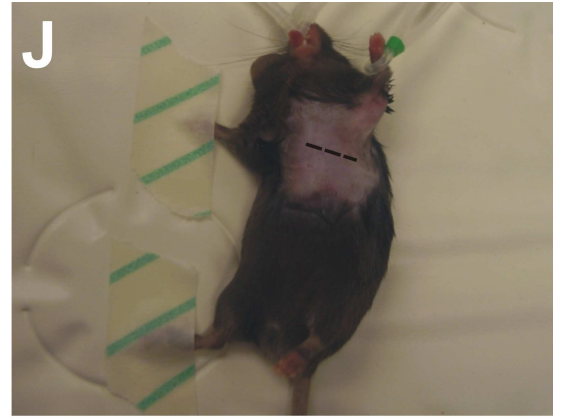
The rib retractors were removed and three sutures were evenly pre-placed along the ribs using 6-0 non-absorbable prolene sutures (*W8711, Johnson & Johnson, U.K.*) (Figure 2.4R). The lungs were reinflated by pinching the expiration tube for 3-4 respiration cycles and then placing the tube underwater in a small beaker (250 ml water) to allow sufficient positive end-expiratory pressure (PEEP) to keep the lungs fully inflated during close-up. This action of placing the tube beneath a depth of ~200 ml water proved more successful than allowing it to remain attached to the machine as it led to a 65% reduction in respiratory-related deaths (data shown in Chapter 3, Figure 3.2). The rib sutures were tied to seal the thoracic cavity, middle suture first, then the adjacent ones. The thoracic muscles were returned back together with the aid of some drops of sterile saline (no sutures) and the skin was sutured with 5-6 simple interrupted sutures using absorbable 6-0 vicryl (*W9575, Johnson & Johnson, U.K.*) (Figure 2.4S). The isoflurane was gradually reduced before being switched off during skin suturing. The mice were given at least 5 min on 100% oxygen before switching to room air while still on the ventilator. Animals were extubated only when they regained consciousness at which point they were placed into a warm recovery cage with soft bedding (Figure 2.4T). The control for this procedure was a sham operation in which the animals underwent exactly the same procedure but without CAL. The suture was initially placed but not tied in the sham animals; however this was found to (i) fall into the thorax and risk infection and (ii) risked causing local damage which may lead to some ischaemia. Therefore sham animals underwent the procedure but without placement of the suture in the heart.

2.1.3.5 Recovery and post-operative care

Animals were monitored closely immediately after surgery to ensure sufficient warmth and oxygen provision if necessary until they were mobile, and then daily thereafter at least three times a day. Post-operative analgesia was provided in the form of buprenorphine (0.1 mg/kg) administered orally in a soft custard feed for three days after the operation and

wounds and body weight were also closely monitored according to Home Office regulations. Mice were given the custard feed in the week before surgery to acclimatise them to it (which was found to improve their interest in it post-surgery) and the custard was provided in a small dish on the cage floor to enhance the animal's ability to reach it. The eating habits and body weight of the animals were recorded daily to ensure the food was being eaten and the analgesia received. After the first week the animals were then returned to normal cages and moved back to the housing area until the time of sacrifice. Any animals found dead underwent autopsy to ascertain the cause of death and a record of the date of death (as day post-operative) was logged.





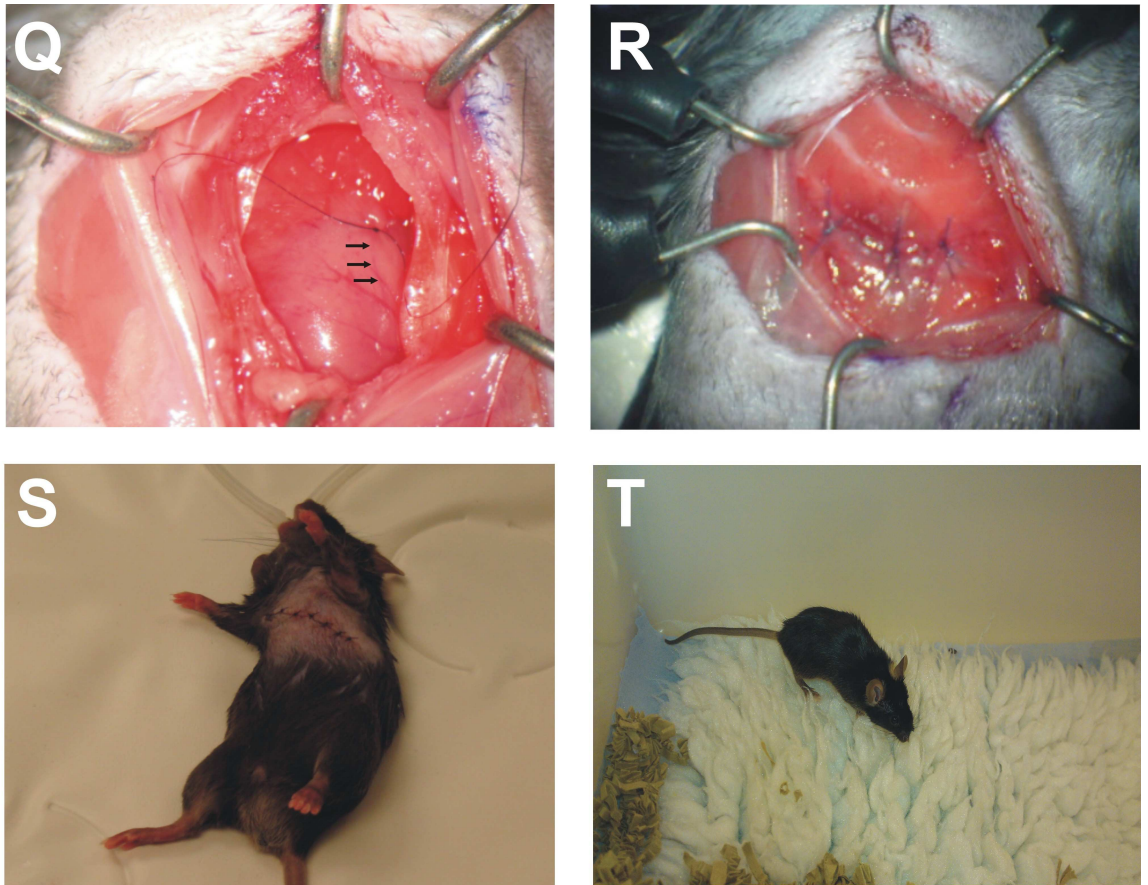


Figure 2.4 Photographs of various stages of the surgical method used for inducing MI in mice.

See details in Section 2.1 describing each image. Dotted line in (J) indicates first incision site and arrows in (Q) indicates the LAD coronary artery.

2.2 Congenic rat model of altered LV mass

2.2.1 Generation of congenic strains

WKY and SHRSP animals, originally obtained from the University of Michigan, were brother-sister mated to produce colonies of WKY and SHRSP at Glasgow as previously described (Dominiczak *et al.*, 1993). Congenic strains were generated using a marker-assisted speed strategy where segments of SHRSP chromosome 14 were introgressed into WKY (to produce a WKY-congenic) and segments of WKY chromosome 14 were introgressed into SHRSP (to produce an SHRSP-congenic). The breeding protocols for these two congenic strains is outwith the scope of this thesis but details have been previously published (Davidson *et al.*, 1995).

2.2.2 Genotyping of congenic strains

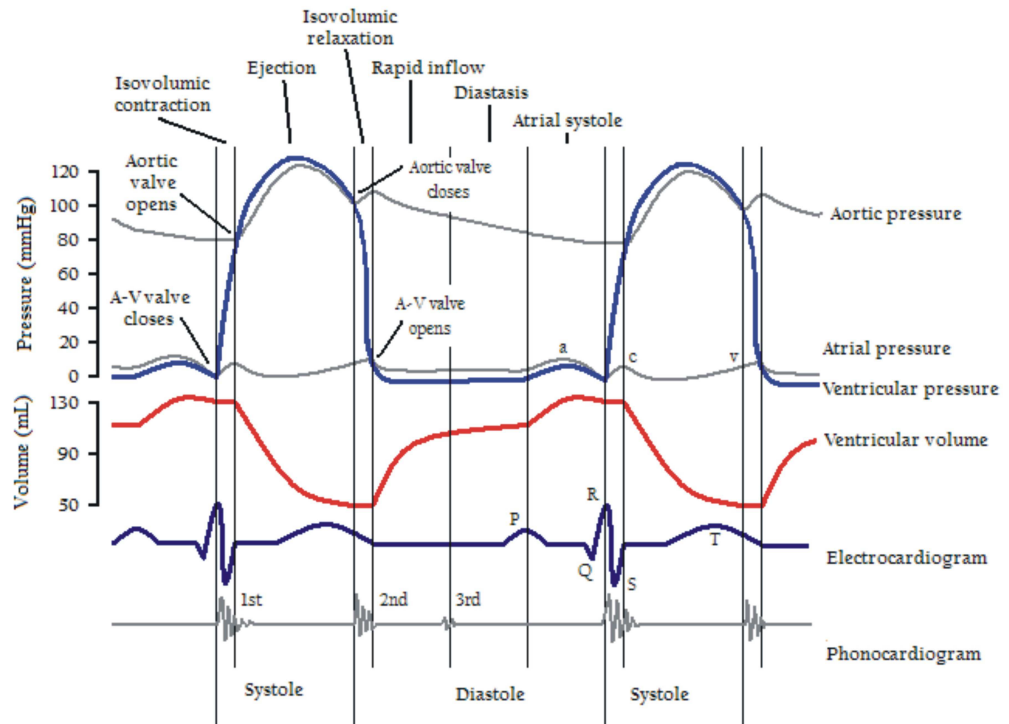
Genotyping was previously performed by Dr Delyth Graham's laboratory at the University of Glasgow. Animals were anaesthetised (isoflurane) and a 4 mm tip from the tail was removed at 4 weeks of age. DNA was extracted from a tail biopsy and analysed using PCR around the 83 polymorphic microsatellite markers from total genomic DNA with the use of specific primer pairs (*Research Genetics, Alabama, USA* or *Sigma Genosys Biotechnology, Cambridge, U.K.*).

2.3 PV measurements

2.3.1 The PV loop

LV pressure can be plotted against LV volume to produce the PV loop (Figure 2.5). The PV loop diagram illustrates instantaneous PV points throughout an entire cardiac cycle and proceeds in an anticlockwise direction depicting the four main stages of the cardiac cycle.

A



B

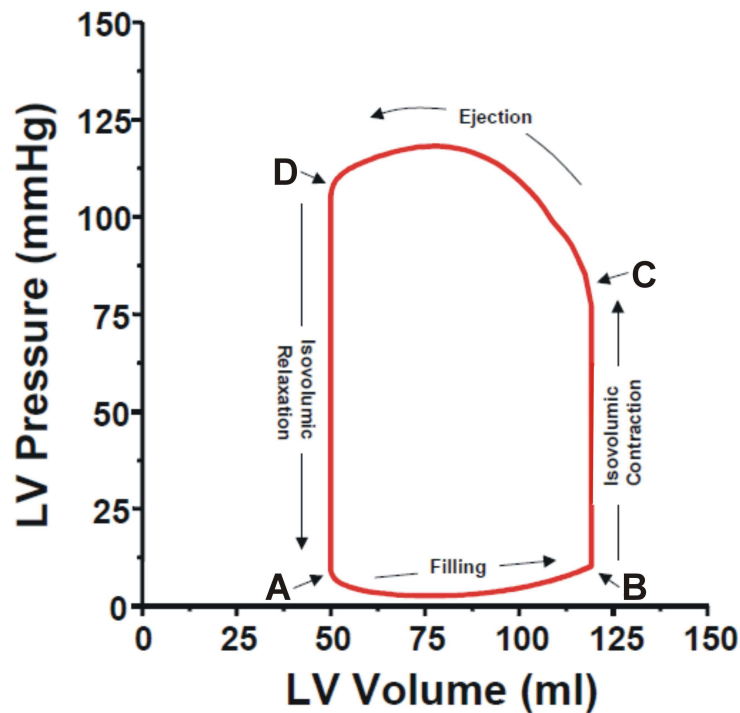


Figure 2.5 LV pressure and volume and the PV loop.

(A) Example pressure (upper blue) and volume (red line) recordings for two cardiac cycles with electrocardiogram (lower blue) also shown. (B) Example PV loop (red line) showing the four stages of a single cardiac cycle. A, mitral valve opens; AB, filling phase; B, mitral valve closes; BC, isovolumetric contraction; C, opening of aortic valve; CD, ejection phase; D, closure of aortic valve; DA, isovolumetric relaxation. Figure (A) taken from (Guyton & Hall, 2006) and (B) taken from (Burkhoff *et al.*, 2005).

2.3.2 Principle of operation

The catheter uses an electric field to measure the volume of blood in the heart. Baan and colleagues (Baan *et al.*, 1984) first proposed a method of correlating the changes in LV volume to the change in electrical resistance of the blood pool within the LV. The conductance catheter has four electrodes located along its axis for the measurement of conductance; two outer excitation electrodes and two inner sensing electrodes. A low-amplitude constant current is applied from the two outer electrodes to produce a local electric field. This electric field passes into the blood, the myocardium and the surrounding structures. The voltage change across these electrodes is inversely proportional to the conductance and is measured by the two inner electrodes. A pressure transducer is located between the two inner electrodes of the catheter for direct pressure measurements within the ventricle (Figure 2.6).

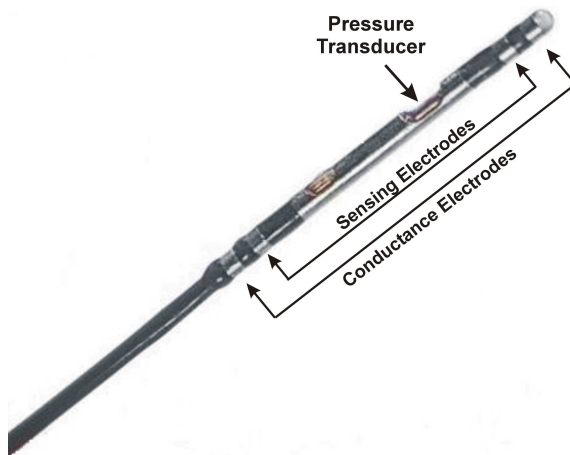


Figure 2.6 Scisense PV catheter.

The pressure transducer and electrodes for measuring volume are indicated. Picture adapted from *Scisense Inc.*

2.3.3 Volume signal correction

The conductance signal is linearly proportional to the volume but requires appropriate calibration (correction) to provide accurate absolute volume measurements. The conductance signal is converted to volume using the following equation described by Baan (Baan *et al.*, 1984) :

$$V_T = \frac{\rho L^2}{\alpha} (V_C - V_P) \quad \text{Eq. 3}$$

Where V_T is the true volume (μl), V_C is the volume measured by the catheter (μl) and V_P is the parallel volume from surrounding conductive structures, ρ represents the resistivity of blood (Ωcm), L represents the length between the electrodes (mm) and α is a constant gain factor dependent on the SV. As the resistivity of blood and the catheter recording segment length remained constant in all experiments, the equation could be simplified to the following (2):

$$V_T = \frac{1}{\alpha}(V_C - V_P) \quad \text{Eq. 4}$$

Two factors are required to correct the volume signal in the above equation, these are: the alpha gain coefficient (α) and the parallel volume offset correction factor (V_P).

2.3.3.1 α gain coefficient

α is a correction factor used to calibrate the SV of the resulting conductance signal to match a standard of comparison (usually by use of a flow probe or echocardiography). This is required because the PV catheter uses point electrodes which means the electric current lines are not straight but curved, introducing non-linearity to the volume signal. α is calculated by adjusting stroke volume (or cardiac output – the product of SV and HR) measured by the catheter to that of stroke volume (or cardiac output) measured by an independent method. Therefore:

$$\alpha = \frac{CO_C}{CO_{True}} \quad \text{Eq. 5}$$

Where CO_C is the cardiac output measured by the catheter and CO_{True} is the independently measured cardiac output.

2.3.3.2 Parallel volume (V_P)

Conductance measurements should correspond to the LV blood pool alone but in reality some of the current leaks into the surrounding myocardium and other structures which are conductive. This introduces an error into the volume calculations and must be corrected to avoid inaccurate over-estimation of the true volume. This is commonly performed using the hypertonic saline dilution method. This involves injecting a bolus of $\sim 10 \mu\text{l}$ (mice) or $\sim 35 \mu\text{l}$ (rats) of high salt solution (e.g. 15% NaCl) intravenously into the animal to transiently increase the conductance with no effect on the pressure. This leads to a

rightward shift in the PV loops. V_p was calculated by solving a series of linear equations to locate the intersection of two lines; one represented by the saline data (plotting EDV against ESV for each beat during the rise phase of the volume trace following the injection of hypertonic saline) and the other by plotting $ESV = EDV$. The latter line ($ESV = EDV$) represents the LV chamber when $ESV = EDV$ (i.e. LV devoid of blood). The value of the intersection between the two lines is equal to the V_p of the surrounding tissue and can be subtracted from the measured volume to obtain true volume – an example of this is shown in Figure 2.7 below.

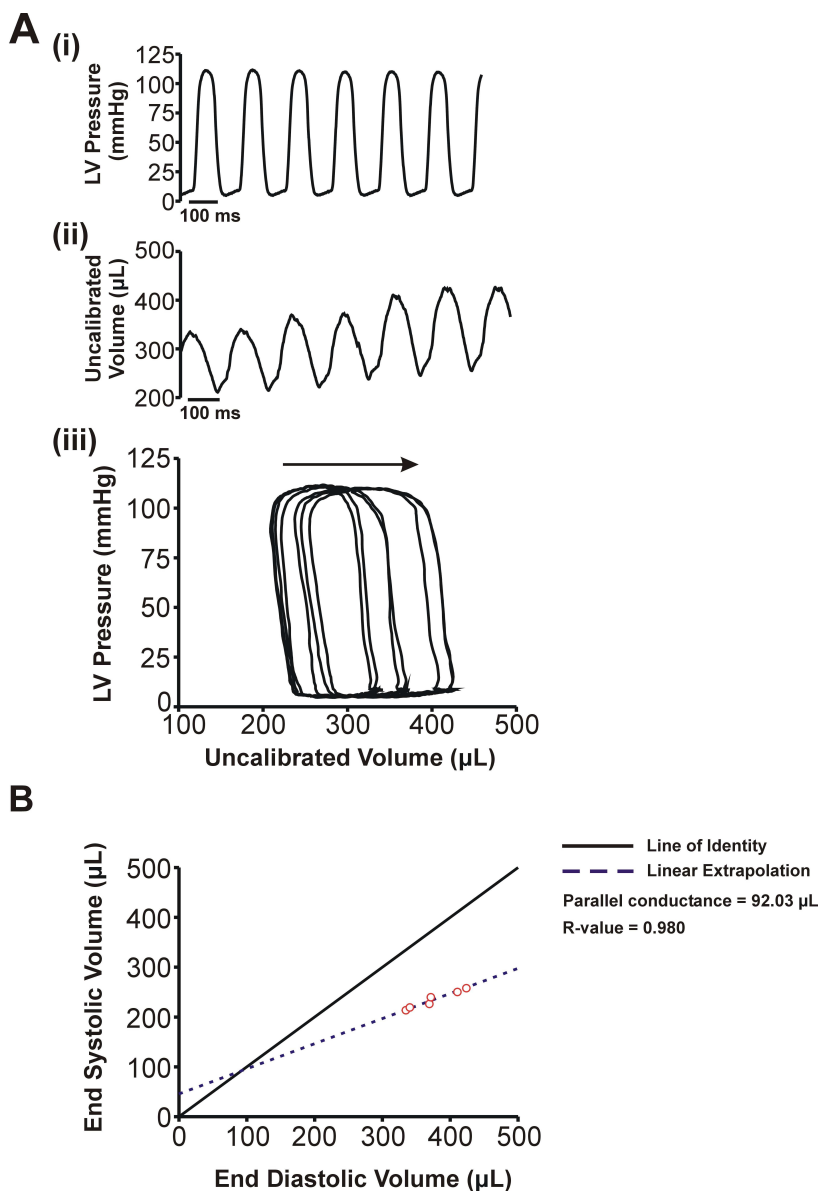


Figure 2.7 Example of parallel volume estimation.

(A-i,ii) Pressure and volume during the hypertonic saline bolus injection and (A-iii) resulting PV loops showing a rightward shift in the loops corresponding to an increase in volume with no change in pressure. (B) ESV and EDV points during the hypertonic saline bolus are plotted and extrapolated – the intersection with the line of unity ($ESV=EDV$) represents the parallel volume. This is an example taken from a stock rat.

2.3.4 Calibration of PV catheters

Prior to *in vivo* PV experiments, the catheter was appropriately calibrated for pressure and volume.

2.3.4.1 Pressure

The catheter was pre-soaked in saline at 37°C in a water bath for at least 45 min before each experiment. The reasons for this were to ensure adequate equilibration with the temperature at which the recordings will be made *in vivo* (37°C) and to ensure maximal stability of the pressure signal. The equipment is also given the same amount of time to warm up before use to minimise electrical drift of the hardware. The signal was calibrated prior to the start of the experiment by a 2-point linear calibration method using built-in values on the power unit (0 mmHg = -2.86 V; 100 mmHg = -0.56 V). Additionally, the pressure sensor was tested using a pressure transducer calibration device (*Delta-Cal 650-950, Utah Medical Products, USA*) which allowed the pressure sensor of the catheter to be calibrated against known output pressures. Immediately prior to use, the sensor was balanced (reset to 0 mmHg) for any electrical drift that may have occurred since calibration by submerging it just below the surface of saline in a bijou at 37°C and adjusting the balance dial until the catheter read 0.00 mmHg.

2.3.4.2 Volume

There are two ways by which the volume signal can be calibrated prior to the beginning of the experiment; (i) using the in-built values on the catheter control unit or (ii) using two cuvette wells of known volume.

(i) Built-in volume calibration

The *Scisense Model FV898B* power unit contains an in-built calibration scale for volume calibration. These are electronic calibration voltage outputs that correspond to specific volumes (5 values for mouse and 5 for rat), two of which can be used for a 2-point calibration similar to the method described above for pressure calibration. However, before using the in-built calibration system a series of calibration experiments were performed to verify the accuracy of this system.

This involved calibrating the catheter with different combinations of two in-built values then measuring the volume read by the catheter in standard wells to assess how closely this

matched the true volume of the well. This approach allowed (i) verification of the accuracy of the in-built system and (ii) selection of the two most suitable in-built values to use based on which combination gave the most accurate result. A polycarbonate block containing cylindrical wells of known volume (*ADInstruments, USA*) were filled with either fresh heparinised blood obtained from rats or mice, depending on the catheter used (mouse blood for the mouse catheter and rat blood for the rat catheter), or using a mock blood solution (described below). These experiments were performed by myself and Heidi Conrad (a summer undergraduate student).

(ii) Cuvette well calibration

These experiments could also be performed using two cuvette wells of known volume for the 2-point calibration instead of calibrating with two in-built values from the machine. The two wells selected were those which corresponded to the normal upper and lower values for LV volumes observed in the mouse or rat heart.

For both of these methods, the preparations were maintained at 37°C in a water bath, clotting of the harvested blood was minimised using low concentration heparin (60 U/ml) added to the blood immediately after collection and the catheter was always centred carefully within the well. The results of these calibration experiments are shown in Figure 2.8. These data reveal that the in-built values 20 and 40 µl showed the greatest unity for the mouse calibrations, and 200 and 300 µl for the rat and were therefore suitable to use for volume calibrations.

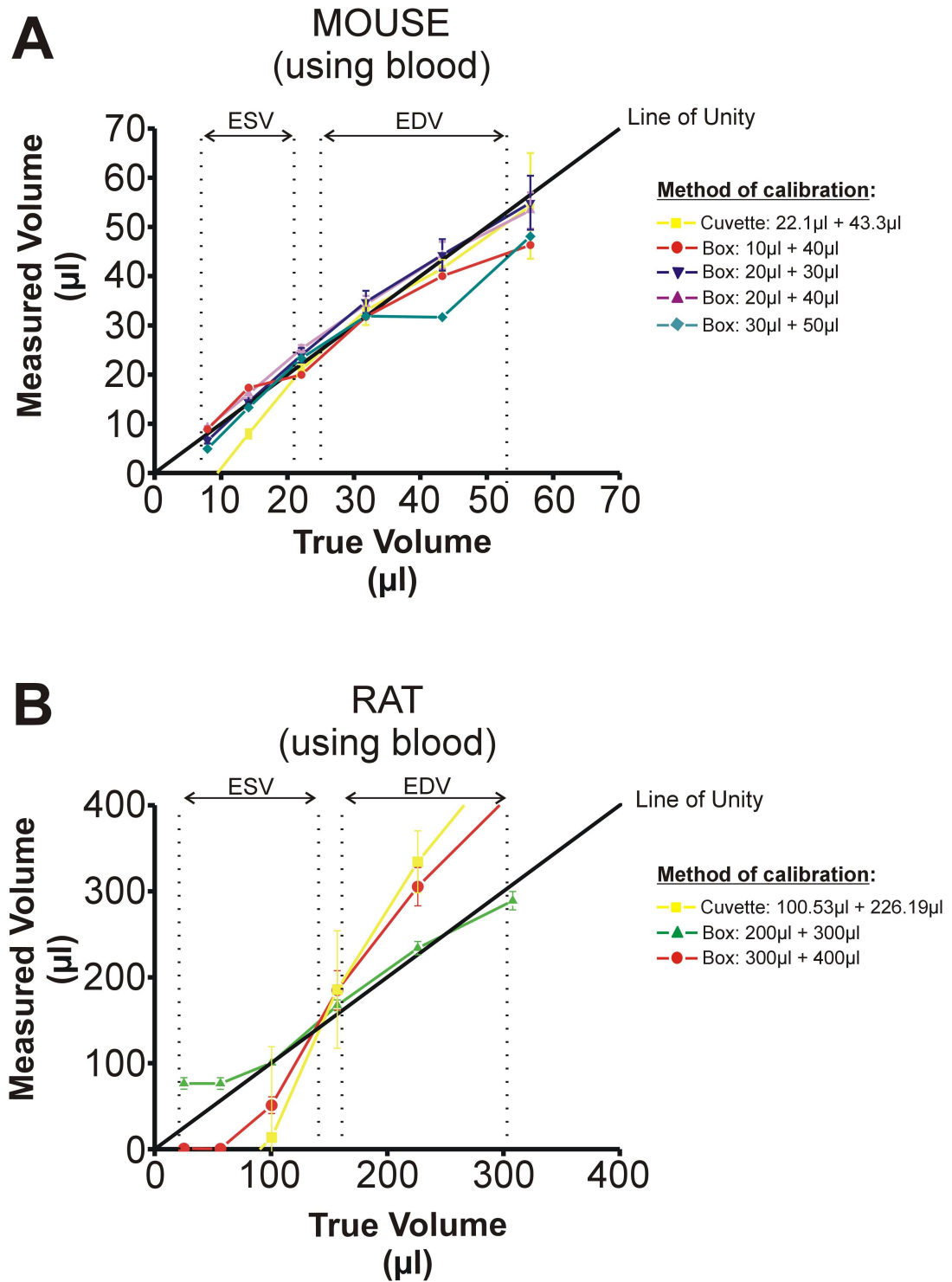


Figure 2.8 Calibration curves using different calibration combinations from the in-built system and a cuvette calibration.

(A-B) Measurements were generated using a mouse or rat PV catheter with freshly harvested heparinised mouse or rat blood respectively in standard cuvette wells of known volume. The combinations shown on the right are the different pairs of values used to calibrate the PV catheter and then the catheter was placed in cuvette wells of increasing known volume. The different calibration curves were compared against a line of unity (black line) where measured volume = true volume to determine the best calibration values to use. The dotted lines represent the normal ESV and EDV ranges for mouse and rat according to (Pacher *et al.*, 2008).

Preparation of a mock blood solution

Under ideal conditions, a sample of blood from the animal would be taken prior to the experiment and used to fill the wells for volume calibration. However, rats and mice have very low circulating blood volumes and therefore would not provide enough blood required to fill the wells. In order to eliminate the need for fresh animal blood before each experiment, an alternative 'mock blood' saline solution can be prepared to match the conductivity of blood and can be used for the calibrations instead. Empirical data has shown that the conductivity of blood for mice and rats are as follows (this has also been verified by our experiments using direct measurement with a conductivity meter):

Mouse blood at 37°C = 7.6 mS

Rat blood at 37°C = 6.3 mS

To prepare a solution that matched these values at 37°C, physiological saline (0.9% NaCl w/v) was diluted with double distilled water and monitored using a conductivity meter (*Amber Science Inc, USA*) calibrated with a standard solution of known conductivity (6.66 mS; *Amber Science Inc, USA*). This was done by submerging the measuring probe of the meter into ~25 ml of the standard solution, moving the probe up and down to dislodge any air bubbles which could affect the readings and adjusting the standardising dial to match the known conductivity. This calibration was required to be performed at a temperature of 25°C in order to be accurate therefore the calibration solution was heated to 25°C in a waterbath. Once the mock blood solution was made it was stored at room temperature and used at 37°C.

Final volume calibration methods used

Prior to the *in vivo* experiments, the volume signal was calibrated either using the in-built volumes within the power unit (all rat experiments and stock mice experiments were calibrated this way), or using two standard cuvette wells (mouse MI studies were performed this way). The two hardware units were different in that one had in-built volume values (*FV866B*) and the other did not (*FV898B*) and is designed to be used for variable segment length catheters. The in-built volume unit (*FV866B*) was suitable for normal rats where physiological LV volumes were expected but in infarcted mouse hearts

post-MI where a dilated LV chamber is common the LV volumes were too large for the range of the *FV866B* and therefore the *FV898B* was used instead for these experiments.

The in-built values used for a 2-point calibration were as follows: 20 and 40 μl for mouse, and 200 and 300 μl for rat. These values were chosen based on verification using calibration experiments (see Section 2.3.4.2). The in-built volumes were unsuitable for the mouse MI functional studies because the larger chamber volumes associated with MI were greater than the maximum volume the in-built system could read for mice. As a result two cuvette volumes were used in combination with the *FV898B* VSL power unit for the 2-point calibration and these were 31.81 and 88.36 μl cuvette wells which were chosen to represent the volume range expected in the mouse infarcted heart. These values were also used for the sham animals. The VSL unit has been previously calibrated in our laboratory and the results published (Elliott *et al.*, 2012; Kelly *et al.*, 2012).

2.3.5 Surgical procedure for insertion of PV catheter into the LV *in vivo*

2.3.5.1 Different surgical approaches available for PV catheter insertion

There are two main surgical approaches which can be used for inserting the PV catheter into the LV of the rodent heart *in vivo*. These are (i) an open-chest approach; involving a thoracotomy by transverse substernal incision of the diaphragm and subsequent insertion of the catheter into the LV *via* direct apical stab or (ii) a closed-chest approach; in which the catheter is inserted *via* the carotid artery and fed retrograde through the aortic valve into the LV. Each method has both advantages and disadvantages and the surgical approach used tends to be largely dependent on the study and the experimental model of cardiac disease used (if applicable).

The **open-chest approach** (*via* the apex of the heart) is frequently used as it tends to be quicker and allows for more direct control over catheter positioning within the heart. Furthermore in models where the aorta has been banded (e.g. in TAC models) or the aortic valve may be severely calcified (e.g. in advanced ageing models) this approach is the more appropriate over the carotid artery method. However, the open-chest approach can be disadvantageous due to the associated lung collapse, compromised myocardial integrity and relatively large tissue trauma which can influence haemodynamic function. In MI models this approach is not suitable as the apical region of the heart will have undergone

extensive remodelling and infarct formation making it inaccessible for the catheter with no stable hold.

The **closed-chest approach** (*via* the carotid artery) is considered to be less invasive than the open-chest method as the lungs remain untouched, the myocardium intact with minimum tissue trauma. This approach therefore tends to be favoured for prolonged experiments which require haemodynamic stability over a long period of time (e.g. drug testing) or for assessment of animals that have undergone MI to avoid damage to the infarcted area.

2.3.5.2 Surgical approach chosen for the different animal models

Mouse MI model: For the reason outlined at the end of the previous paragraph, the closed-chest approach was used for the mouse MI model in this thesis (including control stock or sham mice for consistency).

Hypertensive and congenic rat model: For the hypertensive/congenic rat model study, there were no structural limitations associated with the phenotype to dictate which surgical method was to be used. Therefore, as it was not clear how the surgical approach (including the choice of mechanical or spontaneous ventilation) could affect haemodynamic function, a series of experiments were performed using cohorts of stock control rats to test the suitability of the open or closed-chest surgical approaches using mechanical and spontaneous ventilation in order to ascertain which was the most appropriate to use. The results from these experiments are covered later in this PV loop section of the chapter (see Section 2.3.10). This work was published in abstract form at The Physiological Society Annual Meeting (Foote & Loughrey, 2010).

The following sections describe the surgical procedure for inserting the PV catheter either *via* (a) a closed-chest approach or (b) an open-chest approach. Where rats and mice were used is specified and any differences in the surgical protocol between the two species are clearly stated.

2.3.5.3 Closed-chest surgical procedure

PV catheter preparation

PV experiments were performed using either a 1.2F (mouse) or 1.4F (rat) PV catheter (*112B-C002* and *212B-B097* respectively, *Scisense Inc., Canada*). The catheter was connected to a *Scisense* PV Unit System (*FV866B* or *FV898B*, *Scisense Inc., Canada*) and given at least 45 min to equilibrate at 37°C prior to use. The catheter was calibrated for pressure and volume at the start of the experiment as described previously (Section 2.3.4).

Anaesthesia and surgical preparation

Animals were anaesthetised with isoflurane (4%) in a closed induction chamber and sustained on a face-mask (4% isoflurane) while the skin from the neck region and upper abdominal areas was shaved and cleaned with a surgical disinfectant (*Hibiscrub, Ecolab Ltd, U.K.*). Mice underwent endotracheal intubation with a 0.8 mm tracheal cannula (*Harvard Apparatus, U.K.*) and were ventilated under 1.5% isoflurane at a respiratory rate of 120 min⁻¹ and a tidal volume of 120 µl (*Hugo Sachs Elektronik MiniVent Type 845, Germany*). Rats were either kept on the face-mask for the rest of the experiment (closed-chest, spontaneous breathing group) or were intubated *via* tracheostomy with an 18G cannula made from an intravenous catheter (closed-chest, mechanically ventilated group). Rats were ventilated under 1.5% isoflurane using a small animal ventilator (*Model 683, Harvard Apparatus, U.K.*) at a respiration rate of 70 breaths.min⁻¹ and a tidal volume of 2.4 ml. Animals were positioned supine on a thermostatically-controlled heat pad controlled by a rectal probe to maintain core body temperature at 37.0 ± 0.5°C (*Harvard Apparatus, U.K.*) and the limbs taped down in place. A midline cervical incision was made and the muscles were carefully retracted on the right side of the neck to expose the right carotid artery. The carotid artery was dissected taking care to avoid damage to the vagus nerve or other blood vessels. Four silk sutures (6-0) were then placed around the carotid artery; one at the distal (cranial) end (tied firmly) to allow anchorage and manipulation of the artery as necessary; one at the proximal (caudal) end (retracted with haemostats to occlude but not tied) to occlude blood flow during cannulation; and two loosely placed middle sutures to secure the catheter in place once inserted. In rats, an arterial clip was also used to provide additional support to the most caudal suture to minimise accidental blood loss; this was not required in the mice as the suture was sufficient for their smaller arteries. Before the catheter was inserted, the other blood vessels required for access during the

experiment (left jugular vein and inferior vena cava (IVC)) were exposed at this time to avoid accidentally moving the catheter during recordings later. The left jugular vein was exposed by extending the cervical incision towards the left shoulder and bluntly dissecting the surrounding muscles to expose the vein. The IVC was exposed following an upper abdominal incision (at the level of the xiphoid cartilage). A suture was placed into the xiphoid cartilage as a means of retraction to expose the area better. Warm swabs soaked in saline were placed on the incision sites for the jugular vein and IVC to avoid heat loss until they were needed.

Catheter insertion

The catheter was then prepared for insertion by rebalancing to zero to correct for any electrical drift and to ensure there was no offset error in the pressure readings. A tiny cut was then made into the carotid arterial wall at the distal end and the tip of the catheter was then inserted into the carotid artery and pushed as far as the last suture (closest to heart end) where it was then tied in place. The last suture was released (and clip removed for rat) and the catheter was advanced into the heart, guided by changes in pressure that were recorded during this time. The time taken from catheter rebalance to entry into the heart was usually <5 min but if for any reason this took longer than 5 min, the catheter was rebalanced in warm saline in the bath. The catheter was positioned optimally with fine movements left or right and advancing or retracting as necessary. Optimal positioning was defined as the tallest and widest loop achievable with the straightest edges; a maximum of 15 min was permitted to reach this. Once positioning was complete, the catheter was secured into place with the sutures and with blu-tak if necessary. Baseline measurements were recorded for 10 min in steady state.

IVC occlusions

During baseline recording, the IVC was occluded using blunt forceps (with plastic coverings over the tips) for ~ 5 beats to transiently reduce inflow to the heart (preload) for the offline calculation of load-independent indices of function. At least three IVC occlusions were performed for each animal to allow a mean value to be taken.

Injection of bolus of hypertonic saline

At the end of the experiment a series of intravenous injections of a small volume (10 μl for mouse; 35 μl for rat) of hypertonic saline (15% NaCl w/v) were administered using a 50 μl Hamilton precision syringe (*Harvard Apparatus, U.K.*) to the left jugular vein to allow subsequent correction for parallel conductance (V_P). 15% NaCl was prepared by dissolving NaCl in double-distilled water in a final volume of 10 ml. Three injections were performed for each animal to enable a mean value to be taken. At the end of the experiment the animals were sacrificed.

2.3.5.4 Open-chest surgical procedure

This technique was applied to rats only. Anaesthesia induction, skin preparation, intubation by tracheostomy and positioning of the animal with temperature control were all performed exactly as described in the previous section (Section 2.3.5.3). A transverse substernal incision was made over the liver and a suture was placed through the xiphoid cartilage to allow retraction of the ribs upwards to expose the thorax. The diaphragm was carefully cut transversely to expose the heart. The catheter was rebalanced and secured on to the surgical table. A small tear was made into the pericardium to free the heart and a 23G needle was inserted into the LV through the apex to make a passage for the catheter which was subsequently inserted. Optimal positioning was achieved following the same criteria as before (the tallest, widest loop with the straightest edges). Baseline recording, IVC occlusions and hypertonic saline injections were all performed as described in the previous section. At the end of the experiment the animals were sacrificed.

2.3.6 Data acquisition

PV data were acquired using the *Scisense* control system (either *FV866B* for stock mice and all rat work; or *FV898B* for sham and MI mice) connected *via* an A/D board to a *Dell* laptop using *LabScribe2* software version 2.241 (*iWorx, New Hampshire, USA*). All PV data were analysed offline using the PV module as part of the *LabScribe2* programme. Data were taken from 20 beats in steady-state (after the 10 min stabilisation period).

2.3.7 Calculation of volume

As noted earlier, the conductance signal is converted to volume using the following equation:

$$V_T = \frac{1}{\alpha}(V_C - V_P) \quad \text{Eq. 6}$$

Where V_T is the true volume (μl), V_C is the volume measured by the catheter (μl) and V_P is the parallel volume (the mean of the three values taken) from surrounding conductive structures and α is a constant gain factor dependent on the SV.

2.3.8 Calculation of alpha (α)

α gain coefficient

α was ascertained using an independent measure of CO by assessing flow through the ascending aorta using a miniature ultrasonic aortic flow probe (*Transonic Systems, USA*). The *Transonic* flow probe is designed to be loosely hooked around a blood vessel and the operation is based on the transmission of ultrasound waves from transducers located opposite a reflecting plate for which the transit time is a function of volume flow intersecting the beam (i.e. blood flow through the vessel) as depicted in Figure 2.9. The *Transonic* flow probe is made up of a probe body which contains two ultrasonic transducers on one side and an acoustic reflector positioned opposite, between the two transducers. One transducer emits an ultrasound wave which intersects the blood vessel in the upstream direction, is reflected by the acoustic reflector, and intersects the vessel again before being received by the upstream transducer where it is converted into electrical signals by the flow meter based on the transit time from one transducer to the other. This sequence of transmission is then repeated but in reverse where the transmitting/receiving roles of the transducers are reversed, followed by the reverse again and so on. During the upstream cycle, the ultrasound wave travels against the flow (increased transit time) and the downstream cycle travels with the flow (decreased transit time by the same flow-dependent amount). The flow meter subtracts the downstream-direction transit time from the upstream-direction transit time and the integrated difference is a measure of the flow through the vessel (*Transonic Systems Operations Manual*).

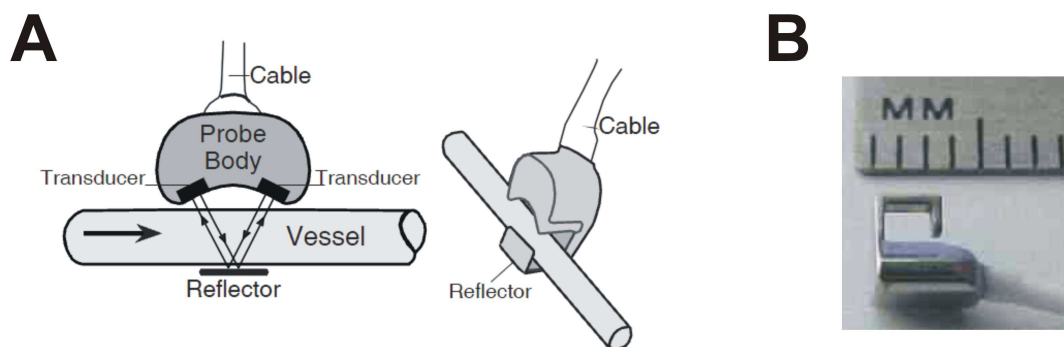


Figure 2.9 Transonic flow probe and mechanism of operation.

(A) Schematic representation of a Transonic flow probe. Two transducers emit alternating signals which intersect the blood flow through the vessel in upstream and downstream directions reflected by the reflector plate located opposite the transducers. Also shown is the view of the probe around the blood vessel from a side-angle. (B) Photograph of a Transonic flow probe for measuring flow in rodents (probe shown is the 1.5PSL for mouse ascending aorta which is the one used for the mouse experiments in this study). Figure courtesy of *Transonic Systems*.

This approach was used for both mouse and rat studies separately. Stock control mice were used for the mouse experiments. For the rat experiments (congenic rat study), the measurements were performed in the parental strains, WKY and SHRSP.

Placement of aortic flow probe *in vivo*

- Prior to use the aortic flow probe was soaked in saline at 37°C for at least an hour before use to allow equilibration with the temperature at which the recordings will be made. Data were acquired using the Transonic System (*Transonic Systems, NY, USA*) with a TS420 flow meter (*Transonic Systems*) and a perivascular flow probe (*1.5PSL* for mouse and *2.5PSL* for rat). A two-point calibration was used using two in-built values (0V = 0 ml.min⁻¹ and 1V = 5 ml.min⁻¹ for mouse; 0V = 0 ml.min⁻¹ and 1V = 20 ml.min⁻¹ for rat).
- Animals were anaesthetised (4% isoflurane) in a closed induction box and then transferred to a face-mask (4% isoflurane) while the skin across the upper chest was shaved and cleaned with a skin disinfectant (*Hibscrub, Ecolab Ltd, U.K.*).

For mice, the animals were intubated with a 0.8 mm O.D tracheal cannula and ventilated at a respiration rate of 120 breaths.min⁻¹ with tidal volume of 120 µl per breath (1.5% isoflurane).

For rats, the animals were intubated *via* tracheostomy (18G IV cannula) and ventilated at a respiration rate of 70 breaths.min⁻¹ with tidal volume of 2.4 ml per breath (1.5% isofluorane).

- Animals were then positioned in a supine-to-left lateral position with the right arm retracted to expose the right side of the chest. An incision was made laterally across the sternum at the level of the second intercostal space. The muscles overlaying the ribs cage were bluntly freed and retracted using elastic blunt-hook retractors. The second intercostal space was perforated and cauterised using a battery-operated cautery pen (*Harvard Apparatus, U.K*) and the ribs were held open using an additional two retractors. The thymus was gently retracted to expose the aortic arch.
- The pericardium was carefully perforated to aid clearing of tissue from around the aorta. The ascending aorta was dissected and a silk suture was loosely placed around this portion to facilitate lifting the aorta into the flow probe. Only the ascending portion of the aorta (prior to any branchings) was used for measurements; this meant that as little flow as possible was missed (only coronary flow was missed). Once the probe was around the aorta, an ultrasound coupling gel (*Surgilube, Transonic Systems, USA*) was injected into the air space between the probe and the aorta to increase acoustic coupling.
- The probe's positioning was adjusted using a micromanipulator until the maximum flow was achieved, taking care not to lose coupling or impede flow. Ascending aortic flow rate was measured by the flow meter and recorded on to a Dell laptop using *LabScribe2* software (*iWorx, New Hampshire, USA*). A 10 min stabilisation period was permitted before taking baseline CO measurements.

Data analysis

Values of CO were taken as the average maximal aortic flow over a 10 s period of trace, defined as the highest flow reading in steady state analysed using *Origin 6.1* (*OriginLab, USA*). The results of these measurements in mice and rats are shown in Figure 2.10 and Figure 2.11, respectively. These results have revealed that the values for CO obtained using the flow probe were not significantly different from those obtained by the PV catheter for mice (7.83 ± 0.75 vs. 8.25 ± 0.53 ml.min⁻¹; flow probe ($n=15$) vs. PV catheter ($n=24$); $P>0.05$; Figure 2.10). The same was true for both strains of rat; WKY ($52.45 \pm$

4.76 vs. 46.51 ± 3.74 ml.min⁻¹; flow probe ($n=6$) vs. PV catheter ($n=5$); $P>0.05$; Figure 2.11) and SHRSP (37.94 ± 1.60 vs. 38.07 ± 4.18 ml.min⁻¹; flow probe ($n=6$) vs. PV catheter ($n=3$); $P>0.05$; Figure 2.11). The value for α was calculated to be 1.05 for mice, 0.89 for WKY rats and 1.00 for SHRSP rats using Equation 3. Therefore the CO measured by the PV catheter has been confirmed by the use of an independent measure and the two separate measures were found to be in agreement; therefore no correction for the volume data for α was required.

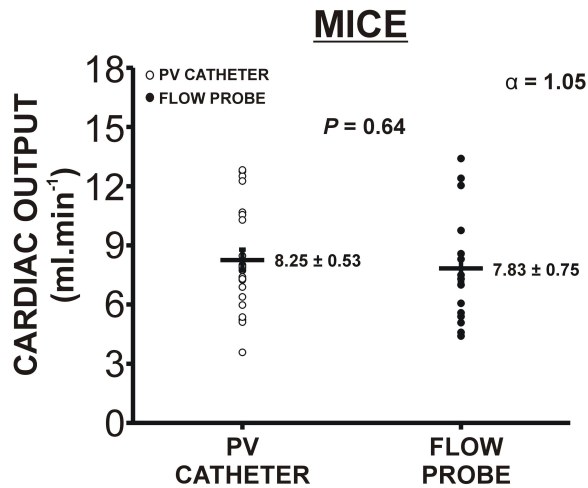


Figure 2.10 Comparison of CO measurements obtained with a PV catheter and an aortic flow probe in mice. Measurements of CO closed-chest using the PV catheter (white circles; $n=24$) compared with measurements of CO open-chest using an aortic flow probe (black circles; $n=15$) in control stock mice.

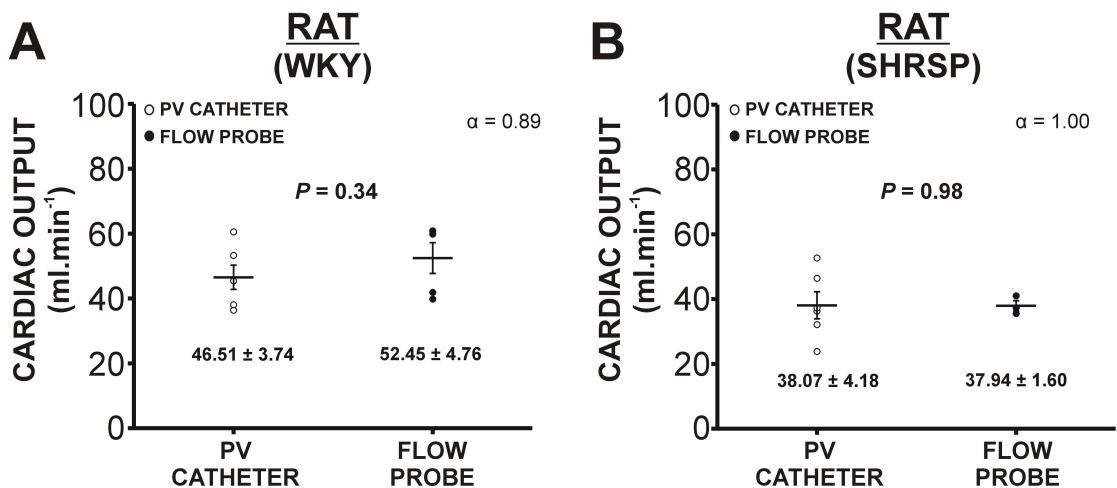


Figure 2.11 Comparison of CO measurements obtained with a PV catheter and an aortic flow probe in rats. Measurements of CO closed-chest using the PV catheter in WKY rats (white circles; $n=6$) compared with open-chest CO measurements with an aortic flow probe (black circles; $n=5$), and in SHRSP rats with the PV catheter (white circles; $n=6$) compared with open-chest aortic flow probe (black circles; $n=3$).

α calculation limitations

- (1) Unfortunately, simultaneous measurements of CO with the PV catheter and the aortic flow probe in the same animal were not possible as this was associated with a very high mortality due to the invasive nature of both procedures.
- (2) Furthermore, for the majority of PV measurements, the carotid artery route was used meaning that a portion of the catheter wire would be present inside the ascending aorta where the flow probe was required to measure from. This was therefore another reason that simultaneous measurements using both the catheter and the flow probe together were not possible. As the majority of the PV catheter measurements were performed under closed-chest conditions (only a proportion of rat experiments were performed open-chest), the aortic flow measurements were initially attempted closed-chest for consistency. This involved accessing the aorta from a cervical incision and 'hooking' the aorta upwards (i.e. the chest cavity was never opened by this method). However this was not feasible and led to difficulty obtaining good probe placement and was also associated with a high level of intra-operative mortality.
- (3) Failing this, the next attempt involved the probe being inserted open-chest by thoracotomy and then closing the chest with sutures; however this was also problematic for the following reasons: (i) the positioning of the probe was altered and often lost acoustic coupling evident by a reduced signal quality; (ii) the cable of the probe did not allow for a complete seal when closing the ribs therefore closed-chest conditions could not be guaranteed, and (iii) alterations in the CO after closing the chest were inconsistent as in some animals CO was found to increase while in others it decreased.

Therefore in light of these problems and the observation that CO data between open and closed chest were not significantly different (data not shown) the open-chest flow probe measurements were used. Placement of the aortic flow probe on the ascending aorta meant that very little of the CO was missed. Only coronary flow (CF) would be missed which is estimated to make up 3-4% and 7% of the total CO in rats and mice, respectively.

Therefore there was a slight underestimation of the CO measured by the flow probe; however due to the small percentage contribution of CF it was decided not to correct for

CF in light of the fact we also did not take CF measurements from these animals to verify against those from the literature.

2.3.9 Calculation of V_p

V_p was estimated offline using *LabScribe2* software (*iWorx, New Hampshire, USA*) using the method described in Section 2.3.3.2. For this calibration, only the volume data from the rising phase following the injection was used. At least three injections were performed for each animal and each one calculated individually to allow a mean value to be taken per animal.

2.3.10 Calculation of load-independent indices

Load-independent indices were obtained by analysing the section of trace corresponding to the IVC occlusions. This was performed offline using *LabScribe2* software (*iWorx, New Hampshire, USA*). The end-diastolic pressure-volume relationship (EDPVR) was assessed by fitting the following non-linear exponential equation to the end-diastolic pressure and volume points from the family of loops obtained during the occlusion:

$$EDP = Cexp^{(\beta*EDV)} \quad \text{Eq. 7}$$

Where EDP is the end-diastolic pressure, EDV is the end-diastolic volume, C is a curve-fitting constant and β is the diastolic stiffness constant (Burkhoff *et al.*, 2005).

2.3.11 Baseline haemodynamic data from control animals

Following completion of all the calibration work, the PV system was then ready to be applied to the animals in the study. Prior to use of the technique in the diseased animals, the system was first refined in a series of stock animals (mice and rats). The main aim of these experiments therefore was to optimise and validate the PV technique and assess its suitability prior to applying the technique to the mouse and rat models of disease in this thesis.

2.3.11.1 Baseline data from stock mice

Aim: Prior to the use of the PV system for functional studies on the MI model, PV measurements were performed using a closed-chest mechanically ventilated approach

(which was also used in sham and MI animals in control stock mice) to assess whether baseline data compared with normal published values for mice (to validate the technique).

Results: The results of these measurements are shown in Table 2.1 and demonstrate that the technique offers a reliable and reproducible approach to measuring LV function in mice with data which were comparable with published ranges for normal mice.

Table 2.1 Baseline haemodynamic parameters of LV function in stock mice compared to published values.

	THIS STUDY (<i>n</i> =24)	PUBLISHED RANGE (Pacher <i>et al.</i> , 2008)
HR (bpm)	560.47 ± 12.0	470 - 620
ESP (mmHg)	102.7 ± 1.4	92 - 118
EDP (mmHg)	3.8 ± 0.6	1 - 6
dP/dt_{max} (mmHg.s⁻¹)	10015.9 ± 312.1	8,200 - 14,200
dP/dt_{min} (mmHg.s⁻¹)	9012.9 ± 419.9	6,700 - 10,500
Tau (ms)	5.8 ± 0.3	4.4 - 7.6
ESV (µl)	14.9 ± 1.3	7 - 21
EDV (µl)	31.2 ± 1.9	25 - 53
SV (µl)	17.7 ± 1.2	17 - 30
CO (ml.min⁻¹)	9.1 ± 0.7	8 - 16
EF (%)	66.1 ± 3.1	55 - 72

2.3.11.2 Comparison of baseline data in stock rats using different surgical techniques

Aim: In order to determine which was the best surgical approach for the rat study, PV measurements were performed in three groups (1-3) of control stock male Wistar rats (BW 310.3 ± 7.2 g) each undergoing a different surgical approach: (1) open-chest approach with mechanical ventilation, (2) closed-chest approach with mechanical ventilation or (3) closed-chest approach with spontaneous ventilation.

Results: Baseline PV data from each group are shown in Table 2.2 and Figure 2.12.

- There were no statistical differences in the following parameters of LV function between the three groups: ESP, EDP, dP/dt_{min}, SV, CO and EF ($P > 0.05$ for all). There were no significant differences in any parameter between the open-chest approach with mechanical ventilation and the closed-chest approach with mechanical ventilation.

- HR was significantly greater in animals that underwent closed-chest with spontaneous breathing approach compared to closed-chest with mechanical ventilation (9.2% greater; $P<0.05$) and compared to animals that underwent the open-chest approach with mechanical ventilation (11.0% greater; $P<0.05$). The only differences in dP/dt_{max} observed were a significant increase (24.7% increase; $P<0.05$) in the closed-chest group with spontaneous breathing compared to the open-chest group with mechanical ventilation. Similarly the relaxation time-constant (τ) was significantly reduced (12.2% lower; $P<0.05$) in the closed-chest with spontaneous breathing group compared to the open-chest with mechanical ventilation group. It cannot be ruled out that these changes observed could be attributed to the differences in HR.
- There was a leftward shift in the PV loops from the closed-chest with spontaneous breathing group compared to both other groups with significantly lower ESV (44.1 and 39.6% lower compared to open-chest with mechanical ventilation and compared to closed-chest with mechanical ventilation, respectively; $P<0.05$ for both) and significantly lower EDV (32.3 and 21.1% lower compared to open-chest with mechanical ventilation and compared to closed-chest with mechanical ventilation, respectively; $P<0.05$ for both).

Table 2.2 Haemodynamic PV indices of LV function in three different groups of rats.

	Open Chest (mechanical ventilation) ($n=9$)	Closed Chest (mechanical ventilation) ($n=4$)	Closed Chest (spontaneous ventilation) ($n=8$)
HR (bpm)	406.6 \pm 7.5	413.4 \pm 11.5 [†]	451.5 \pm 9.4*
ESP (mmHg)	114.9 \pm 3.3	118.0 \pm 10.0	123.5 \pm 4.2
EDP (mmHg)	6.1 \pm 0.6	3.9 \pm 0.9	6.4 \pm 0.8
dP/dt_{max} (mmHg.s ⁻¹)	8208.8 \pm 487.7	8462.9 \pm 427.0	11238.8 \pm 639.7*
dP/dt_{min} (mmHg.s ⁻¹)	9997.8 \pm 510.8	9263.7 \pm 682.3	10055.1 \pm 289.6
Tau (ms)	8.2 \pm 0.2	7.6 \pm 0.3	7.2 \pm 0.3*
ESV (μ l)	99.9 \pm 14.7	92.4 \pm 10.1 [†]	55.8 \pm 10.0*
EDV (μ l)	252.1 \pm 16.2	216.3 \pm 3.1 [†]	170.7 \pm 13.5*
SV (μ l)	150.5 \pm 16.4	122.9 \pm 9.9	111.5 \pm 10.4
CO (ml.min ⁻¹)	61.3 \pm 7.4	51.0 \pm 4.9	50.6 \pm 5.4
EF (%)	62.0 \pm 4.8	56.8 \pm 4.5	66.7 \pm 5.5

* $P<0.05$ between closed-chest with spontaneous ventilation and open-chest with mechanical ventilation. [†] $P<0.05$ between closed-chest with spontaneous ventilation and closed-chest with mechanical ventilation.

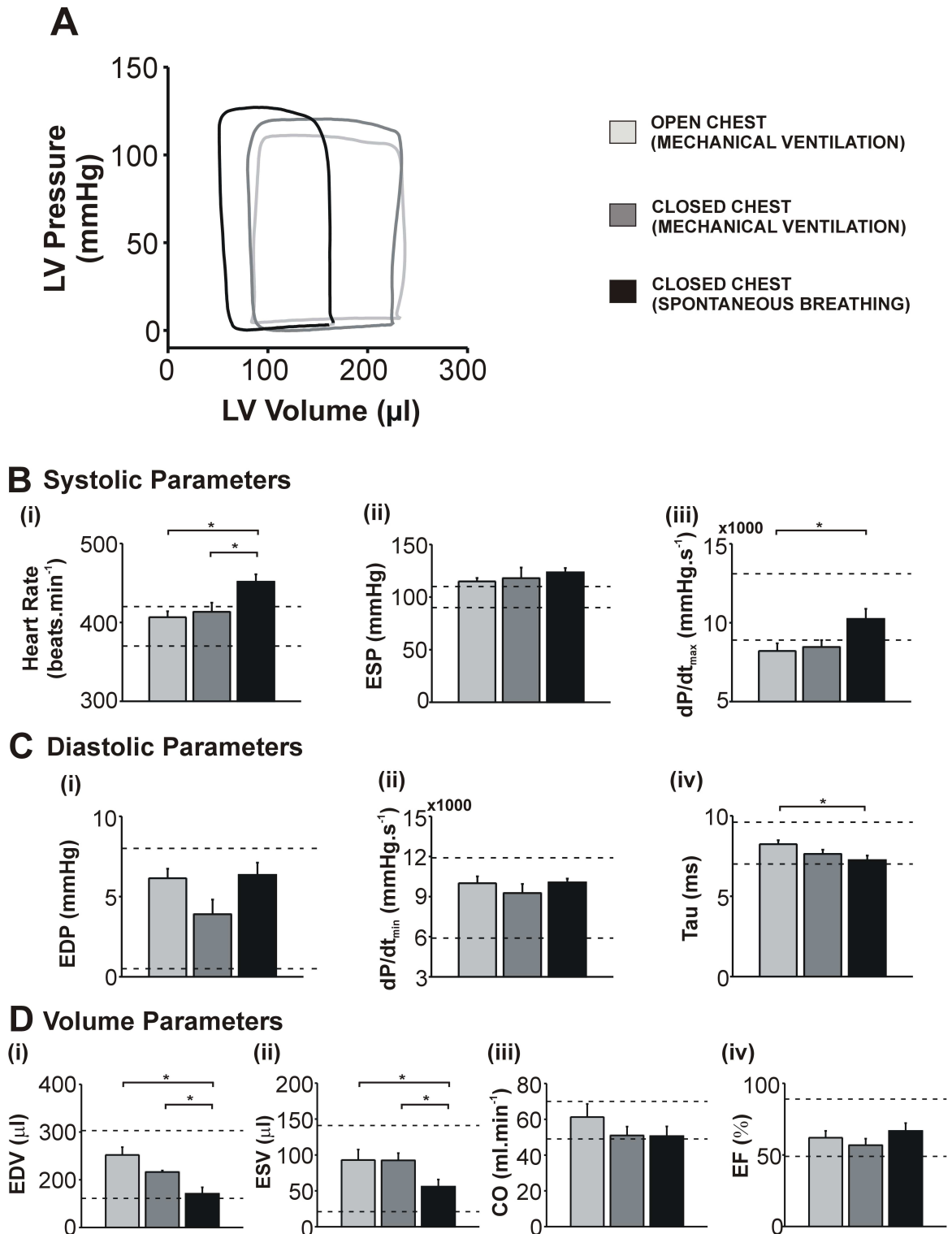


Figure 2.12 Comparison of haemodynamic parameters using different surgical approaches for PV catheterisation in rats.

(A) Representative PV loops using each method. (B i-iii): Comparison of systolic functional parameters, (C i-iii): Diastolic functional parameters, (D i-iii) Volume parameters using the open-chest (apical) approach with mechanical ventilation (light grey bars $n=8$), the closed-chest approach with mechanical ventilation (dark grey bars $n=4$) and the closed-chest approach with spontaneous breathing (black bars $n=8$). Data shown are mean \pm SEM. * $P<0.05$. Dotted lines represent the normal published range for rats under closed-chest conditions (Pacher *et al.*, 2008).

Summary: Collectively, these data demonstrate that when using mechanical ventilation there were no differences in LV performance between an open-chest and a closed-chest approach. This observation however was not in agreement with other studies which have reported differences in LV function using PV methodology between open and closed-chest - it has been shown that ventilated mice undergoing open-chest approaches have larger EF, larger SV and a leftward shift in volume parameters compared to ventilated closed-chest approaches, which the authors state may be due to the reduced intra-thoracic pressures caused by opening the thorax (Lips *et al.*, 2004). This study is not however directly comparable with ours due to the differences in species use and the use of different anaesthesia (sodium pentobarbital and not isoflurane). HR alterations in our study may be as a result of the mode of ventilation: animals maintained on the facemask have greater HR than mechanically ventilated animals (open and closed chest). It is possible that by controlled artificial ventilation there is a more constant delivery rate and volume of anaesthesia owing to the more cardio depressive effect than spontaneous breathing. However exact measurements of rate and flow during spontaneous breathing were not measured. In light of these data that the least cardio depressive LV pressure effects were observed when using the closed-chest approach (spontaneous breathing) group, this group was therefore selected as the method of choice for the congenic rat PV measurements in Chapter 5.

2.4 ECG

2.4.1 ECG as a method of assessing cardiac function *in vivo*

ECG is a non-invasive method for recording the electrical activity of the heart. Electrical signals generated in the heart through depolarisation and repolarisation during the different phases of the cardiac cycle can be detected by placement of recording electrodes in a standard configuration on the body of the subject. The ECG recording, displayed as changes in voltage over time, can then be used to measure electrical functioning of the heart. ECG measurements in this study were used for to assess the frequency of cardiac arrhythmias in the mouse MI model.

2.4.2 Protocol for measuring ECG

Mice were anaesthetised with isoflurane in a closed induction box (4%; 1.5 L.min⁻¹) and maintained under spontaneous breathing conditions through a face mask during recordings (1.5-2% isoflurane; 1.0 L.min⁻¹). Body temperature was maintained at 37 ± 0.5°C using a

rectal thermocouple probe connected to a feedback control unit with heat-pad (*Harvard Apparatus, U.K.*). Animals were positioned supine and sub-dermal needle electrodes (*Grass Technologies, USA*) were placed subcutaneously into the right forelimb (positive electrode), the left hind limb (negative electrode) and the right hind limb (ground electrode) to form a lead II configuration. Recordings were filtered through a high-pass filter of 0.03 Hz and a low-pass filter of 2 kHz at a sampling rate of 2000 samples.s⁻¹ and recorded for a 5-min period after allowing ~ 1 min for stabilisation of the signal. Electrical interference was minimised by switching off any electrical items on the recording table that were not required and by ensuring the electrode wires were not in contact with each other. ECG measurements were taken 10 min prior to the induction of MI, during CAL and 10 min after CAL (this was only performed for a cohort of MI procedures), and was also performed at 4-wk/8-wk time points post-MI prior to PV catheter measurements.

2.4.3 Data analysis

ECG data were acquired using an ETH-256C amplifier unit (*iWorx, New Hampshire, USA*). Signals were recorded on to a *Dell* laptop using *LabScribe2* software (*iWorx, New Hampshire, USA*) and analysed offline by counting the number of arrhythmic events that occurred in the 5 min recording period only (excluding the initial 1 min stabilisation period). Arrhythmic events were defined as any abnormal beats outside the normal sinus rhythm. These were always counted as single beats even when they occurred one after the other. Tachycardic episodes where normal P-QRS-T beats were not clear were rare and if encountered the episode was counted as one arrhythmic event.

2.5 Organ harvest and weighing

The protocol used for harvesting organs was the same for mice and rats. Animals were killed using a Schedule 1 method (cervical dislocation) and the following organs were harvested: heart, lungs, liver and, in some cases thymus (more details on the individual organs are detailed below). All organs were weighed using a precision electronic balance (readability 0.00001g).

2.5.1 Heart

The heart was rapidly excised and washed in a beaker of ice-cold saline (0.9% NaCl). Excess tissue was trimmed off and the aorta was cut transversely, mounted on to a cannula attached to a syringe and perfused retrograde with ice-cold saline to rinse all blood out of

the coronary vessels. The whole heart (which included intact ventricles, atria and major vessels) was then blotted dry on tissue paper, photographed and weighed. Heart tissue was then either fixed in formalin for histological experiments or snap-frozen in liquid nitrogen and stored at -80°C until needed for biochemical experiments. Hearts fixed in formalin included the whole heart (intact ventricles, atria and major vessels). Heart tissue that was snap-frozen was either intact ventricular tissue only (atria and major vessels removed) or dissected regions (infarct, peri-infarct, remote LV and RV).

2.5.2 Lungs and liver

For lung and liver measurements, the entire organ (including all lobes) was removed, blotted dry and weighed but not stored for any further experiments.

2.5.3 Thymus

For thymus harvest, the entire thymus was removed and rinsed in saline to remove any blood and then either fixed in formalin or snap-frozen in liquid nitrogen and stored at -80°C until required.

2.5.4 Tibial length for normalisation of organ weights

The length of the animal's left tibia was measured for normalisation of organ weights; this was performed post-mortem by making an incision along the length of the left leg and dissecting the tibia from surrounding muscle. Tibial length was defined as the distance from the medial condyle to the medial malleolus.

2.6 Preparation of histological sections of the heart

2.6.1 Mouse heart sections

All histological sectioning and sectioning of mouse tissue was performed by Mrs Lynn Stevenson at the University of Glasgow. Hearts were given a minimum fixation time of 24 hr in 10% neutral buffered formalin (*CellPath, U.K.*) after which time they were embedded into a wax block until required for sectioning. The heart was sliced parallel to the long axis of the heart every 250-300 µm using a microtome to produce serial sections 1µm thick per heart (this equated to approximately half of the heart as a whole being used). At every 250-300 µm interval, two adjacent sections were taken, one for each histological stain: (i) Haematoxylin and Eosin (H&E), a stain in which the haematoxylin component stains cell

nuclei blue and the eosin component stains all other eosinophilic structures (generally intracellular and extracellular structures) in pink/red and (ii) Sirius red, a collagen-specific dye that stains nuclei black, muscle and red blood cells yellow and collagen in red (Section 2.7.1.2 for full descriptions). At the mid-point depth of the heart (defined by the largest ventricular cavity size), two sections were taken for RUNX1 staining (positive and negative) (see Section 2.11).

2.6.2 Rat heart sections

Histological sectioning and staining for the rat tissue was performed by Mr Andy Carswell at the University of Glasgow. Harvested rat hearts were fixed in 10% neutral buffered formalin (*CellPath, U.K.*) for a minimum of 24 h to allow sufficient penetration of the tissue. Hearts were then paraffin-embedded and sectioned transversely at the LV apex using a microtome to produce 3 μm -thick sections.

2.7 Staining of heart sections

2.7.1 Mouse heart sections

Cut sections of the heart were deparaffinised in a clearing agent which removes alcohol and makes the section hydrophobic (*Citroclear; TSC Biosciences, U.K.*) and rehydrated through decreasing concentrations of ethanol: 100% ethanol for 2 min, 70% ethanol for 1 min followed by cold tap water for 1 min. Sections were then treated either using one of the following protocols depending on the stain required:

2.7.1.1 H&E staining

For H&E staining, the principle is as follows: Haematin is a complex formed from aluminium ions and an oxidation product of haematoxylin. In acidic conditions, haematin binds to lysine residues of nuclear histones *via* a metallic ion (aluminium) mordant. The stain is usually applied for longer than necessary to ensure saturation of the chemical binding sites and this leads to an undesirable over-staining – the discoloration is selectively removed by controlled leaching in acidic alcohol termed ‘differentiation’ (*NovaUltra* guidelines). The protocol therefore involved submerging the sections in Gill’s haematoxylin for 5 min (which stains all nuclei blue), washed in tap water, differentiated in 1% acid alcohol, and rinsed again in water. Sections were then immersed in Scott’s Tap Water Substitute (STWS; a blueing reagent) to arrest differentiation and turn the nuclei

blue. Normal tap water is not alkaline enough for this and is the reason for using STWS. This is followed by a 5 min treatment with Eosin to turn the eosinophilic structures shades of pink/red before a final wash in water.

2.7.1.2 Sirius red staining

For Sirius red staining, the principle is based on the affinity of the Sirius red dye with collagen fibrils. Collagen has a high affinity for acid (anionic) dyes of large molecular size which can bind through electrostatic attraction *via* van der Waals forces (Lyon, 1991). The protocol used was as follows: sections were submerged in Celestine blue (which stains nuclei) for 5 min, washed in tap water, placed in Gill's haematoxylin for 5 min (also stains nuclei) and washed again with water. The sections were placed in STWS (to arrest differentiation and turn the nuclei blue) followed by another wash in water before staining with Sirius red for 6 min (which stains collagen red/orange and muscle/cytoplasm yellow) and a final wash in water.

After completion of one of the above protocols, the sections were dehydrated through increasing concentrations of alcohol (70% for 1 min, 100% for 2 min); this was to remove any residual water that could affect the clearing and mounting. The sections were then cleared and mounted with dibutyl phthalate xylene (DPX) mounting medium which is a synthetic resin used to allow a coverslip to be attached to the section while preserving the stain.

2.7.2 Rat heart sections

For *Sirius red staining*, sections were deparaffinised using 2 x washes with a clearing agent (*Histoclear, Fisher Scientific, U.K*) followed by rehydration in 100% ethanol, 90% ethanol, 70% ethanol then distilled water for 7 min in each solution. Sections were then stained for 1 h with Sirius red, followed by differentiation in 2 x washes of acid water (for differentiation) and 2 x washes of tap water for 5 min each. Sections were then dehydrated through 70% ethanol, 90% ethanol, 100% ethanol and *Histoclear* (2 x washes) for 7 min each. The dehydrated sections were then coverslip-mounted with a mounting agent (*Histomount, Invitrogen, U.K.*). Rat tissue histology was performed in a different laboratory which is why some of the reagents were from different suppliers compared to the mouse tissue work; however the principles of the technique were the same.

2.8 Histological morphometry of the mouse heart

For each mouse heart, at least five serial sections (taken from a depth of at least 250 μm into the heart; 250-300 μm apart) were examined for morphometric and infarct size measurements to ensure a range of depths through the heart were examined avoiding bias. All sections were examined with an *Olympus BX51* microscope and images were captured with an *Olympus DP71* camera with the use of *Cell D (Olympus, Germany)* software. H&E stained images were used to identify qualitative histopathologic features in myocardial tissue following MI.

2.8.1 Infarct thickness

Infarct wall thickness was measured using serial H&E sections of the heart as shown in Figure 2.13. Infarct thickness was defined as the distance between the endocardium and epicardium of the infarcted myocardium indicated by the red area on the corresponding Sirius red image (or equivalent sham apex) disregarding any papillary muscles. This was performed using a line drawn perpendicular to the curvature of the ventricular wall and the distance measured with *ImageJ*. Measurements were calculated using at least 5 sections taken from middle of the heart 250-300 μm apart (each 1 μm thick) and averaging 3 equally spaced measurements along the infarct wall (starting at the apex and taking one either side) in each slide to yield a final mean infarct thickness for each heart.

2.8.2 LV chamber size

LV chamber area was measured from the same H&E sections using *ImageJ* by tracing the area of the LV using the freehand tool as shown in Figure 2.13. This was performed on all sections of the heart to yield a mean value for LV area per heart.

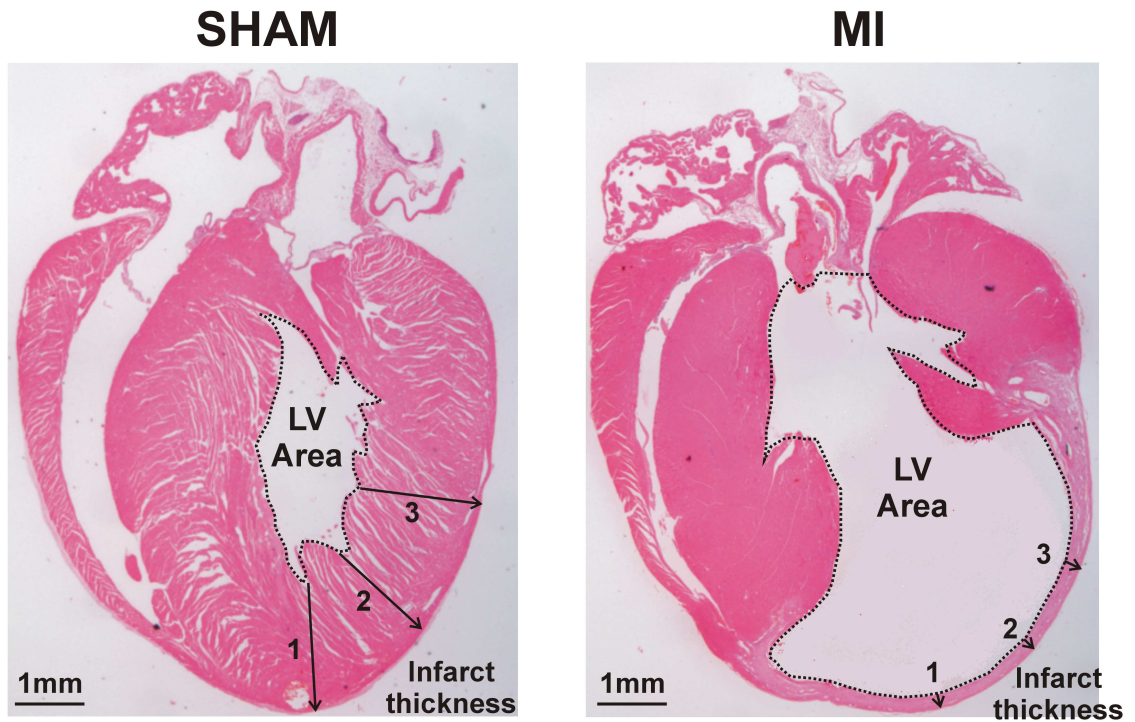


Figure 2.13 Diagram showing how measurements of infarct thickness and LV area were measured.

Infarct thickness was taken at three points along the infarcted region (or equivalent sham region) as indicated by the arrows. LV area was measured by drawing around the circumference of the LV cavity and calculating the area enclosed within, as indicated by the dotted lines. Both infarct thickness and LV area were measured using *ImageJ* software.

2.8.3 Infarct size measurements

Infarct size was measured on sections stained with Sirius red using a length-based approach similar to the method published by Takagawa *et al.* (2007). Briefly, four lengths were measured from each heart section: epicardial infarct length, endocardial infarct length, epicardial remaining LV circumference and endocardial remaining LV circumference as shown in Figure 2.14. The infarct included all infarcted myocardium which was >50% of the total thickness of the myocardium. Epicardial and endocardial infarct ratios were then calculated by dividing the sum of epicardial or endocardial lengths from all sections by the sum of all epicardial or endocardial circumferences from all sections respectively. Infarct size was then calculated using the following equation:

$$\text{Infarct size (\%)} = \frac{\text{EPI infarct ratio} + \text{ENDO infarct ratio}}{2} \times 100 \quad \text{Eq. 8}$$

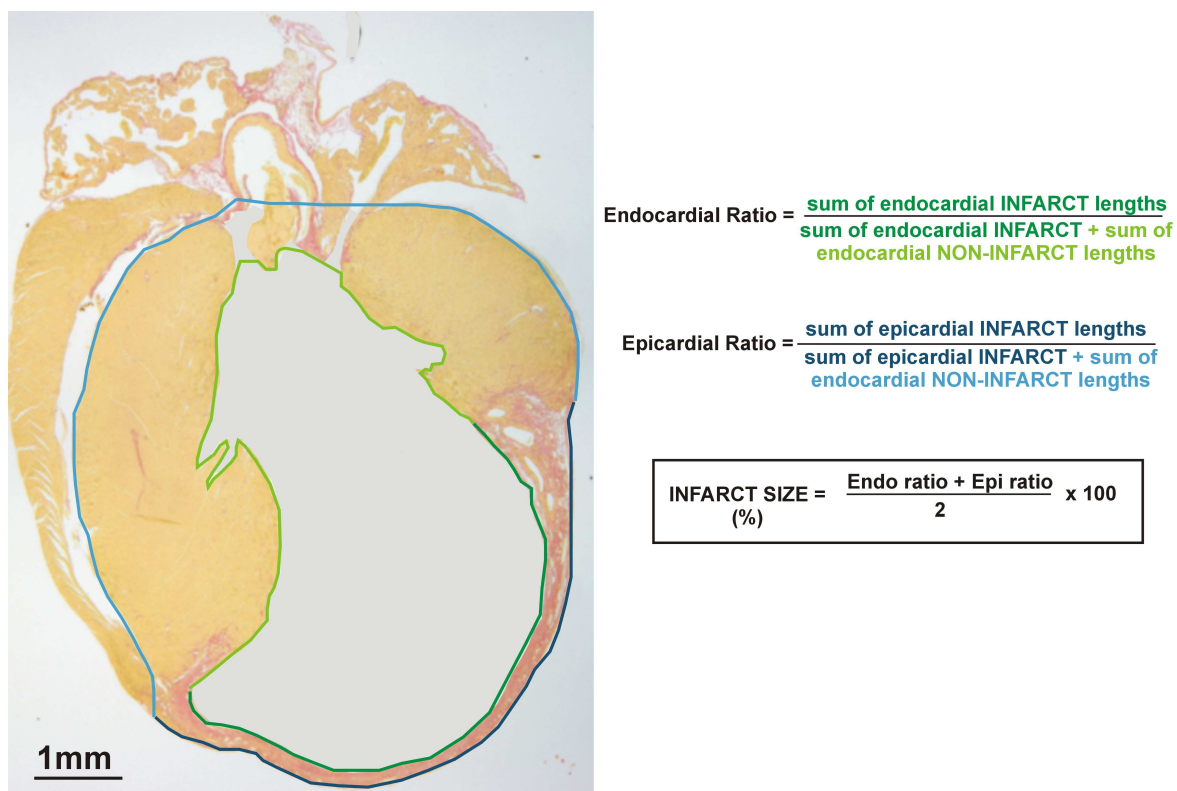


Figure 2.14 Measurement of infarct size using Sirius red sections of the heart.

Four lengths were traced: epicardial infarct length (dark blue), endocardial infarct length (dark green), epicardial remaining LV circumference (light blue) and endocardial remaining LV circumference (light green). These were used from all sections of the same heart to calculate the endocardial infarct ratio and epicardial infarct ratio (equations for each shown). Infarct size was then calculated using the formula shown above.

2.9 Collagen quantification

Sections of the heart stained with Sirius red, either longitudinal whole heart sections (mouse) or transverse apical LV sections (rat) were examined and photographed under x 10 magnification using an *Olympus Bx40* microscope with a camera (*3.3 RTV, QImaging, Canada*) and associated software (*QCapture, QImaging, Canada*). Images were analysed using *ImageProPlus (Media Cybernetics, USA)* software.

2.9.1 Collagen quantification in rat hearts (perivascular vs. interstitial fibrosis)

For the congenic rat model study, a square of fixed area (300 x 300 pixels which was equivalent to 102 μm^2) was drawn and positioned over an area of interest (see below) and the number of red pixels, defined by a set colour threshold, was measured within this square by the software (Figure 2.15). The amount of red staining inside this square could then be expressed as a percentage of the total pixels contained within the square (300 x 300

= 90,000). Four areas were taken for each rat section (1 perivascular, 3 interstitial regions). The square was placed either over a blood vessel or an area of interstitium adjacent to a blood vessel to assess differences in perivascular and interstitial cardiac fibrosis, respectively. Perivascular fibrosis was assessed in at least 5 randomly selected vessels per heart. Blood vessels with comparable lumen size were selected for as much as possible and only vessels which could fit into the box were used and only vessels which were $\sim <50\%$ the size of the box were used. Interstitial fibrosis was measured in areas adjacent to the blood vessels; three separate adjacent areas to each blood vessel were used for this and a mean value taken. Interstitial areas contained no obvious blood vessels or other structures. All perivascular and interstitial measurements were then averaged to give a mean value of perivascular and interstitial fibrosis for each heart.

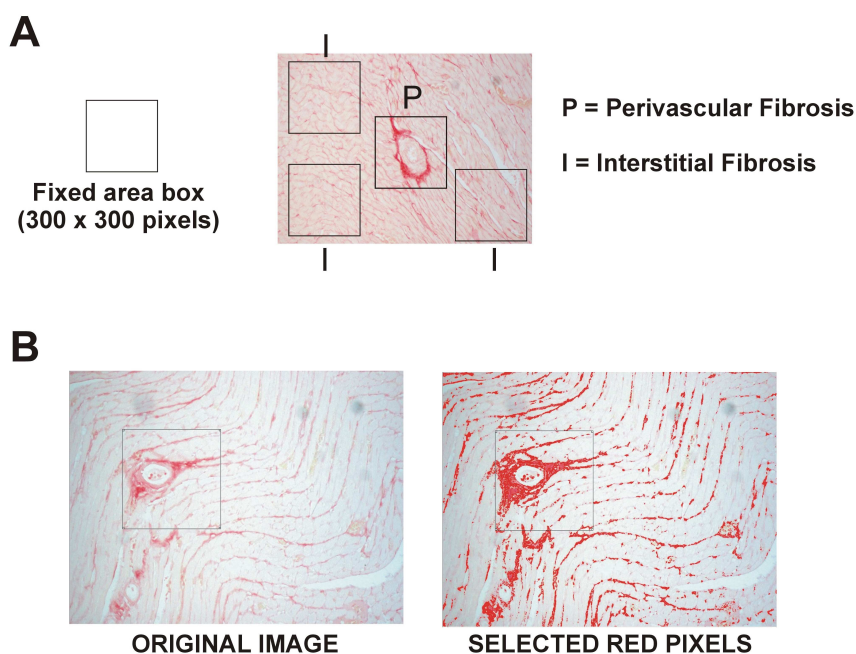


Figure 2.15 Diagram showing how perivascular and interstitial fibrosis was measured in the rat hearts using *ImageProPlus*.

(A) A box of fixed area (300×300 pixels or $100 \mu\text{m}^2$) was drawn around a blood vessel and three separate adjacent interstitial areas for each image. Five different areas of each LV were performed like this. (B) Red pixels of a set threshold were selected to measure collagen-positive red areas. Positive collagen area was expressed as the percentage of red pixels to total pixels (90,000) as defined by the fixed area box.

2.9.2 Collagen quantification in mouse hearts

For mouse (MI) model studies, the total number of red pixels in each heart was expressed as a percentage of the total pixels to measure the percentage of red-staining in each heart.

2.10 Mouse cardiomyocyte isolation

2.10.1 Mouse cardiomyocyte isolation protocol

Mice were killed by a Schedule 1 method (cervical dislocation) and then placed in a dorsal position with the arms and legs taped down. The chest cavity was opened and the heart rapidly excised and immersed in ice-cold cell isolation buffer. Cell isolation buffer was a Krebs-Henseleit (KH) solution containing the following (in mM): NaCl (130), HEPES (25), KCl (5.4), NaH₂PO₄ (0.33), MgCl₂·6H₂O (0.5) and glucose (22). Using a dissection microscope, the ascending aorta was cleared of surrounding tissue and cut transversely (below the level of the branches), positioned on to the cannula (attached to the perfusion apparatus; Figure 2.16A) and secured with a silk suture (6-0). Once the heart was secured, the perfusion was started and the cannula was moved to a vertical position held by a helping-hand device (*Maplin Electronics, U.K.*) (Figure 2.16B). All perfusion solutions were maintained at 37°C through a heated water bath and water-jacketed perfusion system. The heart was initially perfused with KH solution for 2-3 min to remove all of the blood and then switched to KH solution containing 0.7 mg.ml⁻¹ collagenase (type I, *Worthington Chemicals, New Jersey, USA*) and 0.07 mg.ml⁻¹ protease (type XIV, *Sigma Aldrich, U.K.*) for 7 min at a flow rate of 4 ml.min⁻¹. After this time, the heart was then perfused with KH containing 0.7% bovine serum albumin (BSA; *Sigma Aldrich, U.K.*) for 6 min. The heart was then cut down from the cannula and the atria and RV were removed. The LV was cut into small pieces in KH with 0.7% BSA solution and gently triturated with a plastic transfer pastette with a large smoothed opening to minimise mechanical tearing during cardiomyocyte dissociation. The cells were sedimented by gentle centrifugation and resuspended in fresh BSA; this was repeated for a further time before finally pooling the two tubes of cells together. The two tubes each contained a suspension of isolated cardiomyocytes; one containing the cells from the first trituration and the other from the second. Ca²⁺ was added gradually and incrementally (by adding 0.1 mM of CaCl₂ every 10 min) to the cells until the final concentration reached 1 mM.

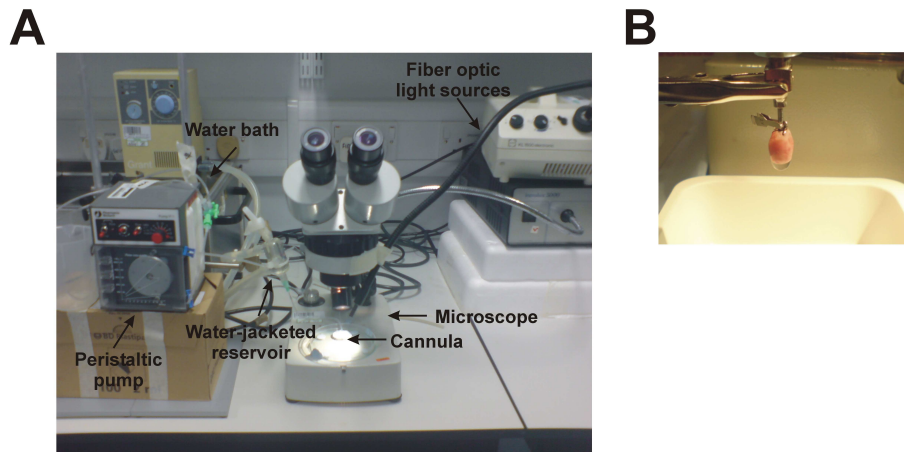


Figure 2.16 Apparatus for mouse ventricular cardiomyocyte isolation.

(A) Experimental set-up and (B) cannula showing mouse heart cannulated during digestion.

2.10.2 Measurements of cardiomyocyte length, width and cross-sectional area

Isolated cardiomyocytes were viewed using a microscope (x 20 magnification; *Nikon Eclipse TE2000-S*) and captured using a camera (*Rolera-XR, QImaging, Canada*) and associated software (*QCapturePro, QImaging, Canada*). Cardiomyocyte length and width was measured by drawing a line end-to-end and measuring the distance using *ImageJ* software as illustrated in Figure 2.17. Measurements were calibrated using a stage micrometer used at the same magnification. Cardiomyocyte cross-sectional area was estimated using the following equation:

$$\text{Cross sectional Area} = \pi \left(\frac{\text{cell width}}{2} \right)^2 \quad \text{Eq. 9}$$

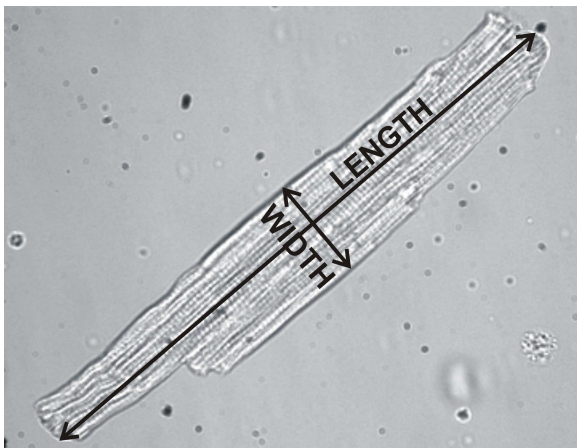


Figure 2.17 Diagram showing how cardiomyocyte width and length were measured.

2.10.3 Filtration of cardiomyocytes to remove other cell types

The filtration approach was based on a published method (Kosloski *et al.*, 2009). Isolated cells were kept on ice while a second cell isolation from a different heart using the same isolation protocol was performed. The cells from the two hearts were then pooled to yield sufficient RNA for subsequent experiments. All of the following steps were performed on ice to minimise RNA degradation.

- A sample of the pooled cells was taken as a pre-filtration control (2 ml) and was lysed in Qiazol lysis buffer (*Qiagen, U.K.*) and stored at -80°C until required. The remaining suspension (~ 8 ml) was poured through a $300\ \mu\text{m}$ nylon mesh filter to separate large fragments of tissue from the cells. 5-10 ml ice-cold Hank's Buffered Saline Solution was then poured through the filter to wash any trapped cells through the filter (HBSS; *Invitrogen, U.K.*). The composition of HBSS was as follows (in mM): KCl (5.33), KH_2PO_4 (0.441), NaHCO_3 (4.17), NaCl (137.93), Na_2HPO_4 (0.338) and glucose (5.56).
- The filtrate was spun, supernatant removed, and resuspended in HBSS and then passed through a second filter mesh ($40\ \mu\text{m}$). Based on this method, cardiomyocytes were caught on this filter and the contents of the filter were rinsed off into a separate tube with ice-cold HBSS, spun and lysed in Qiazol lysis buffer and stored at -80°C until required as the purified cardiomyocyte sample.
- The study on which this filtration method is based (Kosloski *et al.*, 2009) recommends the use of *RNAlater*, a stabilising agent which permeates cells to protect RNA from degradation, for subsequent use of the cells in gene expression studies. However they have used *RNAlater* as a tissue storage medium for their biopsy samples prior to the isolation of the cells; whereas in our study the heart was not stored prior to the dissociation of the cells (i.e. hearts were harvested fresh from the animal). *RNAlater* was used initially to store the newly isolated cells based on Kosloski *et al.*'s paper which found that *RNAlater* significantly enhanced RNA yields; however the *RNAlater* solution was found to cause the cardiomyocytes to 'clump' together and due to the density of the solution this required higher force centrifugation to pellet the cells which causing greater loss of cells through mechanical damage. Therefore *RNAlater* was no longer used; instead cells were continually kept on ice, rapidly lysed and stored at -80°C which was sufficient to protect the RNA as was shown by comparable yields and quality as determined by the use of a *NanoDrop* spectrophotometer and *Agilent*

Bioanalyser technologies, both of which are covered in more detail in the later sections of this chapter (Section 2.12.2).

2.11 Immunohistochemistry

2.11.1 Staining protocol

IHC refers to the process of detecting antigens (protein of interest) through the binding of antibodies. A common approach to visualising this antibody-antigen interaction is using an antibody which is conjugated to an enzyme that catalyses a colour-producing reaction. This process typically utilises two antibodies, a primary and secondary antibody, which are added in a step-wise fashion. The primary antibody is typically unlabelled (does not contain any conjugate molecules attached) and has been raised specifically against the antigen of interest. The secondary antibody binds to immunoglobulins of the primary antibody and is conjugated to a reporter enzyme (e.g. peroxidase) which, in the presence of a chromogenic substrate, catalyses a colour-producing reaction to indicate the presence of the antigen. A common reporter enzyme/chromogen combination is the horseradish peroxidase (HRP) enzyme with the chromogen 3,3'-diaminobenzidine tetrahydrochloride (DAB). In the presence of HRP, DAB produces a brown precipitate which is insoluble in alcohol. The overall process can therefore be summarised in three steps: (i) application of a primary antibody; (ii) application of a HRP-labelled secondary antibody and (iii) application of DAB to produce the brown colour (Figure 2.18). Prior to this 3-step process the tissue often needs specific preparatory steps: these include antigen retrieval and blocking of endogenous peroxidase activity. Antigen retrieval is necessary to expose the epitopes of the antigen which may have become obscured during the fixation process; this is usually performed by heating which breaks the protein cross-links formed by formalin thereby uncovering epitopes. Blocking of endogenous peroxidase is necessary when using DAB which could react non-specifically and lead to background staining; therefore it is normal procedure to treat the samples with a blocking agent (commonly hydrogen peroxide) to block endogenous peroxidase activity.

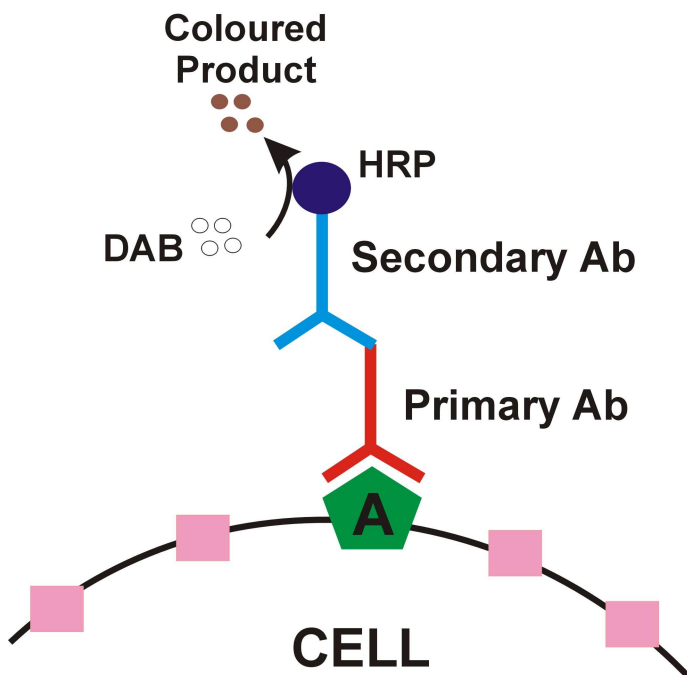


Figure 2.18 Schematic representation of the principle of IHC staining.

Sequential binding of primary antibody to antigen (A) followed by an enzyme-labelled secondary antibody. HRP catalyses the conversion of the chromogen DAB into a brown coloured precipitate. A; antigen. HRP; horseradish peroxidase. DAB; 3,3' diaminobenzidine tetrahydrochloride. Diagram adapted from *Leinco Technologies Inc.*

All IHC was performed by Mrs Lynn Stevenson at the University of Glasgow. Sections were cut, dewaxed and rehydrated as described in the previous sections (Section 2.6.1 and 2.7.1). The buffer used for washing sections between applications was tris-buffered saline (TBS) with 0.05% Tween at pH 7.5 and is used as it lowers surface tension allowing more complete coverage of the reagents applied. Sections were rinsed with buffer and incubated in a pressure cooker for 1 min 40 s at 125°C for antigen retrieval. Sections were loaded into an autostainer machine (*Dako, Glostrup, Denmark*) and the following steps were performed by the machine all at room temperature: 1 x buffer rinse, treatment with peroxidase blocking reagent (*Dako, Glostrup, Denmark*) for 5 min followed by 3 x 5 min buffer rinses. Sections were then incubated for 60 min with the primary antibody (rabbit polyclonal 1:400, ab61753 or ab35962; *Abcam, U.K.*) for RUNX1 or with antibody dilution buffer (negative control) followed by 2 x 5 min buffer washes. The primary antibody was then labelled with a secondary antibody (anti-rabbit) attached to an HRP conjugate (*Dako EnVision system, Dako, Denmark*) for 30 min. After 2 x 5 min further buffer washes, the sections were treated with 2 x 5 min incubations with the chromogen DAB (*K5007 Dako, Denmark*). After 3 washes in water, counterstaining was performed using Gill's haematoxylin for 26 s followed by one last wash with water – counterstaining

provides contrast to aid visualisation of the primary stain. Sections were then dehydrated and mounted using DPX mounting medium.

2.11.2 Quantification of IHC staining

Positive RUNX1 staining was quantified by counting positively-stained nuclei (brown) as a percentage of the total nuclei within fields at different regions of the heart. Sections were examined under a microscope (x60 lens; *Olympus Bx51*) and photographed using a camera (*Olympus DP71*) with accompanying software (*Cell D*). Images were imported into *ImageJ* and a grid (5 boxes long x 4 boxes wide) was fitted over the full size of the image to facilitate nuclear counting. Three photographs were taken from each region of the heart (infarct, peri-infarct, remote LV and RV) resulting in 12 in total per heart. The total number of positively-stained nuclei (brown coloured) and negatively-stained nuclei (blue coloured) were counted in each region and the percentage positive staining was calculated using the following equation:

$$\% \text{ RUNX1 positive staining} = \left(\frac{\text{number of brown nuclei}}{\text{number of brown nuclei} + \text{number of blue nuclei}} \right) \times 100$$

Eq. 10

As the different cell types present were not specifically labelled with markers, no discrimination was made to exclude positive nuclei from any cell type. Positive staining included any nucleus which was predominantly brown. Where it looked like there may be two overlapping nuclei, this was counted as one only. This was repeated for three areas per region and a mean value taken.

2.12 RNA extraction, cDNA synthesis and qRT-PCR

2.12.1 Gene expression based on quantification of messenger RNA levels

The level at which a particular gene is expressed in a given tissue can be measured by quantifying that gene's messenger RNA (mRNA) levels. An mRNA molecule contains the sequence of a particular gene (or the 'blueprint') which will later be translated into a protein. A cell's total mRNA therefore contains all the mRNA from all the genes which are actively being transcribed in that particular cell. By isolating the total mRNA from a tissue sample and then selecting the mRNA for a particular gene only, the levels of mRNA can be quantified and the amount of gene expressed in that sample determined. This is

achieved by the technique of qRT-PCR. If a gene is expressed at higher levels, there will be a greater abundance of mRNA for that gene, therefore a greater number of cDNA molecules which will be detected quicker during the qRT-PCR reaction. As RNA cannot serve as a template for qRT-PCR it must be synthesised into double-stranded complementary DNA (cDNA) by a method called reverse transcription (RT). Therefore the entire process from the biological sample to gene expression data consists of three main stages: (i) extraction of RNA from the biological sample, (ii) synthesis of cDNA from the RNA template, and (iii) qRT-PCR using the cDNA. Each of these steps will be described in turn and for each, the principle behind the technique will be described followed by the laboratory protocol used for each.

2.12.2 RNA extraction

2.12.2.1 Principle of the procedure of RNA extraction

RNA extraction is the isolation and purification of RNA from biological samples. One of the most common ways to do this is using a guanidine thiocyanate/phenol/chloroform extraction method. Cells or tissue are homogenised in a lysis buffer containing guanidine thiocyanate which dissolves cells membranes releasing the cellular contents into the lysate. After lysis, a phenol/chloroform extraction is performed on the lysate. The lysis buffer contains phenol and when chloroform is added these solvents separate into two phases by centrifugation: a clear upper aqueous phase (chloroform) and a bright pink lower organic phase (phenol). RNA partitions to the upper phase, DNA to the interphase and proteins to the lower phase. The upper phase (containing the RNA) can then be collected with a pipette and added to a spin column for purification. A spin column is a small plastic capped tube similar to an eppendorff containing a silica membrane to which the RNA binds while other substances can be washed away thus permitting the purification of the RNA. Ethanol is added to provide appropriate binding conditions for the RNA to bind to the membrane of the column followed by various wash buffers designed to support binding of the RNA and wash away any contaminants (such as phenol or proteins). Finally, the RNA is eluted (released) from the membrane by addition of water which neutralises the pH and reduces the affinity for RNA-binding to the membrane. The purified RNA can then be collected and used for downstream reactions.

2.12.2.2 Full procedure for RNA extraction

The RNA extraction procedure was the same for mouse and rat tissue. RNA extraction is complicated by the ubiquitous presence of ribonuclease enzymes (RNases) which are naturally present on the skin of users and can also be present on laboratory benches and glassware. RNases can rapidly degrade RNA if appropriate laboratory practice is not adopted throughout the RNA extraction procedure. Therefore for all RNA work, gloves were worn at all times, the bench was cleaned with a spray that eliminates RNases (*RNAZap, Ambion, U.K.*) and RNase/DNase-free tubes and pipette tips were used throughout to minimise degradation of RNA. Total RNA was extracted from frozen heart tissue using the miRNeasy Mini Kit (*Qiagen, U.K.*) according to the protocol included with the kit. This kit contains the necessary reagents for the full extraction protocol: lysis buffer, two wash buffers (*Buffer RWT* and *Buffer RPE*), RNase-free water and spin-columns. The exact composition of buffers RWT and RPE are protected by the supplier (*Qiagen*) but they both contain high concentrations of ethanol and guanidine thiocyanate to facilitate binding of RNA to the silica membrane and remove traces of proteins and organic salts, respectively. Chloroform was not supplied by the kit and was acquired separately (*Fisher Scientific, U.K.*). The full protocol was as follows:

- The tissue was weighed and then homogenised in 700 μl of lysis buffer provided by the kit through high-speed shaking (*TissueLyser, Qiagen, U.K.*) with steel beads (supplied ready-made by *Qiagen, U.K.*). Homogenisation was performed in 30s intervals and checked after each shake to assess level of tissue breakdown and minimise over- homogenisation. Homogenisation was deemed complete when no solid tissue pieces remained (this usually took < 5 min).
- The steel bead was removed and the samples were treated with 140 μl chloroform (*Fisher Scientific, U.K.*) and spun at 4°C for 15 min using a temperature-controlled centrifuge (*Model 5415R, Lab Mark, Czech Republic*) for phase separation. After this time, the uppermost layer containing RNA was collected with a pipette into a separate tube, leaving DNA (middle layer) and proteins (bottom layer) behind.
- RNA was then treated with ethanol and applied to a spin column where the ethanol facilitates binding of the RNA to the silica membrane of the column. The spin column was then treated with washing buffers (*buffer RWT* and *buffer RPE*) to remove any contaminants (e.g. proteins or organic salts) followed by a 15-min on-column digestion

with DNase (*DNase I, Qiagen, U.K.*) (i.e. DNase is added directly to the silica membrane of the column) to remove any accidental carry-over of genomic DNA.

- RNA was then eluted in RNase-free water – this means that the RNA is lifted from the silica membrane by the water which raises the pH to >8.5 increasing the charge on the surface of the membrane reducing the affinity for RNA-binding which means it can be collected in the water that passes through the membrane. The RNA extracted at this stage represents the total RNA (including all mRNA from all different genes) that was present in the tissue sample.

Once the RNA has been extracted, there are three quality control checks to be performed which are recommended at this stage prior to further use in downstream reactions. These include assessment of (i) RNA quantity (yield), (ii) RNA purity and (iii) RNA integrity. These factors are important because cDNA synthesis requires a minimum template amount (yield is important), any chemical impurities can adversely affect the reverse transcriptase enzyme (purity is important) and degraded RNA can lead to shorter cDNA fragments which could underestimate the results (integrity is important).

(i)-(ii) The quantity and purity of the RNA were measured using a Nanodrop ND-1000 Spectrophotometer (*Nanodrop Technologies/Thermo Scientific, U.K.*). The Nanodrop ND-1000 is a spectrophotometer which measures the absorbance of light between 220-320 nm of a sample of nucleic acid - the absorbance is linearly proportional to the concentration of molecules within the sample and can be used to quantify the concentration of nucleic acid in a sample based on this (Beer-Lambert law). The machine requires only a small amount of sample (0.5-1 μ l) which is pipetted on to a measurement pedestal. An 'arm' is closed down on to the pedestal and a liquid sample column is formed between the two surfaces through which UV light can be passed and the absorbance measured. RNA absorbs light maximally at 260 nm and the absorbance ratios 260/280 nm and 260/230 nm provide information on the purity of the RNA sample. Pure RNA will have a 260/280 ratio of 1.9-2.1 (<1.9 indicates protein contamination) and a 260/230 ratio of 1.8-2.3 (<1.8 indicates organic contamination by phenol).

(iii) RNA integrity was determined using the Agilent Bioanalyzer 2100 (*Agilent Technologies, U.K.*); this step was performed by Julie Galbraith or Jing Wang at the Functional Genomics Centre at the University of Glasgow. This method is based on capillary electrophoresis with a fluorescent dye that binds to RNA. Capillary

electrophoresis of a (total) RNA sample shows two distinct peaks corresponding to the two ribosomal RNA (rRNA) species in the sample: 18S and 28S and in a sample with low degradation the baseline between the peaks should be relatively flat (Figure 2.19).

How the Agilent Bioanalyzer 2100 works: The machine uses a chip which contains wells for the samples with micro-channels between the wells. The chip is prepared by filling the micro-channels with a sieving polymer matrix gel and a fluorescence dye and the samples of RNA are then loaded into the wells along with a size ladder. Once the micro-channels and wells are filled, a 16-electrode pin cartridge fits into the wells of the chip and the charged molecules of RNA are driven by the voltage gradient, separated according to size with smaller fragments migrating further than larger ones. The dye molecules intercalate into the RNA strands which allows them to be visualised by laser-induced fluorescence. The result is visualised as an electropherogram where the amount of fluorescence is proportional to the amount of RNA at a given size. An algorithm known as the RNA Integrity Number (RIN) has been developed to indicate the integrity of the RNA sample based on 8 different features of the electrophoretic output trace (total 28S/18S ratio, 28S peak height, area under 28S peak, 18S and 28S area compared to area of the fast region, linear regression of end-point of fast area, number of detectable fragments in fast region, presence or absence of 18S peak and relation of the overall mean to the median) (Schroeder *et al.*, 2006). Based on these criteria, computer software calculates the RIN number on a scale from 1-10 by order of increasing RNA integrity (1-badly degraded; 10-highly intact). It is generally accepted that samples with a RIN >5 (but preferably >8) are suitable for qRT-PCR experiments (Fleige & Pfaffl, 2006) although this is largely dependent on the individual study. For this thesis, only RNA that met the following criteria were used ($A_{260}/A_{280} > 1.8$ and $RIN > 7$).

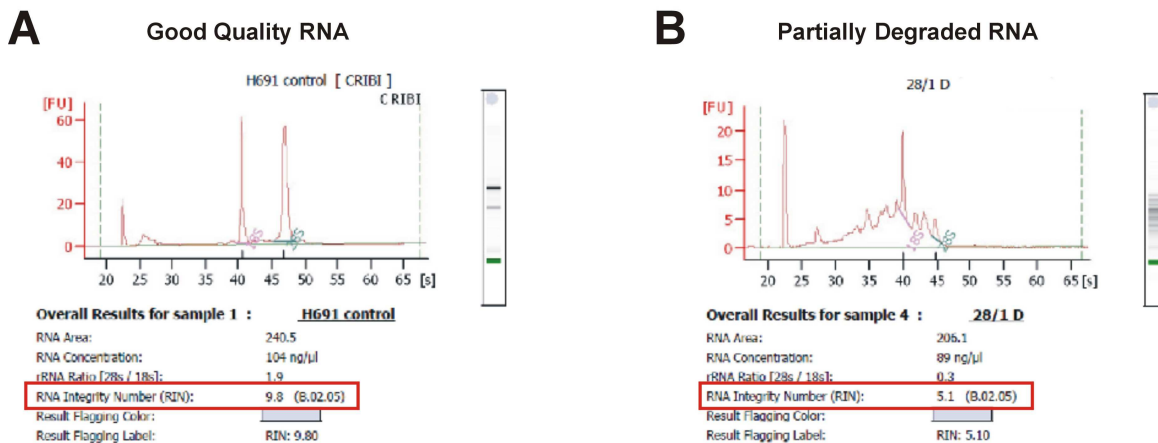


Figure 2.19 Example electrophoresis output traces from the *Agilent Bioanalyzer* showing analysis of RNA integrity.

(A) Good quality RNA is visible with two prominent 18S and 28S peaks with a 28S/18S ratio of ~2 and a flat baseline – RIN value of 9.8. (B) Example where RNA degradation is visible as a decrease in the 18S and 28S peaks with an increase in smaller degradation fragments resulting in a noisier baseline – RIN value of 5.1. Figure courtesy of *Agilent Technologies*.

2.12.3 Synthesis of cDNA

2.12.3.1 Principle of procedure of cDNA synthesis

RNA is not a suitable template for a qRT-PCR experiment which requires double-stranded DNA to work therefore the RNA must be transcribed into cDNA. This is performed by the process of reverse transcription in which single-stranded mRNA is transcribed into double-stranded DNA (i.e. the *reverse* to the normal transcription process in which DNA is transcribed to mRNA) as depicted in Figure 2.20. This is performed using oligonucleotide primers of poly-thymine (oligo-dT primers) that specifically bind to the poly-A tail of all mRNAs and direct the enzyme reverse transcriptase (RNA-dependent) to synthesise a new strand using dNTPs (A, T, C and G). This forms an mRNA:DNA hybrid (one strand is the mRNA and the other the newly synthesised cDNA strand) for all the mRNAs in the sample. In order to synthesise a new cDNA strand to replace the mRNA strand, the mRNA must be digested with an enzyme, usually RNase H. Once the mRNA strand is digested, the single-stranded cDNA forms a hairpin loop on itself due to its hydrophobic nature and this serves as the ‘primer’ to direct synthesis of the complementary new strand of cDNA by a DNA-dependent DNA polymerase. The result is double-stranded cDNA derived from the original template mRNA sequence.

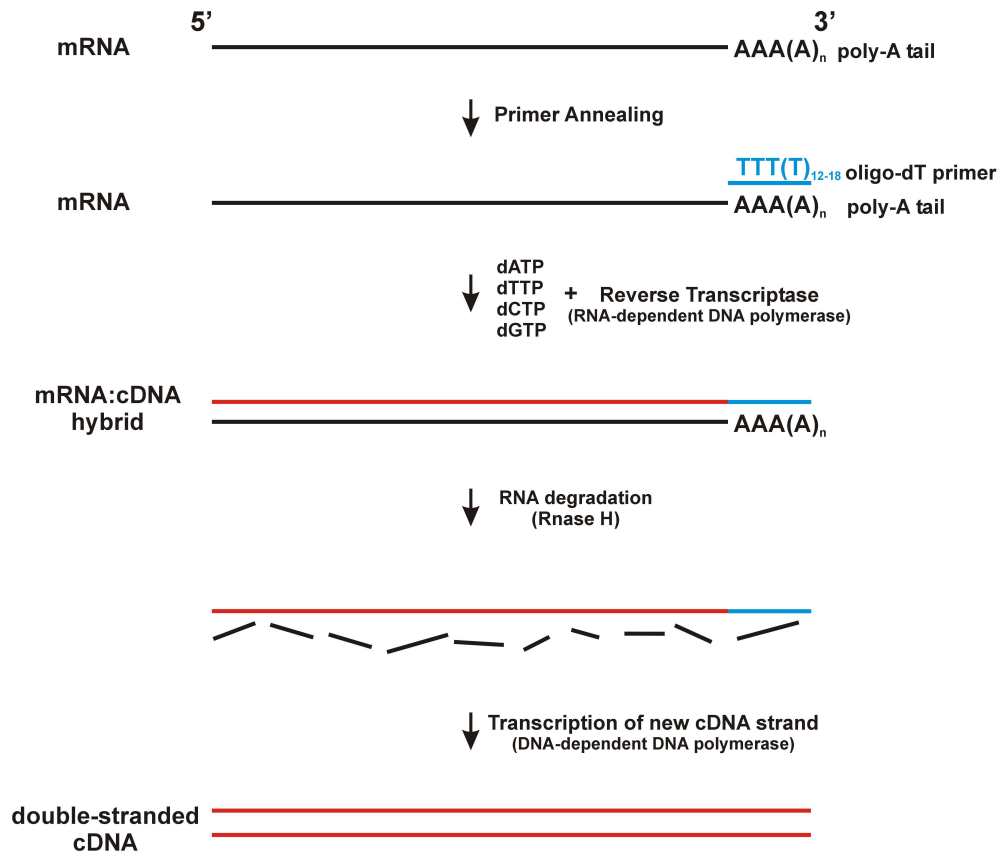


Figure 2.20 cDNA synthesis by reverse transcription.

2.12.3.2 Full protocol for cDNA synthesis

As was the case with the RNA extraction protocol, the cDNA synthesis protocol was the same for mouse and rat samples. Prior to the synthesis of cDNA, the RNA was given a second treatment of DNase to ensure complete removal of contaminating genomic DNA; this was done by incubating the RNA with a different DNase I (*Turbo DNA-free*, Ambion, U.K.) for 25 min at 37°C. After this time a DNase-inhibitor was added to inactivate the DNase enzyme (*DNase Inactivation Reagent* provided with *Turbo DNA-free* kit, Ambion, U.K.). First strand cDNA was synthesised from 1 µg RNA (measured by the *Nanodrop Spectrophotometer* as previously described) by reverse transcription using the *Omniscript Reverse Transcription* kit (*Qiagen*, U.K.). This kit contains the reagents necessary for the protocol including the reverse transcriptase enzyme (catalyses synthesis of cDNA strands and degrades RNA in RNA:cDNA hybrids), dNTPs ('building blocks' for the new cDNA strands), buffer RT (contains Mg²⁺ for optimal reverse transcriptase activity) and RNase/DNase free water for dilutions or as a substitution for the reverse transcriptase enzyme in control reactions. The *Omniscript* reverse transcriptase enzyme contains three distinct enzymatic functions: (i) RNA-dependent reverse transcription (catalyse the

synthesis of cDNA from an RNA template), (ii) DNA-dependent reverse transcription (catalyse the synthesis of cDNA from a cDNA template) and (iii) RNase H (degradation of RNA in RNA:cDNA hybrids only). Additional reagents that were not provided in this kit but were necessary for the reaction were oligo-dT primers (*Qiagen, U.K.*) and an RNase inhibitor (*RNase-Out, Invitrogen, U.K.*) for removal of contaminating RNases (this does not affect the RNase activity of the *Omniscript* reverse transcriptase enzyme). The final composition of the reaction is shown in Table 2.3 to give a final volume of 50 μ l and the reaction was performed in an incubator at 37°C for 1 h. Reactions containing RNase/DNase-free water instead of reverse transcriptase enzyme served as negative RT controls (denoted RT-). The resulting cDNA produced at this stage contains all the cDNA of all the genes that were present in the original tissue sample, transcribed from all the mRNAs in the sample. The cDNA corresponding to the gene of interest (e.g. *Runx* or *Gapdh*) is selectively amplified in the final stage using gene-specific primers by qRT-PCR allowing quantification of the expression of the gene of interest.

Table 2.3 Reverse transcription reaction components.

Component	Volume (per reaction)	Final concentration
<u>Master mix</u>		
10x Buffer RT	5 μ l	1x
dNTP mix (5 mM each)	5 μ l	0.5 mM each dNTP
Oligo-dT primer (10 mM)	5 μ l	1 μ M
RNase inhibitor (10 units/ μ l)	2.5 μ l	25 units (per 50 μ l reaction)
Reverse transcriptase	2.5 μ l	10 units (per 50 μ l reaction)
RNase-free water	Variable*	-
<u>RNA</u>	Variable*	1 μ g
Total Volume	50 μ l	-

* Variable depending on available RNA concentration. Final volume is made up with RNase/DNase-free water.

2.12.4 Verification of cDNA synthesis

Prior to qRT-PCR, newly synthesised cDNA (including RT- controls) were tested for the presence of double-stranded DNA to verify successful reverse transcription. This was done using conventional PCR amplification. Conventional PCR amplification is based on the same principle of exponential amplification by the three-step process of denaturing, primer annealing, and strand extension as previously described. It differs from qRT-PCR in that the reactions do not contain any fluorescence labelling therefore the product is not detected as it accumulates but rather at the end-stage post-amplification by agarose gel

electrophoresis. Conventional PCR was sufficient for this stage in verifying presence of cDNA. The protocol for this was as follows:

Conventional PCR: For these experiments the PCR was run beyond 27 cycles to ensure the product is collected from the plateau phase (maximum accumulated product). PCR reactions were conducted in 10 μ l final volume containing 0.5 μ l cDNA, 1 μ l PCR custom-made master mix (*Thermo Scientific, U.K.*), 2 μ l primers (10 μ M) for *Runx1* (rat-specific or mouse-specific as appropriate; *Quantitect, Qiagen, USA*) or glyceraldehyde-3-phosphate dehydrogenase (*Gapdh*) (*Eurofins MWG Operon, Germany*) and 0.1 μ l Taq DNA polymerase (*Thermo Scientific, U.K.*). A layer of oil was placed on the top of the reaction mix to avoid loss of solution by evaporation in the machine. Reactions were performed using a *Stratagene RoboCycler* PCR machine (which provided cyclic heating conditions) for either 30 cycles (*Gapdh*) or 40 cycles (*Runx1*) to ensure analysis was taken from the plateau phase of the reaction (Figure 2.23). Each cycle was 50s at 95°C, 50s at 55°C and 1 min at 65°C. Amplified PCR products were then visualised by gel electrophoresis.

Gel electrophoresis: Gel electrophoresis can be used to separate DNA fragments by size and charge. DNA from the PCR reaction can be loaded into wells of an agarose gel and by application of an electric field, the negatively-charged DNA moves through the agarose matrix towards the positive electrode with shorter fragments migrating further than longer fragments. The gel is treated with a fluorescent dye called ethidium bromide which allows the final bands on the gel to be visualised under UV light.

Preparation of the gel: A 2% agarose gel was prepared fresh using powdered agarose (*NuSieve; Fisher Scientific, U.K.*) dissolved in 0.5x Tris/Borate/EDTA (TBE) buffer in a final volume of 250 ml and heating in a standard microwave for approximately 2.5 min. The composition of TBE buffer for a 0.5x stock was (in mM): Tris (44.5), boric acid (44.5) and EDTA (1.0). Once the agarose was completely dissolved the liquid gel was cooled prior to pouring to prevent damage to the plastic gel tray (to approximately below 60°C) by holding the bottle containing the gel under cold running tap water for 5 min. After this time, 10mg/ml EtBr (*Invitrogen, U.K.*) was added to the liquid gel, swirled to mix, and the gel was then poured into a Perspex gel tray and left for 30 min to set with gel combs in place to create the wells. Once the gel was set, the gel combs were removed and the gel was placed into a gel tank with 0.5x TBE buffer.

Loading and running the gel: 3 µl PCR product (final amplified cDNA) was mixed with 2 µl loading dye and added to each well. Loading dye (6x; *Promega, U.K.*) contains bromophenol blue dye (which allows coloured visualisation of the gel electrophoresis progress) and Ficoll, a high molecular weight (MW) polysaccharide (which increases the density of the sample to a level greater than the surrounding TBE buffer to ensure it falls to the bottom of the well). A 100 bp DNA size ladder (5 µl) was run alongside each run (*Promega, U.K.*) to allow size comparisons of the fragments to be made. The gel electrophoresis was run for 30 min at 160V. Successful RT reactions were confirmed by positive single bands of correct size for RT+ samples (120 bp for *Runx1* and 140 bp for *Gapdh*) and no band in RT- control samples (RT negative reaction - water instead of RT enzyme) (Figure 2.21).

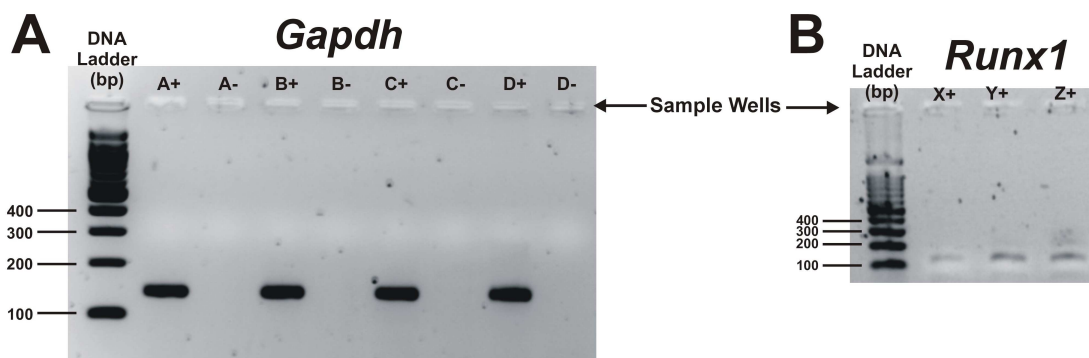


Figure 2.21 Example gels from DNA gel electrophoresis to verify reverse transcription and appropriate size products.

(A) Samples of cDNA from positive (+) and negative (-) reverse transcription reactions amplified with conventional PCR using *Gapdh* primers. Positive samples show a single, distinct band of appropriate length (140 bp) with no bands present in negative control reactions. (B) Samples of cDNA from positive (+) samples only to verify a single, distinct band of appropriate size for *Runx1* amplicons (120 bp). Primers for *Gapdh* were used to confirm positive and negative samples (*Runx1* primers were used when confirming amplicon length for *Runx1*).

2.12.5 qRT-PCR

2.12.5.1 Principle of PCR

The principle of PCR (both qRT-PCR and conventional PCR) is based on the amplification or replication of DNA (derived from the mRNA) to produce more DNA. This involves first denaturing double-stranded DNA by applying a high temperature (~90-98°C) which separates the DNA into two single strands. Short DNA sequences known as primers which have been selected to flank the DNA sequence of interest can then anneal to the single strands when the temperature is reduced to 50-65°C. At a slightly higher temperature of 72-80°C an enzyme known as DNA polymerase begins synthesising two new strands

which are complementary to the template strands by incorporating nucleotide bases (adenine, thymine, cytosine and guanine) provided in the reaction (this process is directed by the primers which indicate the start site). This results in two new strands and doubling of the original DNA (1 copy to 2 copies of DNA). This represents two new templates for the next cycle in which these three main temperature-dependent steps are repeated again. The entire process is continually repeated in cycles to produce exponential doubling of DNA at each cycle for the sequence of interest. PCR reactions take place in plastic tubes within a thermal cycler machine and require the following components:

Component	Function
<u>Master-mix:</u>	
Buffer	Maintains the master-mix at the appropriate pH for the reaction.
Deoxynucleotide triphosphates (dNTPs)	Provide energy and nucleotides for the synthesis of DNA. Each nucleotide base must be added in equal concentration to avoid mismatch of bases.
Primers specific to gene of interest	Short pieces of DNA (20-30 bp) that bind to the DNA allowing the polymerase enzyme to initiate the incorporation of dNTPs.
Polymerase	A heat-stable enzyme that adds dNTPs to the DNA template strand.
<u>DNA sample:</u>	
Template DNA	Sample of DNA to be amplified by the PCR reaction.

The PCR process: PCR usually consists of 20-40 repeated cycles with each cycle made up of a defined series of temperature steps depending on the activity of the DNA polymerase, the concentration of dNTPs and divalent cations, and the melting temperature of the primers, as outlined below and summarised in Figure 2.22:

- (1) **Initiation:** This step involves heating the reaction to 94-98°C and held for 1-9 min and is only required if the DNA polymerase requires ‘heat-start’ activation.

- (2) **Denaturation:** The reaction is then heated to 94-98°C for 20-60s which disrupts the hydrogen bonds between the complementary bases which hold the two DNA strands together, therefore causing the two strands to separate (or 'melt').
- (3) **Annealing:** The reaction is lowered to 50-65°C for 20-60s which allows the primers to anneal to the single-stranded DNA template. DNA polymerase then binds to the primer-template hybrid.
- (4) **Elongation (extension):** The reaction is then heated to 72-80°C which is the optimum temperature for DNA polymerase (a temperature of 72°C is used for *Taq* polymerase). The DNA polymerase synthesises a new strand by adding dNTPs to the template strand in the 5' to 3' direction. Under optimal conditions the amount of target DNA doubles at each extension step.
- (5) **Final elongation:** A single step may be performed after the last cycle to ensure any remaining single-stranded DNA is fully extended. This step usually involves heating to 70-74°C for 5-15 min.
- (6) **Final hold:** The final step can be applied for an indefinite time at 4-15°C which holds the reaction until the user is ready to collect it from the machine.

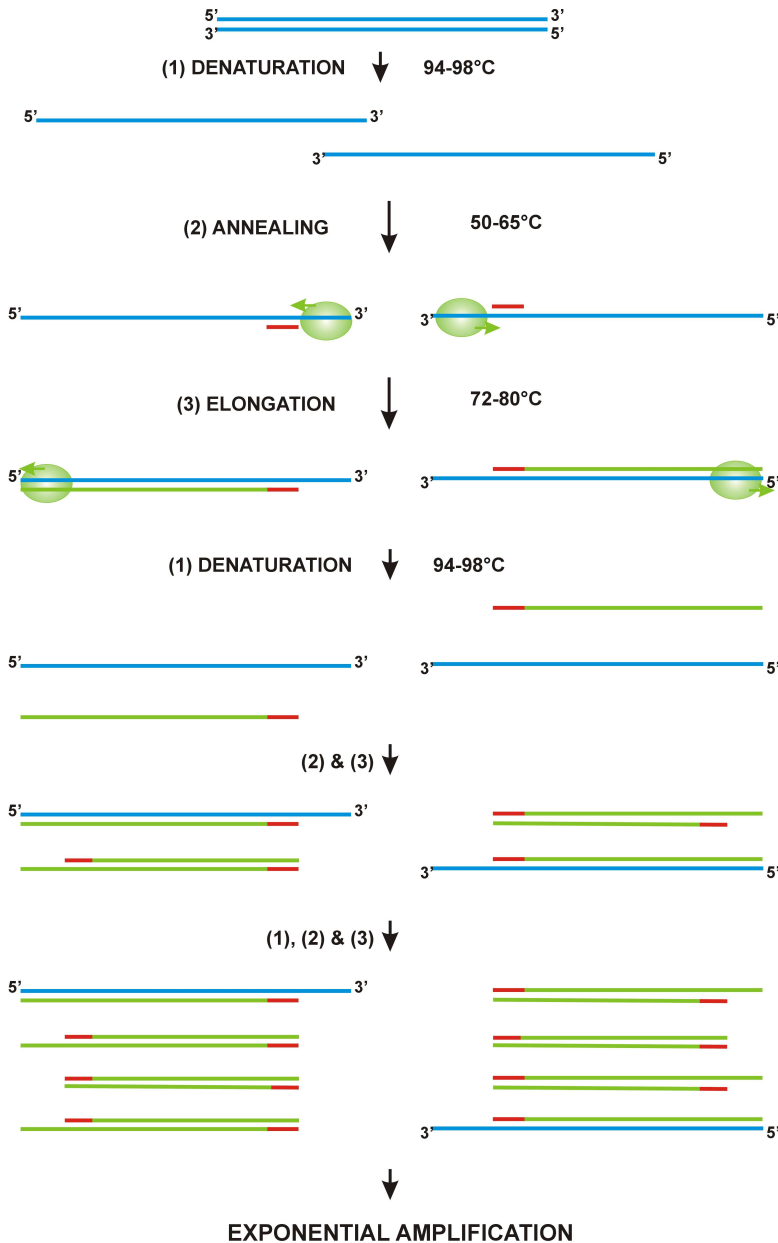


Figure 2.22 Schematic representation of the PCR process.

(1) Denaturation at 94-98°C (2) Annealing at 50-65°C (3) Elongation at 72-80°C. Three cycles are shown. Blue lines represent the DNA template to which primers (red lines) anneal and are extended by DNA polymerase (green circle) to produce shorter DNA products (green lines) which are then used as templates as the PCR progresses.

Stages of a PCR reaction: The complete PCR process can be divided into three main phases; (1) exponential phase, during which there is exact doubling of the product after each cycle; (2) linear phase, during which the reaction components are being consumed and the reaction is slowing; and (3) plateau phase, during which the reaction components have been exhausted and no more product is being made (Figure 2.23).

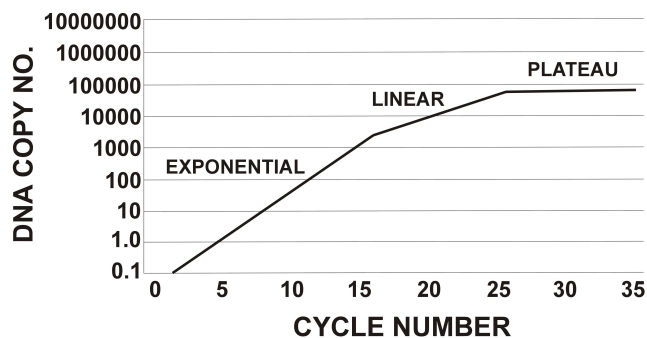


Figure 2.23 Phases of a conventional PCR reaction.

Conventional vs. quantitative qRT-PCR: Conventional PCR uses agarose gel with ethidium bromide for detection of PCR product (which is the amplified DNA) at the final phase or end-point of the reaction as described previously in Section 2.12.4. Conventional PCR is sufficient for simply detecting the presence of double-stranded cDNA to verify appropriate RT as described; however for gene expression studies it is limited in that it permits only semi-quantitative analysis of target gene levels (due to the insensitivity of the ethidium bromide) and since the analysis is taken from near the end-point of the reaction it is often associated with poor precision as the reaction has often proceeded past the exponential stage and products may therefore have begun to degrade. Conventional PCR has been replaced by real-time quantitative reverse transcription PCR (qRT-PCR) which differs in that it includes a fluorescent dye into the reaction to allow detection of target DNA as the reaction is occurring (i.e. in real time) rather than at the end-point of the reaction. This makes qRT-PCR more accurate than the conventional PCR method. Reporter dyes may be sequence-specific, for example the well-known *Taqman* probe, an oligonucleotide specific to the target sequence labelled with two fluorophores (a reporter and a quencher dye). As long as the two fluorophores remain in close proximity they do not emit a fluorescence signal; however during the extension phase of replication the action of *Taq* polymerase cleaves the 5' end of the probe allowing the two dyes to become separated therefore as product accumulates the fluorescence increases. Reporter dyes may also be non-specific, for example SYBR green, which binds to the minor groove of double-stranded DNA and as the reaction proceeds and product increases the fluorescent signal also increases (Figure 2.24). Further details on the processing of qRT-PCR data is covered in the later sections.

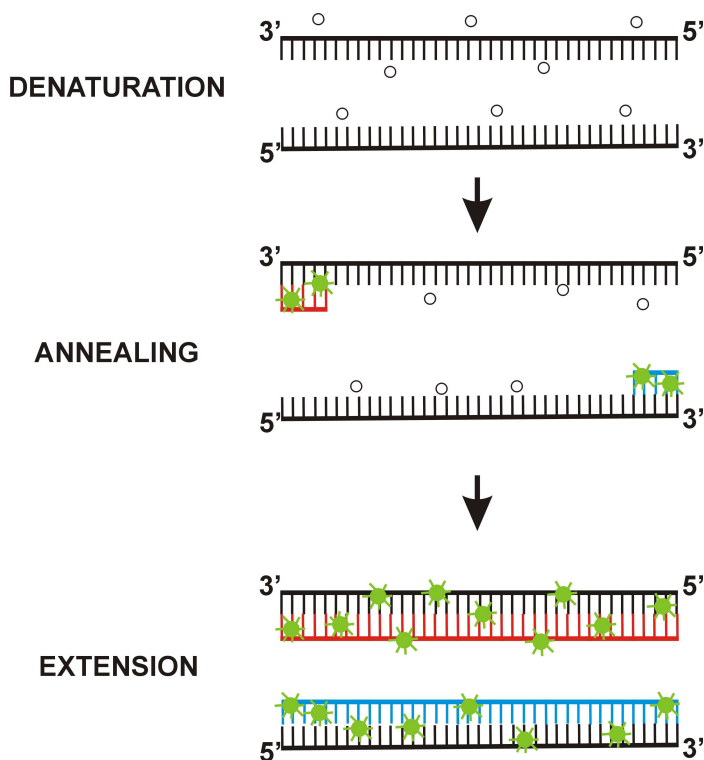


Figure 2.24 SYBR green binding during PCR amplification.

SYBR green (green circles) binds to double-stranded DNA and can be used to measure the abundance of template DNA at the end of the extension step of the PCR reaction.

2.12.5.2 Full protocol for qRT-PCR

For this thesis, qRT-PCR was used to assess *Runx* mRNA levels in either whole heart samples (LV + RV) or in dissected regions of the heart (infarct, peri-infarct, remote LV and RV). For regional work, the RV was selected as the region to which other regions were compared as the RV represented a comparison for the LV and represented the furthest region from the infarcted region.

Preparation for qRT-PCR: All reagents were thawed and kept on ice and all qRT-PCR reactions were prepared in a laminar flow hood to prevent aerosol contamination of cDNA or primers. Gloves and a laboratory coat were worn at all times to further minimise any contamination. Synthesised cDNA was diluted 1:5 with RNase/DNase-free water (final volume 30 μ l) to allow a manageable volume (2 μ l) for pipetting to reduce error. Either 96-well or 384-well plates specifically designed for qRT-PCR were used (*Applied Biosystems, U.K.*) depending on the number of samples. *Runx* was detected with the appropriate *Runx*-specific primers (*Qiagen, U.K.*). These primers have also been bioinformatically validated for high sensitivity (excludes short nucleotide polymorphisms (SNP) therefore more accurate), have high efficiency and high specificity with short

amplicon length (120bp) which have better efficiency as less SYBR green is incorporated. A master-mix was prepared to minimise variation of reagent concentration between wells; two were prepared, one for each gene (*Runx1* and the housekeeper, *Gapdh*) enough to contain the following in each well:

Table 2.4 qRT-PCR mastermix reaction components.

	<u><i>Gapdh</i></u>	<u><i>Runx</i></u>
<u>Master-Mix:</u>		
RNase/DNase-free H ₂ O	4 µl	6 µl
SYBR green mix*	10 µl	10 µl
Forward Primer (F)	2 µl	2 µl (F & R)
Reverse Primer (R)	2 µl	
<u>cDNA:</u>		
cDNA	(2 µl)	(2 µl)
Final Volume:	20 µl	20 µl

*The SYBR green mix (*Applied Biosystems, U.K.*) contains SYBR Green dye (the main reporter dye which intercalates with double-stranded DNA to indicate the quantity of DNA accumulating during the amplification process), an *Amplitaq Gold* DNA polymerase (catalyses synthesis of new DNA), dNTPs (the building blocks of the new strand) and a ROX dye (an internal passive reference dye to normalise non-PCR related fluorescence fluctuations that may be caused by pipetting error or sample evaporation).

Sample loading: 2 µl of cDNA sample was added to each well followed by 18 µl of the master-mix (final volume 20 µl) with centrifugations of 1500 rpm between the addition of cDNA and master-mix to ensure all drops of solution fall to the bottom of the well. An optical adhesive cover film was applied to the top of the plate to prevent loss of solution through evaporation.

qRT-PCR reaction: The qRT-PCR reaction was then performed in an ABI 7500 machine with *Sequence Detection* software (*Applied Biosystems, U.K.*) to measure relative gene expression. The cycle conditions were as follows: initial 2 min at 50°C followed by 10 min at 95°C to heat-start (activate) the *Taq* polymerase enzyme, then 40 cycles where each cycle was 95°C for 10 min, 60°C for 1 min. *Runx* was detected using *Runx* primers (*Qiagen, USA*) normalised to *Gapdh* (*Eurofins MWG Operon, Germany*). At the end of the 40 cycles, the machine was set to perform a melting curve. This is an important step for SYBR green based detection as SYBR green will bind to any double-stranded DNA

therefore this stage was performed to ensure that no contaminating DNA is present in the sample which could affect the results. The melting step is performed immediately after the 40 cycles by slowly ramping up the temperature of the reaction from 60-95°C causing the DNA to denature while continually collecting fluorescence during this time. The melting point is the temperature (T_m) at which the two DNA strands separate causing the fluorescence to rapidly decrease. Melting curve analysis is described in the section that follows (Section 2.12.6.1). In all qRT-PCR experiments, template-free (no cDNA) controls and RT- controls were always run in parallel with positive samples and each sample was run in triplicate for each experiment. Baselines and thresholds were calculated automatically by the software (see below for more detail on these parameters).

2.12.6 Interpretation of qRT-PCR data

This section aims to cover the interpretation of qRT-PCR data and covers the following: (i) the theory behind the qRT-PCR amplification curve; (ii) analysis of the qRT-PCR data followed by (iii) example calculations showing how the data was analysed for the different areas of the study.

2.12.6.1 Theory of the qRT-PCR amplification curve

Figure 2.25 shows graphical representations of typical qRT-PCR output amplification plots. An amplification plot is the normalised fluorescence signal of the reporter dye (e.g. SYBR green) plotted against the PCR cycle number. DNA is being amplified at each cycle therefore as the PCR reaction proceeds (cycle number increases) the number of DNA products increases and as fluorescence is directly proportional to DNA concentration (more fluorescence with more DNA), the fluorescence also increases (Figure 2.25A).

Baseline fluorescence: In qRT-PCR, the fluorescence does not become detectable for the initial cycles of the reaction as the DNA concentration has not accumulated to a level where the fluorescence is detectable by the machine; the fluorescence during the initial cycles of the reaction where it is not changing is referred to as the baseline fluorescence (Figure 2.25A). The fluorescence signal shown in the amplification plot is the *normalised* fluorescence of the reporter dye (R_n). R_n is the ratio of the fluorescence by the reporter dye (e.g. SYBR green) to the fluorescence of a passive reference dye. A passive reference dye is required to normalise non-PCR related fluctuations in fluorescence due to pipetting or sample evaporation, a commonly used example is the ROX dye for use in *Applied Biosystems* machines. The software automatically normalises this. Typically the delta- R_n

(ΔR_n) is used in amplification plots which is R_n with the baseline fluorescence subtracted ($\Delta R_n = R_n - \text{baseline}$).

Cycle threshold (Ct): Following the initial cycles whereby the fluorescence is unchanged, the amount of DNA accumulating during the amplification process will begin to reach detectable fluorescence levels and there is a sudden increase in the fluorescence signal. The cycle at which this increase in fluorescence becomes detectable is known as the threshold cycle (Ct). It is the Ct which defines the quantification of gene expression. The higher the starting copy number of a gene (greater number of cDNA molecules containing the gene sequence) the earlier the increase in fluorescence (i.e. the earlier the Ct). Therefore the Ct is inversely related to the level of gene expression - the smaller the Ct, the higher the gene expression. The Ct is defined by a threshold fluorescence set either manually by the user or more often by the software package which has auto-threshold and auto-baseline features. The threshold is the ΔR_n used for which above this defines the Ct of the reaction. The threshold must be set above the baseline but low enough to be within the exponential phase of the amplification curve. The Ct is derived from the intersection of the amplification plot with this threshold line (Figure 2.25A-B).

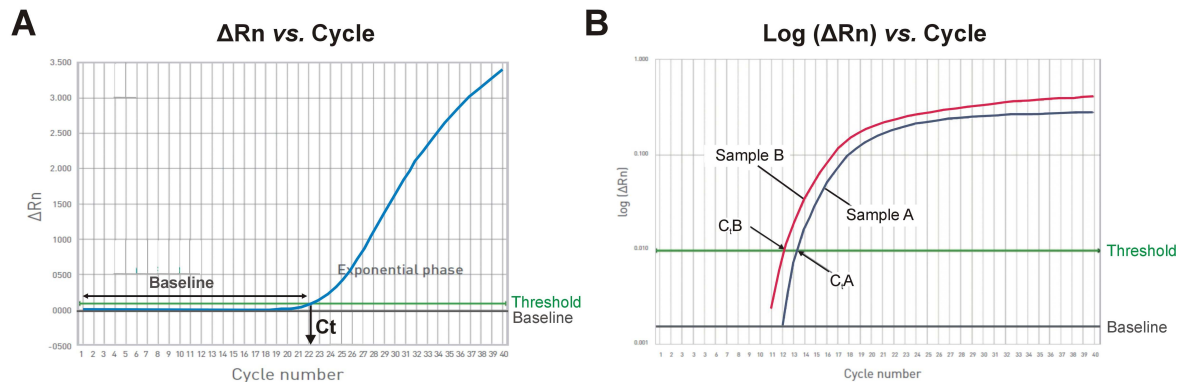


Figure 2.25 Graphical representation of qRT-PCR data.

(A) A typical qRT-PCR amplification curve where ΔR_n is plotted against PCR cycle number (R_n is the normalised reporter fluorescence; ΔR_n is the R_n minus the baseline). During the initial cycles the fluorescence does not reach a detectable level, this is known as the baseline (indicated). The cycle at which the amplification curve intersects the threshold (green line) is the Ct, as shown. (B) An example amplification curve plotted using the $\log(\Delta R_n)$ against PCR cycle for two samples (A; blue and B; red). The green line is the threshold (set at the same level for both samples); the gray line is the baseline. As the Ct determines the expression levels of the gene present in the sample in an inverse manner (lower Ct, higher gene levels) and sample B has an earlier (lower) Ct (C_{tB}) than sample A (C_{tA}), sample B therefore has higher expression of the gene of interest than sample A. Figure adapted from *Applied Biosystems* guide *Real-time PCR: understanding Ct*.

Melting curve analysis: Melting curves show the melting temperature (T_m) for samples which is dependent on the base composition and length of the DNA present in the sample. All DNA from the same primers should have the same T_m resulting in a single peak in the melting curve; the presence of other peaks indicates contamination – this may be from contaminating DNA or from primer-dimers (which are formed when primers anneal to themselves). Primer-dimers are easily identified by smaller peaks to the left of the main peak as they are smaller in size and therefore have lower T_m . An example of melting curve analysis is shown in Figure 2.26. For this thesis, primer-specificity was confirmed in samples by single peak melting curves with no primer-dimer formations. Only samples with a single peak on a melting curve were included.

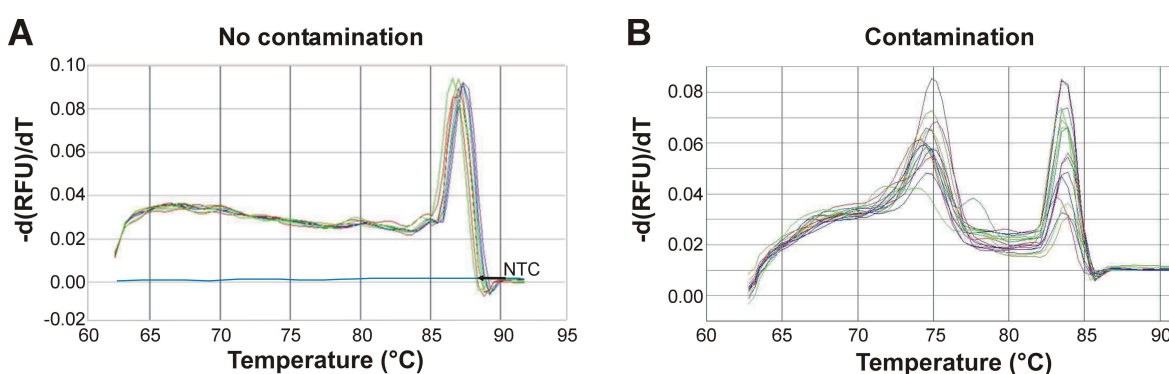


Figure 2.26 Example melting curves from the qRT-PCR dissociation stage.

Melting curves are plotted as the derivative of fluorescence $d(\text{rfu})/dT$ against temperature. The derivative is often plotted as it is useful for identifying different peaks. (A) Melting curves with a single peak at the same T_m indicating no contamination. The no template control (NTC) samples should have a straight line as there should be no DNA in the sample. (B) Multiple peaks present indicating contamination. Some of the peaks on the left may be from primer-dimers as there are smaller peaks melting at a lower temperature. All samples in this thesis were tested by melting curve analysis and only those which showed a single peak were included. Figure adapted from *Gunster Biotech Ltd*.

2.12.6.2 Analysis of qRT-PCR data

There are two different methods which can be used to quantify qRT-PCR data: absolute or relative quantification. Absolute quantification provides an exact copy number of the gene using a standard curve approach whereas relative quantification presents the expression levels relative to a specific control (e.g. treated vs. non-treated). Absolute quantification is only usually used when the precise quantity of amplified DNA is required (e.g. for viral load studies where the absolute number of viral copies in the sample is to be determined). But when comparing between groups, relative quantitation is sufficient.

2.12.6.3 Analysis of qRT-PCR data by the comparative C_t method

One of the most common methods of analysing relative qRT-PCR data is using the comparative C_t method (known as the $2^{-\Delta\Delta C_t}$ method) (Schmittgen & Livak, 2008). The equation for this is:

$$\text{Fold change} = 2^{-\Delta\Delta C_t} \quad \text{Eq. 11}$$

Where $\Delta\Delta C_t = [(C_t \text{ target gene} - C_t \text{ reference gene})_{\text{SAMPLE A}} - (C_t \text{ target gene} - C_t \text{ reference gene})_{\text{SAMPLE B}}]$. The derivation of this formula can be found in the appendix.

The result is the fold change in expression of the gene of interest between one sample and another (e.g. treated *vs.* untreated). The sample to which the others are compared against is known as the calibrator sample and is typically the control, for example a healthy subject in a disease study. Where the data is required to be as single data points (i.e. not compared to a calibrator sample) it is acceptable to use $2^{-\Delta C_t}$ or 2^{-C_t} . Where samples have been run in triplicate, the mean C_t is used for the equations above. For this thesis qRT-PCR results were analysed using comparative C_t calculations; either $2^{-\Delta\Delta C_t}$ (regional comparisons relative to RV region), $2^{-\Delta C_t}$ (whole heart or RV region between sham and MI) or 2^{-C_t} (*Gapdh* stability) as recommended by accepted published methods (Schmittgen & Livak, 2008). Example calculations for each of these are detailed below. Statistical significance between regions within the same heart was tested using ANOVA with multiple regression analysis performed with SPSS software. This involved selecting the RQ as the dependent variable for the analysis. An example of how this was calculated is shown in Figure 2.27.

A

	RQ	RV	Infarct	Periinfarct	RemoteLV
1	1.00	1.00	.0	.0	.0
2	1.00	1.00	.0	.0	.0
3	1.00	1.00	.0	.0	.0
4	1.00	1.00	.0	.0	.0
5	1.00	1.00	.0	.0	.0
6	1.00	1.00	.0	.0	.0
7	1.00	1.00	.0	.0	.0
8	1.00	1.00	.0	.0	.0
9	5.21	.0	1.00	.0	.0
10	4.40	.0	1.00	.0	.0
11	7.62	.0	1.00	.0	.0
12	1.73	.0	1.00	.0	.0
13	8.23	.0	1.00	.0	.0
14	2.83	.0	1.00	.0	.0
15	2.40	.0	1.00	.0	.0
16	8.46	.0	1.00	.0	.0
17	1.49	.0	.0	1.00	.0
18	1.55	.0	.0	1.00	.0
19	2.50	.0	.0	1.00	.0
20	5.90	.0	.0	1.00	.0
21	2.92	.0	.0	1.00	.0
22	.94	.0	.0	.0	1.00
23	1.63	.0	.0	.0	1.00

B

Model Summary

Model	R	R Square	Adjusted R Square	Std. Error of the Estimate
1	.746 ^a	.556	.503	1.63912

a. Predictors: (Constant), RemoteLV, Periinfarct, Infarct

ANOVA^b

Model		Sum of Squares	df	Mean Square	F	Sig.
1	Regression	84.144	3	28.048	10.439	.000 ^a
	Residual	67.168	25	2.687		
	Total	151.312	28			

a. Predictors: (Constant), RemoteLV, Periinfarct, Infarct

b. Dependent Variable: RQ

Coefficients^a

Model		Unstandardized Coefficients		Standardized Coefficients	t	Sig.
		B	Std. Error	Beta		
1	(Constant)	1.000	.580		1.726	.097
	Infarct	4.110	.820	.804	5.015	.000
	Periinfarct	1.826	.848	.342	2.152	.041
	RemoteLV	.133	.885	.024	.151	.881

a. Dependent Variable: RQ

Figure 2.27 Example outputs of statistical analysis of qRT-PCR data using SPSS software.

(A) The data set as a grid of dummy variables by a yes (1) or no (0) system – where there is 1.00 means the RQ corresponds to the appropriate region in the column; RQ is selected as the dependent variable to assess whether there is a statistical difference between the RQ in each region. (B) Output view showing the overall ANOVA *P* value and the individual *P* values for each region. These results were also verified with separate ANOVA testing.

For comparisons of specific regions between sham and MI using unpaired samples, the student's t-test was used. A value of $P < 0.05$ was considered significant. All data were tested for normal distribution using a histogram plot and by plotting residuals.

Example 1: analysis of gene expression between sham and MI – whole heart samples.

SHAM					MI				
	<i>Runx</i> C_T	<i>Gapdh</i> C_T	ΔC_T	$2^{-\Delta C_T}$		<i>Runx</i> C_T	<i>Gapdh</i> C_T	ΔC_T	$2^{-\Delta C_T}$
	17.37	17.80				15.16	17.68		
	16.99	17.41				15.03	17.78		
	16.89	17.94				15.22	17.87		
Mean	17.08	17.72	-0.63	1.55	Mean	15.14	17.78	-2.64	6.25

Figure 2.28 Sample qRT-PCR data analysis of mouse MI tissue using the $2^{-\Delta C_T}$ method.

Samples were analysed using qRT-PCR and the C_T data from the *SDS* software was imported into Microsoft Excel. Each sample was performed in triplicate, represented by three C_T values for each gene in this example. Two samples are shown; whole heart (LV + RV) homogenate for a (i) 4-wk sham heart and a (ii) 4-wk MI heart.

As the whole heart samples were from separate animals, there was no means to justify pairing any MI sample with a particular sham sample; therefore it was not appropriate to use the $2^{-\Delta\Delta C_T}$ method, and instead the $2^{-\Delta C_T}$ value for MI was used for the calculations. The individual $2^{-\Delta C_T}$ value (mean of the triplicates) for each MI heart was divided by the mean sham value (mean of all sham $2^{-\Delta C_T}$ values) and then multiplied by 100 to calculate the percentage change in *Runx* expression using the formula shown below. In the above example, *Runx* expression in the MI heart is increased to 403% of levels in the sham heart.

$$\% \text{ change} = \frac{MI(2^{-\Delta C_T})}{\text{mean Sham}(2^{-\Delta C_T})} \times 100 \quad \text{Eq. 12}$$

Example 2: analysis of gene expression between sham and MI – heart region samples.

MI - RV region						MI - Peri infarct region					
	<i>Runx</i> C _T	<i>Gapdh</i> C _T	ΔC_T	$\Delta\Delta C_T$	$2^{-\Delta\Delta C_T}$		<i>Runx</i> C _T	<i>Gapdh</i> C _T	ΔC_T	$\Delta\Delta C_T$	$2^{-\Delta\Delta C_T}$
	25.04	18.24					24.09	18.19			
	24.92	18.19					24.86	17.94			
	25.54	18.58					24.28	18.19			
Mean	25.16	18.34	6.83	0.00	1.00	Mean	24.41	18.11	6.30	-0.53	1.44

Figure 2.29 Sample qRT-PCR data analysis of mouse MI tissue using the $2^{-\Delta\Delta C_T}$ method.

Samples were analysed using qRT-PCR and the Ct data from the *SDS* software was imported into Microsoft Excel. Each sample was performed in triplicate, represented by three Ct values for each gene in this example. Two regional samples are shown, both from the same heart; the RV region and the peri-infarct region. The RV region was the region to which all other regions of the respective hearts were normalised.

For regional heart samples, the $2^{-\Delta\Delta C_T}$ method was used to compare the infarct, peri-infarct and remote LV (or equivalent sham regions) to the RV region of that respective heart. An example of this is shown in the table above where data from the RV region and the peri-infarct of an MI heart is shown (both regions have come from the same heart). The calculation is performed in a step-wise order: (1) Calculate ΔC_T (mean *Runx* Ct – mean *Gapdh* Ct) for the region; (2) Calculate $\Delta\Delta C_T$ (ΔC_T of region of interest – ΔC_T of RV); (3) Calculate $2^{-\Delta\Delta C_T}$, the value is expressed as the relative quantitation (RQ) value. In the example above, *Runx* expression is 1.44-fold higher in the peri-infarct region of the MI heart than the respective RV.

Example 3: analysis of gene expression between the four different rat strains – whole LV samples.

WKY					WKY-congenic				
	<i>Runx</i> C _T	<i>Gapdh</i> C _T	ΔC_T	$2^{-\Delta C_T}$		<i>Runx</i> C _T	<i>Gapdh</i> C _T	ΔC_T	$2^{-\Delta C_T}$
	15.34	14.62				16.44	14.63		
	15.25	14.38				16.39	14.88		
	15.20	14.84				16.58	14.69		
Mean	15.26	14.61	0.65	0.64	Mean	16.47	14.73	1.74	0.30

Figure 2.30 Sample qRT-PCR data analysis of congenic rat tissue using the $2^{-\Delta C_T}$ method.

Samples were analysed using qRT-PCR and the Ct data from the *SDS* software was imported into Microsoft Excel. Each sample was performed in triplicate, represented by three Ct values for each gene in this example. Two samples are shown; whole LV homogenates for a (i) WKY heart and a (ii) WKY-congenic heart.

Runx expression between the different rat strains was compared using the $2^{-\Delta C_t}$ method. This method was chosen because, like the whole heart MI samples, there was no reason to pair samples with each other therefore the $2^{-\Delta\Delta C_t}$ method was not appropriate to use. Instead the mean \pm SEM for each strain was calculated from single data points using the $2^{-\Delta C_t}$ value. In this example above, the WKY-congenic shows a 2-fold reduction in *Runx1* expression compared to WKY.

2.12.7 Limitations of the technique

qRT-PCR has several advantages in that it is fast, extremely sensitive, highly reproducible and can be integrated into high-throughput systems making it a very powerful tool for performing accurate gene expression. However despite these advantages there are caveats associated with qRT-PCR. The most common is the selection of a suitable reference gene. It is necessary to use a housekeeping/reference gene in qRT-PCR as a normalisation strategy to control for error between samples. Performing each well in triplicate controls for pipetting error but the housekeeping gene is required to control for differences in cDNA concentration *not* due to pipetting error. Housekeeping genes are usually cellular maintenance genes that regulate basic functions of the cell and are therefore ubiquitously and ideally uniformly expressed during all experimental conditions. They serve as a 'common denominator' to which the target gene is normalised and control for variation in the amount of starting material between samples, e.g. from variation in (i) RNA integrity, (ii) differences in RT efficiencies, and (iii) cDNA sample loading variation.

- (i) Variations in RNA integrity (and purity) can occur if the RNA becomes degraded due to exposure to RNases or improper storage, and contaminants (phenol or proteins) may be present from incomplete purification during the RNA extraction process. Degraded RNA can lead to shorter cDNA products and contaminants in the RNA can affect the activity of the reverse transcriptase enzyme therefore leading to reduced cDNA. This would result in a lower gene expression of the housekeeping gene and would indicate that the altered expression of the target gene of interest would be questionable.
- (ii) The reverse transcription process should occur with 100% efficiency (that is, 1 μ g RNA is converted into 1 μ g cDNA). In reality, this is not always the case and this may be due to factors that affect the activity of the transcriptase enzyme such as the presence of contaminants (as described before), incorrect temperature ($>42^\circ\text{C}$ reduces the activity of the *Omniscript* transcriptase enzyme; *Qiagen Omniscript Kit handbook*)

or incorrect concentration of primers (including degradation of primers) and dNTPs. To minimise these problems, only RNA of minimum purity ($A_{260}/A_{280} > 1.8$) was used, reactions were performed in a controlled incubator at 37°C and reagents were kept on ice and stored at -20°C to minimise degradation, and primers/dNTPs were always mixed by gentle vortex prior to use to ensure thorough mixing. If the efficiency of the reaction was markedly affected this would lead to a reduction in the concentration of cDNA, which would result in a lower gene expression of the housekeeping gene and therefore indicate that the altered expression of the target gene of interest would be questionable.

- (iii) The third source of variation could arise from cDNA sample loading – this means that if unequal cDNA concentrations were used between different samples, for example if the cDNA was not diluted correctly or if too little/too much was added (this does not include minor errors which are not always avoidable due to the nature of pipetting). Incorrect starting cDNA template could bias results leading to over/under-representation of true gene expression levels which would be informed by the over/underexpression of the housekeeping gene. This was avoided as much as possible by ensuring dilutions of 1:5 of cDNA were always performed as accurately as possible.

2.12.7.1 Choice of suitable housekeeping gene

Without appropriate normalisation to a housekeeping gene, small differences between genes of interest may be missed (variability in the housekeeping gene would obscure small changes making them difficult to detect), or results may be misrepresented – for example fluctuations in the housekeeping gene can lead to over/under-estimation in the expression of the gene of interest (if the housekeeper expression is reduced or increased respectively) and this can make it extremely difficult to interpret the real changes. A suitable housekeeping gene is one which shows no differences in expression between the treatment groups. It is best practice to test a number of different housekeeping genes and choose the most suitable rather than arbitrarily selecting a single unvalidated gene. For this thesis a preliminary study was performed to test three different housekeeping genes based on some of the most stable in mouse MI according to previous housekeeping gene studies: *Gapdh* (a glycolysis enzyme), ribosomal protein P0 (*Rplp0*) and hypoxanthine-guanine phosphoriboyltransferase (*Hprt*; an enzyme involved in purine nucleotide generation).

Gapdh is widely used in cardiovascular studies and is the most frequently reported housekeeping gene in the literature for MI (as researched by Brattelid *et al.*, 2010). However there are discrepancies in the literature in the suitability of *Gapdh* in mouse MI; for example *Gapdh* has been reported to be one of the most stable genes in mouse MI (Brattelid *et al.*, 2010) but contrary to this, it has also been revealed as the one of the least stable in mouse infarcted tissue (Everaert *et al.*, 2011). *Gapdh* was also found to be the most stable housekeeping gene in rat infarcted and peri-infarct tissue (Zhao *et al.*, 2011). However it is being increasingly accepted that housekeeping genes behave very differently depending on the study design and the experimental conditions involved. Therefore while a housekeeping gene may be unsuitable for one study, it may be acceptable under similar conditions of another. Following the advice of Everaert *et al.*, 2011 which warned against the use of *Gapdh* in mouse infarction tissue, we also tested their recommended alternative gene reported to be the least variable in mouse MI (*Hprt*). *Rplp0* was additionally chosen as it has been shown to be stable regardless of cardiac disease state (Moniotte *et al.*, 2001) and ribosomal genes also feature highly as non-variable genes in MI (Everaert *et al.*, 2011; Perez *et al.*, 2007). These three housekeeping genes (*Gapdh*, *Rplp0* and *Hprt*) were therefore quantified using qRT-PCR and were ranked based on a criteria of low variance published by Mane *et al.*, 2008 (Mane *et al.*, 2008). This method is based on the idea that under ideal conditions, fluctuations in housekeeping gene expression would not vary much from a mean (i.e. have low standard deviation (SD)). Therefore the variance was assessed in the Ct and each candidate gene was ranked based on the SD (see example calculation below).

Example 4: analysis of stability of the housekeeper gene

MI Model – whole heart samples:

Using the data from Example 1 above, the *Gapdh* Cts for sham whole heart were (17.8, 17.4, 17.9) and whole heart MI were (17.7, 17.8, 17.9). The method for assessing the suitability of the housekeeping gene between whole heart groups (sham vs. MI) was based on comparing the fold change between groups using the mean (of the triplicates) Ct for 2^{-Ct} as recommended by published methods (Schmittgen & Livak, 2008). For the values given in this example, the mean *Gapdh* Ct for sham and MI were 17.7 and 17.8 respectively. The fold change between the two is MI/sham ($17.8/17.7$) = 1.01 which equates to 1% fold-change between sham and MI and by using the *P* value to indicate whether the differences were significant also aided in determining the suitability of the housekeeping gene – in this

example therefore it was suitable between this pair. This method was used for all animals by taking the mean 2^{-Ct} value for all animals (sham and MI).

MI Model – regional heart samples (SD method):

For regional variations, as there were more than two samples, fold-change between all four was not possible using the above method. Therefore the method used was based on the SD between the regions as mentioned above and published by Mane *et al.* (2008). The SD calculation was performed as follows: (i) firstly, the mean Ct for each individual region from all hearts (sham and MI) were compared and tested for statistical significant differences using ANOVA (with Tukey post-test) to yield a *P* value as shown in Figure 2.31A(i),B(i); a *P* value of <0.05 signified that the raw Ct values between sham and MI were significantly different and the housekeeping gene being tested was unsuitable (ii) secondly, the regional mean Ct values were pooled to yield a single mean Ct for either sham or MI; (iii) the SD between this single sham and single MI mean Ct value was calculated using the standard formula for SD:

$$SD = \sqrt{\frac{\sum(x - \bar{x})^2}{n - 1}} \quad \text{Eq. 13}$$

Where \sum is the sum of, x is a value in the data set, \bar{x} is the mean of all values in the data set, n is the number of values in the data set.

The resulting SD of each housekeeping gene is shown in red in Figure 2.31; the SD value was used to rank the genes in order with lowest SD being most suitable and highest SD the least suitable gene.

Results: The results of this method are shown in Figure 2.31 and these data have shown that *Gapdh* was the most stable gene of the three with the lowest SD and showed no significant differences in expression between sham and MI. *Hprt* was tested in the infarct region and showed that there was a small but significant difference in the Ct values between sham and MI with a high SD, therefore *Hprt* was considered the least suitable in this study. *Rplp0* was the neither the best nor worst of the three, however data was only available from $n=1$ sham therefore the results were somewhat inconclusive for this gene. Based on these validation experiments, *Gapdh* was chosen as the housekeeping gene for all mouse qRT-PCR experiments. Based on these results, *Gapdh* was also tested for

suitability in the different strains of rat heart tissue for the congenic rat model studies and was also found to be stable with no significant differences observed between the 4 strains (Figure 2.32).

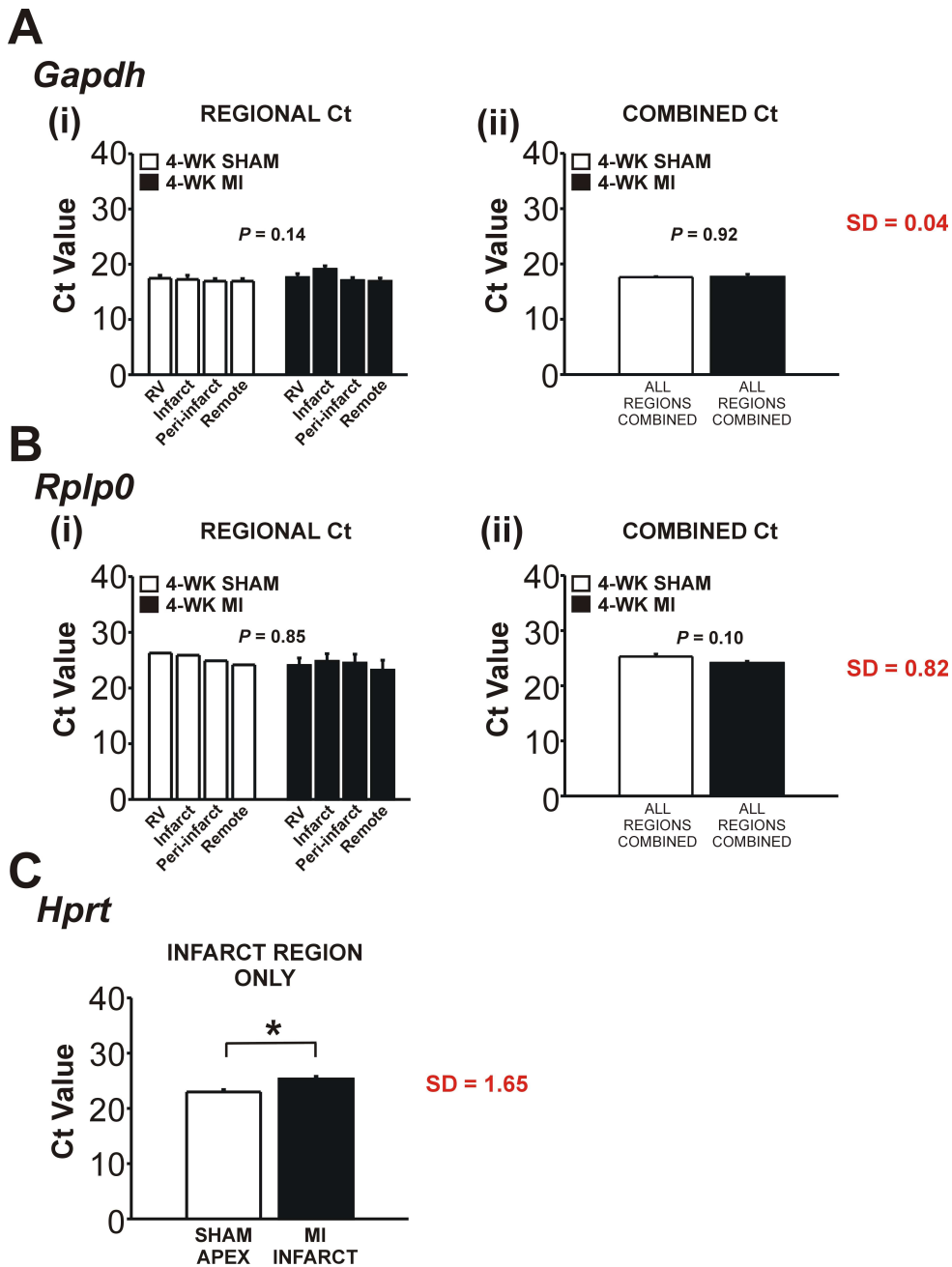


Figure 2.31 Comparison of different housekeeping genes for qRT-PCR between sham and MI hearts.

(A-i) Comparison of raw Ct values from different regions of 4-wk sham hearts ($n=5$) and 4-wk MI hearts ($n=8$) and (A-ii) values for the regions combined using *Gapdh*. (B-i) Comparison of raw Ct values from different regions of 4-wk sham hearts ($n=1$) and 4-wk MI hearts ($n=5$) and (B-ii) values for the regions combined using *RPL0*. (C) Comparison of raw Ct values from 4-wk sham apex ($n=3$) and 4-wk MI infarct region ($n=3$). The standard deviations (SD) between the two groups for each housekeeping gene are shown in red. The P value indicates whether there were any significant differences in the mean Ct value between groups overall and was used in conjunction with the SD method. $*P<0.05$ using ANOVA for more than two groups (regional data) or student's unpaired t-test for comparisons between two groups only (combined regions).

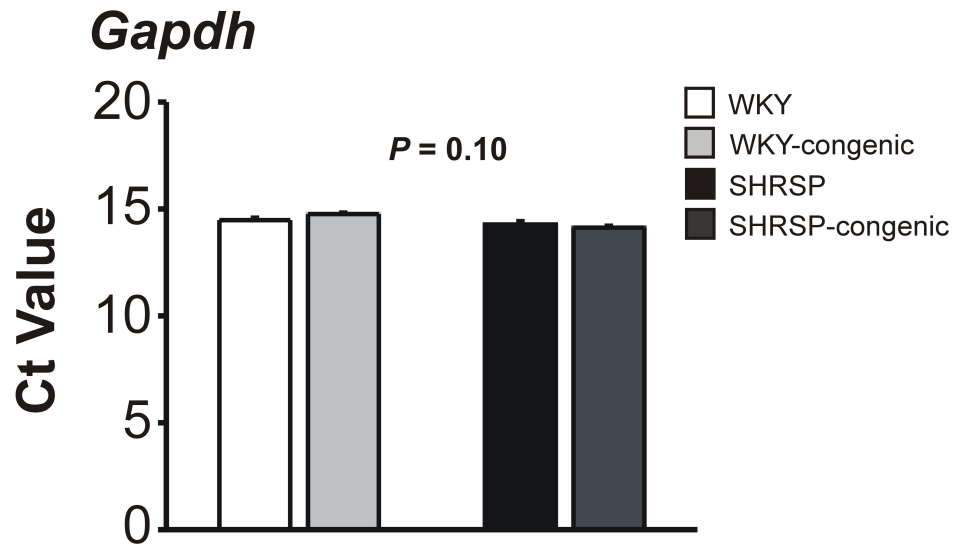


Figure 2.32 Validation of *Gapdh* as a suitable housekeeping gene between four different rat strains.

Raw Ct values are shown for each group; WKY (white bar; $n=5$), WKY-congenic (light grey bar; $n=5$), SHRSP (black bar; $n=5$) and SHRSP-congenic (dark grey bar; $n=5$). Statistical significance was tested using ANOVA with a Tukey multiple comparisons post-test. The resulting P value from this ANOVA test across the four groups is shown. These data indicate that there was no significant difference in the Ct value of *Gapdh* between the hearts from the four different rat strains overall.

CHAPTER 3

Characterisation of a mouse model of myocardial infarction

3.1 Introduction

3.1.1 MI is a serious public health problem

CVD is the leading cause of death in Europe and the U.S. estimated to account for 49% and 37% of all mortalities respectively (Petersen *et al.*, 2005; Thom *et al.*, 2006). The majority of CVD-related deaths are due to coronary heart disease (Petersen *et al.*, 2005; Thom *et al.*, 2006) which is the atherosclerotic narrowing or thrombus occlusion of coronary arteries, both of which can lead to MI and eventual HF (Libby, 2001). Despite considerable progress in the prevention and treatment of CVD, MI leading to HF continues to be a highly prevalent source of morbidity and mortality (Allender *et al.*, 2006). Current treatments for MI such as coronary artery bypass, percutaneous interventions and dissolution thrombotic therapies are successful in slowing the disease and improving patient symptoms and quality of life (Hermanides & Ottervanger, 2008), however, paradoxically the advances in the treatment of MI have led to an increased prevalence of chronic HF; this is because patients are surviving the initial insult but have to live with a severely compromised heart (Thomas *et al.*, 2008). More effective treatments are therefore required to slow the progression of HF.

3.1.2 Need for an animal model of MI

In order to manage and treat MI and HF more effectively, it is important to understand the pathophysiology and underlying mechanisms of the disease so that suitable therapeutic treatments can be developed. Experimental animal models that closely resemble human disease characteristics have proven invaluable for this (Hasenfuss, 1998; Klocke *et al.*, 2007). Much of the work that has advanced our understanding of MI and HF over the past four decades would not have been possible without the use of animal models. CVD research performed on animals has yielded invaluable information about alterations in neurohormonal activity (McCullagh *et al.*, 1972), myocardial function (Magovern *et al.*, 1992) and molecular changes (Dodd *et al.*, 1993) that occur in the failing heart after MI. Animal models of MI and HF are therefore highly beneficial for CVD research.

3.1.3 Surgical methods of inducing MI in an animal model

As mentioned previously, human MI is characterised by atherosclerotic narrowing of coronary arteries (Libby, 2001). Animal models of MI are therefore based on methods that result in partial or complete occlusion of a coronary artery. This is typically performed

through the use of surgical intervention methods. The advantage of using a surgical approach rather than alternative methods such as dietary (Wilson & Hartroft, 1970) or genetic-inducing strategies (Chu *et al.*, 2002) to induce natural atherosclerotic development is that surgical methods allow more precise control over timing, location and extent of infarction which provides more reproducible results. Depending on the nature of ischaemic injury required for the purposes of the study, a number of different methods have been described utilising physical occluders, freezing and ligation approaches. Most surgical interventions involve placing the animal under anaesthesia, performing a left thoracotomy to expose the heart and implementing the relevant coronary artery occlusion method (Klocke *et al.*, 2007). The most widely used method of inducing MI in an animal is by ligating a coronary artery using a band (large animals) or thin suture (small animals) (Klocke *et al.*, 2007). Alternative methods have been reported and each method has numerous advantages and disadvantages associated with the suitability of inducing MI similar to the human phenotype, descriptions of each are detailed below.

3.1.3.1 Occluding devices

Occluder devices such as hydraulic or ameroid occluders have been described in large animal models, for example swine (Harada *et al.*, 1994) as a method of inducing MI through coronary artery stenosis (Roth *et al.*, 1987). These occluders are constriction devices that are implanted around the coronary artery and either inflated (balloon occluder or hydraulic occluder) or constricted (ameroid) to a controlled extent to cause partial or complete occlusion. These occluders are useful in that they can gradually occlude over a long period of time that will allow formation of collaterals therefore mimicking human MI (St Louis *et al.*, 2000), however implantation requires a high level of surgical expertise and moreover due to their size are restricted to use in larger animals only (Dixon & Spinale, 2009).

3.1.3.2 Embolisation

Another example of an animal model of MI is based on intracoronary embolisation with microspheres or agarose beads using catheter-mediated injections (Sabbah *et al.*, 1991). This technique is advantageous in that it closely resembles the clinical cause of MI in humans due to the embolisation of atherosclerotic and thrombus plaques that build up inside the artery wall (Topol & Yadav, 2000). There is also the added advantage that the embolising agents are administered percutaneously, therefore the risk of infection or inflammation associated with thoracotomy is reduced (Erbel & Heusch, 2000). The

technique has been successful at inducing LV dysfunction, myocardial fibrosis and hypertrophy in dogs (Sabbah *et al.*, 1991) however due to the nature of the technique it is also restricted to larger animal models only (Grund *et al.*, 1999).

3.1.3.3 Cryoinjury

Cryoinjury is another method of inducing infarction which has been described in smaller animal models such as rats (Ciulla *et al.*, 2004) and mice (van den Bos *et al.*, 2005). This involves applying a cryoprobe to the LV free wall for approximately 10 s and the freezing temperature (-175 to -190°C) disrupts coronary blood flow. Cryoinjury is unique among these methods in that cell death occurs immediately as a result of the freezing insult, rather than from a developing ischaemia process and therefore it does not induce the injury in the same way that a naturally developing ischaemia-induced injury occurs in human MI (van den Bos *et al.*, 2005). Cryoinfarctions in mice have been shown to cause reduced contractility and diastolic dysfunction to a similar extent as coronary artery ligation after 8 weeks, however the injury results in smaller infarct sizes, not always transmural and with only modest LV structural remodelling (van den Bos *et al.*, 2005).

3.1.3.4 Coronary artery ligation

CAL is the most commonly used approach for surgically inducing MI; this involves tying a ligature around a coronary artery for either transient or permanent occlusion (Klocke *et al.*, 2007). CAL has been extensively used for a large number of years as a very effective method of inducing MI in a variety of animal species including dog (Hood, Jr. *et al.*, 1967), sheep (Gorman, III *et al.*, 1998), rabbit (Smith *et al.*, 2006), rat (Pfeffer *et al.*, 1979b) and mouse (Michael *et al.*, 1999). CAL does have some drawbacks, one being the damage made around the ligature; inserting a suture into the myocardium inevitably will include muscle mass as well as veins, nerves and lymphatic vessels which could affect the level of coronary artery stenosis (Klocke *et al.*, 2007). CAL is subject to infarcts with varying size which may mean a large group of animals may be required (Zimmer *et al.*, 1990). Despite its limitations, the CAL technique has many advantages which make it a very attractive choice for surgical MI methods. Firstly, the ability to produce a range of infarct sizes can also be considered a strength of the technique as it provides flexibility in the extent of infarction that may be useful for the study. Secondly, CAL is not restricted to larger animals as some of the other techniques are, and is therefore suitable for rodents including mice, which have become increasingly popular in the field of cardiac research due to the availability of transgenic strains in this species (Rockman *et al.*, 1994;Svenson

et al., 2003). The ligature can be placed for either permanent or temporary occlusion and therefore can be used for ischaemia-reperfusion (I/R) models as well as permanent occlusion models providing greater scope for use (Michael *et al.*, 1995).

3.1.4 How well does CAL-induced experimental MI resemble human MI?

If an animal model is to be used to study human disease it is imperative that the animal model closely resembles the human disease as far as possible. MI is caused by acute occlusion of coronary arteries in human patients by thrombosis and leads to a cascade of events that ultimately alter the functional and structural properties of the heart that can eventually lead to the development of HF.

3.1.4.1 Characteristics of human MI

The loss of contractile mass from the infarcted area causes an acute reduction in cardiac pump function. Stroke volume and cardiac output however are initially maintained through the action of adrenergic signalling pathways which increase Ca^{2+} influx and SR activity to increase contractility in the surviving cardiomyocytes (Levick, 2010). Enhanced contractility in the surviving myocardium is believed to induce cardiomyocyte hypertrophy, whereby individual cardiomyocytes through the action of increased sarcomeres have the ability to increase in cell size, thereby increasing contractile mass and offering further support against the wall stress demands (Pfeffer & Braunwald, 1990). Over time, the ventricles dilate further increasing the work of the surviving myocardium (Weisman & Healy, 1987). The dilated ventricle is further supported by increased deposition of collagen within the infarcted region to provide structural support and preserve the structural integrity of the myocardium (French & Kramer, 2007). These adaptive responses which maintain SV and CO within normal physiological ranges are collectively known as compensatory remodelling. However, persistent strain on the surviving cardiomyocytes leads to abnormalities in their Ca^{2+} -handling properties: Ca^{2+} transient and action potential durations are prolonged and SR Ca^{2+} uptake rates are slowed (Pogwizd *et al.*, 2001). Initially this can cause diastolic dysfunction but with preserved systolic function. These changes are responsible for the slowing of contraction and relaxation rates and prolonged relaxation duration that ultimately lead to impaired contraction and relaxation of the ventricles. As contraction and relaxation abnormalities worsen to the point where the heart cannot maintain a sufficient CO, this is classified as HF (McMurray & Pfeffer, 2005). Therefore in summary, human MI can present

diminished systolic and diastolic function, ventricular dilation and infarct thinning with increased collagen deposition (French & Kramer, 2007).

3.1.4.2 CAL-induced experimental MI

The CAL method has been applied to large animals such as the dog and pig but it is reportedly problematic in these species due to high mortality rates (>50% in dog) mainly from ventricular tachycardia (Hood, Jr. *et al.*, 1967). Moreover, dogs have a very extensive collateral coronary circulation which therefore restricts infarct size to only 20% of the LV in many cases and as a result produces only minor haemodynamic alterations (Hood, Jr. *et al.*, 1967). Therefore CAL-induced MI is commonly used in smaller laboratory species such as the rat and mouse largely because of the lower costs associated and with the recent technological advances in miniature instruments for measuring cardiac parameters they have become popular species for use in cardiac research (Patten & Hall-Porter, 2009). CAL models in the rat have been well-documented. CAL-induced MI results in impaired LV function with reduced systolic function and increased filling pressures in rats (Pfeffer *et al.*, 1979b). Rats with infarctions greater than 46% of the LV develop congestive HF after 3-6 weeks with elevated filling pressures and reduced cardiac output (Pfeffer *et al.*, 1991b). As mentioned previously, the mouse has become a popular species of choice for the MI model as it carries the unique ability to manipulate specific genes that may be important for post-infarction remodelling not possible with any other species (Svenson *et al.*, 2003). The mouse, like the rat, demonstrates both systolic and diastolic dysfunction (Shioura *et al.*, 2007) with evidence of LV remodelling (Sam *et al.*, 2000). Further details of the phenotype of murine models of MI reported by others are described in Table 3.1.

Table 3.1 Characteristics of murine models of MI using the permanent CAL method.

Animals	Phenotype	Reference
Male and female Kummung mice (24-30g).	Myocardial necrosis after 24h Infarct size $44.3 \pm 2.9\%$ of LV after 24h	Wang <i>et al.</i> A simple and fast experimental model of myocardial infarction in the mouse (2006).
Male C57Bl/6 mice (20-25g; 6-10 wk old).	33% survival after 1-wk 30.8% reduction in ESP compared to sham after 1-wk	Degabriele <i>et al.</i> Critical appraisal of the mouse model of myocardial infarction (2004).
Male Swiss mice (30-45g; 10-12 wk old).	3-fold reduction in LV wall thickness (5-wk post-MI) 2.1-fold increase in LV diameter (5-wk post-MI) Infarct size $47.7 \pm 5.2\%$ of LV circumference (5-wk post-MI) Positive Sirius red collagen levels peaked 7.8-fold higher than sham at 2-wk, dropped thereafter but remained ~2-fold higher at 3-wk and 5-wk No differences in HW/BW ratio by 5-wk post-MI Reduction LV ESP, dP/dt _{max} , dP/dt _{min} (exact fold change not available)	Lutgens <i>et al.</i> Chronic myocardial infarction in the mouse: cardiac structural and functional changes (1999).
Male and female C57Bl/6 mice (18-22g; 8-10 wk old).	At 2-wk post-MI: 60% survival 1.7-fold increase in LV mass compared to sham Increased systolic (1.7-fold) and diastolic (1.3-fold) diameter (echo) compared to sham. Fractional shortening reduced by 30.9% of sham (echo).	Kumar <i>et al.</i> Distinct mouse coronary anatomy and myocardial infarction consequent to ligation (2005).
Female C57Bl/6 mice (20-25g; 4-6 wk old).	At 9-days post-MI: 60% survival 2.5-fold increase in EDV (MRI) 6.6-fold increase in ESV (MRI) EF reduced from 72 to 31%	Caiani <i>et al.</i> Analysis of regional left ventricular function in the post-infarct mouse by magnetic resonance imaging with retrospective gating (2008).
Male C57Bl/6 mice (6 wk old).	Apoptosis of cardiomyocytes at 48h	Bialik <i>et al.</i> Myocyte apoptosis during myocardial infarction in the mouse localizes to hypoxic regions but occurs independently of p53 (1997).
Male C57Bl/6 mice (20-25g; 8-10 wk old)	At 6-wk post-MI: 68% survival Infarct size $38.6 \pm 15.2\%$ 12.4% reduction in SBP 41.0% increase in EDP 24.1 and 28.2% reduction in dP/dt _{max} and dP/dt _{min} 14% increase in LV mass/BW ratio 25.6% increase in end-diastolic diameter (echo) 40.7% increase in end-systolic diameter (echo) 36.4% reduction in fractional shortening (echo)	Patten <i>et al.</i> Ventricular remodelling in a mouse model of myocardial infarction (1998).
Male C57Bl/6 mice (10-12 wk old).	Collagen accumulation at days 7-14, scar completed by day 21 Infarct size $47.3 \pm 5\%$ (4-wk), $45.3 \pm 5\%$ (8-wk) 60% increase in HW/BW ratio at 4-wk post-MI No change in lung weights at 4-wk or 8-wk nor by 24-wk	Yang <i>et al.</i> Myocardial infarction and cardiac remodelling in mice (2002).
Male C57Bl.6 mice (20-30g; 10 wk old).	Survival after 12-mo 70% Decrease in EF from 64% to 33% at 6-mo 100% increase in EDP at both 6- and 12-mo 38% increase in LV hypertrophy at 6-mo 53% increase in LV chamber size at 6-mo Infarct size $40.7 \pm 1.9\%$	Pons <i>et al.</i> Survival, haemodynamics and cardiac remodelling follow up in mice after myocardial infarction (2003).

Given the well-documented success of the CAL method in mouse models of MI and its close similarities to the human disease phenotype, the CAL model was the choice of method for inducing experimental MI in mice for the work in this thesis. Furthermore, there are also a number of projects anticipated that require genetic manipulation in this model and therefore the mouse was the best species to use for this.

3.1.5 Aims

The aims of the work presented in this chapter were to perform a detailed characterisation of the mouse model of MI in terms of (i) cardiac structural and functional alterations and (ii) associated surgical success rates and survival characteristics of the model. As this was a new model in our laboratory, it was necessary to characterise the phenotype (including both mechanical and electrical activity) to ensure the model developed LV dysfunction. It was hypothesised that inducing MI in mice by CAL would produce a model of LV dysfunction and structural remodelling comparable with other published mouse models of MI using the CAL method.

3.2 Methods

3.2.1 Induction of MI

Adult male C57Bl/6 mice (aged 8-10 weeks; 20-25 g) underwent MI by CAL as previously detailed in the General Methods Section 2.1. Control sham-operated mice underwent the same procedure but without CAL. Mice were permitted to recover up to 4 or 8 weeks following the procedure at which point they underwent *in vivo* functional assessment (PV loop and analysis) and their hearts were harvested for subsequent morphological and histological analyses as described in the General Methods Section 2.3 and 2.4. Animals were inspected daily for mortality and any found dead underwent post-mortem analysis to identify the cause of death.

3.2.2 Experimental timeline

A schematic of the experimental timeline is shown in Figure 3.1. Following CAL, animals were randomly assigned to one of the two following groups: (i) 4-wk group and (ii) 8-wk group as detailed above. Sham-operated animals were also randomly assigned to one of the two study groups (4-wk or 8-wk).

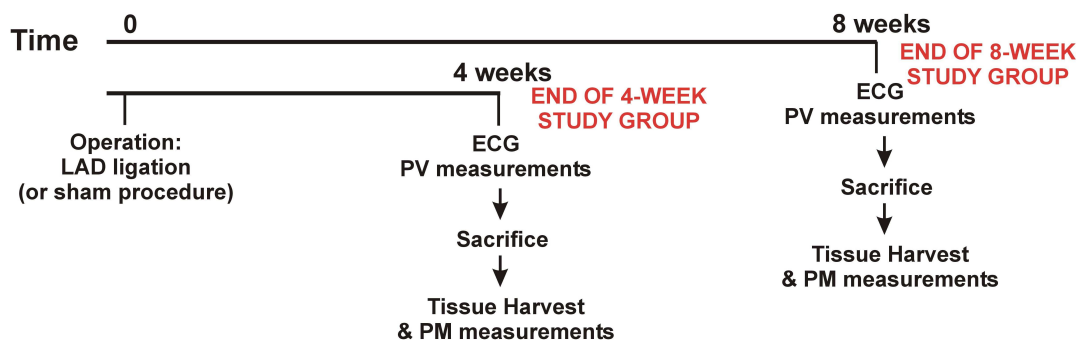


Figure 3.1 CAL model experimental time line.

3.2.3 Haemodynamic assessment of LV function

Mice underwent PV measurements either at 4 wk or at 8 wk after MI as described in the General Method Section 2.3. Briefly, mice were anaesthetised (4% isoflurane), intubated with a 0.7 mm cannula and ventilated using a rodent respirator (1.5-2% isoflurane, 120 μ l tidal volume, 120 breaths per minute). A rectal thermocouple probe connected to a feedback control unit maintained core body temperature of the animal between $37.0 \pm 0.5^\circ\text{C}$ throughout the procedure. Following a midline cervical incision, a 1.2F PV catheter (*SciSense, Ontario, Canada*) was inserted into the LV of the heart *via* the right common carotid artery. PV data were recorded at baseline and during reduced preload by transient vena cava occlusion. The parallel conductance of surrounding conductive structures was offset by administering an intravenous 10 μ l bolus of 15% hypertonic saline.

3.2.4 Assessment of electrical cardiac function

Mice underwent ECG assessment either during the CAL surgery, and/or at 4 wk or at 8 wk after MI as described in the General Methods Section 2.4. Briefly, mice were anaesthetised and sustained under spontaneous breathing conditions through a face mask (1.5-2% isoflurane) while a rectal thermocouple probe connected to a feedback control unit maintained core body temperature at $37.0 \pm 0.5^\circ\text{C}$. Subdermal needle leads were placed on the front and hind forelimbs in a lead II configuration and ECG measurements were recorded for a 5 minute time period.

3.2.5 Harvesting of hearts

Animals were sacrificed at 4 or 8 wk after MI and the heart was removed and washed in ice-cold saline (0.9% NaCl w/v). The aorta was cut transversely, mounted on to a 23G

cannula attached to a syringe and perfused retrograde with ice-cold saline to rinse blood out of the coronary vessels. Hearts were blotted dry on tissue paper and weighed using a precision electronic balance and subsequently either fixed in formalin for histological analysis or snap-frozen in liquid nitrogen and stored at -80°C until needed for biochemical experiments.

3.2.6 Preparation of heart sections

Hearts taken for histological analysis included the whole intact heart (atria, ventricles and major blood vessels). Hearts were given a minimum fixation time of 24 hr in formalin to allow sufficient time for fixative to penetrate the tissue. After sufficient fixation, hearts were embedded into a wax block until required for sectioning. The heart was sliced parallel to the long axis of the heart to produce multiple sections $1\mu\text{m}$ thick with an interval of 250-300 μm between each section. At each interval, adjacent sections were taken, one for each stain: (i) H&E, (ii) Sirius red and (iii) RUNX1-specific antibody (for work detailed in Chapter 4).

3.2.7 Morphometry and infarct measurements

For each heart, at least five serial sections (approximately 250-300 μm between each section) were taken for morphometric and infarct size measurements to ensure a range of depths through the heart. All sections were examined with an *Olympus BX51* microscope and images were captured with an *Olympus DP71* camera with the use of *Cell D* software.

3.2.7.1 LV wall thickness and LV area

LV wall thickness and LV area were measured using serial H&E sections of each heart as described in the General Methods Section 2.8.1 and 2.8.2. The wall thickness was measured as the distance between the endocardium and epicardium of the infarcted myocardium using a line perpendicular to the curvature of the ventricular wall. LV area was measured from the same sections by tracing around the endocardium inside the LV. Both chamber size and wall thickness were measured using *ImageJ* software and measurements were performed on all sections of each heart to yield a mean value for each heart. Qualitative histopathological changes in myocardial tissue following MI were assessed using H&E and Sirius red stained sections of the heart.

3.2.7.2 Infarct size

Infarct size was measured on sections stained with Sirius red using a length-based approach similar to the method published by Takagawa *et al.*, 2007 as described in the General Methods Section 2.8.3. Briefly, four lengths were measured from each heart section: epicardial infarct length, endocardial infarct length, epicardial total circumference and endocardial total circumference. The infarct included all infarcted myocardium which was >50% of the total thickness of the myocardium. Epicardial and endocardial infarct ratios were then calculated by dividing the sum of epicardial or endocardial lengths from all sections by the sum of all epicardial or endocardial circumferences from all sections respectively. Infarct size was then calculated using the following equation:

$$\text{Infarct size (\%)} = \frac{\text{EPI infarct ratio} + \text{ENDO infarct ratio}}{2} \times 100 \quad \text{Eq. 14}$$

3.2.7.3 Collagen levels

Collagen levels in the heart were estimated from Sirius red sections using *ImageProPlus* software as described in the General Methods Section 2.9.2. The number of red pixels above a set threshold of red colour were counted and expressed as a percentage of total pixels in the heart.

3.2.8 Lung and liver weights

The lungs and liver were harvested, blotted dry on tissue paper and weighed using a precision electronic balance as described in the General Methods Section 2.3. Tibial length measurements were also taken as a normalising reference for lung, liver and heart weights. Since the animals were at an age where they may still be growing, the tibial length was used as a more accurate normalising reference than body weight.

3.2.9 Cardiomyocyte isolation and measurements of cell length, width and estimated cross-sectional area

Cardiomyocytes were isolated using a standard digestion protocol with collagenase and protease from 4-wk sham and 4-wk MI hearts as described in the General Methods Section 2.10.1. Briefly, hearts were removed and perfused retrogradely at 4 ml.min⁻¹ with a modified KH solution containing 0.7 mg.ml⁻¹ collagenase (*type I, Worthington, New Jersey USA*) and 0.07 mg.ml⁻¹ protease (*type XIV, Sigma Aldrich, UK*) for 7 minutes followed by

6 minutes of KH solution containing 0.7% bovine serum albumin (BSA, *Sigma Aldrich, UK*). The perfusion was then stopped and the LV free wall cut into strips and mixed in KH solution with 0.7% BSA to yield a cell suspension of single cardiomyocytes. Isolated cardiomyocytes were visualised by light microscopy and captured using a camera (*Q imaging Rolera-XR*) and *QCapturePro software*. Cardiomyocyte length and width was determined from a group of hearts using *ImageJ* software and cross-sectional area was estimated using the equation as detailed in the General Methods Section 2.10.2.

$$\text{Cross sectional Area} = \pi \left(\frac{\text{cell width}}{2} \right)^2 \quad \text{Eq. 15}$$

3.2.10 Data recording and statistical analysis

All PV and ECG data were recorded on a *Dell* laptop using *LabScribe2* software at a sampling rate of 1000 samples.s⁻¹ and analysed offline using *LabScribe2* software. All data in the text and figures are expressed as mean ± SEM. Statistical significance was measured using student's paired or unpaired t-test for comparisons between a maximum of two groups, or ANOVA followed by the Bonferroni or Tukey post-hoc test where appropriate for comparing more than two groups. For the survival study, Kaplan-Meier analysis was used and statistical significance tested using the Log-rank (Mantel-Cox) test. A *P* value of <0.05 was considered statistically significant.

3.3 Results

3.3.1 Survival following MI

Mice underwent surgically induced MI (*n*=137) or a sham operation (*n*=60). Survival data for these procedures are presented in Figure 3.2. As shown in Figure 3.2A (i), MI leads to significantly reduced survival (end-point survival rate 63% after MI vs. 100% for sham operations; *P*<0.05). Of the 197 mice that underwent surgery, 73 did not survive to the end of the study and reasons for this are shown in Figure 3.2A (ii). 50% of the deaths were due to cardiac rupture, 45% occurred intra-operatively (28% of these were attributable to mechanical ventilation issues; the other 17% were related to another unidentified aspect of the surgical procedure), 4% developed severe clinical symptoms within the first week of MI (extreme dyspnoea, lethargy and rapid weight loss) and were killed humanely using an appropriate Schedule 1 method; the remaining 1% died after the first week of the procedure for reasons that could not be identified from a post-mortem. The majority of

deaths following MI occurred within the first week of the operation (99%) and it was very rare to lose animals beyond the first week (1%). As this was a new model in our laboratory, efforts were made to minimise mortalities to achieve the highest possible success (survival) rates. Figure 3.2A (iii) shows how mortality changed over the course of learning the technique and how this affected the overall survival. The current values are denoted by the last point on the graph of Figure 3.2A (iii). It can be seen that with experience of the technique, deaths from ventilation issues and from cardiac rupture were reduced by 64.8% and 86.1% respectively (current *vs.* highest incidence). Intra-operative deaths were reduced by 100% to zero (current *vs.* highest incidence). In reducing mortalities over the course of developing the technique, the overall survival rate of the model was increased by 63.3% (current *vs.* lowest incidence). Current survival success rates were 78% for MI and 100% for sham-operated animals.

3.3.1.1 Cardiac rupture

The most common cause of mortality in this model was cardiac rupture. All animals were monitored daily and any animals found dead were examined by autopsy for evidence of cardiac rupture. Cardiac rupture was confirmed by the presence of a pool of clotted blood surrounding the heart within the chest cavity (Figure 3.2B(i-a) and by the presence of a visible tear on the LV free wall of the heart (Figure 3.2B(i-b)). Cardiac rupture always occurred in the first week of MI between day 3-6 (Figure 3.2B (ii)); it did not occur before day 3 nor after day 7.

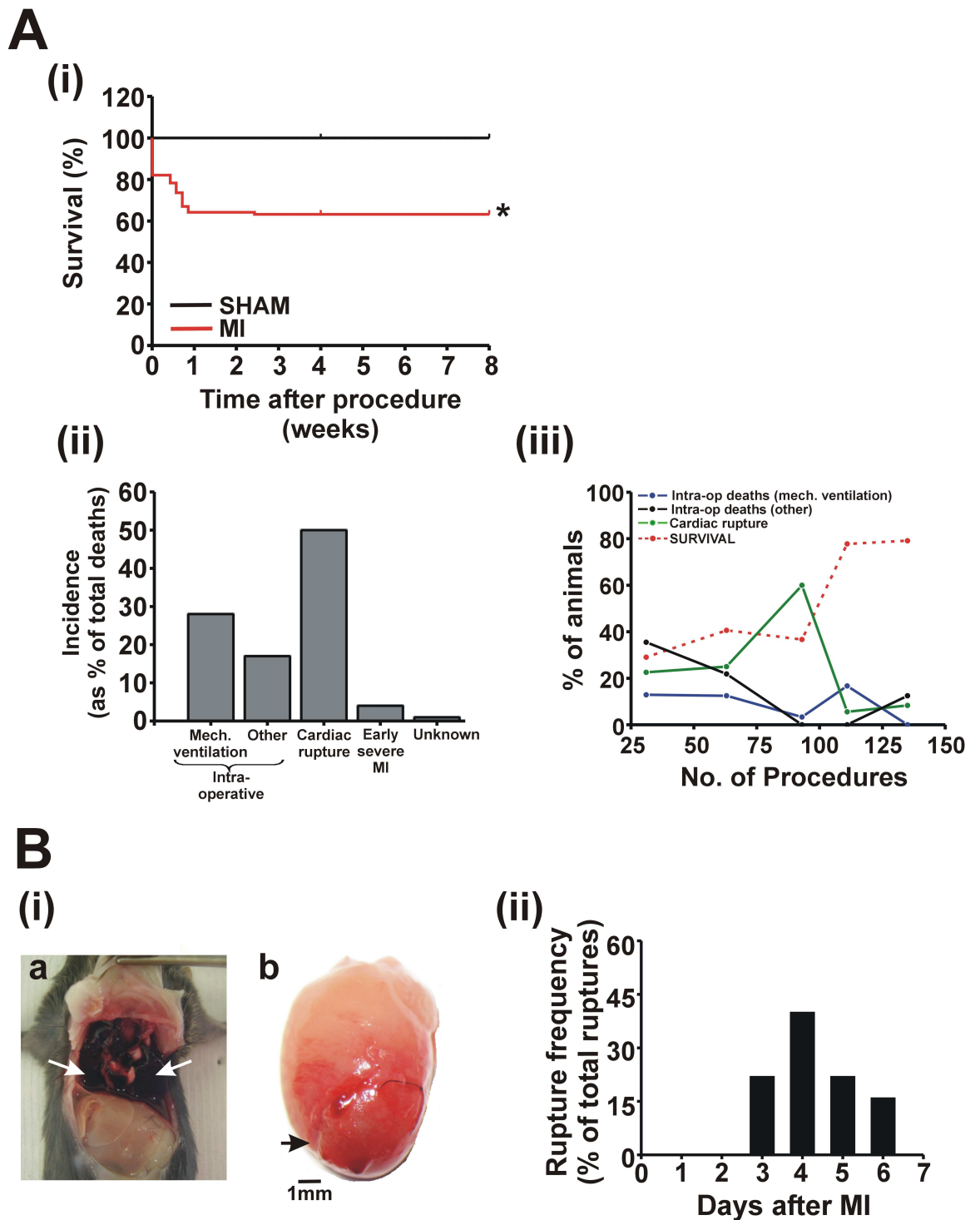


Figure 3.2 Survival following MI.

(A-i) Kaplan-Meier survival curves for mice undergoing CAL to produce MI (red line) compared to sham procedure (black line). Animals removed from the study at their respective time points (4 or 8 weeks) are represented by ticks at these time points on the survival curve to indicate removal from the study rather than death from the CAL procedure. * $P < 0.05$ Log-rank (Mantel-Cox) test. (A-ii) Reasons why mice did not survive CAL. (A-iii) Success rates associated with experience of the CAL technique. (B-i) Photograph of an animal that died as a result of cardiac rupture showing blood in the chest cavity (white arrows; (a)) and the site of rupture on the heart (black arrow; (b)). (B-ii) Incidence of cardiac rupture showing the frequency of rupture in the days following MI.

3.3.2 Effect of MI on haemodynamic LV function

LV PV loop measurements were used to assess changes in LV function 4-wk and 8-wk post-MI. The results of these measurements are presented in Figure 3.3, Figure 3.4 and summarised in Table 3.2 and described below. Results are expressed as the percentage change compared to the respective time-matched sham.

3.3.2.1 Effect of MI on LV pressure and volume traces and HR

Figure 3.3A (i-iv) shows typical LV pressure and volume traces from 4-wk sham, 4-wk MI, 8-wk sham and 8-wk MI. The resultant PV loops from these traces are summarised in Figure 3.3B. Heart rate was not statistically different across the four groups (545.1 ± 13.3 (4-wk sham; $n=10$); 552.7 ± 10.2 (4-wk MI; $n=13$); 572.0 ± 14.6 (8-wk sham; $n=5$); 546.2 ± 18.0 (8-wk MI; $n=7$) bpm; $P>0.05$; Figure 3.3C).

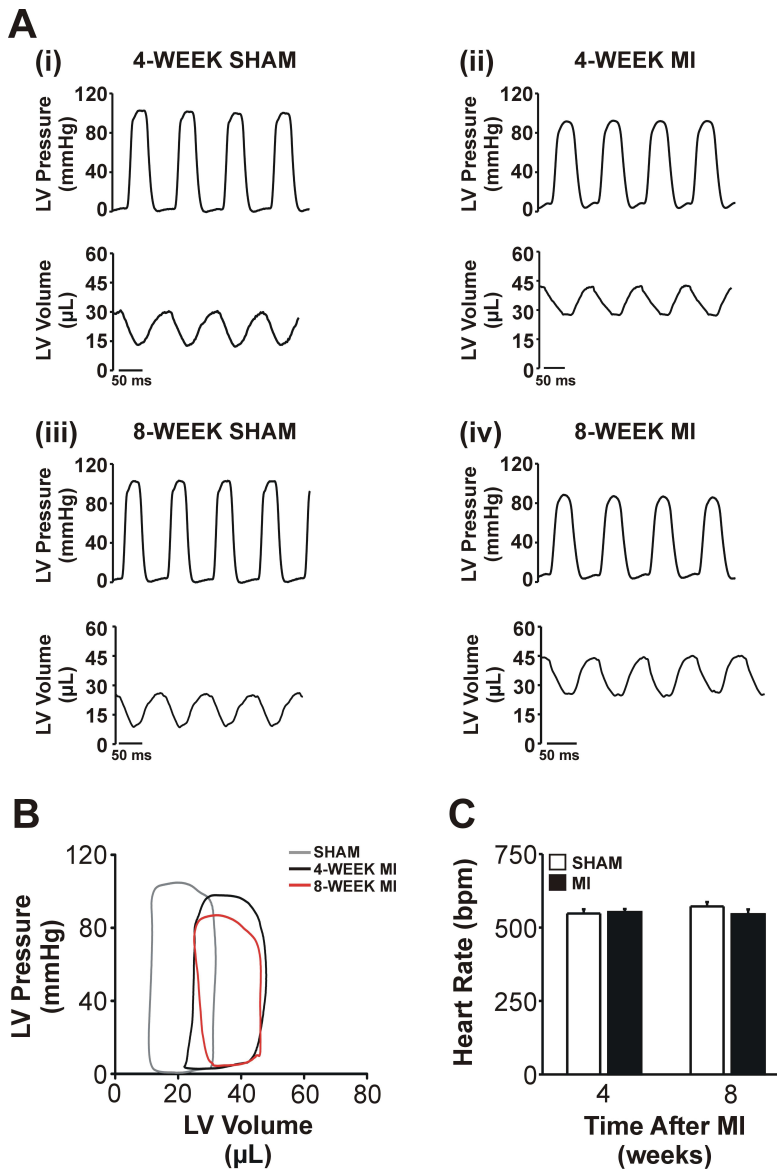


Figure 3.3 Effects of MI on pressure, volume and heart rate.

(A-i-iv) Representative pressure and volume traces from sham and MI hearts at 4-wk and 8-wk time points. (B)

Representative PV loops from sham and MI hearts at 4-wk and 8-wk time points. (C) Heart rates from 4-wk sham ($n=10$), 4-wk MI ($n=13$), 8-wk sham ($n=5$) and 8-wk MI ($n=7$).

3.3.2.2 Effect of MI on systolic functional parameters of the heart

Figure 3.4A shows the effect of MI on parameters of systolic function. LV end-systolic pressure (ESP), a measure of contractility, was significantly reduced to 88.0% of control sham levels at 4-wk post-MI (4-wk MI ($n=13$) vs. 4-wk sham ($n=10$); $P<0.05$) and to 82.0% of control sham levels at 8-wk post-MI (8-wk MI ($n=7$) vs. 8-wk sham ($n=5$); $P<0.05$; Figure 3.3A (i-iv), B; Figure 3.4A (i)). Similarly, the maximum rate of rise of LV pressure (dP/dt_{\max}) which is another index of contractility, was significantly reduced to 78.6% of control sham levels at 4-wk post-MI (4-wk MI ($n=13$) vs. 4-wk sham ($n=10$); $P<0.05$) and to 59.7% of control sham levels at 8-wk post-MI (8-wk MI ($n=7$) vs. 8-wk

sham ($n=5$); $P<0.05$; Figure 3.4A (ii)). Another measure of systolic performance is the ejection fraction (EF) which is equal to (stroke volume/end-diastolic volume)*100; MI led to a significant reduction in EF to 63.5% of control sham levels at 4-wk post-MI (4-wk MI ($n=13$) vs. 4-wk sham ($n=10$); $P<0.05$) and to 65.2% of control sham levels at 8-wk post-MI (8-wk MI ($n=7$) vs. 8-wk sham ($n=5$); $P<0.05$; Figure 3.4A (iii)). Cardiac output, however, remained unchanged following MI after 4-wk post-MI (7.9 ± 1.3 vs. 9.5 ± 1.2 ml.min⁻¹; 4-wk MI ($n=13$) vs. 4-wk sham ($n=10$); $P>0.05$) and 8-wk post-MI (10.1 ± 1.4 vs. 10.1 ± 0.6 ml.min⁻¹; 8-wk MI ($n=7$) vs. 8-wk sham ($n=5$); $P>0.05$; Figure 3.4A (iv)). There was no further decline in systolic function from 4-wk to 8-wk post-MI for any parameter.

3.3.2.3 Effect of MI on diastolic functional parameters of the heart

Figure 3.4B shows the effect of MI on parameters of diastolic function. LV end-diastolic pressure (EDP) is a measure of diastolic function and was significantly increased to 198.1% of control sham levels at 4-wk post-MI (4-wk MI ($n=13$) vs. 4-wk sham ($n=10$); $P<0.05$) and to 280.8% of control sham levels at 8-wk post-MI (8-wk MI ($n=7$) vs. 8-wk sham ($n=5$); $P<0.05$; Figure 3.3A (i-iv), B; Figure 3.4B (i)). Similarly, the maximum rate of fall of LV pressure (dP/dt_{max}) which is another measure of diastolic function was significantly reduced to 58.9% of control sham levels at 4-wk post-MI (4-wk MI ($n=13$) vs. 4-wk sham ($n=10$); $P<0.05$) and to 58.3% of control sham levels at 8-wk post-MI (8-wk MI ($n=7$) vs. 8-wk sham ($n=5$); $P<0.05$; Figure 3.4B (ii)). Another index of diastolic function is the time constant Tau (τ) which describes the rate of LV pressure decay during isovolumetric relaxation - τ was significantly increased to 155.9% of control sham levels at 4-wk post-MI (4-wk MI ($n=13$) vs. 4-wk sham ($n=10$); $P<0.05$) and to 168.0% of control sham levels at 8-wk post-MI (8-wk MI ($n=7$) vs. 8-wk sham ($n=5$); $P<0.05$; Figure 3.4B (iii)).

3.3.2.4 Effect of MI on load-independent measures of LV function

The end-diastolic pressure-volume relationship (EDPVR) was measured to assess a load-independent measure of diastolic function in terms of myocardial compliance and stiffness. The myocardial stiffness constant (β ; calculated from an exponential fit of the end-diastolic PV data points) is a load-independent measure of diastolic function in terms of stiffness of the myocardium and was significantly increased by 2.5-fold of control sham levels at 4-wk post-MI (4-wk MI ($n=13$) vs. 4-wk sham ($n=10$); $P<0.05$) and by 13.8-fold of control sham levels at 8-wk post-MI (8-wk MI ($n=7$) vs. 8-wk sham ($n=5$); $P<0.05$; Figure 3.4B (iv)).

Hearts were progressively stiffer by 2.5-fold at 8-wk compared to 4-wk post-MI (8-wk MI ($n=7$) vs. 4-wk MI ($n=5$); $P<0.05$; Figure 3.3B (iv)). EDPVR was the only diastolic parameter that was found to progressively change from 4-wk to 8-wk post-MI; no other parameters of diastolic function were found to change between 4-wk and 8-wk post-MI.

3.3.2.5 Effect of MI on volume parameters

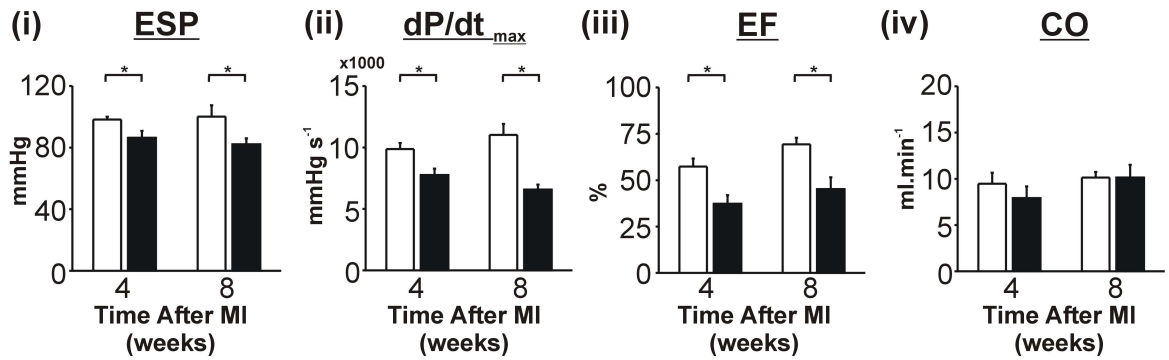
Figure 3.4C shows the effect of MI on LV volume parameters. LV end-diastolic volume (EDV) and end-systolic volume (ESV) are measured of the LV blood volumes at end-diastole and end-systole, respectively and are useful indicators of any change in LV volume as a result of chamber dilation for example. EDV was significantly increased to 141.1% of control sham levels at 4-wk post-MI (4-wk MI ($n=13$) vs. 4-wk sham ($n=10$); $P<0.05$) and to 168.4% of control sham levels at 8-wk post-MI (8-wk MI ($n=7$) vs. 8-wk sham ($n=5$); $P<0.05$; Figure 3.3A (i-iv); Figure 3.4C (i)). Similarly, ESV was significantly increased to 215.0% of control sham levels at 4-wk post-MI (4-wk MI ($n=13$) vs. 4-wk sham ($n=10$); $P<0.05$) and to 301.2% of control sham levels at 8-wk post-MI (8-wk MI ($n=7$) vs. 8-wk sham ($n=5$); $P<0.05$; Figure 3.3A (i-iv); Figure 3.4C (ii)). Stroke volume (SV) was unchanged after MI at both 4-wk post-MI (15.0 ± 2.2 vs. 17.6 ± 2.1 μ l; 4-wk MI ($n=13$) vs. 4-wk sham ($n=10$); $P<0.05$) and at 8-wk post-MI (18.7 ± 2.1 vs. 17.8 ± 1.3 μ l; 8-wk MI ($n=7$) vs. 8-wk sham ($n=5$); $P>0.05$; Figure 3.4C (iii)). There was no further change in volume parameters from 4-wk to 8-wk post-MI.

Table 3.2 Effect of myocardial infarction on haemodynamic indices of LV function in mice.

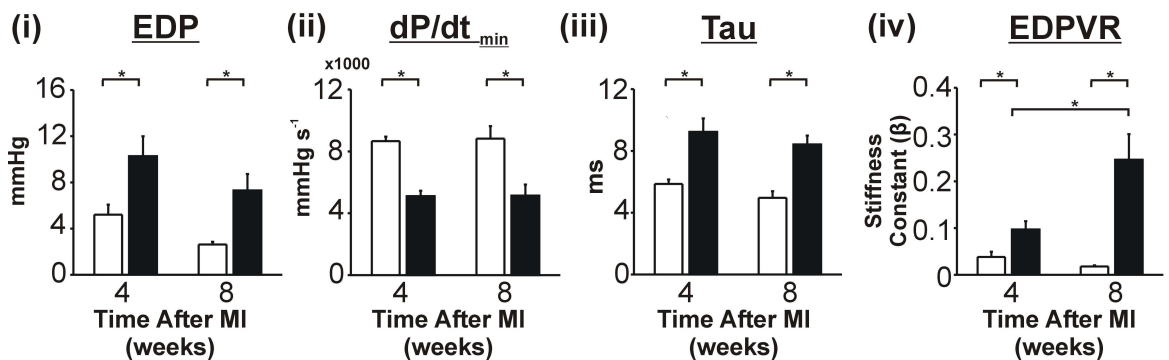
	4-wk SHAM	4-wk MI	8-wk SHAM	8-wk MI
HR (bpm)	545.1 ± 13.3	552.7 ± 10.2	572.0 ± 14.6	546.2 ± 18.0
ESP (mmHg)	98.2 ± 1.8	86.4 ± 4.4*	100.1 ± 7.4	82.1 ± 3.9*
EDP (mmHg)	5.2 ± 0.9	10.3 ± 1.7*	2.6 ± 0.2	7.3 ± 1.4*
dP/dt_{max} (mmHg.s⁻¹)	9872.8 ± 489.2	7761.5 ± 516.3*	11023.0 ± 893.9	6575.9 ± 399.9*
dP/dt_{min} (mmHg.s⁻¹)	8663.3 ± 292.0	5106.8 ± 351.4*	8826.9 ± 804.7	5141.7 ± 711.2*
Tau (ms)	5.9 ± 0.3	9.2 ± 0.9*	5.0 ± 0.4	8.4 ± 0.6*
EDPVR	0.038 ± 0.011	0.097 ± 0.018*	0.018 ± 0.002	0.246 ± 0.05*†
ESV (µl)	12.7 ± 2.2	27.4 ± 3.4*	8.5 ± 2.0	25.6 ± 4.4*
EDV (µl)	29.7 ± 3.9	41.9 ± 3.3*	26.3 ± 3.3	44.3 ± 5.5*
SV (µl)	17.6 ± 2.1	15.0 ± 2.2	17.8 ± 1.3	18.7 ± 2.1
CO (ml.min-1)	9.5 ± 1.2	7.9 ± 1.3	10.1 ± 0.6	10.1 ± 1.4
EF (%)	58.7 ± 4.0	37.3 ± 4.6*	69.3 ± 3.5	45.2 ± 6.4*

HR = heart rate; ESP = end-systolic pressure; dP/dt_{max} = maximal rate of rise of pressure; EF = ejection fraction; CO = cardiac output; EDP = end-diastolic pressure; -dP/dt_{min} = maximal rate of fall in pressure; Tau = time relaxation constant; EDPVR = end-diastolic pressure-volume relationship stiffness constant. Values are expressed as mean ± SEM. * $P < 0.05$ vs. time-matched sham control. † $P < 0.05$ between 4-wk MI vs. 8-wk MI.

A SYSTOLIC FUNCTION



B DIASTOLIC FUNCTION



C VOLUME PARAMETERS

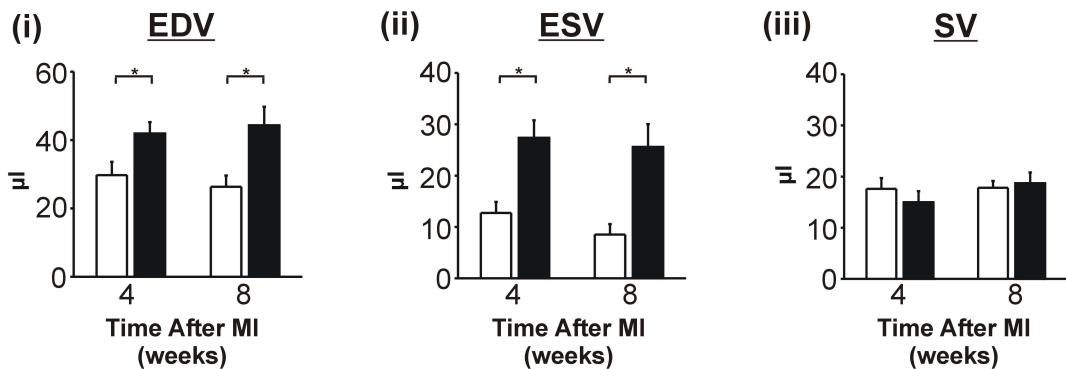


Figure 3.4 Effects of MI on haemodynamic indices of LV function in mice.

Effect of MI on systolic functional parameters (A i-iv), diastolic functional parameters (B i-iv) and volume parameters (C i-iii) in 4-wk sham (white bar; $n=10$), 4-wk MI (black bar; $n=13$), 8-wk sham (white bar; $n=5$) and 8-wk MI (black bar; $n=7$). Data shown are mean \pm SEM; * $P<0.05$.

3.3.3 Effect of MI on the electrical properties of the heart

ECG measurements were used to measure changes in the electrical properties of the heart after MI. ECG was used during the induction of MI in a cohort of animals as a method of validating successful CAL. Representative ECG recordings before, during and after CAL are shown in Figure 3.5 which show an increase in the ST-segment during CAL which can still be seen 10 min after CAL (Figure 3.5A (i-iii)). ECG measurements were also recorded 4-wk and 8-wk after MI. Representative ECGs from sham, 4-wk MI and 8-wk MI are shown in Figure 3.5B. It can be seen from these recordings that MI causes the development of a negative Q wave, ST depression and T-wave inversion, based on the morphology of the ECG alone (not quantified). Any arrhythmic events that occurred in the 5 min recording period were counted offline. Sham animals showed no arrhythmic events and therefore the 4-wk and 8-wk shams were combined into a single group. Animals with MI were found to have a significantly increased frequency of arrhythmias in the form of ventricular premature complexes (VPC) both at 4-wk (0.10 ± 0.04 ; 4-wk MI ($n=18$) vs. sham ($n=18$); $P<0.05$; Figure 3.5C (ii)) and 8-wk post-MI (0.04 ± 0.02 ; 8-wk MI ($n=7$) vs. sham ($n=18$); $P<0.05$; Figure 3.4C (ii)). These arrhythmias were identified as VPC by their larger QRS complexes with a deflection in the opposite direction to the normal sinus rhythm and a larger T wave consistent with a VPC. These were identified based on their morphology alone. There were no statistical differences in the frequency of VPC arrhythmias between 4-wk and 8-wk post-MI ($P>0.05$).

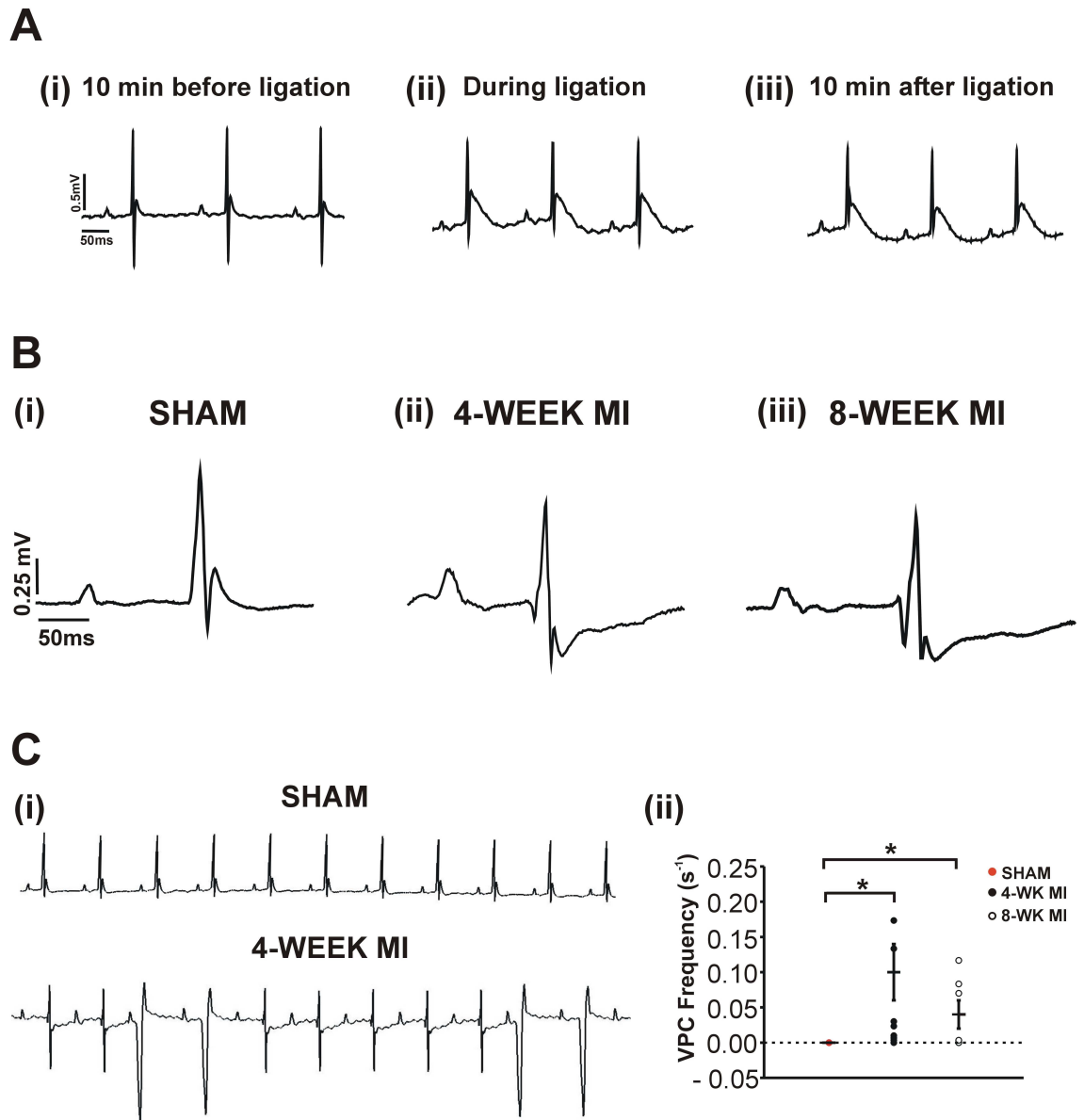


Figure 3.5 Effect of MI on the electric properties of the heart.

(A-i-iii) Representative electrocardiograms from mice before (i), during (ii) and after CAL (iii). (B-i-iii) Representative electrocardiograms from (i) sham, (ii) 4-wk MI and (iii) 8-wk MI. (C-i) Representative electrocardiograms for arrhythmia analysis from 4-wk sham and 4-wk MI after MI. (C-ii) Frequency of VPC arrhythmias in sham (both 4-wk and 8-wk shams; $n=18$; red circles), 4-wk MI ($n=18$; black circles) and 8-wk MI ($n=7$; open circles).

3.3.4 Effect of MI on the structural properties of the heart

3.3.4.1 Heart weight

Heart weight relative to TL was found to be significantly increased 4-wk post-MI (10.7 ± 0.5 vs. 8.9 ± 0.4 mg/mm; 4-wk MI ($n=15$) vs. 4-wk sham ($n=22$); $P<0.05$; Figure 3.6A-B) and 8-wk post MI (13.4 ± 1.4 vs. 9.3 ± 0.4 mg/mm; 8-wk MI ($n=12$) vs. 8-wk sham ($n=11$); $P<0.05$; Figure 3.6A-B). Hearts were also found to be progressively heavier as the MI developed from 4-wk to 8-wk (13.4 ± 1.4 vs. 10.7 ± 0.5 mg/mm; 8-wk MI ($n=12$) vs. 4-wk MI ($n=15$); $P<0.05$; Figure 3.6A-B).

3.3.4.2 Cardiomyocyte size

One factor that may be contributing to an increase in the weight of the heart after MI is an increase in the size of the individual cardiomyocytes. Cardiomyocyte cell dimension measurements (measured at 4-wk post-MI only) indicated a small but significant increase in cardiomyocyte length 4-wk post-MI (148.9 ± 3.2 vs. 130.7 ± 3.1 μm ; 4-wk MI ($n=3$ hearts; $n=63$ cells) vs. 4-wk sham ($n=3$ hearts; $n=79$ cells); $P<0.05$; Figure 3.6C(i-ii). Conversely, there were no statistical differences observed in cardiomyocyte width at 4-wk post-MI (30.4 ± 1.3 vs. 28.1 ± 0.9 μm ; 4-wk MI ($n=3$ hearts) vs. 4-wk sham ($n=3$ hearts); $P>0.05$; Figure 3.6(i,iii). There was also no significant differences in cardiomyocyte cross-sectional area at 4-wk post-MI (809.9 ± 73.1 vs. 665.0 ± 40.9 μm^2 ; 4-wk MI ($n=3$ hearts) vs. 4-wk sham ($n=3$ hearts); $P<0.05$; Figure 3.6C(i,iv).

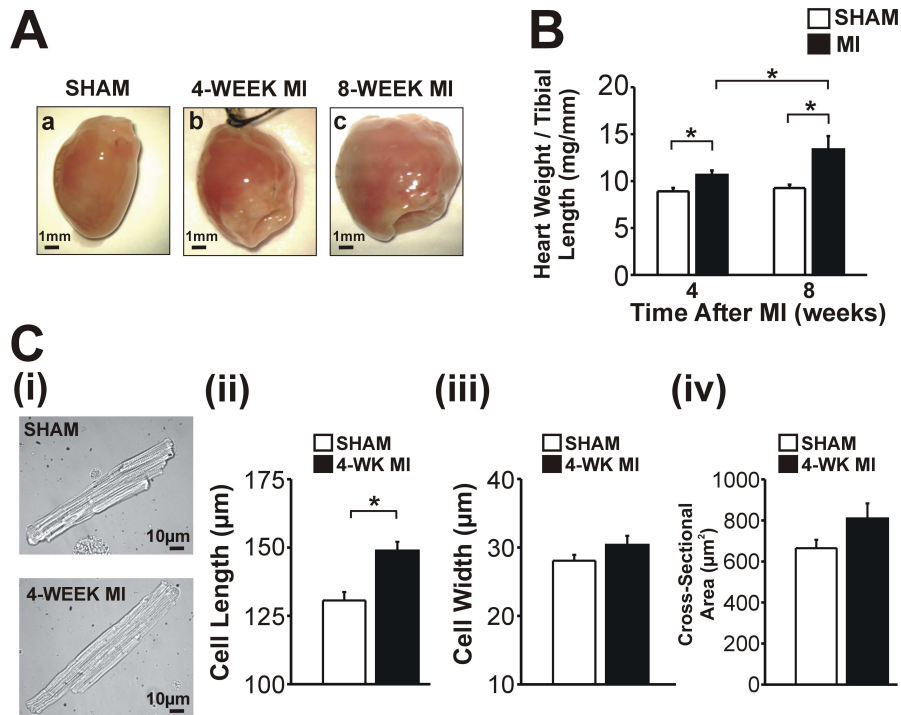


Figure 3.6 Effect of MI on heart weight and cardiomyocyte size.

(A-a-c) Representative photographs of the heart from (a) 4-wk sham, (b) 4-wk MI and (c) 8-wk after MI. (B) Effect of MI on heart weight (normalised to tibial length) for 4-wk sham ($n=15$), 4-wk MI ($n=22$), 8-wk sham ($n=12$) and 8-wk MI ($n=11$). (C-i) Typical cardiomyocytes from a 4-wk sham and 4-wk MI heart. C (ii-iv) Effect of MI on (ii) cell length, (iii) cell width and (iv) estimated cross-sectional area for 4-wk sham ($n=79$ cells; $n=3$ hearts) and 4-wk MI ($n=63$ cells; $n=3$ hearts). Data shown are mean \pm SEM. * $P<0.05$.

3.3.4.3 LV dimensions

Histological H&E-stained sections of the heart were used to quantify LV wall thickness and LV chamber area (Figure 3.7A (i-iii)).

LV wall thickness was found to be unchanged in sham-operated animals from 4-wk to 8-wk (1.96 ± 0.46 vs. 1.30 ± 0.06 mm; 4-wk sham ($n=4$) vs. 8-wk sham ($n=5$); $P>0.05$; Figure 3.7B). MI resulted in thinning of the LV free wall after 4-wk compared to the respective time-matched sham (0.19 ± 0.02 vs. 1.96 ± 0.46 mm; 4-wk MI ($n=5$) vs. 4-wk sham ($n=4$); $P<0.05$; Figure 3.7B) and after 8-wk (0.32 ± 0.10 vs. 1.30 ± 0.06 mm; 8-wk MI ($n=4$) vs. 8-wk sham ($n=5$); $P<0.05$; Figure 3.7B). There were no statistical differences in the degree of LV wall thinning between 4-wk MI and 8-wk MI (0.19 ± 0.02 vs. 0.32 ± 0.10 mm; 4-wk MI ($n=5$) vs. 8-wk MI ($n=4$); $P<0.05$; Figure 3.7B).

LV chamber area in sham-operated animals was not statistically different from 4-wk to 8-wk (5.3 ± 0.7 vs. 7.0 ± 0.3 mm²; 4-wk sham ($n=4$) vs. 8-wk sham ($n=5$); $P>0.05$; Figure 3.7C). After MI, LV area was significantly increased at 4-wk compared to the respective

time-matched sham (19.3 ± 3.7 vs. 5.3 ± 0.7 mm²; 4-wk MI ($n=5$) vs. 4-wk sham ($n=4$); $P<0.05$; Figure 3.7C) and at 8-wk (17.2 ± 3.5 vs. 7.0 ± 0.3 mm²; 8-wk MI ($n=4$) vs. 8-wk sham ($n=5$); $P<0.05$; Figure 3.7C). There were no significant differences in LV area observed between the 4-wk MI and 8-wk MI groups (19.3 ± 3.7 vs. 17.2 ± 3.5 mm²; 4-wk MI ($n=5$) vs. 8-wk MI ($n=4$); $P>0.05$; Figure 3.7C).

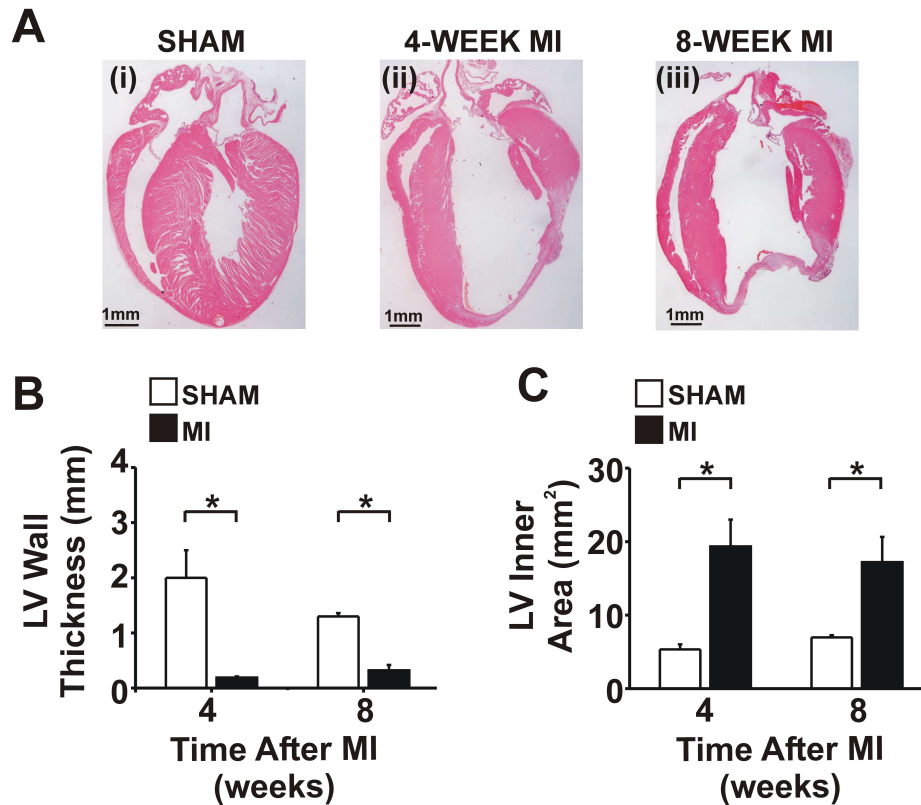


Figure 3.7 Altered LV dimensions after MI.

A (i-iii) Representative H&E sections of the heart from 4-wk sham, 4-wk MI and 8-wk MI. (B) LV infarct thickness and (C) LV chamber area measured using H&E sections for 4-wk sham (white bar; $n=4$), 4-wk MI (black bar; $n=5$), 8-wk sham (white bar; $n=5$) and 8-wk MI (black bar; $n=4$). * $P<0.05$

3.3.4.4 Infarct size

Sirius red sections of the heart were used to quantify infarct size (Figure 3.8A (i-iii)). The mean infarct size after 4-wk and 8-wk post-MI was 36.6 ± 4.2 and $39.4 \pm 5.4\%$ of the LV respectively (Figure 3.8B) indicating that there were no differences in the infarct size between the two time points (36.6 ± 4.2 vs. $39.4 \pm 5.3\%$; 4-wk MI ($n=4$) vs. 8-wk MI ($n=3$); $P>0.05$; Figure 3.8B). Sham animals showed no infarction.

3.3.4.5 Collagen deposition (cardiac fibrosis)

Collagen content was measured from the collagen positive (red-stained) area in Sirius red sections of the heart (Figure 3.8A (i-iii)). 4-wk and 8-wk shams were combined. Collagen levels were expressed as a percentage of the whole heart. After MI there was a significant increase in collagen content in the heart after 4-wk (13.2 ± 2.2 vs. $4.4 \pm 0.7\%$; 4-wk MI ($n=4$) vs. sham ($n=3$); $P<0.05$; Figure 3.8C) and after 8-wk (20.5 ± 4.5 vs. $4.4 \pm 0.7\%$; 8-wk MI ($n=3$) vs. sham ($n=3$); $P<0.05$; Figure 3.8C). There were no significant differences in collagen content between 4-wk and 8-wk hearts post-MI.

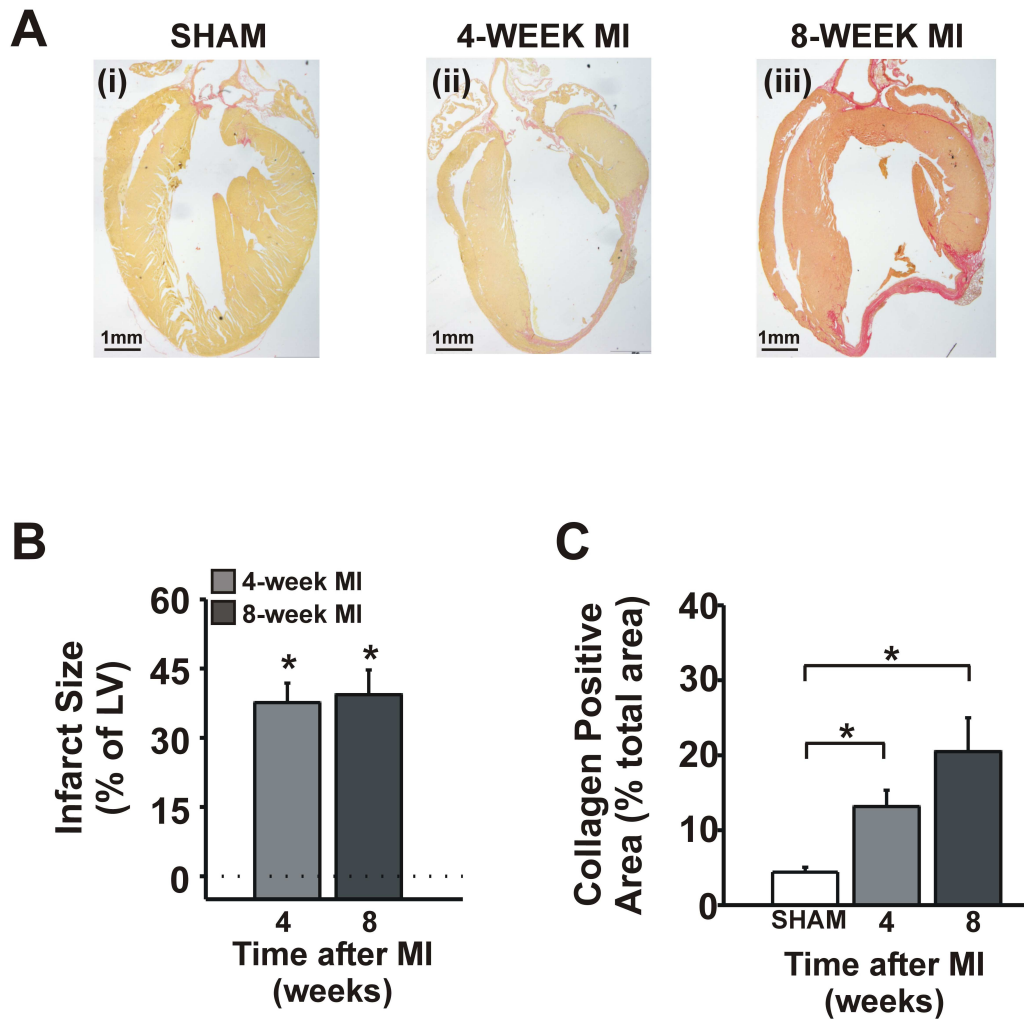


Figure 3.8 Infarct size and collagen content after MI.

(A i-iii) Representative Sirius red sections of the heart from (i) sham, (ii) 4-wk MI and (iii) 8-wk MI. (B) Infarct size after 4-wk MI ($n=4$; light grey bar) and 8-wk MI ($n=3$; dark grey bar). * $P<0.05$ compared to sham (dotted line). (C) Collagen levels in the heart as a percentage of the whole heart in sham ($n=3$; white bar), 4-wk MI ($n=4$; grey bar) and 8-wk MI ($n=3$; black bar). * $P<0.05$ between two groups indicated by connecting bars.

3.3.5 Effect of MI on lung and liver weight

There were no statistical differences in lung weight at 4-wk post-MI (7.1 ± 0.4 vs. 7.2 ± 0.4 mg/mm; 4-wk MI ($n=22$) vs. 4-wk sham ($n=15$) $P>0.05$; Figure 3.9A) nor at 8-wk post-MI (7.2 ± 0.7 vs. 6.8 ± 0.2 mg/mm; 8-wk MI ($n=11$) vs. 8-wk sham ($n=12$) $P>0.05$; Figure 3.9A). Similarly, there were also no statistical differences in liver weight at 4-wk post-MI (67.5 ± 1.8 vs. 66.6 ± 2.8 mg/mm; 4-wk MI ($n=22$) vs. 4-wk sham ($n=15$) $P>0.05$; Figure 3.9B) and at 8-wk post-MI (70.0 ± 2.1 vs. 65.9 ± 2.6 mg/mm; 8-wk MI ($n=11$) vs. 8-wk sham ($n=12$) $P>0.05$; Figure 3.9B).

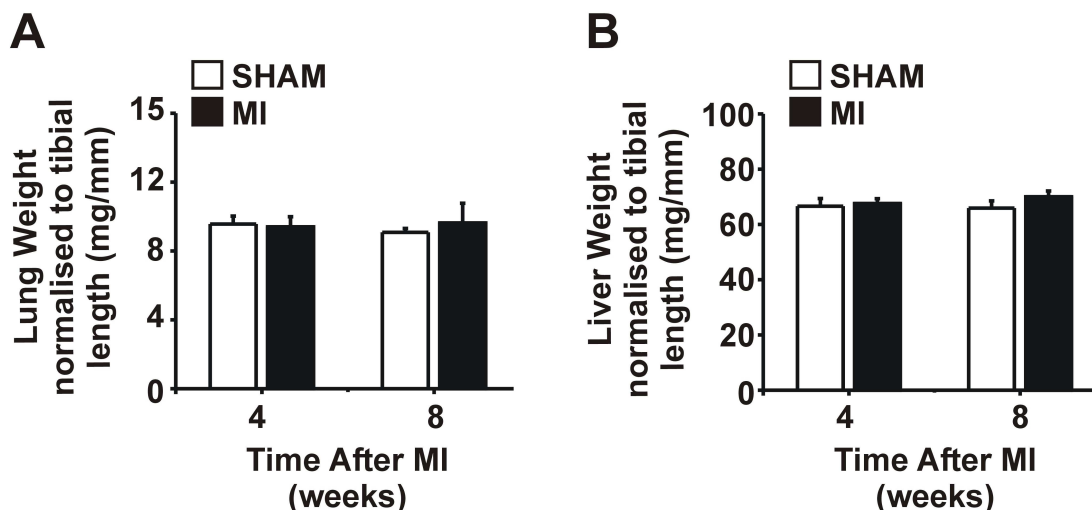


Figure 3.9 Lung and liver weights after MI.

(A) Lung weight in 4-wk sham ($n=15$), 4-wk MI ($n=22$), 8-wk sham ($n=12$) and 8-wk MI ($n=11$). (B) Liver weight in 4-wk sham ($n=15$), 4-wk MI ($n=22$), 8-wk sham ($n=12$) and 8-wk MI ($n=11$).

3.4 Discussion

For this study, a model of MI was produced in the mouse using the well-established CAL method. The results presented in this chapter demonstrate that this method produced a model with altered cardiac functional and structural properties consistent with LV remodelling during MI.

3.4.1 Inducing MI leads to reduced survival

Inducing MI in mice experimentally is known to be associated with a higher incidence of mortality compared to animals undergoing the sham procedure (Sam *et al.*, 2000; van Laake *et al.*, 2007). The current mortality in our model was 27% for animals undergoing CAL (compared to 0% in shams); which saw an improvement in survival by approximately 3-fold since first learning the technique for the study. Mortality associated with CAL-induced MI in mice is about 32-50% (Gehrmann *et al.*, 2001; Kuhlmann *et al.*, 2006) therefore the mortality for our model was low compared with the published literature for this species.

3.4.1.1 Reasons for reduced survival

Nearly all (99%) of the deaths from CAL occurred within the first week of the operation which is a consistent finding in mouse MI models (Lutgens *et al.*, 1999; Patten, 1998). Sudden deaths beyond the first week were uncommon in our model (1% of all deaths) but

these have been known to occur in murine MI models beyond the first week although these tend to be a significantly smaller proportion compared to the first week drop-out: Patten reported a small proportion of deaths (8.8% of their deaths) which occurred at days 20, 28 and 32 post-operative (Patten, 1998) and Yang have reported 1% of sudden deaths at 2-wk, 4-wk and 8-wk with 3% of sudden deaths at 16-wk and 24-wk (Yang *et al.*, 2002).

Intra-operative mortality: In the present study, nearly half of all mortalities (45%) occurred intra-operatively and were mainly due to respiratory problems from mechanical ventilation. It was necessary to mechanically ventilate the animals to prevent respiratory insufficiency from lung collapse during thoracotomy; however, due to the animal's small size and complex respiratory patterns (e.g. high respiration rate (RR) and low inspiratory time to total time of the respiratory cycle (T_i/T_T)), mechanical ventilation in mice can be inherently difficult (Schwarte *et al.*, 2000). There is also the associated high risk of pneumothorax with open-chest procedures which occurs when air is not fully displaced from the chest and the lungs cannot fully inflate which can also lead to respiratory insufficiency. In this model, deaths from mechanical ventilation were either due to (i) pneumothorax as previously described, or (ii) an over-inflation of the lungs, which may have been caused by too great a pressure at the inlet port. Efforts were made to minimise ventilation-related deaths and improve overall survival. These included (i) placing the expiratory tube under water during closing up to increase PEEP and reduce the chance of lung collapse, (ii) ensuring patency in the tracheal cannula and associated tubing at all times, (iii) use of appropriate tidal volumes and respiration rates for the body weight of the animal (as recommended by the manufacturer of the ventilator, *Harvard Apparatus*, Germany). Together these methods were successful in reducing ventilation-related deaths to 0% and improved overall survival by 65% during the course of refining the model as shown in Figure 3.2A(iii). Novel methods for inducing CAL in mice without the need for mechanical ventilation are emerging like the method by Gao *et al.*, (2010) in which a "heart pop-out" approach is used to eliminate the need for ventilation and is found to produce identical infarct sizes and a similar level of dysfunction as the conventional method but with less tissue damage and better survival. This may be beneficial to investigators using mouse MI models to help reduce intra-operative mortality (Gao *et al.*'s method showed reduced mortality from 52.3% to 32.5% without need for mechanical ventilation). The other intra-operative deaths observed in the present study that were not caused by respiratory problems were for reasons that could not be identified; it's possible that the CAL may have triggered fatal arrhythmias. Alternatively, as Figure 3.2A(iii)

shows, these deaths were highest at the beginning of the course of learning the technique therefore it may have been related to inexperience.

3.4.1.2 The main cause of reduced survival was cardiac rupture

The largest loss of animals after the CAL procedure was from cardiac rupture which occurred in 27% of animals overall (constituting 50% of all deaths) as shown in Figure 3.2A(ii). Cardiac rupture is a feature of acute MI which is believed to occur from persistent stretching of weakened myocardium causing it to rupture (Schuster & Bulkley, 1979). The increased abundance and activity of MMP enzymes in the early stages of acute MI is believed to be the major contributor to this event (Heymans *et al.*, 1999; Matsumura *et al.*, 2005). Cardiac rupture can occur in human patients with MI although it is rare (occurs in 3% of MI patients) (Brener & Tschopp, 2009) and is also a feature of mouse models of MI; the mouse is the only laboratory species reported to demonstrate cardiac rupture like humans (Gao *et al.*, 2010b; Sane *et al.*, 2009). Mouse rupture models have provided valuable insight into the principal mechanisms of rupture as well as the associated risk factors for developing rupture. A common finding appears to be that the occurrence of rupture requires a critical extent of infarction (Gao, 2005; Gao *et al.*, 2010b). It has also been reported that the gender and strain of mice plays a role in the risk of rupture with males being at greater risk than females (59% for males *vs.* 23% for females) (Gao, 2005) and the greatest incidence occurring in the 129sv strain compared to the C57Bl/6 strain (62% for 129sv *vs.* 33% for C57Bl/6) (Gao, 2005). Ageing is also a factor for rupture incidence; older mice (12 months old) demonstrated greater LV remodelling with a higher incidence of rupture (40.7%) compared to younger mice (3 months old; 18.3%) (Yang *et al.*, 2008). In light of these reports, a lower risk strain (C57Bl/6) and younger animals (8-10 weeks of age) were used for this study to try to minimise the incidence of rupture and promote full recovery to the 4-wk and 8-wk time points. From these studies, rupture incidence for male C57Bl/6 mice were reported to be 27% and 33% (Gao, 2005; Gao *et al.*, 2010b) which is very comparable with our rupture rate (27%). Cardiac rupture was easily identifiable at autopsy following sudden death by the presence of blood clots within the chest surrounding the heart and by the presence of a visible tear on the LV free wall, although the latter was not always clearly evident. The time-window for this event was always within the first week of MI peaking at day 3-5 which is consistent with what others have seen in mouse models of post-infarct rupture (Gao, 2005; van der Borne, 2009).

3.4.2 MI alters the structural properties of the heart

3.4.2.1 MI causes LV chamber dilation and wall thinning

MI induces a series of complex changes to the size, shape and function of the heart as part of LV remodelling (Pfeffer & Braunwald, 1990). One of the earliest features of remodelling after MI is LV chamber dilation caused by infarct expansion through loss of cardiomyocytes (Weisman *et al.*, 1988) or side-to-side slippage of cardiomyocytes (Gerdes & Capasso, 1995; Olivetti *et al.*, 1990). Side-slippage of cardiomyocytes occurs because of the loss of collagen holding the cells together through degradation by MMPs which permits them to move (Whittaker *et al.*, 1991). Cardiomyocyte cell death also contributes to the process because as they die, the neighbouring viable cells are no longer held in place and are also able to slip (Gajarsa & Kloner, 2011). In the present study, it was found that after 4-wk and 8-wk post-MI, mice displayed a ≈ 3.6 -fold and ≈ 2.5 -fold increase respectively in LV chamber area together with reduction in LV infarct thickness by 90% and 75% respectively, findings which are consistent with a dilated LV chamber. These measurements were taken from histological slices post-mortem which are acceptably less accurate than for example *in vivo* imaging methods such as echocardiography and MRI due to the tissue shrinkage associated with histological processing which may underestimate true dimensions. However, efforts were made to enable as accurate measurements as possible using histology methods by use of serial sections and using area-based chamber size measurements rather than radius/diameter which could be subject to error if there was any deformation of the heart on the slide. Despite histological limitations, a study by Nahrendorf *et al.* (2000) found that MRI vs. histologic-based methods of LV dimensions correlated well ($R=0.97$) in a rat MI model which is encouraging for the measurements in our study (Nahrendorf *et al.*, 2000). Furthermore the findings are further supported by increased end-diastolic LV volumes observed by PV methodology in the 4-wk and 8-wk infarcted heart also consistent with LV chamber dilation. Chamber dilation leads to an increase in systolic and diastolic wall stress; this occurs because the increase in LV radius increases the wall stress and oxygen demand by Laplace's law (Pfeffer *et al.*, 1991a). Elevated wall stress triggers eccentric hypertrophy (end-to-end lengthwise cell enlargement) in the non-infarcted myocardium by causing altered expression of genes which encode contractile proteins (e.g. β myosin heavy chain) for assembly of new sarcomeres (Sadoshima *et al.*, 1992). Over time however as the heart undergoes ongoing remodelling, cardiac function significantly deteriorates as the LV chamber becomes so enlarged that it begins to severely impair contractile function. Dilated cardiomyopathy is a

serious problem for patients as once this stage is reached it is very difficult to reverse; approximately 1 in 3 cases of congestive HF are due to a dilated cardiomyopathy (Jameson *et al.*, 2005).

3.4.2.2 MI leads to cardiac hypertrophy

A dilated ventricle can trigger hypertrophy of surviving myocardium in attempts to attenuate further dilation, offset the elevated load and wall stress resulting from infarct expansion and stabilise contractile function (Sutton & Sharpe, 2000). There are two forms of hypertrophy (concentric and eccentric) which is determined by the type of load applied to the heart. Pressure overload causes cardiomyocyte thickening (concentric hypertrophy) by the parallel addition of new sarcomeres, while volume overload elicits cardiomyocyte lengthening (eccentric hypertrophy) by the in-series addition of new sarcomeres. LV remodelling post-MI is primarily a state of volume overload and thus leads to cardiomyocyte lengthening as part of eccentric hypertrophy (French & Kramer, 2007). Cardiomyocytes in the non-infarcted regions can increase in length as a result of in-series addition of sarcomeres as described previously (Gerdes & Capasso, 1995) which at the organ level manifests as an increase in heart weight. In the present study, hearts showed a progressive increase in heart weight (increased heart weight-to-tibial length ratio) after MI, with heavier hearts after 4-wk which continued to increase by 8-wk. Concurrent with the increased heart weight was a 14% increase in cardiomyocyte length but no change in cardiomyocyte width at 4-wk post-MI (but no significant differences in cardiomyocyte cross-sectional area) as shown in Figure 3.6C(ii-iii). This is in agreement with what others have found, for example Zhang *et al.* (1998) reported a 10% increase in cardiomyocyte cell length with no change in cell width 3-wk post-MI in a rat model (Zhang *et al.*, 1998) and Scherrer-Crosbie *et al.* (2001) also found no change in cardiomyocyte width in a mouse model of MI after 4-wk (Scherrer-Crosbie *et al.*, 2001). An increase in cardiomyocyte length with no change in cell width is consistent with eccentric hypertrophy observed in MI, although concentric hypertrophy has been known to occur during MI in addition to eccentric hypertrophy (Runge & Patterson, 2006). Together these results demonstrate the hearts have undergone hypertrophy consistent with LV remodelling after MI and that cardiomyocyte elongation is likely to be contributing to the increase in heart weight observed.

3.4.2.3 MI causes increased collagen deposition

Another important characteristic of remodelling is the increased synthesis and deposition of collagen to support the weakened myocardium and stabilise the infarct (Van *et al.*, 2000). After MI, collagen levels in the heart were found to increase 3-fold and 4.7-fold after 4-wk and 8-wk respectively. Collagen levels tended to be higher at 8-wk (compared to 4-wk) however this did not reach statistical significance. This may be due to low *n* numbers for this group (sham *n*=3, 8-wk MI *n*=3) and larger numbers may have shown a statistical difference. Increased collagen deposition could explain why no further dilation was observed from 4-wk to 8-wk as collagen can prevent cardiomyocyte slippage, one of the primary causes of LV expansion and dilation (Whittaker *et al.*, 1991). Fibrosis after MI can also decrease the compliance of the ventricle leading to stiffer myocardium during diastole (Raya *et al.*, 1988; Litwin *et al.*, 1991). This occurs because excessive accumulation of collagen around myofibres reduces the passive viscoelasticity of the myocardium which limits normal diastolic recoil, impairs tissue compliance and compromises length-dependent muscle fibre shortening (Burlew & Weber, 2002). Therefore, the increased cardiac collagen observed may explain why the ventricles were stiffer after MI as PV data using the EDPVR demonstrated. A trend towards higher collagen levels at 8-wk would parallel with the progressively stiffer ventricle at 8-wk. Increased myocardial stiffness has been known to occur in the post-MI heart during the healing phase in humans (Diamond & Forrester, 1972) and experimental animal models (Hood, Jr. *et al.*, 1970) which is in agreement with the results found in this present study. However investigations have also led to variable findings regarding cardiac stiffness post-MI, these refer to the very early stages of MI (<1 day). Forrester *et al.* (1972) found a significant increase in LV compliance (reduced stiffness) 1 hr after induction of MI in the canine model (Forrester *et al.*, 1972). Increased myocardial stiffness is a major cause of diastolic dysfunction which is important because diastolic dysfunction is considered an independent predictor of mortality in CVD patients (Aljaroudi *et al.*, 2012).

3.4.2.4 The CAL technique produces comparable infarct sizes

Data from other mouse MI models have reported that the CAL method can produce infarct sizes from 25-50% (Lutgens *et al.*, 1999; Patten, 1998). Using the CAL method in our model produced a mean infarct size of 37.6 ± 4.2 and $39.4 \pm 5.4\%$ at 4-wk and 8-wk respectively. This model therefore had infarcts of comparable size with other mouse infarct models. Infarct size was not different between 4-wk and 8-wk. This suggests that

the size of the infarct had reached completion by 4-wk with no further increase in size thereafter to 8-wk. Yang *et al.* (2002) reported a similar finding with identical infarct sizes in mice post-MI of (as % of LV) $47.3 \pm 5\%$ at 4-wk and $45.3 \pm 5\%$ at 8-wk ($P > 0.05$) – through further examinations at different time points (3-wk, 4-wk, 8-wk, 16-wk and 24-wk) they found that the infarct formation was complete by 3-wk and infarct size did not increase after this point (Yang *et al.*, 2002). Based on these findings this may explain why no change in infarct size was observed in our model from 4-wk to 8-wk as the infarct may have reached its full size by 3-wk. Despite equivalent infarct size, the progressive increase in cardiac weight observed between 4-wk and 8-wk suggests the hypertrophic response could have occurred independently of infarct size and may be a time-related response. This result does however differ from previous reports: for example the current view is that after MI, the extent of cellular hypertrophy in surviving tissue is proportional to the magnitude of cardiomyocyte loss which has been demonstrated in a number of studies showing a positive correlation between the extent of cardiomyocyte hypertrophy with infarct size in rats (Anversa *et al.*, 1986; Anversa *et al.*, 1990). However hypertrophy is known to be a progressive process which can increase over the course of the remodelling period with time and may not be strictly regulated by the degree of infarction as has been shown in mice where heart weight continued to increase with no change in infarct size (Yang *et al.*, 2002).

3.4.3 Early onset of structural remodelling can have adverse effects

A small percentage (5%) of animals undergoing CAL developed very severe symptoms in the first week after the procedure including severe respiratory distress which autopsy assessment revealed may be due to severe adverse remodelling. These animals displayed a marked increase in heart weight (32% greater than 4-wk MI $P < 0.05$; data not shown) which was comparable to the level seen at 8-wk (15.7 ± 3.0 vs. 13.4 ± 1.4 mg/mm; severe MI ($n=4$) vs. 8-wk MI ($n=11$); $P < 0.05$; data not shown). However, these hearts developed a greater degree of adverse remodelling in terms of significantly greater chamber dilation (than 4-wk and 8-wk hearts; see below) and also evidence of severe pulmonary congestion in these animals which showed 65% increase in lung weight when compared to both 4-wk and 8-wk animals respectively. This may explain why animals at 8-wk MI (which had comparable HW/TL ratio to the animals with the severe phenotype) did not exhibit the same symptoms. It is likely that these animals were suffering from acute congestive HF, however due to the severity of their condition it was not possible to perform any functional

measurements on them to confirm this. Examination of histological heart sections also revealed that these animals had severe LV chamber dilation compared to animals that survived to 4-wk and 8-wk post-MI, as mentioned above, with 1.9-fold and 2.1-fold greater chamber area respectively. Advanced dilation and wall thinning does not usually occur until the chronic phase of MI in mice (Bayat *et al.*, 2002), however the level of acute adverse remodelling observed in these animals may explain their symptoms. Severe dilation causes an increase in systolic wall stress (Pfeffer & Braunwald, 1990) and loss of cardiomyocyte contractility (Gomez *et al.*, 2001) to a level that significantly affects the pump function of the heart and reduce the EF and CO to a level insufficient to meet the demands of the body, leading to HF (Isaaz *et al.*, 1989). The findings from this small subset of animals ($n=2$) are consistent with a study by Gao *et al.*, 2000 who have reported a similar small subset of mice that did not survive past the first week of CAL and showed significant chamber dilation compared to mice that survived to longer time points (Gao *et al.*, 2000).

3.4.4 MI leads to impairment of cardiac function

After chronic MI in mice, chamber dilation and infarct thinning can adversely lead to systolic and diastolic dysfunction (Pfeffer *et al.*, 1991b). LV PV measurements are considered the ‘gold standard’ for measuring cardiac function *in vivo* and in this model, PV measurements revealed an overall decline in cardiac function after MI. There was a significant reduction in contractile function at 4-wk and 8-wk post-MI as evidenced by reduced LVESP and reduced dP/dt_{max} . There was also a significant decrease in diastolic function with raised LVEDP and reduced relaxation rates ($-dP/dt_{min}$) and duration of relaxation (τ) consistent with impaired relaxation and filling. Systolic and diastolic function were reduced to the same degree at 4-wk and 8-wk, suggesting there was no further deterioration in function from 4-wk to 8-wk after MI. This has been observed by others; one study reported no further decline in dP/dt_{max} and EF beyond 12-wk post-MI in mice (Pons *et al.*, 2003) while another showed no further worsening of function in terms of ESP, dP/dt_{max} and dP/dt_{min} between 1-wk and 3-wk post MI in mice (Lutgens *et al.*, 1999). This finding is consistent with the sustained structural properties between 4-wk and 8-wk such as infarct size, degree of LV dilation and infarct thickness. The progressive increase in cardiac weight did not improve function between 4-wk and 8-wk; however it may have contributed towards protecting the heart from further decline. Alternatively, it may be that the degree of remodelling had not reached advanced stages and the heart was still well compensated. This is confirmed by the finding that, despite marked LV dysfunction,

hearts had preserved SV and CO after 4-wk and 8-wk. This is known to occur during compensated remodelling post-MI where there is surprisingly little change in the SV due to a compensatory rise in LV filling pressure – an increase in both EDP and EDV (the latter through dilation) shifts the ventricular function curve upwards restoring contractile energy through the Frank-Starling mechanism allowing SV and CO to be near normal (Levick, 2010). Although there are reports which have observed a reduction in CO in mouse models of MI by 8-wk (Shioura *et al.*, 2007), it has also been found that CO is conserved after 8-wk in mice with MI similar to the findings of the present study; for example it has been previously shown from PV loop measurements in a mouse model of MI that there was no reduction in CO by 12-wk post-MI compared to sham (Pons *et al.*, 2003). In our mouse model conservation of SV and CO would suggest the hearts had not reached the stages of HF by 8-wk. Examinations of the liver and lung weights have further confirmed this by the absence of any signs of systemic or pulmonary congestion. These findings are not unusual as it has been reported that it can take up to 18 weeks for mice with MI to start showing signs of HF (Bayat *et al.*, 2002).

3.4.5 MI alters electrical activity and increases the frequency of cardiac arrhythmia

As well as mechanical dysfunction, MI can alter the normal electrical functioning of the heart. This occurs because the infarcted myocardium represents an area of altered substrate for the normal depolarisation and repolarisation of the heart leading to conduction disturbances (Peters, 1995). Our model demonstrated conduction abnormalities associated with ventricular depolarisation and repolarisation such as negative Q waves, ST depression and T-wave inversion. These findings are consistent with what has been reported on changes in ECG seen in mouse MI (Wehrens *et al.*, 2000). These morphological changes observed on the ECG were very similar between 4-wk and 8-wk. The model also showed an increased propensity for ventricular arrhythmias in the form of VPC. VPC arrhythmias are the most common type of cardiac arrhythmia in MI and occur when an action potential is fired from a region other than the SA node prior to normal conduction resulting in a premature or ectopic beat (Horan & Kennedy, 1984). These occur during MI as a result of the myocardial scarring disrupting the normal conduction system of the heart. Furthermore due to the loss of cell-cell communication by the scarred tissue (Peters, 1995) neighbouring cardiomyocytes are more likely to depolarise spontaneously ('irritated myocytes') and fire off premature beats – this explains why VPCs usually arise from the infarct or peri-infarct

regions (Bogun *et al.*, 2008). At the molecular level, VPCs largely occur due to the remodelling of (i) ion channels, (ii) Ca^{2+} handling proteins and (iii) gap junction proteins which predispose the heart to electrical disturbances mainly after depolarisations. For example, during MI NCX is known to be up-regulated which increases the inward $\text{I}_{\text{Na/Ca}}$ during SR release leading to extrusion of a larger fraction of released Ca^{2+} (increasing the transient inward Na^+ current, I_{ti}). There is also a reduction in the inward rectifier K^+ current (I_{K1}) which for any given I_{ti} could produce a greater depolarisation which means that it may be more likely to trigger an AP (Pogwizd *et al.*, 2001). The incidence of VPC arrhythmias is markedly increased in heart disease (by 90% in patients with coronary artery disease and ischaemia) (Ghuran & Camm, 2001). VPCs are an important predictor of adverse outcome; in patients with MI, a frequency of >10 VPC per hour is associated with a greater risk of sudden death (Laidlaw *et al.*, 2007). In our model, the frequency of VPC arrhythmia was not different between 4-wk and 8-wk which is not surprising given the similar degree of LV remodelling between these two groups. Collectively, the findings reveal that our mouse model demonstrates cardiac arrhythmias consistent with MI.

3.4.6 Summary

In summary, these data show that the mouse model of MI developed for this study demonstrates both structural and functional alterations of the heart comparable with other published mouse models of MI using the CAL method. This model is therefore a suitable model of MI for use in subsequent studies in this thesis.

CHAPTER 4

Expression of *Runx* in the heart in a mouse model of myocardial infarction

4.1 Introduction

MI is the leading cause of HF and premature death (Scarborough, 2010). The loss of viable myocardium after MI triggers a sequence of structural and geometric alterations to the heart as part of LV remodelling which can eventually lead to progressive dysfunction and the inability of the ventricle to maintain output sufficient for the body's metabolic needs (Weber *et al.*, 1991a). LV remodelling is a complex process involving a multitude of cellular and molecular mechanisms (Colucci, 1997). While these mechanisms are believed to be beneficial initially, many of them can become detrimental and lead to long-term adverse effects in patients (Pfeffer & Braunwald, 1990). Despite extensive investigations, the specific pathophysiological pathways responsible for the decline into HF are not fully understood. Novel insight into the regulatory mechanisms that contribute to the subsequent decompensatory processes of post-infarction remodelling are therefore required to slow this deterioration process and improve treatment strategies.

4.1.1 Altered gene expression in MI

Clinical and animal studies of MI have revealed a number of cellular changes that contribute to the functional and structural changes of remodelling including cardiomyocyte hypertrophy (Litwin *et al.*, 1991) and ECM alterations (Van *et al.*, 2000). Although the molecular mechanisms involved in remodelling are numerous and complex, it is clear that substantial alterations in gene expression are involved to afford the changes observed. Altered gene expression after MI has been widely reported in both human and experimental animal models (Stanton *et al.*, 2000;Gidh-Jain *et al.*, 1998;LaFramboise *et al.*, 2005). Studies have revealed that MI can modify the expression of genes involved in calcium-handling (Swynghedauw, 1991), contractile function (Yue *et al.*, 1998), the ECM (Weber, 1997) and the RAA system (Holtz, 1998).

4.1.1.1 Altered gene expression in different regions of the heart in MI

Changes in gene expression can be seen as a global change across the whole heart but studies particularly from rodent models of MI have shown that altered gene expression post-MI can occur differentially and tends to be selective for specific regions of the heart (Melle *et al.*, 2006;Xu *et al.*, 2004;Schneider *et al.*, 2007). Most commonly, genes are altered differently in the infarcted versus non-infarcted regions. In the early post-infarction period (24-48 h) a broad range of genes are activated or up-regulated in the remote region while many are repressed in the infarct region; the specific cell types were not specified

(LaFramboise *et al.*, 2005). Early remote gene expression is largely activation of genes involved in the inflammatory response including the interleukins (IL1 α , IL1 β , IL6, IL12 α , IL18) which can increase 1.5 – 5 fold and the TNF α superfamily which have been observed in mice to increase ~2 fold compared to sham equivalent regions (LaFramboise *et al.*, 2005) as part of the initial compensatory phase to limit injury expansion (Brivaniou & Darnell, 2002; Frangogiannis *et al.*, 2002). Other genes which show increased expression in the remote region at this early time point include homeobox genes which encode homeobox transcription factors which are involved in developmental processes (RAX, LH2, HOXA1; 2-4 fold increase compared to sham) and zinc finger factors which are a group of transcription factors (ZPF103, HR, GATA1; 2-3 fold increase compared to the matching sham region) (LaFramboise *et al.*, 2005).

Conversely, at a later stage of the MI (4-wk) the reciprocal pattern between infarct and remote regions is reversed, and many genes are up-regulated in the infarcted region while expression in the remote is reduced. Genes up-regulated in the infarct region are mainly ECM genes (collagen 5A3, MET1A, P4HB, contactin, osteoadherin, osteopontin) (Frangogiannis *et al.*, 2002a; Jugdutt, 2003). Genes which show early increase in the remote but low expression in the infarct (24h) but then lower in the remote and higher in the infarct at the later time point (4-wk) include the genes encoding MMPs which degrade collagen (MMPs 2, 9, 12, 23; 2-5 fold higher in infarct compared to sham), ADAM15 (glycoproteins for cell adhesion; up 2 fold in infarct compared to sham) and metallothioneine 1 and 3 involved in zinc binding which increase 2 fold in the infarct compared to the equivalent sham region (LaFramboise *et al.*, 2005). In the weeks after the MI, a large number of gene expression alterations are reported to occur in the infarct and peri-infarct regions only with little or no change in areas remote; these include genes encoding TGF- β 1, part of a super family of cytokines although the cell type was not specified (Vandervelde *et al.*, 2007), fibulin-2, a Ca²⁺-binding glycoprotein located in the vascular endothelial cells only (Tsuda *et al.*, 2012) and fibroblast growth factor receptor 1 (FGFR-1) found to be 1.4 fold higher in cardiomyocytes (Wang *et al.*, 2007) which all show increased levels in the peri-infarct alone. Regional patterns of altered gene expression are not surprising given the disparate remodelling processes in each region of the infarcted heart, more details on this are discussed later (French & Kramer, 2007). This may largely be contributing to the difficulty in trying to resolve the molecular mechanisms associated with adverse remodelling and HF.

4.1.2 Transcription factors in MI

Microarray technology has emerged as a large-scale approach for the identification of altered target genes during MI (Kaab *et al.*, 2004). In one study, this approach identified over 700 different genes which were altered after MI in the remodelled myocardium alone (Stanton *et al.*, 2000) and this is believed only to represent a fraction of the genes which show altered expression patterns after MI. However gene expression profiles are complex and require detailed understanding of the precise regulatory mechanisms underlying the control of their expression patterns. Transcription factors have therefore emerged as important targets in cardiac disease as they directly regulate the expression of many cardiac genes in response to specific physiological and pathophysiological signals. Furthermore, one of the earliest responses following cardiac injury is the activation of transcription factors (LaFramboise *et al.*, 2005). Transcription factors are therefore key for understanding the regulatory mechanisms and coordinated changes in cardiac gene expression during disease (Buermans *et al.*, 2005; Bruneau, 2002). Examples of transcription factors which have been shown to have altered expression post-MI are detailed below.

CARP and TSC-22: Additionally, the transcription factors CARP and transforming growth factor- β -stimulated clone (TSC)-22 both show elevated levels of expression in rat remodelled myocardium and have specific roles in cardiac gene regulation (Stanton *et al.*, 2000). CARP is constitutively expressed in the heart (within the nucleus of cardiomyocytes) and is up-regulated in a variety of different cardiac pathologies; including failing canine ventricular tissue (Zolk *et al.*, 2002), hypertrophied mouse hearts (Ihara *et al.*, 2002), hypertrophied rat models (aortic banding, SHR and Dahl salt-sensitive rats) (Aihara *et al.*, 2000) and also in explanted ventricular tissue from human HF patients (Zolk *et al.*, 2002). CARP is believed to be induced by both acute and chronic pressure-overload and stress pathways (Aihara *et al.*, 2000) and leads to contractile disturbances through repression of genes encoding contractile proteins. TSC-22 is also over-expressed in rat remodelled cardiac tissue and is believed to be important for mediating cardiac myofibroblast differentiation (Yan *et al.*, 2011).

HIF1- α : Another example of a transcription factor which has been characterised during MI is the hypoxia-inducible factor 1 alpha (HIF1- α) which activates gene expression of glycolytic enzymes and glucose transporters (Semenza *et al.*, 1994; Semenza, 1996). HIF1- α levels are increased in the nuclei of cardiomyocytes of the heart by ~ 2 fold in a rat

model of MI and hamster model of cardiomyopathy and HF (Kakinuma *et al.*, 2001). The same study revealed that HIF1- α mRNA was increased ~3.3 fold in cultured rat cardiomyocytes that were treated with a mitochondrial inhibitor Cobalt(II) Chloride (CoCl₂), therefore this degree of mRNA increase in HIF1- α led to an increase in glycolysis believed to be a protective response against impaired energy metabolism during MI (Kakinuma *et al.*, 2001). Transgenic studies with HIF1- α in mice have revealed that HIF1- α is required to reduce the extent of infarction (infarct size) and limit the progression of dysfunction in mice post-MI by promoting angiogenesis (Kido *et al.*, 2005).

WT-1: Recently the transcription factor Wilms' tumour protein (WT-1) has also been shown to have altered expression in MI (Finsen *et al.*, 2004). WT-1 expression was increased in non-infarcted myocardium (cell type not specified). WT-1 is known to be a transcriptional regulator of syndecans, a family of transmembrane proteoglycans which have also themselves been implicated in MI (Finsen *et al.*, 2004) as having increased expression in non-infarcted mouse myocardium post-MI and have been shown to be critical mediators in cardiac fibrosis (Frangogiannis, 2010).

4.1.3 RUNX transcription factors

As detailed in Introduction chapter (Chapter 1) RUNX proteins are novel transcription factors in the context of myocardial injury. RUNX1 has been shown to be up-regulated in the human heart in response to MI relative to healthy hearts (Gattenlohner *et al.*, 2003) and may represent a novel candidate gene for myocardial injury. RUNX1 has been shown to selectively regulate the expression of genes that encode important muscle proteins during disrupted electrical activity (e.g. in skeletal muscle) which are also found in cardiac tissue such as phospholamban, sodium channel type V, osteopontin and thrombospondin (Wang *et al.*, 2005). During these conditions RUNX1 elicited a protective role in the diseased muscle which may also be applicable to similar conditions of disrupted electrical activity in cardiac injury. RUNX2 has also been shown to have negligible expression in the healthy heart (negative with IHC in normal rat cardiomyocytes) (Custodio *et al.*, 2012) but is up-regulated under conditions of myocardial disease such as human DCM and HCM (Sanoudou *et al.*, 2005), aortic valve calcification (Garg *et al.*, 2005), atherosclerosis plaque formation (Tyson *et al.*, 2003) and during myocardial fibrosis and dysfunction (Elsherif *et al.*, 2008). RUNX3 expression during cardiac disease is virtually unknown. However, due to its links with RUNX1 cross-regulation (Levanon *et al.*, 2001a) and, like RUNX2, it is a direct target of Notch signalling pathways which are known to be altered in

cardiac disease (Fu *et al.*, 2011) it is therefore possible there may be altered expression patterns of RUNX3 like the other RUNX proteins. Despite this information, knowledge of the expression of RUNX proteins within the heart during CVD is limited. RUNX expression has not clearly been investigated in terms of its altered expression during cardiac disease in an animal model of MI. No evidence currently exists on their expression in different regions of the heart, over different time-points post-MI or any links with the cardiac expression in relation to the functioning of the heart.

4.1.4 Aims

The aims of the work in this chapter were to perform a detailed characterisation of the expression of *Runx* gene/protein expression in a mouse model of MI in terms of changes in expression, including how these changes develop over time, and in particular regions of the heart, and examine the links with dysfunction in response to MI.

4.2 Methods

4.2.1 Induction of MI

Mice underwent MI as described previously in the General Methods Section 2.1. Sham controls underwent the same procedure but without ligation. All subsequent experimental measurements detailed in this chapter were carried out either 4-wk or 8-wk post-MI except in the case of animals which developed severe MI (characterised by symptoms of laboured breathing, lung congestion and significant LV chamber dilation) which were sacrificed after 1-wk.

4.2.2 Tissue harvest

4.2.2.1 Heart tissue

At the appropriate time-point after MI, hearts were rapidly excised and perfused retrograde *via* the aorta with ice-cold saline to remove the blood. For heart tissue required for qRT-PCR, the atria and blood vessels at the base of the heart were removed and then either the intact ventricles were snap-frozen (whole heart measurements) or hearts were dissected into regions (regional measurements). This was performed using a microsurgical microscope by carefully dissecting away the infarct region (easily distinguishable as the whitened/fibrous thinned area), the peri-infarct (defined as the ring of myocardium around the infarct ~1mm in width; Sirius red stained images of the heart provided knowledge of

the location of the peri-infarct in relation to the scar), an area of remote LV furthest from the infarct at the base of the heart and an area of RV free wall to yield four different regions which were snap-frozen separately in liquid nitrogen. Care was taken not to include any scar tissue in any regions other than the infarct by removing the whole scar region first and examining that the other regions did not contain any fibrous (whitened) tissue under high magnification (x25). The ‘equivalent*’ regions of the sham heart were harvested as controls by dissecting a region of apex (to match the infarct), a 1 mm region adjacent to the apex (to match the peri-infarct) and similar regions of remote LV and RV free wall as in the infarcted heart. These will be labelled sham apex, sham ‘peri-infarct’ and sham remote LV throughout. All heart tissue was stored at -80°C until needed. Hearts for IHC were also perfused to remove all blood and the whole intact heart (including ventricles, atria and major blood vessels) was placed into 10% neutral buffered formalin for a minimum of 24 h.

4.2.2.2 Positive and negative control tissue

Adult mouse thymus was harvested either from stock mice or sham mice as positive control tissue for IHC as all RUNX proteins are highly expressed in adult thymus (Satake *et al.*, 1995; Woolf *et al.*, 2003). The thymus is located in the upper thoracic region and lies close to the base of the heart (as shown in Figure 4.1). Briefly, the entire thymus (both lobes) was removed and rinsed in ice-cold saline to remove any blood and placed in 10% neutral buffered formalin for a minimum of 24 h.

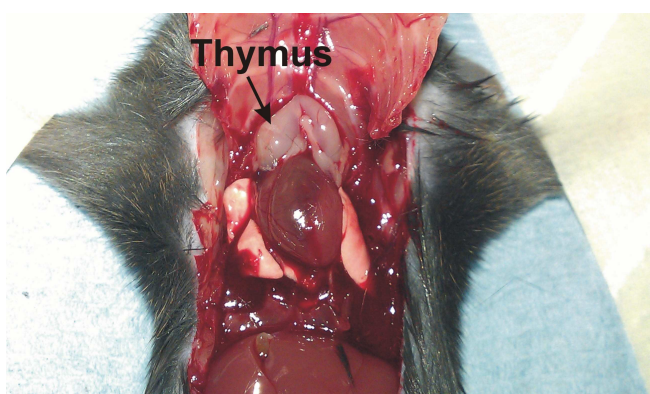


Figure 4.1 Location of mouse thymus in the upper thorax above the base of the heart.

Arrow indicates the location of the thymus.

* When referring to corresponding sham heart regions that do not by definition exist (e.g. peri-infarct) but are necessary to show control for the same region in the MI heart, these will be indicated by single inverted commas (e.g. sham ‘peri-infarct’) where appropriate. The sham control region for the infarct will be denoted as the sham apex. Remote LV will be stated the same for both sham and MI hearts.

4.2.3 Cardiomyocyte isolation and purification

Adult male C57Bl/6 control stock mice which had not undergone any previous surgery were used for these set of experiments. LV cardiomyocytes were isolated as described previously in the General Methods Section 2.10.1. The cells were kept on ice while a second cell isolation from a different heart using the same procedure was performed. The cells from the two hearts were then pooled to yield sufficient RNA for subsequent experiments. Cardiomyocytes were separated from other cell types using a filtration method as detailed in Section 2.10.3 of the General Methods. All of the following steps were performed on ice to minimise RNA degradation. A sample of the pooled cells (2 ml) was taken prior to any filtration as a pre-filtration control (i.e. containing all cell types) and was lysed in *Qiazol* lysis buffer and stored at -80°C until required. The remaining suspension was passed through a series of filters: firstly, a 300 µm nylon filter to separate large fragments of tissue from the cells followed by a 40 µm nylon filter to catch the cardiomyocytes with washes in between with ice-cold HBSS. Cardiomyocytes caught on the 40 µm filter were rinsed off into a separate tube with ice-cold HBSS, spun and lysed in *Qiazol* lysis buffer and stored at -80°C until required as the purified cardiomyocyte sample. This method was performed in order to verify the presence of *Runx* in cardiomyocytes alone by separating cardiomyocytes from other cell types (mostly fibroblasts and smooth muscle cells) using a filtration method published by (Kosloski *et al.*, 2009). The authors of this method report that this produces a purified population of >98% cardiomyocytes.

4.2.4 IHC and quantitative imaging

4.2.4.1 IHC

The heart was removed, perfused to remove all blood and placed into 10% neutral buffered formalin as noted in Section 4.2.2.1 above before being submitted to the Histopathology Unit. All immunohistochemistry was performed by Mrs Lynn Stevenson at the Histopathology Unit at the University of Glasgow as described fully in the General Methods Section 2.11. Briefly, following adequate fixation hearts were embedded in paraffin wax and 1 µm-thick longitudinal sections were cut parallel to the long axis of the heart. Sections were incubated for 60 min with a primary antibody (rabbit polyclonal 1:400, *Abcam*, U.K.) for RUNX1 or with antibody dilution buffer (negative control) followed by 30 min with a biotinylated secondary antibody (anti-rabbit) attached to a HRP conjugate (*Dako EnVision system*, *Dako*, *Denmark*). Sections were then treated with 2 x 5

min incubations with the chromagen DAB (*K5007 Dako, Denmark*) before the final dehydration and mounting.

4.2.4.2 Quantification of IHC staining

Sections were examined under a microscope (*Olympus Bx51*) and photographed using a camera (*Olympus DP71*) with accompanying software (*Cell D*) and analysed using *ImageJ*. A 5x4 grid (*ImageJ* plug-in) was fitted over the image to facilitate counting. The total number of positively-stained nuclei (brown coloured) and negatively-stained nuclei (blue coloured) were counted in each region (using a 60x lens) and the percentage positive staining was calculated using the following equation:

$$\% \text{ RUNX1 positive staining} = \left(\frac{\text{number of brown nuclei}}{\text{number of brown nuclei} + \text{number of blue nuclei}} \right) \times 100$$

Eq. 16

As the different cell types present were not specifically labelled with markers, no discrimination was made to exclude positive nuclei from any cell type. Positive staining included any nucleus which was predominantly brown. Where it looked like there may be two overlapping nuclei, this was counted as one only. This was repeated for three areas per region and a mean value taken.

4.2.5 RNA extraction

Total RNA was extracted from frozen heart tissue or frozen cell lysates using the miRNeasy Mini Kit (*Qiagen, U.K.*) based on a guanidine thiocyanate/phenol/chloroform extraction method followed by ethanol precipitation according to the manufacturer's protocol (full details are described in the General Methods Section 2.12). RNA extraction included on-column treatment with DNase I (*Qiagen, U.K.*) for 15 min at room temperature to remove genomic DNA. RNA yield and purity was determined by measuring the absorbance at 260 nm and absorbance ratio 260/280 nm, respectively with a Nanodrop ND-1000 Spectrophotometer (*Nanodrop Technologies/Thermo Scientific, U.K.*). RNA integrity was further determined by UV spectrophotometry and electrophoretogram (*Bioanalyzer 2100, Agilent Technologies, U.K.*). Only RNA that met minimum purity standards (260/280 >1.8 and RIN >7) was used for subsequent experiments. RNA was then incubated with a second DNase I treatment (*Turbo DNA-free, Ambion, U.K.*) for 25 min at 37°C.

4.2.6 cDNA synthesis

First strand cDNA was synthesised from 1 µg RNA by reverse transcription (RT) performed at 37°C for 1 h with Omniscript reverse transcriptase (*Qiagen, U.K.*) in a final volume of 50 µl containing dNTP, RNase inhibitors and oligo dT primers (*Omniscript Reverse Transcription kit, Qiagen, U.K.*). Reactions containing RNase/DNase-free water instead of reverse transcriptase enzyme served as negative RT controls (denoted RT⁻).

4.2.7 Verification of cDNA synthesis

cDNA (and RT⁻ controls) samples were tested to verify successful RT using conventional PCR amplification. PCR reactions were conducted in 10 µl final volume containing cDNA, PCR master mix (*Thermo Scientific, U.K.*), appropriate primers for *Runx* (*Quantitect, Qiagen, USA*) or *Gapdh* (*Eurofins MWG Operon, Germany*) and Taq DNA polymerase (*Thermo Scientific, U.K.*). Reactions were performed using a *Stratagene RoboCycler* PCR machine for either 30 cycles (*Gapdh*) or 40 cycles (*Runx1*) to ensure analysis was taken from the plateau phase of the reaction. Each cycle was 50s at 95°C, 50s at 55°C and 1 min at 65°C. Amplified PCR products were then visualised by gel electrophoresis on a 2% agarose gel (*NuSieve*; prepared fresh) treated with EtBr and using 3 µl PCR product mixed with 2 µl loading buffer into each well. A DNA size ladder was run alongside each run (*Promega, U.K.*). Successful RT reactions were confirmed by positive single bands of correct size for RT⁺ samples and no band in RT⁻ control samples.

4.2.8 qRT-PCR

qRT-PCR was performed with cDNA and SYBR Green master mix (*Applied Biosystems, U.K.*) in 20 µl final volume reactions using the ABI 7500 machine with Sequence Detection software (*Applied Biosystems, U.K.*) to measure relative gene expression. *Runx1-3* were detected using appropriate *Runx* primers (1, 2 or 3; all *Qiagen, USA*) normalised to *Gapdh* (*Eurofins MWG Operon, Germany*) for heart tissue studies or *PPIA* (*Qiagen, U.K.*) for purified cardiomyocyte preparations. (*Gapdh* was found to be the most stable gene for the MI heart tissue work while *PPIA* was recommended as a stable gene for the cell preparations according to the published method used for the protocol by (Kosloski *et al.*, 2009)). In all qRT-PCR experiments, template-free (no cDNA) controls and RT⁻ controls were always run in parallel with positive samples and each sample was run in triplicate for each experiment.

4.2.9 Interpretation of qRT-PCR data

qRT-PCR results were analysed using comparative Ct calculations; either $2^{-\Delta\Delta C_t}$ (regional comparisons relative to RV region), $2^{-\Delta C_t}$ (whole heart or RV region between sham and MI) or 2^{-C_t} (*Gapdh* stability) as recommended by accepted published methods (Schmittgen & Livak, 2008). Statistical significance between regions within the same heart was tested using multiple regression analysis performed with SPSS software. For comparisons of specific regions between sham and MI using unpaired samples, the student's unpaired t-test was used. A value of $P < 0.05$ was considered significant. All data were tested for normal distribution using a histogram plot and by plotting residuals. Triplicate measurements of Ct were assessed and any outliers removed using the Grubb's Test for removing outliers as an accepted published method for normalising qRT-PCR data (Burns *et al.*, 2005b). This was only used when Cts were >1 Ct different to the others in the triplicate set. A Grubb's statistic of >1.00 was the criteria for removing an outlier value. The formula for the Grubb's test is as follows:

$$G = \frac{|Y_i - \bar{Y}|}{SD} \quad \text{Eq. 17}$$

Where G is the test statistic associated with the Grubb's Test, Y_i is the i th observation from the data set (suspected outlier), \bar{Y} is the sample mean (with outlier included) and SD is the standard deviation of the data set (with outlier included).

4.3 Results

4.3.1 Expression of *Runx1* in the whole heart post-MI

Runx1 mRNA levels were assessed in whole heart homogenates (LV + RV) 4-wk post-MI using qRT-PCR. The results demonstrated firstly that *Runx1* was present in sham hearts indicating a basal expression of *Runx1* in the normal mouse heart (mean *Runx1* Ct value of 20.6 ± 0.7). Although acceptable Ct ranges for detectable expression have not been specifically defined, it is generally considered in the literature (and from personal communication with companies specialising in qRT-PCR) that Cts ≤ 30 represent strong abundance of the gene, Cts of 31-35 indicate very low expression but in some cases can still be acceptable, and Cts of 38-40 indicate extremely weak/barely detectable expression (Goni *et al.*, 2009; Sigma Aldrich, 2010). The second finding was that *Runx1* expression was significantly increased in the MI heart 4-wk post-MI to 247.7% of levels in 4-wk sham hearts ($247.7 \pm 66.3\%$ increase; 4-wk MI ($n=7$) compared to 4-wk sham (100%; $n=6$); $P < 0.05$; Figure 4.2A). This was calculated using the ratio of ($2^{-\Delta Ct}$ (MI)/mean $2^{-\Delta Ct}$ (sham)) * 100. Expression of the housekeeping gene *Gapdh* was not different between sham and MI for whole heart expression as shown by equivalent Ct values (15.7 ± 0.5 vs. 15.6 ± 0.3 raw Ct; 4-wk sham ($n=6$) vs. 4-wk MI ($n=7$); $P > 0.05$; Figure 4.2B(i)) and equivalent expression ($2.6 \times 10^{-5} \pm 8.9 \times 10^{-6}$ vs. $2.3 \times 10^{-5} \pm 6.1 \times 10^{-6}$; $2^{-Ct(\text{Gapdh})}$; 4-wk sham ($n=6$) vs. 4-wk MI ($n=7$); $P > 0.05$; Figure 4.2B(ii)) between sham and MI indicating that *Gapdh* was a suitable internal control gene for these measurements.

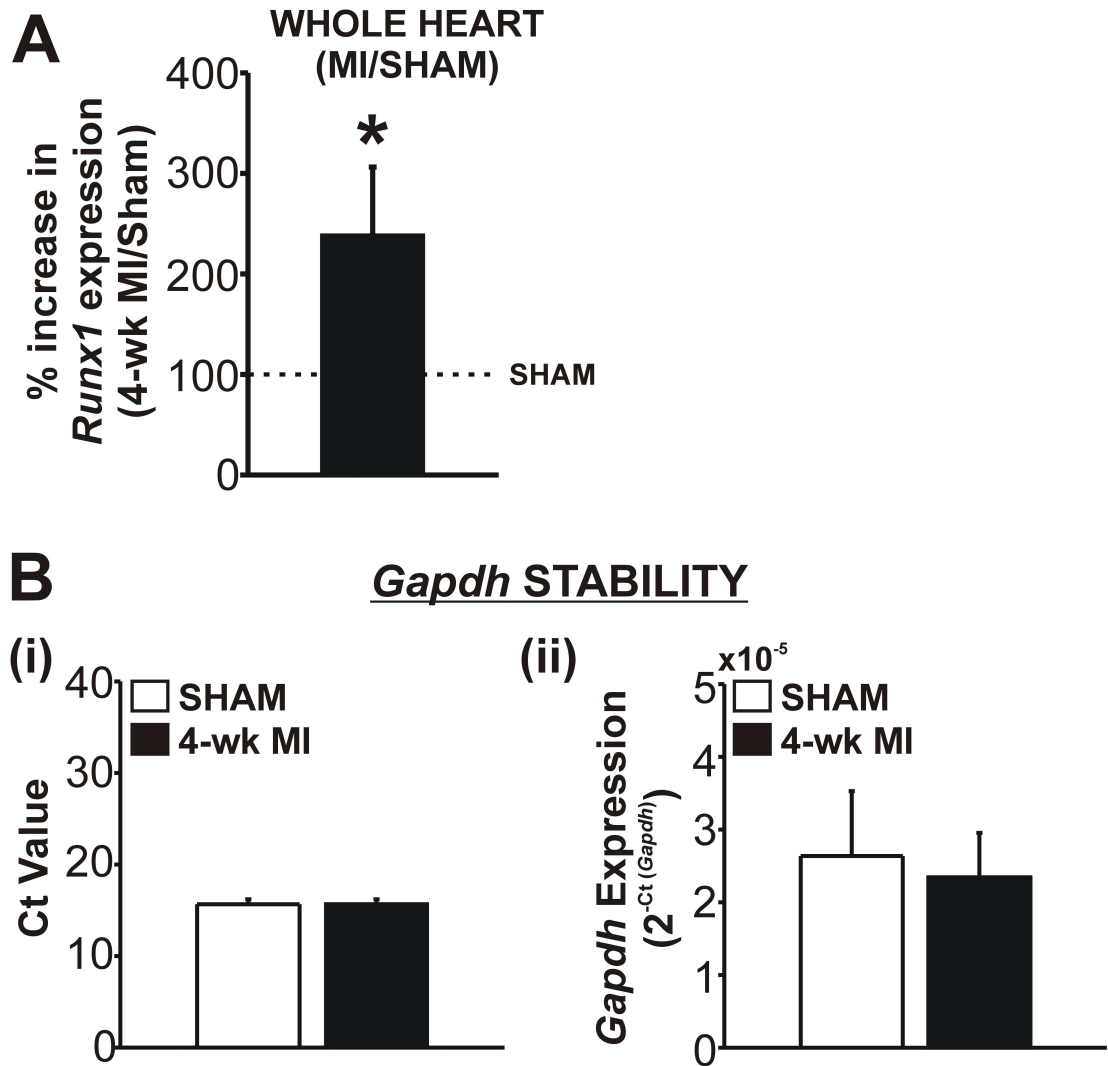


Figure 4.2 *Runx1* expression and *Gapdh* stability in the whole heart 4 weeks post-MI.

(A) *Runx1* gene expression measured by qRT-PCR using *Runx1* specific primers on whole heart homogenates (LV + RV) from 4-wk MI hearts ($n=7$; black bar) relative to 4-wk sham hearts ($n=6$; dotted line). (B (i)) Raw Ct values for the housekeeping gene *Gapdh* between sham ($n=6$; white bar) and 4-wk MI hearts ($n=7$; black bar). (B (ii)) Resulting fold change in *Gapdh* between sham ($n=6$; white bar) and 4-wk MI hearts ($n=7$; black bar). Data presented are mean \pm SEM. * $P < 0.05$.

4.3.2 Expression of *Runx1* in different regions of the heart post-MI

Runx1 expression was measured in different regions of the heart: infarct, peri-infarct, remote LV and RV to assess regional variation at 4-wk post-MI. Expression in each region was normalised to *Gapdh* and expressed relative to the non-infarcted RV region of the same heart (RV set to 1.0) using the comparative Ct ($2^{-\Delta\Delta C_t}$) method. *Runx1* levels in the RV region were not different between 4-wk sham and 4-wk MI as analysed using the $2^{-\Delta C_t}$ method (0.23 ± 0.06 vs. 0.20 ± 0.09 $2^{-\Delta C_t}$; 4-wk sham ($n=5$) vs. 4-wk MI ($n=6$); $P>0.05$; Figure 4.3A(ii)) which permitted regional comparisons between sham and MI.

4.3.2.1 *Runx1* expression in regions of the 4-wk sham heart

Results from qRT-PCR revealed that *Runx1* expression was uniform across all regions of the sham heart with no differences between any of the regions compared to the sham RV which was set to 1.0. These differences were measured using the $2^{-\Delta\Delta C_t}$ method. This was true for the sham apex (1.4 ± 0.2 vs. 1.0 RQ; sham apex ($n=4$) vs. sham RV ($n=4$); $P>0.05$; Figure 4.3A(i)), the 'peri-infarct' equivalent sham region (1.1 ± 0.1 vs. 1.0 RQ; sham 'peri-infarct' ($n=4$) vs. sham RV ($n=4$); $P>0.05$; Figure 4.3A(i)) and the sham remote LV (1.2 ± 0.1 vs. 1.0 RQ; sham remote LV ($n=4$) vs. sham RV ($n=4$); $P>0.05$; Figure 4.3A(i)).

4.3.2.2 *Runx1* expression in regions of the 4-wk MI heart

Runx1 expression was significantly increased in the infarct region of 4-wk MI hearts compared to the MI heart's respective RV (5.1 ± 1.0 vs. 1.0 RQ; MI infarct ($n=8$) vs. MI RV ($n=8$); $P<0.05$; Figure 4.3A(i)). The peri-infarct region of 4-wk MI hearts showed significantly higher *Runx1* expression compared to its own RV region (1.8 ± 0.2 vs. 1.0 RQ; MI peri-infarct ($n=8$) vs. MI RV ($n=8$); $P<0.05$; Figure 4.3A(i)). There were no significant differences observed between the remote LV region of the 4-wk MI heart compared to its respective RV region (1.4 ± 0.2 vs. 1.0 RQ; MI remote LV ($n=8$) vs. MI RV ($n=8$); $P>0.05$; Figure 4.3A(i)).

4.3.2.3 Comparison of regional *Runx1* expression between 4-wk MI and 4-wk sham

Comparing each region between sham and MI (both at the 4-wk time point) showed that the infarct region of the MI heart had significantly higher levels of *Runx1* expression than the equivalent apical sham region (5.1 ± 1.0 vs. 1.4 ± 0.2 RQ to its respective RV region;

4-wk MI ($n=8$) vs. 4-wk sham ($n=4$); $P<0.05$; Figure 4.3A(i)). *Runx1* was significantly increased in the peri-infarct region of 4-wk MI hearts compared to the equivalent 'peri-infarct' region of the 4-wk sham heart (1.8 ± 0.2 vs. 1.1 ± 0.1 RQ to its respective RV region; 4-wk MI ($n=8$) vs. 4-wk sham ($n=4$); $P<0.05$; Figure 4.3A(i)). *Runx1* expression was not significantly different in the remote LV of 4-wk MI hearts compared to the remote LV region of 4-wk sham hearts (1.4 ± 0.2 vs. 1.2 ± 0.1 RQ to its respective RV region; 4-wk MI ($n=8$) vs. 4-wk sham ($n=4$); $P>0.05$; Figure 4.3A(i)).

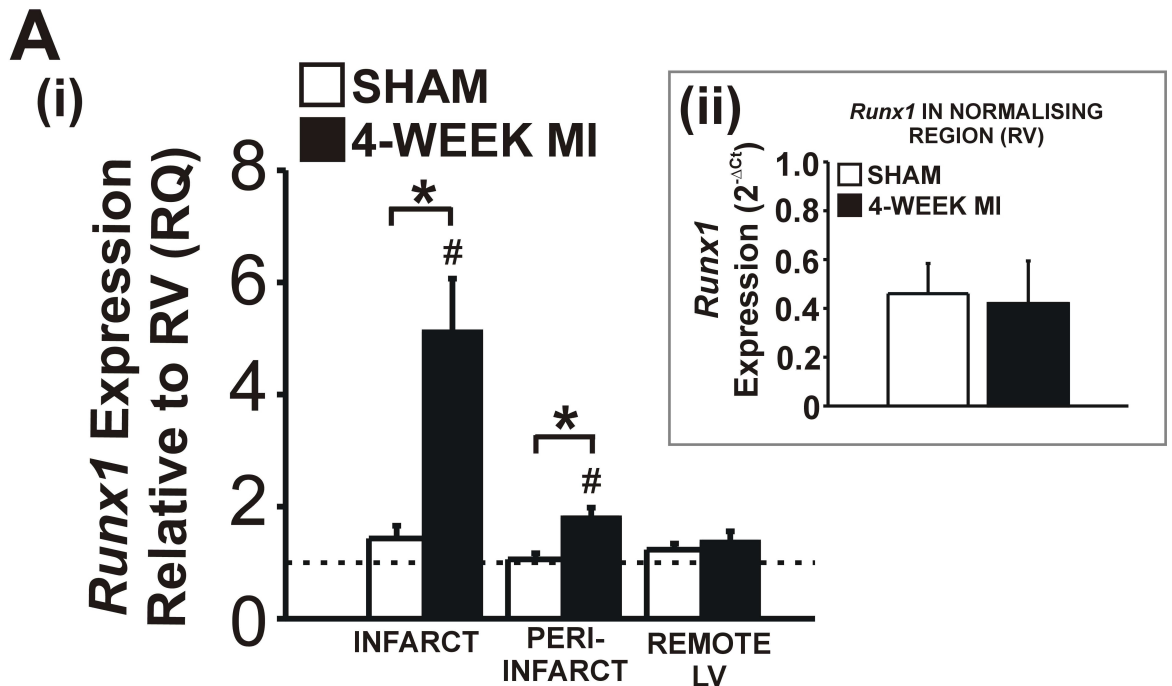


Figure 4.3 Regional expression of *Runx1* 4 weeks post-MI.

(A (i)) *Runx1* expression measured by qRT-PCR in different regions of the heart in 4-wk sham ($n=4$) and 4-wk MI hearts ($n=8$); infarct, peri-infarct and remote LV were expressed relative to their respective RV region (dotted line). (A (ii)) *Runx1* expression in the RV regions between 4-wk sham ($n=5$) and 4-wk MI ($n=6$). # $P<0.05$ between region of interest and the RV of the same heart; * $P<0.05$ between MI and sham.

4.3.3 Expression of *Runx1* at different time points post-MI

Regional *Runx1* gene expression levels were additionally determined at different time points post-MI (Figure 4.4). Regional expression at the **4-wk time point** has been described in the previous section (Section 4.3.2).

At the **8-wk time point** *Runx1* expression in the RV region between 8-wk sham and 8-wk MI was not different as analysed using the $2^{-\Delta\text{Ct}}$ method (0.010 ± 0.004 vs. 0.010 ± 0.005 $2^{-\Delta\text{Ct}}$; 8-wk sham vs. 8-wk MI; $P > 0.05$; Figure 4.4A(ii)). This allowed for comparisons between 8-wk sham and 8-wk MI to be made.

4.3.3.1 *Runx1* expression in regions of the 8-wk sham heart

As was observed in the sham heart at 4-wk, there were no differences in *Runx1* expression between the different regions of the 8-wk sham heart (compared to the 8-wk sham heart's respective RV) as measured using the $2^{-\Delta\Delta\text{Ct}}$ method. This was the case for the 8-wk sham apex (1.1 ± 0.2 vs. 1.0 RQ; sham apex ($n=4$) vs. sham RV ($n=4$); $P > 0.05$; Figure 4.4A(i)), the 'peri-infarct' equivalent 8-wk sham region (1.2 ± 0.2 vs. 1.0 RQ; sham 'peri-infarct' ($n=4$) vs. sham RV ($n=4$); $P > 0.05$; Figure 4.4A(i)) and the sham remote LV (0.8 ± 0.2 vs. 1.0 RQ; sham remote LV ($n=4$) vs. sham RV ($n=4$); $P > 0.05$; Figure 4.4A(i)).

4.3.3.2 *Runx1* expression in regions of the 8-wk MI heart

All regions of the 8-wk MI heart were also compared relative to their non-infarcted RV region within the same heart using the $2^{-\Delta\Delta\text{Ct}}$ method. 8-wk MI hearts demonstrated a significant increase in *Runx1* expression in the infarct region compared to the respective RV of the 8-wk MI heart (3.7 ± 0.9 vs. 1.0 RQ; MI infarct ($n=8$) vs. MI RV ($n=8$); $P < 0.05$; Figure 4.4A(i)). *Runx1* expression was also significantly increased in the peri-infarct region compared to the respective 8-wk MI RV (2.2 ± 0.3 vs. 1.0 RQ; MI peri-infarct ($n=8$) vs. MI RV ($n=8$); $P < 0.05$; Figure 4.4A(i)). The remote LV region of the 8-wk MI heart also showed significantly elevated levels of *Runx1* expression compared to the respective 8-wk MI RV (2.7 ± 0.6 vs. 1.0 RQ; MI remote LV ($n=8$) vs. MI RV ($n=8$); $P < 0.05$; Figure 4.4A(i)).

4.3.3.3 Comparison of regional *Runx1* expression between 8-wk MI and 8-wk sham

Also similar to 4-wk MI, 8-wk MI hearts also demonstrated a significant increase in *Runx1* expression in the infarct region compared to the equivalent region in 8-wk sham (3.7 ± 0.9 vs. 1.1 ± 0.2 RQ to respective RV region; 8-wk MI ($n=8$) vs. 8-wk sham ($n=4$); $P<0.05$; Figure 4.4A(i)). Similar to the situation at 4-wk, the level of *Runx1* expression in the peri-infarct region at 8-wk post-MI was significantly higher compared to the corresponding 8-wk sham region (2.2 ± 0.3 vs. 1.2 ± 0.2 RQ; 8-wk MI ($n=8$) vs. 8-wk sham ($n=4$); $P<0.05$; Figure 4.4A(i)). Interestingly at 8-wk, *Runx1* expression was significantly elevated in the remote region of the 8-wk MI heart compared to 8-wk sham remote (2.7 ± 0.6 vs. 0.8 ± 0.2 RQ to respective RV region; 8-wk MI ($n=8$) vs. 8-wk sham ($n=4$); $P<0.05$; Figure 4.4A(i)). This finding of increased expression in the 8-wk remote LV compared to 8-wk sham remote is in contrast to the observations at 4-wk in which there was no significant change in *Runx1* levels in the remote region between 4-wk MI and 4-wk sham.

4.3.3.4 *Runx1* expression between 4-wk MI and 8-wk MI

Expression levels of *Runx1* in the infarct region between 4-wk MI and 8-wk MI were not significantly different (5.1 ± 1.0 vs. 3.7 ± 0.9 RQ to respective RV region; 4-wk MI ($n=8$) vs. 8-wk MI ($n=8$); $P>0.05$; Figure 4.4B). There were also no significant differences in the expression of *Runx1* in the peri-infarct regions in the 4-wk and 8-wk MI heart (1.8 ± 0.2 vs. 2.2 ± 0.3 RQ to respective RV region; 4-wk MI ($n=8$) vs. 8-wk MI ($n=8$); $P>0.05$; Figure 4.4B). However, in contrast to the similar expression levels in the infarct and peri-infarct regions, there was a significantly greater level of *Runx1* expression in the remote LV at 8-wk MI than the remote LV at 4-wk MI (1.4 ± 0.2 vs. 2.7 ± 0.6 RQ to respective RV region; 4-wk MI ($n=8$) vs. 8-wk MI ($n=8$); $P<0.05$); Figure 4.4B).

4.3.3.5 *Runx1* expression at 1-wk in a severe MI phenotype

The highest level of *Runx1* expression was observed at a 1-wk time point following a severe MI phenotype (as defined by symptoms of laboured breathing, severe infarct thinning and lung congestion; see Section 3.4.3 Chapter 3). It is believed that animals in this condition were suffering from acute HF although it was not possible to confirm this by functional assessment due to the severity of their condition. These animals were killed in the interest of their welfare and the hearts excised immediately and treated in the same way as the other time points. However, due to the small proportion of animals developing this phenotype, only one heart was available for qRT-PCR analysis from this group ($n=1$).

1-wk sham: The control 1-wk sham heart showed the following levels of *Runx1* expression across the four regions: sham apex (0.3 vs. 1.0 RQ to respective RV; sham apex ($n=1$) vs. sham RV ($n=1$); Figure 4.4C(i)), the peri-infarct (1.1 vs. 1.0 RQ to respective RV; sham 'peri-infarct' ($n=1$) vs. sham RV ($n=1$); Figure 4.4C(i)) and the remote LV (1.4 vs. 1.0 RQ to respective RV; sham remote LV ($n=1$) vs. sham RV ($n=1$); Figure 4.4C(i)).

1-wk MI heart: The 1-wk MI heart with the severe MI phenotype showed a high level of *Runx1* expression in the infarct region compared to the respective MI RV (12.0 vs. 1.0 RQ; MI infarct ($n=1$) vs. MI RV ($n=1$); Figure 4.4C(i)). A similar high level of *Runx1* was found in the peri-infarct region (11.5 vs. 1.0 RQ; MI peri-infarct ($n=1$) vs. MI RV ($n=1$); Figure 4.4C(i)). The remote LV showed the following (1.9 vs. 1.0 RQ; MI remote LV ($n=1$) vs. MI RV ($n=1$); Figure 4.4C(i)).

1-wk sham vs. 1-wk MI: Comparing the 1-wk MI with the 1-wk sham showed higher levels of *Runx1* in the infarct region (12.0 vs. 0.3 RQ; MI infarct ($n=1$) vs. sham apex ($n=1$); Figure 4.4C(i)) and in the peri-infarct region (11.5 vs. 1.1 RQ; MI peri-infarct ($n=1$) vs. sham 'peri-infarct' ($n=1$); Figure 4.4C(i)). The remote LV between the MI and sham were as follows: (1.9 vs. 1.4 RQ; MI remote LV ($n=1$) vs. sham remote LV ($n=1$); Figure 4.4C(i)). However due to a very small proportion ($n=3$) of animals developing this very severe phenotype and only 1 heart ($n=1$) being available for qRT-PCR measurements, this observation represents data from only one animal for sham and MI and therefore it was not possible to perform any statistics on this data set.

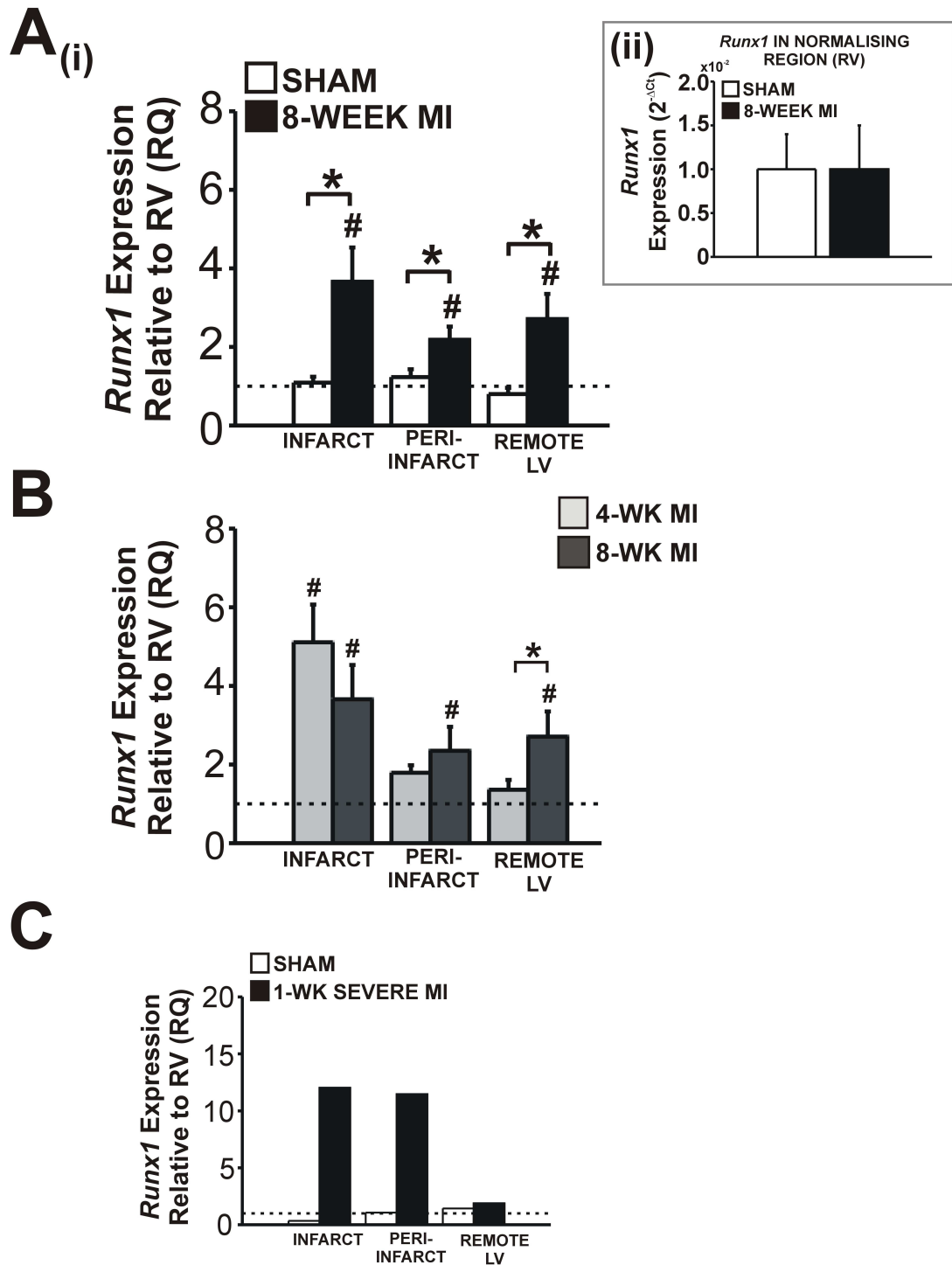


Figure 4.4 Regional *Runx1* expression at different time points post-MI.

(A (i)) Regional *Runx1* expression in 8-wk MI hearts ($n=6$; black bars) compared to 8-wk sham hearts ($n=4$; white bars) measured by qRT-PCR using *Runx1* specific primers; each region is expressed relative to its respective RV region (dotted line). A (ii) *Runx1* expression in the RV region (normalising region) between groups. (B) Comparison of *Runx1* expression in different regions of the infarcted heart between 4-wk (light grey bars) and 8-wk MI (dark grey bars) hearts as compared to the respective RV region (dotted line). (C (i)) *Runx1* expression in 1-wk animals showing symptoms of severe MI ($n=1$; black bars) compared to 1-week sham ($n=1$; white bars); each region expressed relative to its respective RV region (dotted line) and (ii) *Runx1* expression in the infarct and peri-infarct only of 1-wk severe MI animals using the mean $2^{-\Delta Ct}$ of infarct and peri-infarct for each animal (sham; $n=1$) and (MI; $n=1$). # $P < 0.05$ between region of interest and the respective RV.; * $P < 0.05$ between MI and sham.

4.3.4 Comparison of regional expression of different *Runx* genes post-MI

In addition to *Runx1*, the other *Runx* genes (*Runx2* and *Runx3*) were also measured in regions of the infarcted heart 4-wk post-MI to compare mRNA expression patterns between the different genes of the *Runx* family. Regional *Runx1* expression data at 4-wk post-MI has been discussed previously in Section 4.3.2.

4.3.4.1 Regional expression of *Runx2* at 4-wk post-MI

4-wk sham heart: As has previously been observed with *Runx1*, the expression of *Runx2* was not different between regions of the 4-wk sham heart. This was ascertained by comparing expression levels in each region relative to each heart's respective RV using the $2^{-\Delta\Delta Ct}$ method. No differences were observed in the 4-wk sham apex (1.1 ± 0.3 vs. 1.0 RQ; sham apex ($n=3$) vs. sham RV ($n=3$); $P>0.05$; Figure 4.5A), or the 'peri-infarct' equivalent 4-wk sham region (0.9 ± 0.1 vs. 1.0 RQ; sham 'peri-infarct' ($n=3$) vs. sham RV ($n=3$); $P>0.05$; Figure 4.5A) nor the sham remote LV (1.2 ± 0.2 vs. 1.0 RQ; sham remote LV ($n=3$) vs. sham RV ($n=3$); $P>0.05$; Figure 4.5A).

4-wk MI heart: *Runx2* expression was also compared in different regions of the 4-wk MI heart. Each region was expressed relative to the respective non-infarcted RV region within the same heart using the $2^{-\Delta\Delta Ct}$ method. As was observed with *Runx1*, *Runx2* expression was significantly elevated in the infarct region of the heart 4-wk post-MI compared to its respective RV of the MI heart (5.3 ± 1.1 vs. 1.0 RQ; MI infarct ($n=7$) vs. MI RV ($n=7$); $P<0.05$; Figure 4.5A). *Runx2* was not altered in the peri-infarct region 4-wk post-MI with no significant differences in expression compared to the respective RV (1.4 ± 0.5 vs. 1.0 RQ; MI peri-infarct ($n=7$) vs. MI RV ($n=7$); $P>0.05$; Figure 4.5A). Similarly there was also no significant differences in *Runx2* expression in the 4-wk MI remote LV compared to the respective RV (1.2 ± 0.3 vs. 1.0 RQ; MI remote LV ($n=7$) vs. MI RV ($n=7$); $P>0.05$; Figure 4.5A).

4-wk sham vs. 4-wk MI: Comparing *Runx2* expression between 4-wk MI regions and the corresponding region of the 4-wk sham heart revealed that *Runx2* expression was higher in the infarct region versus the 4-wk sham apex (5.3 ± 1.1 vs. 1.1 ± 0.3 RQ to respective RV; MI infarct ($n=7$) vs. sham apex ($n=3$); $P<0.05$; Figure 4.5A). *Runx2* expression in the 4-wk MI heart was not significantly different to the 4-wk sham heart in the peri-infarct region (1.4 ± 0.5 vs. 0.9 ± 0.1 RQ to respective RV; MI peri-infarct ($n=7$) vs. sham 'peri-

infarct' ($n=3$); $P>0.05$; Figure 4.5A) or the remote LV region (1.2 ± 0.3 vs. 1.2 ± 0.2 RQ to respective RV; MI remote LV ($n=7$) vs. sham remote LV ($n=3$); $P>0.05$; Figure 4.5A).

4.3.4.2 Regional expression of *Runx3* at 4-wk post-MI

4-wk sham heart: Similar to the results from *Runx1* and *Runx2*, the results for *Runx3* expression showed no significant differences across the regions of the 4-wk sham heart. This was true for the sham apex compared to the respective RV (0.9 ± 0.2 vs. 1.0 RQ; sham apex ($n=3$) vs. sham RV ($n=3$); $P>0.05$; Figure 4.5B), for the sham 'peri-infarct' region (1.1 ± 0.1 vs. 1.0 RQ; sham 'peri-infarct' ($n=3$) vs. sham RV ($n=3$); $P>0.05$; Figure 4.5B), and for the sham remote LV (1.0 ± 0.3 vs. 1.0 RQ; sham remote LV ($n=3$) vs. sham RV ($n=3$); $P>0.05$; Figure 4.5B).

4-wk MI heart: In the 4-wk MI heart, *Runx3* expression was significantly elevated in the infarct region compared to the non-infarcted RV of the MI heart (11.0 ± 2.0 vs. 1.0 RQ; MI infarct ($n=7$) vs. MI RV ($n=7$); $P<0.05$; Figure 4.5B). *Runx3* levels were also significantly elevated in the peri-infarct region compared to the RV of the MI heart (4.3 ± 1.0 vs. 1.0 RQ; MI peri-infarct ($n=7$) vs. MI RV ($n=7$); $P<0.05$; Figure 4.5B). No differences were observed in *Runx3* expression between the LV remote and the RV of the MI heart (2.0 ± 0.8 vs. 1.0 RQ; MI remote LV ($n=7$) vs. MI RV ($n=7$); $P>0.05$; Figure 4.5B).

4-wk sham vs. 4-wk MI: In addition to the regional expression within the 4-wk sham and 4-wk MI heart individually (comparing each to their respective RV of the same heart), the regional differences were also compared between 4-wk MI and the corresponding region of the sham heart. *Runx3* was found to be significantly higher in the infarct region of the MI heart compared to the equivalent sham apex region (11.0 ± 2.0 vs. 0.9 ± 0.2 RQ to respective RV region; MI infarct ($n=7$) vs. sham apex ($n=3$); $P<0.05$; Figure 4.5B). *Runx3* was also significantly higher in the peri-infarct region of the MI heart compared to the sham 'peri-infarct' region (4.3 ± 1.0 vs. 1.1 ± 0.1 RQ to respective RV region; MI peri-infarct ($n=7$) vs. sham 'peri-infarct' ($n=3$); $P<0.05$; Figure 4.5B). No differences were observed in the levels of *Runx3* between the LV remote of the MI heart with the LV remote of the sham heart (2.0 ± 0.8 vs. 1.0 ± 0.3 RQ to respective RV region; MI remote LV ($n=7$) vs. sham remote LV ($n=3$); $P>0.05$; Figure 4.5B).

4.3.4.3 Comparison of *Runx1-3* expression in the 4-wk MI heart

Expression patterns of the three *Runx* genes (1-3) were assessed to compare how their regional differences in MI compared with each other. *Runx3* showed the greatest degree of elevated expression in the infarct region with expression levels significantly greater than *Runx1* (11.0 ± 2.0 vs. 5.1 ± 1.0 RQ to respective RV region; *Runx3* MI infarct ($n=7$) vs. *Runx1* MI infarct ($n=8$); $P<0.05$; Figure 4.5C) and *Runx2* (11.0 ± 2.0 vs. 5.3 ± 1.1 RQ to respective RV region; *Runx3* MI infarct ($n=7$) vs. *Runx2* MI infarct ($n=7$); $P<0.05$; Figure 4.5C). *Runx3* also showed the greatest degree of elevated expression in the peri-infarct post-MI compared to *Runx2* only (4.3 ± 1.0 vs. 1.4 ± 0.5 RQ to respective RV region; *Runx3* MI peri-infarct ($n=7$) vs. *Runx2* MI peri-infarct ($n=7$); $P<0.05$; Figure 4.5C) but not compared to *Runx1* (4.3 ± 1.0 vs. 1.8 ± 0.2 RQ to respective RV region; *Runx3* MI peri-infarct ($n=7$) vs. *Runx1* MI peri-infarct ($n=8$); $P>0.05$; Figure 4.5C). *Runx1* and *Runx2* were altered to the same degree as each other post-MI with equivalent expression levels in the infarct (5.1 ± 1.0 vs. 5.3 ± 1.1 RQ to respective RV region; *Runx1* MI infarct ($n=8$) vs. *Runx2* MI infarct ($n=7$); $P>0.05$; Figure 4.5C) and peri-infarct regions (1.8 ± 0.2 vs. 1.4 ± 0.5 RQ to respective RV region; *Runx1* MI peri-infarct ($n=8$) vs. *Runx2* MI peri-infarct ($n=7$); $P>0.05$; Figure 4.5C). All three *Runx* genes showed a similar level of expression in the remote LV with no significant differences between the three (1.4 ± 0.2 vs. 1.2 ± 0.3 vs. 2.0 ± 0.8 RQ to respective RV region; *Runx1* MI remote LV ($n=8$) vs. *Runx2* MI remote LV ($n=7$) vs. *Runx3* MI remote LV ($n=7$); $P>0.05$ between all three; Figure 4.5C).

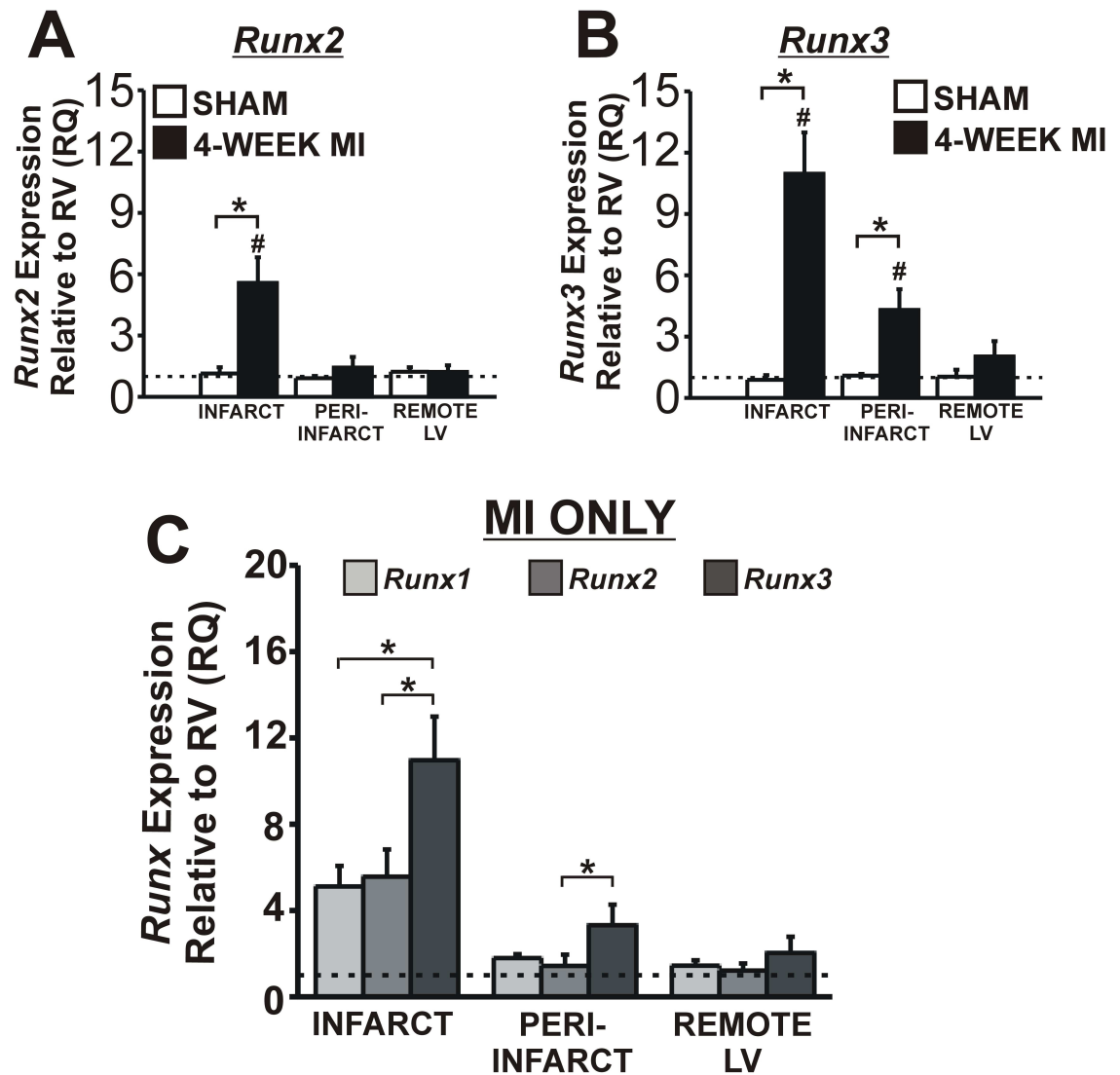


Figure 4.5 Expression of different *Runx* genes post-MI.

(A) Expression of *Runx2* in different regions of sham ($n=3$) or 4-wk MI ($n=7$) hearts using qRT-PCR. (B) Expression of *Runx3* in different regions of sham ($n=3$) or 4-wk MI ($n=7$) hearts using qRT-PCR. (C) Comparison of all three *Runx* genes for each region of the infarcted heart after 4-wk. Data presented are mean \pm SEM. # $P < 0.05$ between region of interest and the RV of the same heart; * $P < 0.05$ between MI and sham.

4.3.5 Links with *Runx* expression and LV function

Further analysis was performed to assess whether changes in *Runx* gene expression correlated with the extent of LV dysfunction. The functional parameters selected for this analysis were the maximal rate of LV pressure rise (dP/dt_{max}) and the maximal rate of LV pressure decay (dP/dt_{min}). These parameters are widely accepted as reliable indicators of myocardial inotropic (dP/dt_{max}) or lusitropic (dP/dt_{min}) state (Kass *et al.*, 1987) and were therefore considered suitable indices of LV function for this part of the study. The RQ values for the three regions of each heart were added up together then divided by 3 to give a single mean RQ value for *Runx* expression per heart for 4-wk sham and for 4-wk MI – calculated as shown below. This value was then paired with the function of that heart to assess the correlation. This was performed for each *Runx* gene (i.e. *Runx1*, *Runx2* and *Runx3*).

$$RQ \text{ value used for correlation study} = \frac{(RQ_{infarct} + RQ_{peri\ infarct} + RQ_{remote\ LV})}{3}$$

Eq. 18

4.3.5.1 Correlations between *Runx1* and LV function

These results revealed that the rise in *Runx1* expression in the heart showed a significant negative correlation with LV function for both parameters investigated. As dP/dt_{max} decreased (myocardial contractility reduced), the expression of *Runx1* increased ($y = -4.4 \times 10^{-4}x + 6.0$; $R = -0.74$; $P < 0.05$; Figure 4.6A(i)). Similarly as dP/dt_{min} decreased (myocardial relaxation impaired), the expression of *Runx1* also increased with significant negative correlation ($y = -4.4 \times 10^{-4}x + 5.1$; $R = -0.95$; $P < 0.05$; Figure 4.6A(ii)).

4.3.5.2 Correlations between *Runx2* and LV function

The results revealed that there was no significant relationship between *Runx2* expression and either dP/dt_{max} ($y = 1.68 \times 10^{-4}x + 0.1$; $R = 0.32$; $P > 0.05$; Figure 4.6B(i)) or dP/dt_{min} ($y = -5.7 \times 10^{-4}x + 1.9$; $R = -0.24$; $P > 0.05$; Figure 4.6B(ii)).

4.3.5.3 Correlations between *Runx3* and LV function

Although a similar trend was observed between *Runx3* and dP/dt_{max} (as had been observed with *Runx1*) the relationship between *Runx3* and dP/dt_{max} did not attain statistical significance ($y = -1.7 \times 10^{-3}x + 17.8$; $R = -0.69$; $P > 0.05$; Figure 4.6C(i)). There was however

a strongly significant negative correlation between *Runx3* expression and dP/dt_{\min} ($y = -1.1 \times 10^{-3}x + 10.6$; $R = -0.99$; $P < 0.0001$; Figure 4.6C(ii)).

4.3.5.4 Correlations with *Runx* expression and LV function excluding the infarct

To assess whether the trends observed were related to size of the infarct, the contribution of *Runx* expression from the infarct region was removed from the analysis. As Figure 4.7 shows the same trends remain even with the contribution of *Runx* expression from the infarct removed.

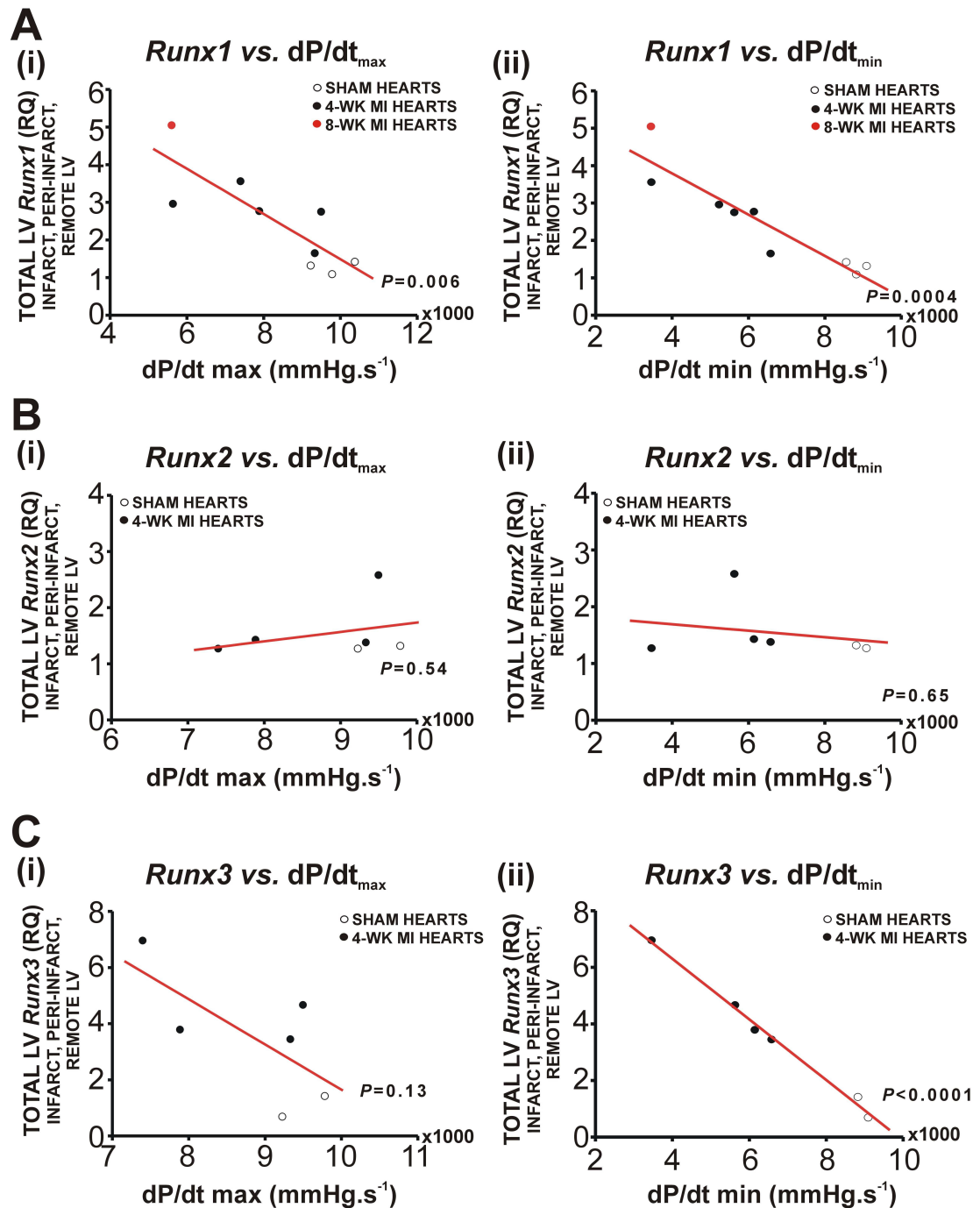


Figure 4.6 Correlations with *Runx* gene expression and LV function.

(A) Linear regression of the mean RQ value for *Runx1* expression of all LV regions relative to their respective RV region in individual MI (4-wk $n=6$; 8-wk $n=1$) and 4-wk sham hearts ($n=3$) 4-wk post-MI plotted against (i) dP/dt_{max} or (ii) dP/dt_{min} (infarct size was not variable between hearts). For dP/dt_{max} ($y=-6.0 \times 10^{-4}x + 7.5$; $R=-0.83$; $P<0.05$) and for dP/dt_{min} ($y=-5.5 \times 10^{-4}x + 8.6$; $R=-0.92$; $P<0.05$). (B) Linear regression of the mean RQ value for *Runx2* expression of all LV regions relative to their respective RV region in individual 4-wk MI ($n=4$) and 4-wk sham hearts ($n=2$) plotted against (i) dP/dt_{max} or (ii) dP/dt_{min} (infarct size was not variable between hearts). For dP/dt_{max} ($y=1.7 \times 10^{-4}x + 0.1$; $R=0.32$; $P>0.05$) and for dP/dt_{min} ($y=-5.7 \times 10^{-5}x + 1.9$; $R=-0.24$; $P>0.05$). (C) Linear regression of the mean RQ value for *Runx3* expression of all LV regions relative to their respective RV region in individual 4-wk MI ($n=4$) and 4-wk sham hearts ($n=2$) plotted against (i) dP/dt_{max} or (ii) dP/dt_{min} (infarct size was not variable between hearts). For dP/dt_{max} ($y=1.7 \times 10^{-3}x + 17.8$; $R=-0.69$; $P>0.05$) and for dP/dt_{min} ($y=-1.1 \times 10^{-3}x + 10.6$; $R=-0.99$; $P>0.05$). Each point in the graph represents an individual heart.

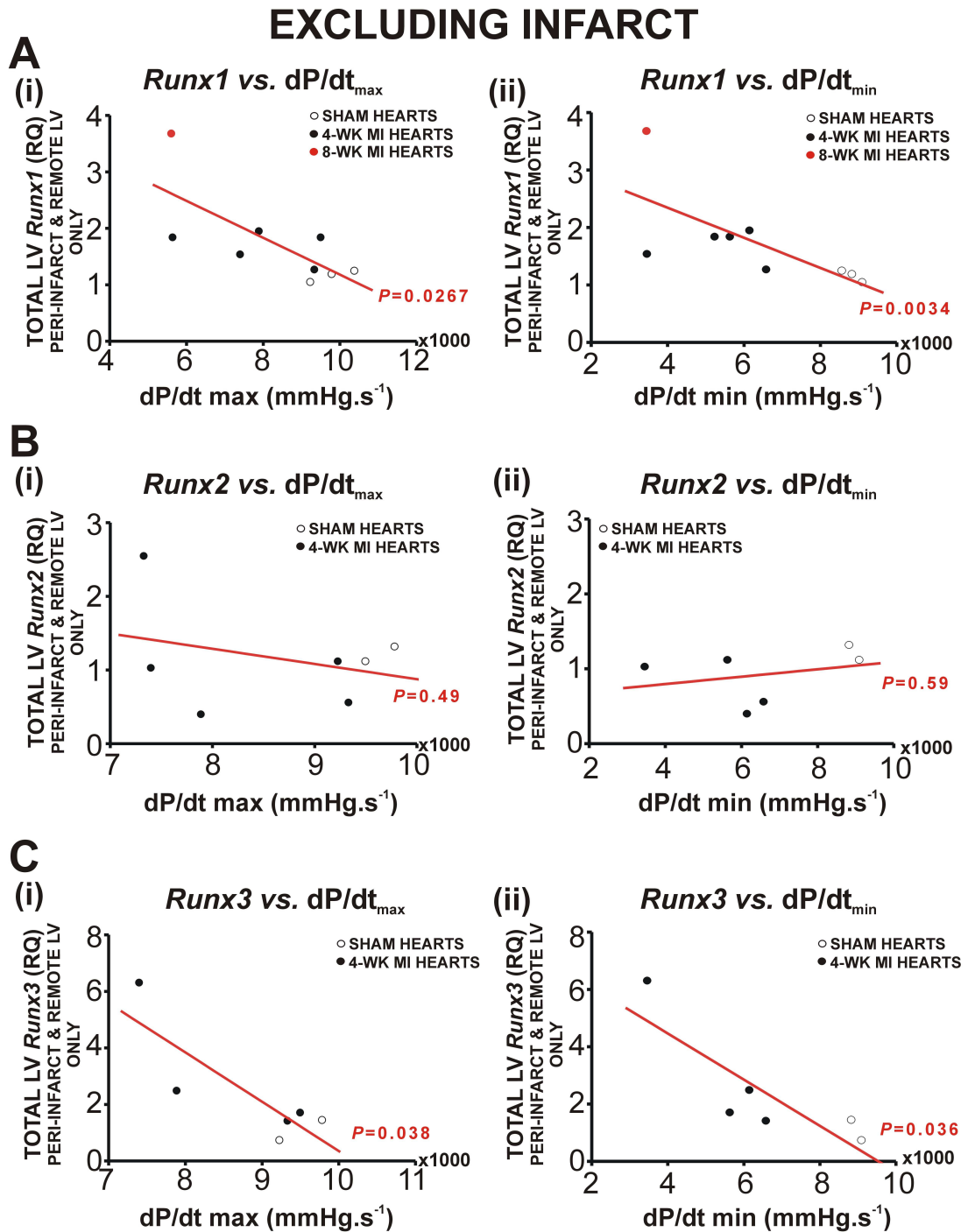


Figure 4.7 Correlations with *Runx* gene expression and LV function (excluding the infarct)

(A) Linear regression of the mean RQ value for *Runx1* expression of all LV regions except the infarct relative to their respective RV region in individual MI (4-wk $n=6$; 8-wk $n=1$) and 4-wk sham hearts ($n=3$) 4-wk post-MI plotted against (i) dP/dt_{max} or (ii) dP/dt_{min} (infarct size was not variable between hearts). For dP/dt_{max} ($y=-3.3 \times 10^{-4}x + 4.4$; $R=-0.73$; $P<0.05$) and for dP/dt_{min} ($y=-2.6 \times 10^{-4}x + 3.4$; $R=-0.71$; $P<0.05$). (B) Linear regression of the mean RQ value for *Runx2* expression of all LV regions relative to their respective RV region in individual 4-wk MI ($n=4$) and 4-wk sham hearts ($n=2$) plotted against (i) dP/dt_{max} or (ii) dP/dt_{min} (infarct size was not variable between hearts). For dP/dt_{max} ($y=-2.1 \times 10^{-4}x + 2.8$; $R=-0.31$; $P>0.05$) and for dP/dt_{min} ($y=-4.9 \times 10^{-5}x + 0.60$; $R=-0.29$; $P>0.05$). (C) Linear regression of the mean RQ value for *Runx3* expression of all LV regions relative to their respective RV region in individual 4-wk MI ($n=4$) and 4-wk sham hearts ($n=2$) plotted against (i) dP/dt_{max} or (ii) dP/dt_{min} (infarct size was not variable between hearts). For dP/dt_{max} ($y=1.7 \times 10^{-3}x + 17.8$; $R=-0.84$; $P>0.05$) and for dP/dt_{min} ($y=-8.1 \times 10^{-3}x + 7.7$; $R=-0.84$; $P>0.05$). Each point in the graph represents an individual heart.

4.3.5.5 Infarct size measurements

To further assess whether the differences observed may be related to infarct size, hearts were photographed with a digital camera and the area of infarction was estimated using *ImageJ* by drawing a line around the infarct (whitened, thinned area) and expressing the area of infarction as a percentage of the total heart (it was not possible to delineate LV from RV in these photographs and this was the reason for expressing infarct size as a percentage of the whole heart i.e. LV + RV). It was not possible to quantify infarct size histologically as previously described in other sections of this thesis for this part of the study as the hearts were to be dissected and snap-frozen (and not be sent for histology). Therefore this method was more limited and permitted only approximation measurements. Infarct size measurements by this method were only possible from 3 out of 6 hearts and the infarct sizes were 31.9, 33.2 and 37.2% (as a % of the total heart) for these hearts. The results revealed that for these specific hearts, no correlation was found between *Runx1* expression and infarct size ($y=0.03x + 2.9$; $R=0.06$; $P>0.05$; Figure 4.8).

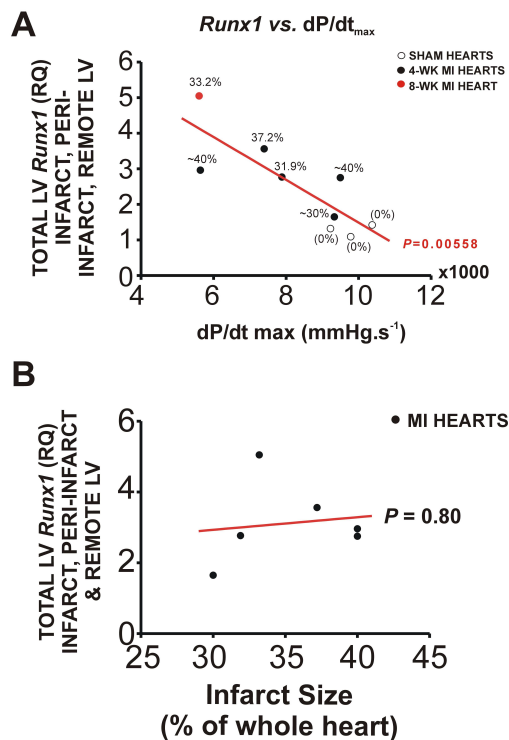


Figure 4.8 Correlation between infarct size and *Runx1* expression.

(A) Example of infarct sizes for individual hearts used for *Runx1* vs. LV function study; $y=-6.0 \times 10^{-4}x + 7.5$, $R=-0.83$; $P<0.05$. Infarct size was estimated for hearts using *ImageJ* and visual inspection. (B) Correlation between *Runx1* expression and infarct size in individual hearts used for the *Runx1* vs. LV function study. Each point on the graph represents individual hearts; $y=0.04x + 1.9$; $R=0.14$; $P>0.05$.

4.3.6 IHC localisation of RUNX1 and quantification of expression

IHC staining was used to visualise the location of RUNX1 in cardiac tissue in sham *vs.* MI (4-wk and 8-wk post-MI). Using two separate RUNX1-specific antibodies, IHC confirmed the presence of RUNX1 in cardiomyocytes (Figure 4.9C(i)), with positive nuclear staining consistent with the nuclear localisation of RUNX1. IHC has confirmed that within the infarct there are surviving cardiomyocytes expressing RUNX1 (Figure 4.11A). Other cell types within the infarct region also showed positive RUNX1 staining; these are believed to be inflammatory cells (lymphocytes) and fibroblasts which were confirmed by examination from an expert pathologist although these types were not labelled with specific markers. RUNX1-positive staining was identified in the sham heart (both 4-wk and 8-wk sham time points) further confirming a basal expression of RUNX1 in the mouse heart before insult. Positive RUNX1 staining was quantified in hearts at 4-wk and 8-wk post-MI using a grid counting method and the percentage positive nuclei in each region was expressed relative to the RV from the same heart using the following ratio (region of interest/RV). Figure 4.9A shows where each region was chosen for analysis in sham hearts and MI hearts. An example of the grid system fitted over the image is shown in Figure 4.9B. Representative images from each region are shown in Figure 4.9C for sham (Figure 4.9C(a-c)), 4-wk MI (Figure 4.9C(d-f)) and 8-wk MI (Figure 4.9C(g-i)), including negative heart tissue control (Figure 4.9C(j)) confirming no positive staining and positive thymus control tissue (Figure 4.9C(k)) showing largely positive staining. IHC results revealed that RUNX1 expression was not found to be different between regions of the sham heart, both at 4-wk (Figure 4.9D (i)) and at 8-wk (Figure 4.9D (ii)).

4.3.6.1 RUNX1-positive staining 4-wk post-MI

The results for RUNX-1 positive staining at the 4-wk time point are shown in Figure 4.9D(i).

4-wk sham hearts: 4-wk sham hearts demonstrated no significant differences in the proportion of RUNX1-positive cells across the different regions (each region is expressed relative to the RV of that heart). This was the case for the sham apex (0.86 ± 0.07 *vs.* 1.00 ratio to respective RV region; 4-wk sham apex ($n=3$) *vs.* 4-wk sham RV ($n=3$); $P>0.05$; Figure 4.9D(i)), the sham ‘peri-infarct’ equivalent (0.85 ± 0.02 *vs.* 1.00 ratio to respective RV region; 4-wk sham ‘peri-infarct’ ($n=3$) *vs.* 4-wk sham RV ($n=3$); $P>0.05$; Figure 4.9D(i)) and the sham remote LV (0.83 ± 0.04 *vs.* 1.00 ratio to respective RV region; 4-wk sham remote LV ($n=3$) *vs.* 4-wk sham RV ($n=3$); $P>0.05$; Figure 4.9D(i)).

4-wk MI hearts: After 4-wk MI, IHC showed that the proportion of RUNX1-positive nuclei was significantly higher in the infarct region of the MI heart compared to its respective RV region (1.81 ± 0.31 vs. 1.0 ratio to respective RV region; 4-wk MI infarct ($n=5$) vs. 4-wk MI RV ($n=5$); $P<0.05$; Figure 4.9D(i)). Similarly RUNX1-positive cells were significantly higher in the peri-infarct region compared to the respective RV (1.57 ± 0.20 vs. 1.0 ratio to respective RV region; 4-wk MI peri-infarct ($n=5$) vs. 4-wk MI RV ($n=5$); $P<0.05$; Figure 4.9D(i)). There were no differences in RUNX1 positive nuclei present in the remote LV compared to the respective RV (1.05 ± 0.08 vs. 1.0 ratio to respective RV region; 4-wk MI remote LV ($n=5$) vs. 4-wk MI RV ($n=5$); $P>0.05$; Figure 4.9D(i)).

4-wk sham vs. 4-wk MI: Comparisons between 4-wk MI and 4-wk sham by region demonstrated that there was a significantly greater proportion of RUNX1-positive staining in the infarct region compared to the corresponding sham apical region (1.81 ± 0.31 vs. 0.86 ± 0.07 ratio to respective RV region; 4-wk MI infarct ($n=5$) vs. 4-wk sham apex ($n=3$); $P<0.05$; Figure 4.9D(i)). This finding was also true for the peri-infarct region compared to the corresponding sham ‘peri-infarct’ region (1.57 ± 0.20 vs. 0.85 ± 0.02 ratio to respective RV region; 4-wk MI peri-infarct ($n=5$) vs. 4-wk sham ‘peri-infarct’ ($n=3$); $P<0.05$; Figure 4.9D(i)). There were no statistical differences between the 4-wk remote LV between sham and MI (1.05 ± 0.08 vs. 0.83 ± 0.04 ratio to respective RV region; 4-wk MI remote LV ($n=5$) vs. 4-wk sham remote LV ($n=3$); $P>0.05$; Figure 4.9D(i)).

4.3.6.2 RUNX1-positive staining 8-wk post-MI

8-wk sham heart: As was observed in the 4-wk sham, the 8-wk sham showed no significant differences in the proportion of RUNX1-positive staining between the different regions, with respect to the RV of the same heart. This was observed for the sham apex region (1.05 ± 0.04 vs. 1.00 ratio to respective RV region; 8-wk sham apex ($n=5$) vs. 8-wk sham RV ($n=5$); $P>0.05$; Figure 4.9D(ii)), was also observed for the ‘peri-infarct’ region (0.99 ± 0.03 vs. 1.00 ratio to respective RV region; 8-wk sham ‘peri-infarct’ ($n=5$) vs. 8-wk sham RV ($n=5$); $P>0.05$; Figure 4.9D(ii)) and for the remote LV region (0.91 ± 0.10 vs. 1.00 ratio to respective RV region; 8-wk sham remote LV ($n=5$) vs. 8-wk RV ($n=5$); $P>0.05$; Figure 4.9D(ii)).

8-wk MI heart: In the 8-wk MI heart, RUNX1-positive staining was significantly higher in the infarct region compared to the RV of the same heart (1.93 ± 0.34 vs. 1.00 ratio to

respective RV region; 8-wk MI infarct ($n=4$) vs. 8-wk MI RV ($n=4$); $P<0.05$; Figure 4.9D(ii)). The same was also true for the peri-infarct region with significantly higher positive staining for RUNX1 compared to the respective RV (1.63 ± 0.30 vs. 1.00 ratio to respective RV region; 8-wk MI peri-infarct ($n=4$) vs. 8-wk MI RV ($n=4$); $P<0.05$; Figure 4.9D(ii)). There was no significant difference in RUNX1 positive nuclei present in the 8-wk remote LV post-MI compared to the respective RV (1.27 ± 0.40 vs. 1.0 ratio to respective RV region; 8-wk MI remote LV ($n=4$) vs. 8-wk MI RV ($n=4$); $P>0.05$; Figure 4.9D(ii)).

8-wk sham vs. 8-wk MI: Comparisons between 8-wk sham hearts and 8-wk MI hearts revealed that there was significantly greater RUNX1-positive staining in the infarct region of the 8-wk MI heart compared to the equivalent sham apical region (1.93 ± 0.34 vs. 1.05 ± 0.04 ratio to respective RV region; 8-wk MI infarct ($n=4$) vs. 8-wk sham apex ($n=5$); $P<0.05$; Figure 4.9D(ii)). Furthermore, positive RUNX1 staining was also significantly higher in the peri-infarct region of the 8-wk MI heart compared to the corresponding region of the 8-wk sham heart (1.63 ± 0.30 vs. 0.99 ± 0.03 ratio to respective RV region; 8-wk MI peri-infarct ($n=4$) vs. 8-wk sham 'peri-infarct' ($n=5$); $P<0.05$; Figure 4.9D(ii)). There were no differences between the 8-wk LV remote of the MI heart compared to the LV remote of the 8-wk sham heart (1.27 ± 0.40 vs. 0.91 ± 0.10 ratio to respective RV region; 8-wk MI remote LV ($n=4$) vs. 8-wk sham remote LV ($n=5$); $P>0.05$; Figure 4.9D(ii)).

4.3.6.3 Comparisons between RUNX1 positive staining between 4-wk and 8-wk MI

RUNX1 was increased in the infarct region to the same extent at 4-wk and 8-wk post-MI (1.81 ± 0.31 vs. 1.93 ± 0.34 ratio to respective RV region; 4-wk MI infarct ($n=5$) vs. 8-wk MI infarct ($n=4$); $P>0.05$; Figure 4.9D(iii)). Similarly the levels of RUNX1 were increased by the same degree in the peri-infarct zone between 4-wk and 8-wk MI (1.57 ± 0.20 vs. 1.63 ± 0.30 ratio to respective RV region; 4-wk MI peri-infarct ($n=5$) vs. 8-wk MI peri-infarct ($n=4$); $P>0.05$; Figure 4.9D(iii)). There was no significant difference in the level of RUNX1 positive staining in the 8-wk remote LV compared to 4-wk remote LV post-MI (1.05 ± 0.08 vs. 1.27 ± 0.40 ratio to respective RV region; 4-wk MI remote LV ($n=5$) vs. 8-wk MI remote LV ($n=4$); $P>0.05$; Figure 4.9D(iii)).

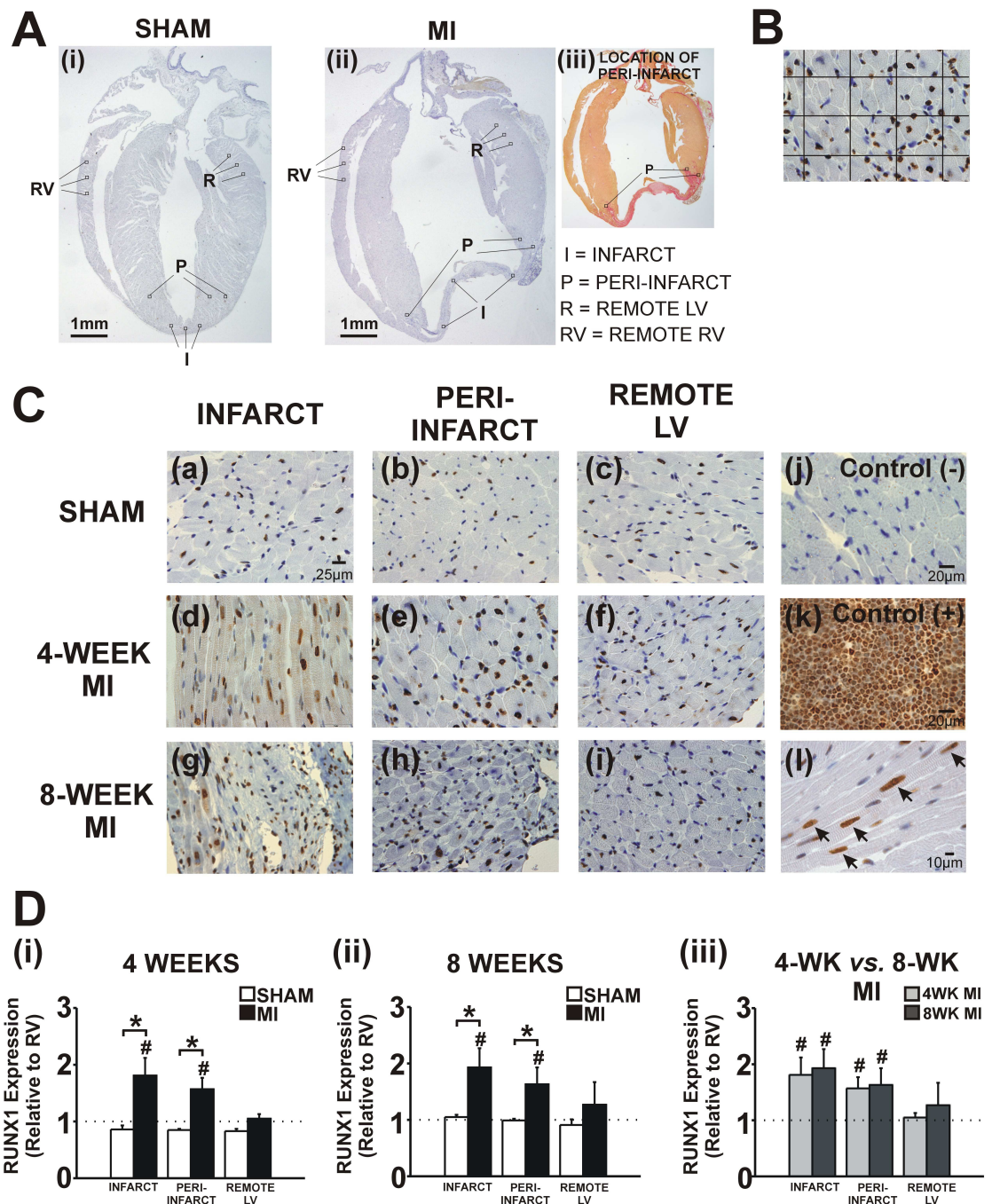


Figure 4.9 IHC expression of RUNX1 at 4-wk and 8-wk post-MI.

(A) Diagram showing where the different regions were analysed for RUNX1 expression in the (i) sham and (ii) MI heart (the peri-infarct region was chosen as accurately as possible with the aid of adjacent Sirius red sections (iii) for each respective heart as they clearly showed where the fibrous infarct (red colour) interfaced the normal myocardium (yellow colour)). (B) Example diagram showing how a grid was fixed over the image to facilitate counting of positively (brown) versus negatively (blue) stained nuclei. (C) Typical images showing expression within the different regions for sham (a-c), 4-wk MI (d-f) and 8-wk MI hearts (g-i). Negative control for heart tissue (antibody dilution buffer instead of primary antibody; j) and positive control tissue (thymus; k) are also shown. Immunohistochemistry of a 4-wk MI heart with a RUNX1-specific antibody – positive nuclear staining in cardiomyocytes indicated by arrows (l). (D (i)) Quantification of RUNX1 expression in each region after 4-wk and (ii) 8-wk MI compared to sham and (iii) comparison of 4-wk MI with 8-wk MI. Each region is expressed relative to the respective RV region (dotted line).

4.3.6.4 Cytoplasmic staining of RUNX1

RUNX1-positive staining was predominantly located within the nuclei of cardiomyocytes; however upon closer inspection it could be seen that some cardiomyocytes showed cytoplasmic staining as well as nuclear staining (Figure 4.10A). The same images for each region (as used for the previous section 4.3.6) were examined and given a score of 0 or 1 (indicating absence (0) or presence (1) of cytoplasmic staining) which was then used to calculate the percentage of hearts that showed cytoplasmic staining per region for each of the four groups (4-wk sham, 4-wk MI, 8-wk sham and 8-wk MI). The results from these data are shown in Figure 4.10B.

4-wk: 4-wk sham hearts showed no cytoplasmic staining in any region of the heart (0% of hearts showed cytoplasmic staining in the 4-wk sham apex, ‘peri-infarct’, remote LV and RV; $n=3$; Figure 4.10B). In 4-wk MI hearts, cytoplasmic staining was present in cardiomyocytes of the infarct region (60% of 4-wk MI hearts) and peri-infarct region (20% of 4-wk MI hearts) only; this was not found in the remote LV (0% of 4-wk MI hearts) or RV regions (0% of 4-wk MI hearts); $n=5$; Figure 4.10B.

8-wk: 8-wk sham hearts, like 4-wk sham hearts, showed no cytoplasmic staining of RUNX1 in any region of the heart (0% of hearts showed cytoplasmic staining in the 8-wk sham apex, ‘peri-infarct’, remote LV and RV; $n=5$; Figure 4.10B). In 8-wk MI hearts RUNX1-positive cytoplasmic staining was present in the infarct region only (in 75% of 8-wk MI hearts) but not in any other region (0% of hearts for peri-infarct, remote LV or RV); $n=4$; Figure 4.10B.

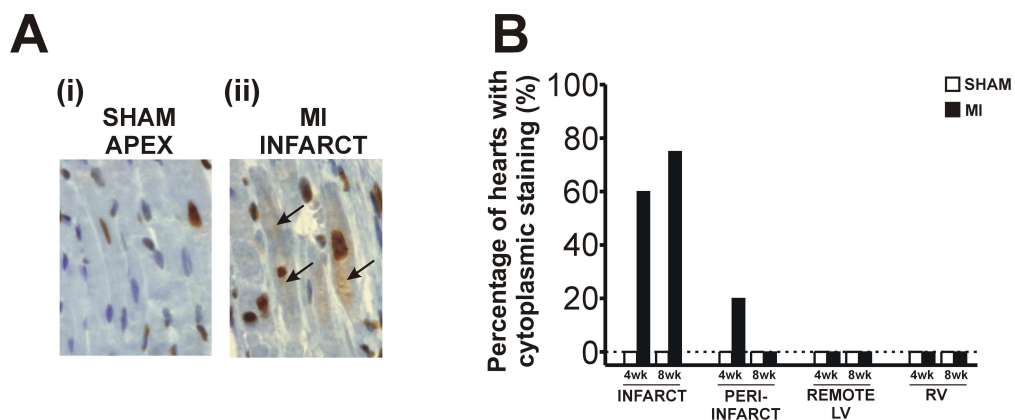


Figure 4.10 Cytoplasmic staining of RUNX1.

(A) Representative examples of IHC staining with RUNX1-specific antibody from (i) a control 4-wk sham apex showing nuclear staining only and (ii) a 4-wk infarct showing nuclear and cytoplasmic staining. Arrows indicate cytoplasmic

staining. (B) Quantification of hearts demonstrating cytoplasmic staining from each group; 4-wk sham ($n=3$), 4-wk sham ($n=5$), 8-wk sham ($n=5$) and 8-wk MI ($n=4$).

4.3.7 Verification of RUNX1 expression in cardiomyocytes

4.3.7.1 RUNX1-specific antibody staining

In order to verify that RUNX1 was present in cardiomyocytes prior to the arrival of the infiltrating cells, IHC and cardiomyocyte purification with qRT-PCR approaches were utilised. As previously shown, IHC showed positive nuclear staining in cardiomyocytes (Figure 4.9C(i)); this has been confirmed using two commercially available and tested polyclonal RUNX1-specific antibodies (61753 and 35962, *Abcam, U.K.*; Figure 4.11A(i-ii)). Some cytoplasmic localisation of RUNX1 was also identified in the surviving cardiomyocytes of the infarct region as shown in Figure 4.11B(i), an observation commonly observed in this region as described in Section 4.3.6.4 previously. Figure 4.11B(ii) shows the presence of viable cardiomyocytes in the infarct region as identified by the yellow colour in Sirius red staining.

4.3.7.2 *Runx1*-specific primers tested on purified cardiomyocytes

Runx1 mRNA levels were measured in a purified population of cardiomyocytes (>98%) according to a published method (Kosloski *et al.*, 2009). *Runx1* was found to be present within this purified population with mean Ct values before purification 27.4 ± 1.0 ($n=2$) and after purification 29.1 ± 0.6 ($n=2$) confirming levels of *Runx1* present in the purified population (Cts <30; Figure 4.11C). These Ct values are significantly greater than those obtained from whole heart (27.4 ± 1.0 vs. 20.6 ± 0.7 raw *Runx1* Ct values; cell preparations prior to filtration ($n=2$) vs. whole heart homogenates ($n=6$); $P<0.05$) or regional homogenates (27.4 ± 1.0 vs. 22.8 ± 1.2 raw *Runx1* Ct values; cell preparations prior to filtration ($n=2$) vs. regional heart homogenates ($n=4$); $P>0.05$) indicating lower gene expression, which is expected given that the starting material is less (cells rather than intact tissue). As described previously (Section 4.3.1), Ct values of less than 30 are generally regarded to represent detectable gene expression. These results revealed that *Runx1* expression decreased following purification, which was expected given the removal of other *Runx1*-containing cell types but expression in the remaining cardiomyocyte population remained evident.

4.3.7.3 *Runx1* expression in LV areas which predominantly contain cardiomyocytes (peri-infarct and remote only)

To assess the levels of *Runx1* gene expression without the contribution from the infarct region, expression levels were examined in the combined regions of the LV excluding the infarct by taking the average RQ of the peri-infarct and remote LV (calculated from the $2^{-\Delta\Delta Ct}$ method relative to the respective RV) for each heart – calculation shown below.

$$RQ\ value = \frac{RQ\ peri\ infarct + RQ\ remote\ LV}{2} \quad \text{Eq. 19}$$

4-wk hearts: These data revealed that the 4-wk sham hearts showed no significant difference in the combined ‘peri-infarct’ and remote LV compared to the RV (1.1 ± 0.1 vs. 1.0 RQ to respective RV region; 4-wk sham combined ‘peri-infarct’ and remote LV vs. 4-wk sham RV; $n=4$; $P>0.05$; Figure 4.11C). However, the combined peri-infarct and remote LV in the 4-wk MI heart showed significantly higher expression of *Runx1* than the RV of the same heart (1.6 ± 0.1 vs. 1.0 RQ to respective RV region; 4-wk MI peri-infarct and remote LV vs. 4-wk MI RV; $n=8$; $P<0.05$; Figure 4.11D). In summary, the results showed that there was 41.2% greater expression of *Runx1* in the combined regions of the 4-wk MI heart.

8-wk hearts: The combined expression in the 8-wk sham ‘peri-infarct’ and LV remote showed no significant differences when compared to the RV of the same heart (1.1 ± 0.3 vs. 1.0 RQ to respective RV region; 8-wk sham combined ‘peri-infarct’ and remote LV vs. 8-wk sham RV; $n=4$; $P>0.05$; Figure 4.11D). In the 8-wk MI heart, the combined peri-infarct and remote LV regions showed significantly greater *Runx1* expression compared to the RV of the same heart (2.4 ± 0.4 vs. 1.0 RQ to respective RV region; 8-wk MI combined peri-infarct and remote LV vs. 8-wk MI RV; $n=6$; $P<0.05$; Figure 4.11D) which represents a 114.3% increase compared to sham (2.1-fold greater; $P<0.05$). Collectively these data have confirmed that *Runx1* expression remains higher in the MI hearts (both at 4-wk and 8-wk) compared to sham even without the contribution from the infarct region (Figure 4.11D).

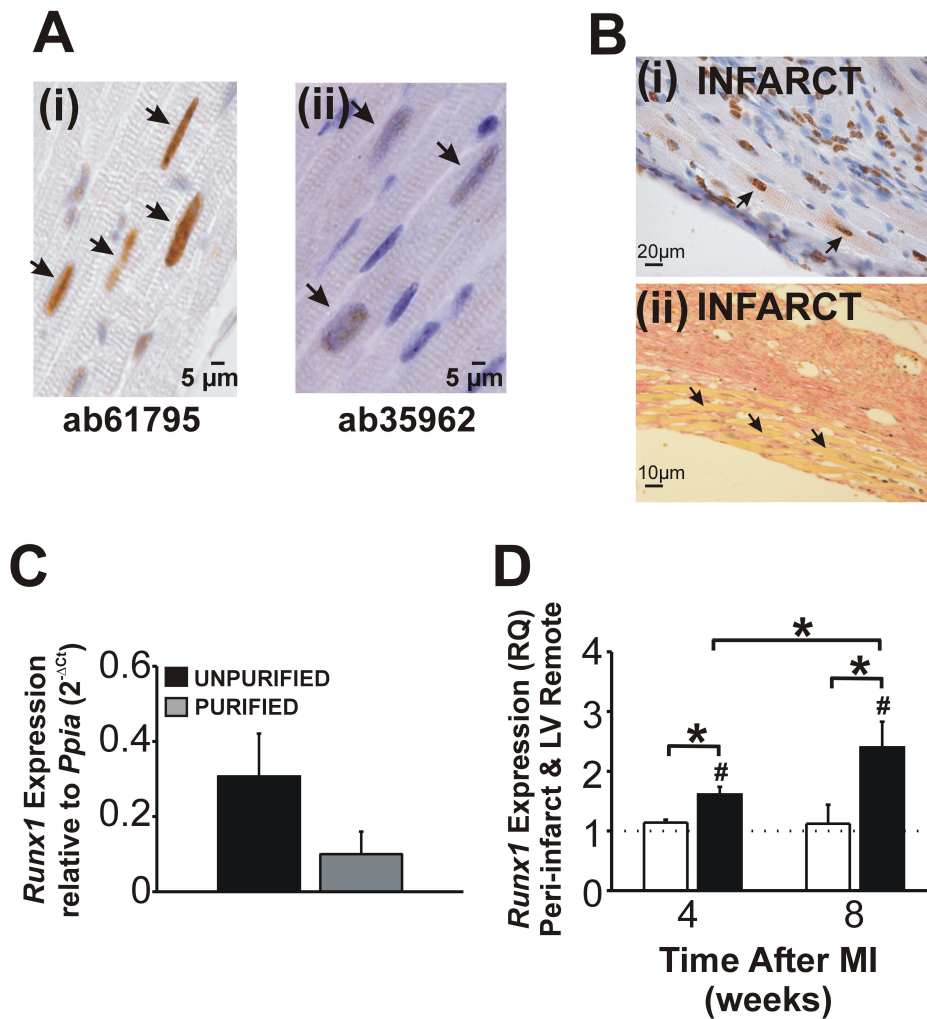


Figure 4.11 Verification of RUNX1 expression in cardiomyocytes.

(A) Examples of nucleic localisation of RUNX1 in cardiomyocytes (identified by striated structure alone) using two different commercially available RUNX1-specific antibodies ((i) ab61795; Abcam, U.K.; and (ii) ab35962; Abcam, U.K.). (B i) Positive RUNX1 staining in cardiomyocytes present within the infarct region (arrows indicate cardiomyocytes) and (ii) Confirmation of presence of viable cardiomyocytes (yellow) in the infarct region by Sirius red staining (areas of fibrosis stained red; arrows indicate viable cardiomyocytes). (C) Results of qRT-PCR performed on unpurified (black bar) and a purified population of cardiomyocytes (grey bar) isolated from a normal mouse heart ($n=2$) and expressed relative to the housekeeping gene PPIA. (D) The mean RQ values for *Runx1* expression of the LV regions excluding the infarct (peri-infarct and remote LV) obtained by qRT-PCR at 4-wk and 8-wk post-MI. # $P<0.05$ between region and respective RV (dotted line); * $P<0.05$ between sham and MI.

4.4 Discussion

Runx genes encode RUNX proteins which are best known as transcriptional regulators of gene expression in major developmental pathways with putative roles in cancer development (Coffman, 2003; Blyth *et al.*, 2005). However more recently the *Runx* genes have been increasingly implicated in specific conditions of tissue injury and/or metabolic stress (Wang *et al.*, 2005; Ghosh *et al.*, 2010; Custodio *et al.*, 2012). RUNX1, a member of the RUNX family and an important regulator of the haematopoietic system, has previously been shown to be up-regulated in damaged muscle including post-ischaemic myocardium of the human heart during ischaemic cardiomyopathy (Gattenlohner *et al.*, 2003). At present, no quantitative data exists on the altered expression of *Runx1* in the heart during MI. This chapter provides quantification and detailed characterisation of the expression of RUNX genes/proteins in response to myocardial injury providing a basis for further investigation into the role the RUNX family plays in the heart under these conditions.

4.4.1 *Runx1* expression is increased post-MI

Firstly, knowledge of RUNX in the heart even under normal conditions is very limited. *Runx1* is known to be expressed in the mammalian heart; this has been demonstrated in embryonic mouse tissue using β -galactosidase-tagged staining (Levanon *et al.*, 2001a; Telfer & Rothenberg, 2001; Levanon *et al.*, 2003) and results from the present study have confirmed a basal expression of *Runx1* in the normal mouse heart. However the major finding from this work is an increased expression of *Runx1* in the heart after MI in a mouse model. In whole ventricular myocardium 4-wks post-MI, *Runx1* mRNA levels were more than double that of sham hearts. An up-regulation of *Runx1* following MI concurs with a previous publication which revealed that in hearts taken from human MI patients there was a significant increase in RUNX1 expression compared to normal human heart tissue (Gattenlohner *et al.*, 2003). These findings combined with those in our mouse model suggest that RUNX1 may be activated by myocardial injury which could indicate a potential role for RUNX1 in the heart following MI. It is possible that increased RUNX1 in the heart can be attributed in part from infiltrating or deposited cells that arrive during the MI injury (e.g. lymphocytes and fibroblasts, respectively) as RUNX1 is known to be present in lymphocytes (Himes *et al.*, 2005) and in cardiac fibroblasts (Wotton *et al.*, 2004) which are present in the heart during remodelling (Nian *et al.*, 2004; McCormick *et al.*, 1994). By examination of the structure of these cell types using IHC and with confirmation from a pathologist we believe these to be lymphocytes (identified by their

small round mononuclear shape) and fibroblasts (identified by their spindled shape with minimal cytoplasm and wavy nuclei). These cell types were not labelled with specific markers so it was not possible to positively confirm their presence. However, the work from this study has shown that the RUNX1 expression does not come solely from the invading cells as we have evidence that RUNX1 is present in cardiomyocytes *prior* to any injury or infiltration: (i) firstly, using qRT-PCR and IHC we have shown that *Runx1* (RUNX1) is present in the normal mouse sham heart (Figure 4.3 & Figure 4.9) and (ii) secondly, by qRT-PCR *Runx1* has been shown to be expressed in a purified population of healthy mouse cardiomyocytes (Figure 4.11). Therefore a proportion of the RUNX1 expression is attributable to invading cell types *as well as* existing cardiomyocytes already there. As Figure 4.11 shows, RUNX1 is expressed in the surviving cardiomyocytes present in the infarct which are visible as layers or islets distributed throughout this region. Cell purification studies in which qRT-PCR was performed on a purified cardiomyocytes population demonstrated that cardiomyocytes contain *Runx1* mRNA confirming that the RUNX1 protein is expressed in cardiomyocytes and not taken up from surrounding cell types which can occur for other proteins during MI (e.g. S100A4) (Schneider *et al.*, 2007).

4.4.2 Elevated *Runx1* expression is localised to areas within and adjacent to the injury

At present, studies that have examined *Runx1* levels in the heart have been from whole heart homogenates only and no information is available on altered *Runx1* expression within different regions of the heart post-MI. The hypothesis that *Runx1* expression in the heart is triggered by myocardial injury is further supported by the observations that increased *Runx1* expression in the mouse heart post-MI was localised to regions within or adjacent to the area of injury (the infarct). As Figure 4.3 shows, higher levels of *Runx1* were observed in the infarct region and in the peri-infarct region compared to areas remote after 4 weeks (this was in contrast to sham hearts which showed no differences in expression in any particular region of the heart). This observation of altered regional distribution of gene expression is a recurrent finding in hearts post-MI. For instance, genes which are down-regulated in the infarct are often increased in the remote zone (e.g. inflammatory genes as described previously) and *vice versa* (when compared to matching sham regions) (LaFramboise *et al.*, 2005). The initial up-regulation of genes in the remote region is important as these tend to be switched on as a compensatory response against the adjacent tissue injury. Regional differences can result from variations in the mechanical, electrical,

remodelled and/or metabolic properties of each region (Kramer *et al.*, 1993;McCormick *et al.*, 1994) as detailed below.

4.4.2.1 Potential triggers in the infarct region

The infarct region represented the region with the highest levels of *Runx1*, *Runx2* and *Runx3* in the heart post-MI compared to an area remote (RV) and compared to the equivalent region of the sham heart. The infarct is primarily made up of a collagen-based matrix and contains infiltrating macrophages, monocytes and neutrophils as part of the inflammatory cascade during infarct repair (Frangogiannis *et al.*, 2002b). These cells are known to express RUNX1 and therefore a contribution of the RUNX1-positive signal in the infarct may be coming from these invading cell types (Himes *et al.*, 2005;Wotton *et al.*, 2004). The repair process and early infarct expansion (characterised by slippage and/or loss of cardiomyocytes) can also trigger changes in gene expression within the surviving cardiomyocytes of the infarct zone (Swynghedauw, 1999). Due to loss of contractile mass in the infarcted region, mechanical function in this region is markedly reduced (Fomovsky & Holmes, 2010). Mechanical instability is known to induce *Runx2* expression in arthritic cartilage (Kamekura *et al.*, 2006); the same may be true for the infarct region and may contribute to the increase in *Runx2* expression in the infarct region. *Runx2* has also been shown to be up-regulated in cardiomyocytes under conditions of myocardial fibrosis during high phosphorous conditions or parathyroid hormone infusion (Custodio *et al.*, 2012) – this is relevant to the present work as the model in our study has been shown to demonstrate myocardial fibrosis and therefore it is possible that the increase in *Runx2* may also be attributed to conditions of myocardial fibrosis in the infarct region in the same way.

4.4.2.2 Potential triggers in the peri-infarct myocardium

The peri-infarct region also demonstrated a significant increase in *Runx1* expression post-MI compared to areas remote and when compared to the equivalent region of the sham heart. The possible triggers for *Runx* up-regulation in the peri-infarct during MI are unclear. Studies investigating the over-expression of NCAM (believed to be linked to RUNX1) in MI have postulated that possible triggers may be related to (i) “communication failures” from disrupted electrical activity in the infarct and peri-infarct, (ii) increased wall stress, or (iii) loss of cell-cell interaction.

(i) Disruptions in electrical activity may be a key stimulus for *Runx1* expression. This has been shown to be the case in injured skeletal muscle in which disruptions in electrical

activity (*via* denervation) are responsible for an increased expression of RUNX1 (Wang *et al.*, 2005). It's possible that alterations in electrical activity which are known to occur in the infarct and peri-infarct (due to loss of cardiomyocytes and remodelling of gap junctions as described previously) (Peters, 1995) may relate to increased RUNX1 expression in the same way.

(ii) Increased wall stress: Close contact between thin-walled infarct and viable myocardium results in an abnormally increased radius of curvature of the myocardium at the infarct margin, leading to elevated wall stress and associated energy demands in the peri-infarct region (Buda *et al.*, 1986;Guccione *et al.*, 2001;Walker *et al.*, 2005). Therefore the peri-infarct is also exposed to high mechanical stress which could also be a trigger for *Runx2*. This is because RUNX2 over-expression during injury, for example in the pathogenesis of osteoarthritis, has been linked to mechanical instability and tensile strain factors (Kamekura *et al.*, 2006). Interestingly, the over-expression of RUNX2 under these conditions was limited to the affected areas with little or no change in the unaffected regions of the tissue at a distance from the injury. These findings further support the up-regulation of *Runx* genes under conditions of insult and a similar pattern of expression bordering areas of the injury.

(iii) Persistent ischaemia in infarct and peri-infarct and the infarct may also be an important trigger for altered *Runx* levels. At present little is known about how the mechanisms by which ischaemic stimuli can regulate gene expression but it may be related to the activation of specific protein kinase cascades (Shimizu *et al.*, 1997). Hypoxia may be an important stimulus but given that RUNX3 is known to be down-regulated in response to hypoxia this may not be the case (Lee *et al.*, 2009).

Importance of altered *Runx* expression in the peri-infarct region: Altered levels of *Runx* in the peri-infarct region is of particular significance because the peri-infarct region has been the subject of intense investigation in MI and is believed to contribute to the decompensatory process that eventually leads to HF (Jackson *et al.*, 2002;Jackson *et al.*, 2003;Narula *et al.*, 2000). Importantly adverse peri-infarct remodelling is believed to be responsible for almost 70% of HF cases (Gheorghiade & Bonow, 1998) and is a major determinant of poor patient outcome as it is very difficult to reverse once established (Gavazzi *et al.*, 1993). Given the importance of the peri-infarct region in the progression to HF, the increased levels of RUNX1 that were observed in this region support the need for further investigation in the role RUNX1 plays in this region during MI.

4.4.2.3 Potential triggers in the remote region

Changes in *Runx1* were not evident in the remote region after 4-wk MI but were significantly increased in this region by 8-wk. The remote region can be defined as the area of non-infarcted myocardium found beyond the peri-infarct region at a distance from the infarcted region. Remote myocardium is largely normal muscle but due to the alterations in ventricular geometry and increased wall stress imposed by the loss of myocardium in the infarcted region this can lead to a hypertrophic response in the remote region which can be a trigger for altered mRNA expression levels. Results from Chapter 3 in this thesis have shown that hearts post-MI show evidence of cardiomyocyte hypertrophy, although it cannot be confirmed definitively if these came from the remote region. However, based on the findings that the hearts showed an overall increase in heart weight despite loss of myocardium in the infarct, this would strongly suggest that the surviving myocardium had undergone hypertrophy. However despite this, *Runx* expression in the remote LV after 4-wk MI was comparable to those seen in the equivalent sham heart suggesting that hypertrophy observed at 4-wk does not seem to have triggered changes in *Runx* expression. It may be that the hypertrophy signals could repress *Runx1* expression (as has been shown in a different animal model of hypertrophy in this thesis; Chapter 5). However *Runx1* was found to be higher in the remote LV region at 8-wk; and from the heart weight data the hearts showed greater muscle mass at 8-wk (compared to 4-wk) therefore it is also possible there may be a hypertrophic threshold below which *Runx1* is not affected.

A further possible trigger for *Runx1* over-expression may be linked to the reactivation of the foetal gene programme commonly observed in the metabolically stressed heart, which has been found to be responsible for regional over-expression of other genes in the mouse infarcted heart (e.g. NCAM) (Iwamura *et al.*, 1977).

4.4.3 RUNX1 may be mislocalised in injured cardiomyocytes

IHC has further confirmed that RUNX1 expression is confined to areas within and around the area of injury in the 4-wk infarcted heart. The RUNX antibodies used in this study have been previously published - ab61753 (*Abcam*, U.K.) was used to detect RUNX1 in the cells of the inferior vena cava in mouse embryos (Nagamachi *et al.*, 2010) and ab35962 (*Abcam*, U.K.) was used to detect RUNX1 in haematopoietic progenitor cells in mouse embryos (Tsunoda *et al.*, 2010). Immunohistochemical analysis has demonstrated that the expression of RUNX1 is localised predominantly to the nuclei of cardiomyocytes, but

upon closer inspection RUNX1 can also be found within the cytoplasm of a proportion of cardiomyocytes within and around the infarct - a difference observed only in the infarcted heart and not present in sham hearts. This may represent a mislocalisation of RUNX1 as RUNX proteins are normally expressed exclusively within the nucleus only (Lu *et al.*, 1995). There are transcription factors which can be expressed both in the nucleus and cytoplasm, for example RBCK1, a protein kinase C-interacting transcription factor located in human embryonic kidney cells (HEK293) (Tatematsu *et al.*, 2005) and HOXA10, a regulator of RUNX2 transcriptional activity located in endometrial stromal cells (Bae *et al.*, 2004). The FOXO transcription factors (FOXO1 and FOXO3) are present in both the nucleus and cytoplasm of embryonic cardiomyocytes (Sengupta *et al.*, 2009). However, RUNX transcription factors have a unique targeting signal in the C terminus called the NLS which is responsible for directing RUNX to discrete foci within the nucleus (Choi *et al.*, 2001) and the sole presence of RUNX protein in the cytoplasm can render it inactive (Choi *et al.*, 2001). Mislocalisation of RUNX1 into the cytoplasm has been reported previously under disease conditions e.g. translocation of the CBF β partner can lead to a CBF β -MYH11 fusion gene (Liu *et al.*, 1995) which has the ability to sequester RUNX1 in the cytoplasm increasing leukamogenic potential (Adya *et al.*, 1998; Lukasik *et al.*, 2002). RUNX3 mislocalisation to the cytoplasm is present in 38% of gastric cancer tumour cells and interestingly it has been shown that hypoxic culture conditions can induce this mislocalisation to the cytoplasm in gastric tumour cells, identified by IHC (Lee *et al.*, 2009). It may be therefore that the hypoxic conditions within the infarcted region of the heart could be responsible for RUNX1 expression within the cytoplasm; this is further supported by the finding that this occurs in cardiomyocytes within the infarct and peri-infarct region only and not in the areas remote. Another possibility is that RUNX1 can be mislocalised to the cytoplasm bound to CBF β , the precise mechanisms by which this occurs remain to be fully elucidated but it is thought to be related to a direct disruption of the NLS (Michaud *et al.*, 2002). CBF β is normally cytoplasmic (Tanaka *et al.*, 1997) and its entry into the nucleus required interaction with the Runt domain (Lu *et al.*, 1995) but the regulatory mechanism involved in this is not clear, it has been proposed that a portion of CBF β remains in the nucleus (Lu *et al.*, 1995); Figure 4.12. Therefore it may be complex underlying pathways initiated as a result of the injury to the heart that could be responsible for causing this mislocalisation.

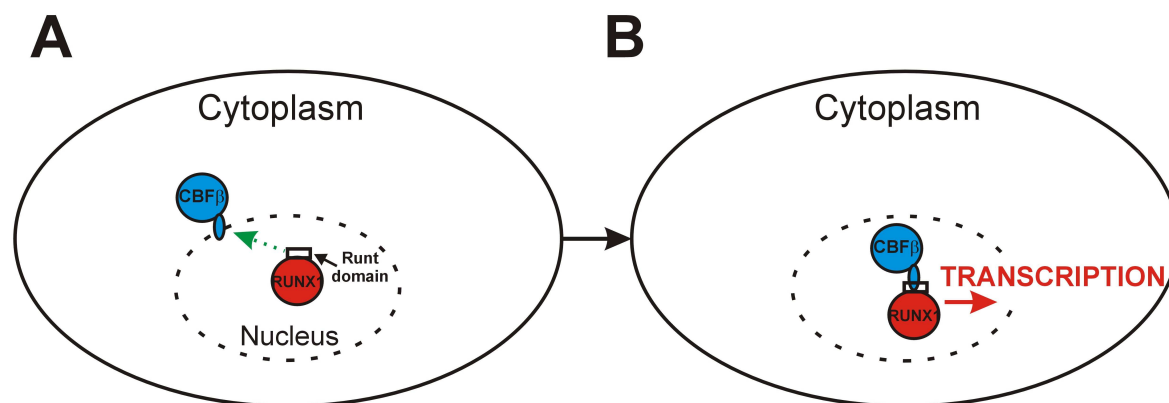


Figure 4.12 Diagram showing possible mechanism for how the CBF β partner unit enters the nucleus to permit formation of the heterodimer complex required for transcription.

(A) CBF β resides in the cytoplasm but a portion is believed to remain inside the nucleus to permit binding to the Runt domain which allows CBF β to enter the nucleus and (B) form a heterodimeric complex to mediate transcription.

4.4.4 Localised regional expression of other genes in MI

Expression in areas of close contact with the injury has been reported by others for example the neural cellular adhesion molecule NCAM is also up-regulated in human MI (Gattenlohner *et al.*, 2003) and in a mouse model of MI (Nagao *et al.*, 2010) and is restricted only to the cardiomyocytes within the infarcted or peri-infarct regions. RUNX1 is believed to have a binding site within the promoter of NCAM and may therefore be involved in the control of its expression. This seems very likely given the strikingly similar pattern in expression between the two. The over-expression of nestin, an intermediate filament protein, after MI is predominantly in the infarct and peri-infarct of mouse infarcted hearts and human end-stage heart failure; this has been shown by immunofluorescence confocal microscopy to be present in cardiomyocytes as well as endothelial cells, smooth muscle cells, neuronal cells and fibroblasts (Scobioala *et al.*, 2008). The multifunctional Ca²⁺-binding protein S100A4 as also been reported to show increased expression in injured cardiomyocytes localised to the peri-infarct in rat MI (twice as high compared to the remote region within the same heart and nearly 5 times higher than the matching sham regions) (Schneider *et al.*, 2007). Although S100A4 is detectable by immunofluorescence confocal microscopy in inflammatory cells (macrophages and leukocytes), fibroblasts and endothelial cells, the staining within cardiomyocytes was exclusively in the peri-infarct; interestingly S100A4 mRNA was not detectable by qRT-PCR in the cardiomyocytes therefore it is believed to be uptaken by the cardiomyocytes rather than expressed by them (Schneider *et al.*, 2007).

4.4.5 Temporal alterations in *Runx1* expression post-MI

4.4.5.1 How do *Runx1* levels compare between 4-wk and 8-wk post-MI?

Runx1 levels remained high in the infarct region by 8-wk post-MI but were not significantly different to those observed in the 4-wk infarct (as shown in Figure 4.4). Similarly, levels of *Runx1* also remained high in the peri-infarct at 8-wk but were not significantly different to those observed at 4-wk MI. It is possible however that the regional distribution is changing by 8-wk as we begin to see higher levels of expression in the remote LV at 8-wk. Interestingly, this is in contrast to normal levels in the remote region at 4-wk signifying a possible temporal response which may be linked to advanced remodelling. In our mouse model, 8-wk MI hearts do show a greater degree of remodelling compared to the 4-wk hearts in terms of greater muscle mass and a trend towards higher cardiac fibrosis (Chapter 3) and therefore this could explain the altered expression seen in the 8-wk remote. Up-regulation of *Runx1* in the remote region at 8-wk is important because it may indicate that *Runx1* up-regulation is not triggered as a result of the initial ischaemic injury, as the remote LV region represents an area which is not subject to the ischaemia (still perfused). Although *Runx1* mRNA was increased in the 8-wk remote region, the level of RUNX1-positive staining by IHC was unchanged. Unfortunately one of the limitations of IHC is that it simply indicates presence or absence of the antigen of interest (in this case RUNX1) and does not provide indication of the quantity of the protein present within each cell. Therefore it is possible that IHC may be underestimating the true *abundance* which could explain the discrepancy between high mRNA but unchanged RUNX1-positive IHC in 8-wk post-MI remote regions. Other techniques that may have been utilised for this include Western Blotting, but for more specific analysis of RUNX1 levels this could involve utilising techniques designed to examine proteins expressed within the nucleus such as isolating nuclear extracts followed by electrophoresis mobility shift assay. Other transcription factors have shown delayed expression post-MI similar to the RUNX1 8-wk remote result in this study; these include the Fox transcription factors for which the FoxO3 and FoxJ2 members only begin to show elevated expression at 8-wk post-MI in the nuclei of cardiomyocytes in the peri-infarct region (Philip-Couderc *et al.*, 2008). Others take even longer; the FoxF2 does not appear higher until 20-wk post-MI (Philip-Couderc *et al.*, 2008).

4.4.5.2 High levels of *Runx1* in 1-wk animals with severe MI phenotype

Interestingly, the greatest degree of *Runx1* was observed during early severe MI at 1-wk indicating there may be a potential link with onset of HF. As Figure 4.4 shows, *Runx1* was over twice as high in the 1-wk infarct compared to 4-wk infarcts, and over three times higher than 8-wk infarcts. 1-wk animals also showed ≈ 6.5 -fold and ≈ 5 -fold higher *Runx1* in the peri-infarct compared to the equivalent regions in the 4-wk and 8-wk hearts, respectively. Although it was not possible to functionally confirm HF in the animals that developed a severe phenotype at 1-wk ($n=3$ in total including the animals for which the hearts were taken for histological assessment described in the previous Chapter 3, Section 3.4.3), previous measurements have revealed they show a marked increase in heart weight with severe lung congestion consistent with congestive HF (Chapter 3). These animals also showed very advanced acute remodelling (substantial infarct thinning; Chapter 3) which may indicate a link with the high levels of *Runx1* expression observed in these circumstances. Unfortunately it must be noted that due to the small number of animals that develop this severe phenotype, the animals are limited to test this further. It is unclear what may be responsible for these high levels of *Runx1* expression whether it is related to an inflammatory response which is known to peak at this time (1-wk) (Bonvini *et al.*, 2005; Frangogiannis *et al.*, 2002) or whether it is related to a more severe remodelling of this condition. Genes are known to show higher levels of mRNA within the infarct and peri-infarct at 1-wk and fall by later time points (4-wk); this has been shown to be the case for a number of genes involved in inflammation, angiogenesis and stem cell factors (as measured by qRT-PCR) including IL-8, TGF- β 1, β FGF, MIP-1 α and IL-10 (Vandervelde *et al.*, 2007).

4.4.6 Other *RUNX* genes show similar altered expression but to varying extents

Knowledge on the altered expression patterns of the other members of the RUNX family (RUNX2 and RUNX3) in the heart during MI is also extremely limited. RUNX2 has been found to be barely detectable in normal rat heart (negative with IHC), however during conditions of elevated phosphorous or parathyroid hormone (both features of chronic kidney disease which can lead to cardiac disease), RUNX2 is found to be up-regulated in cardiomyocytes and coronary arteries (Custodio *et al.*, 2012). This finding is another example linking tissue stress with RUNX expression. Tissue stress in this context refers to damage, injury or overload of the specialised functioning of the tissue that disturbs normal nutrient and/or energy supply. In our study, all three *Runx* genes showed increased mRNA

levels post-MI with a very similar regional distribution pattern. This is not surprising given that all three RUNX proteins bind *via* the same highly conserved DNA motif known as the *Runt* domain located at the N-terminus of the RUNX protein (Kagoshima *et al.*, 1993;Crute *et al.*, 1996) and all require the CBF β for DNA binding (Ogawa *et al.*, 1993). As a result the *RUNX* genes employ very similar roles, albeit in different lineages. *Runx2* showed increased expression within the infarcted region of the heart post-MI only. The *Notch1* gene, a member of the Notch signalling family, has been reported to be up-regulated ~3-fold in cardiomyocytes of the peri-infarct of mice 4-days post-MI (Gude *et al.*, 2008); as Notch is known to inhibit *Runx2* (Zamurovic *et al.*, 2004) this may explain why *Runx2* showed no change in expression in this region (while the other *Runx* genes did). *Runx1* and *Runx3* demonstrated expression within both the infarct and the peri-infarct with no change in remote LV expression after 4-wk. *RUNX3* is also a known direct target of the Notch signalling pathway but unlike *RUNX2*, is activated by increased Notch (Fu *et al.*, 2011). This could explain the increased levels of *Runx3* mRNA in the peri-infarct region as Notch is activated in this region post-MI in mice (Gude *et al.*, 2008) as described above which could be contributing to an increased expression of *Runx3* in this region. The similarity in pattern between *Runx1* and *Runx3* is not unusual as the two have been known to overlap or cross-regulate in other systems e.g. both the haematopoietic system and during thymopoiesis more than they do with *Runx2* (Levanon *et al.*, 2001a;Woolf *et al.*, 2003). Furthermore, during murine embryogenesis *Runx3* is only detected in organs that also express *Runx1* (Levanon *et al.*, 2001a) which also supports the possibility of cross-regulation. In gastric cancer, both *RUNX1* and *RUNX3* are down-regulated while no changes were observed in *RUNX2* (Sakakura *et al.*, 2005). Although there were similarities to *Runx1* in the expression pattern, *Runx3* showed a more exaggerated response than the other two *Runx* genes within the infarct and peri-infarct regions, the reasons for this however are not clear. Together these findings further support the idea that the *RUNX* family are differentially altered in the heart during MI which therefore warrants further investigation into the possible role *RUNX* may have in the heart during MI.

4.4.7 Functional role of *RUNX1* in cardiomyocytes

The functional role of *RUNX* in the heart remains to be fully elucidated. From *Runx1*-knockout studies in skeletal muscle, a small group of 29 genes were identified as transcriptional targets for *RUNX1*, many of which are also not only important for cardiac myocardial structure, but demonstrate altered patterns of expression during cardiac disease.

For example RUNX1 can activate the expression of the gene for osteopontin (*Sbp1*) (Wang *et al.*, 2005), a matricellular protein which is expressed at low levels in the healthy, unstressed heart but increases in cardiomyocytes during the onset of cardiac hypertrophy (Graf *et al.*, 1997), MI (Trueblood *et al.*, 2001) and advanced heart failure (Stawowy *et al.*, 2002). RUNX2 is also known to regulate osteopontin by activating its expression (Ducy, 2000). This may be important as osteopontin is believed to be involved in the coordination of intracellular signals required to integrate myofibroblast proliferation, migration, and ECM deposition in the post-infarcted heart to ensure the mechanical properties of the heart are not compromised further (Singh *et al.*, 2010). There are also links to sodium channel type V (*Scn5a*) which is activated by RUNX1 (Wang *et al.*, 2005) and mutations of the *Scn5a* gene have been associated with Long QT syndrome and fatal cardiac arrhythmias (Zhang *et al.*, 2007). Thrombospondin-1 and 4 (*Tsp*) are secretory proteins which are also induced by RUNX1 (Wang *et al.*, 2005) and selectively over-expressed in the peri-infarct myocardium post-MI in cardiomyocytes as well as endothelial cells and macrophages (Dewald *et al.*, 2005; Paoni & Lowe, 2001; Sezaki *et al.*, 2005) and is believed to prevent adverse remodelling by regulating the inflammatory response during MI (Sezaki *et al.*, 2005).

4.4.7.1 Phospholamban a key target?

A particular key target for RUNX1 may be phospholamban (Pln), an integral regulatory protein which controls the rate of Ca^{2+} movement across the SR membrane through association with SERCA. When Pln is unphosphorylated, the rate of Ca^{2+} movement is reduced through inhibition of SERCA, and upon phosphorylation of Pln, Ca^{2+} movement increases. Failing heart muscle exhibits distinct changes in intracellular Ca^{2+} handling, including impaired removal of cytosolic Ca^{2+} ; reduced Ca^{2+} loading of the SR with down-regulation of SERCA2; and defects in SR Ca^{2+} release (Marx *et al.*, 2000; Morgan, 1991). Thus contractility impairment in heart failure has been linked to increased inhibition of SERCA due to (i) increases in phospholamban/SERCA2 expression and (ii) decreases in Pln phosphorylation (Chu & Kranias, 2006). Increased RUNX1 levels could therefore be affecting the expression of Pln which may be having detrimental consequences for the heart during post-MI remodelling. In denervated skeletal muscle, knockout of *Runx1* led to an 82% reduction in *Pln* gene expression compared to wild-type denervated muscle (Wang *et al.*, 2005). Therefore these data suggest that *Pln* gene expression is activated/maintained by *Runx1*. It is not known whether *Runx1* up-regulation in cardiac muscle would affect *Pln* to the same extent; however it is known that transgenic mice with a 2-fold

cardiac-specific over-expression in Pln protein (2-9 extra copies of *Pln* gene) demonstrate reduced cardiomyocyte contractility with reduced Ca^{2+} transient amplitude (to 83% of wild-type) and significant prolongation of Ca^{2+} decay (to 131% of wild-type) (Kadambi *et al.*, 1996). Therefore, an elevation in the *Runx1* observed in the heart post-MI could lead to an increase in *Pln* expression and subsequently alter normal Ca^{2+} handling and overall functioning of the heart.

Preliminary data supporting a link with phospholamban: Further to potential links between RUNX over-expression and cardiac dysfunction, preliminary data from our laboratory has shown that rabbit cardiomyocytes over-expressing RUNX1 demonstrate altered Ca^{2+} handling with reduced peak systolic Ca^{2+} , slower decay of the Ca^{2+} transient and reduced SR content all consistent with reduced contractile function (data not shown). These data suggest elevated RUNX1 levels may have a detrimental effect in cardiomyocytes. These data would support the hypothesis of potential over-expression of *Pln* and subsequent inhibition of SERCA which may be responsible for the altered handling and reduced cardiomyocyte contractions observed. These data have revealed that RUNX1-overexpression shows adverse effects in cardiac muscle which is in contrast to the protective effects of RUNX1 observed in skeletal muscle during injury. In skeletal muscle RUNX1 was necessary in the muscle after denervation to protect against wasting, myofibrillar disorganisation and autophagy; however the data from our group suggests that the situation is different in cardiac muscle and that unlike skeletal muscle, RUNX1 shows a detrimental effect rather than a positive protective one.

4.4.7.2 Possible links with *Runx* expression and degree of dysfunction.

The work in this thesis has shown that there are significant correlations between mean regional *Runx1* and *Runx3* expression and cardiac function in the heart post-MI i.e. higher *Runx1* and *Runx3* expression in hearts with greatest dysfunction (with and without shams included in the analysis). *Runx2* shows no correlations with cardiac function. However, the degree of LV dysfunction can be influenced by the size of the infarct which has been shown to be the case in a separate small cohort of hearts (in which infarct size was measured histologically) i.e. larger infarct size, lower function. *Runx* mRNA levels are highest in the infarct region - therefore it becomes difficult to ascertain whether it is the larger infarct size or the increased *Runx* expression that leads to reduced cardiac function.

- 1) One way to test this would be to assess the infarct size of the hearts that have been used for *Runx* expression experiments. If the infarct size was not different between hearts, it would give more confidence that the relationship is not as a result of the infarct size. However, due to the nature of the tissue preparation for these experiments (fresh hearts dissected and immediately snap-frozen) it was not possible to accurately assess infarct size histologically in these hearts. Infarct size therefore could only be estimated from photographs of the heart under magnification and estimated based on the percentage of infarcted area by means of tracing around the surface of the infarct using image analysis software – this was only possible from a very small number of hearts ($n=3$). Using these three hearts by this method, there were no significant differences observed in infarct size and no correlation observed between infarct size and *Runx1* expression. This would suggest that the relationship between *Runx* expression and level of cardiac dysfunction was not influenced by infarct size. However when infarct size was measured histologically in a separate group of hearts the level of dysfunction was proportional to the infarct size. The reasons for the discrepancy may be related to the method of measuring infarct size with the ‘tracing round’ method being less accurate than the more thorough length-based quantification from serial histology sections where the infarct is clearly delineated from Sirius red staining. Furthermore the small sample size is a limiting factor in the accuracy of the results.

- 2) A similar approach would be to assess whether the degree of *Runx* expression in the infarct region itself changes with degree of dysfunction; although this region shows the highest levels of *Runx1*, *Runx2* and *Runx3*, if no correlations with function and *Runx* gene expression were observed in this region it would invalidate the original problem of the infarct’s contribution to *Runx*/dysfunction. Following analysis however this was found not to be the case - when assessing the infarct alone, *Runx1* and *Runx3* correlate significantly with dysfunction (with and without shams included) indicating hearts with greatest dysfunction express more *Runx1* and *Runx3* in the infarct alone. There was no correlation with *Runx2* expression and function in the infarct region. In attempts to eliminate the influence of the infarct on the analysis, the contribution of *Runx* expression from the infarct was removed from the analysis and the relationship between *Runx* expression and dysfunction was still the same. This indicates that there was still a significant correlation between *Runx* expression and level of dysfunction even without the contribution from the infarct. There are however some points to consider with this observation: (i) firstly the infarct size may have already affected the

function of the heart (larger infarcts do lead to reduced function) but it is unclear if this would play a part in the peri-infarct and remote LV *Runx* expression. It is possible that with greater damage there was reduced function and a subsequent increase in *Runx* in the surviving regions as well as the infarcted tissue – therefore this point may only affect the functional side of the relationship; (ii) secondly, the peri-infarct could be contaminated with infarct expression (although efforts were made to ensure careful dissection of the infarct and peri-infarct from each other during tissue collection, it is very difficult to be completely certain that no overlap of scar tissue was present in the peri-infarct). However, it was tested to see whether there was any correlation between *Runx* expression in the infarct and peri-infarct region of the same heart (i.e. did the hearts with the highest level of *Runx* in the infarct also have the highest level of *Runx* in the peri-infarct of the same heart?). The results showed that there were no significant correlations suggesting that the peri-infarct expression had not been affected by the infarct of the same heart (and contamination therefore was unlikely). Furthermore, the remote region was tested as there would be no risk of contaminating scar tissue in this region, but no correlations were found between the expression of any *Runx* gene and cardiac function in this region - it must be noted that these were 4-wk post-MI hearts and *Runx1* levels are not different from basal sham levels in the remote LV at 4-wk.

- 3) In a separate animal model of cardiac disease in which there is no infarct (hypertension/LVH) the model showed the same pattern with significantly higher *Runx1* expression in hearts with greatest dysfunction therefore owing more strength that it may not be related to the infarct. This data is discussed in more detail in Chapter 5. Although infarct size post-MI is an important determinant of the extent of dysfunction in humans (Masci *et al.*, 2011) and mouse models (Gao *et al.*, 2000; Patten, 1998; Takagawa *et al.*, 2007), the degree of adverse remodelling is not always solely related to the amount of damage sustained (Ambler *et al.*, 2008). Genes can influence function independently of infarct size; this has been shown in transgenic mouse studies: mice deficient in the gene for myeloperoxidase had improved function compared to wild-type mice despite equivalent infarct size (Vasilyev *et al.*, 2005) and over-expression of the gene for glutathione peroxidase in mice reduces adverse LV remodelling independently of infarct size (Shiomi *et al.*, 2004). Therefore it is possible for *Runx* genes to have a potential role in the dysfunction observed independent of infarct size, however at present it is not clear whether infarct size is contributing to the effects seen in this study.

4.4.8 Summary

Collectively, the findings described in this chapter have revealed in detail that during MI there are changes in the expression of the *Runx* genes in terms of abundance, regional distribution, time course and (very preliminary indications of) association with onset of severe MI and HF. Additionally there were similarities in the regional expression pattern of the other *Runx* genes but differences in their extent of altered expression. One of the first areas to investigate further would be to ascertain that RUNX1 increases in cardiomyocytes during MI. The work in this chapter has shown that RUNX1 is increased in the heart post-MI and is present in cardiomyocytes during MI but it remains to be shown that the levels of RUNX in the cardiomyocytes increase. Further experiments for this work would involve further over-expression of recombinant RUNX protein within cultured mouse cardiomyocytes to verify that the changes in Ca²⁺ handling could be repeated in the mouse (rabbit cardiomyocytes survive better in culture than mouse cardiomyocytes which is the reason why the preliminary experiments were performed in rabbit). To evaluate whether increased expression of *Runx1* is having an adverse effect on function post-MI, two approaches could be taken; (i) genetic over-expression of *Runx1* into the heart *via in vivo* adenoviral vector delivery prior to the induction of MI (followed by functional measurements *in vivo* and at the cardiomyocyte level after MI) or (ii) genetic ablation of *Runx1* using transgenic mice with cardiac-specific knockout of *Runx1* (global knockout is embryonically lethal) followed by functional measurements. Biochemical analyses of Pln expression (both phosphorylated and unphosphorylated forms) in the mouse MI cardiac tissue would also be very informative to assess whether levels of the phosphorylated Pln were reduced and unphosphorylated levels increased as a means to explain a possible mechanism by which RUNX1 may be adversely affecting cardiomyocyte function.

Conclusion: In conclusion, the up-regulation of RUNX in the heart post-MI may reflect an important role in the regulation of post-infarction remodelling and warrants further investigation.

CHAPTER 5

Characterisation of cardiac function and *Runx1* expression in a congenic rat model of altered left ventricular mass

5.1 Introduction

5.1.1 Altered *RUNX* gene expression in cardiac disease

Experimental animal models of cardiac disease can provide valuable insight into the underlying molecular mechanisms associated with the development of HF. This includes the identification of causative genes related to a particular disease or the alteration of specific genes during the disease. The adverse LV remodelling process that occurs in response to cardiac disease can trigger changes in cardiac gene expression, for example genes regulating calcium (Ca^{2+}) handling (Swynghedauw, 1991), contraction (Yue *et al.*, 1998), the ECM (Weber, 1997) and the RAA system (Holtz, 1998). More recently, transcription factors have emerged as important targets in elucidating the mechanisms of altered gene expression as many genes affected during remodelling are under the control of transcription factors (Kaab *et al.*, 2004). As the previous chapter in this thesis has shown, the gene encoding RUNX1, a transcriptional regulator of the RUNX family is over-expressed in the mouse heart during MI, similar to what has been shown previously in human MI (Gattenlohner *et al.*, 2003). However, although knowledge of cardiac RUNX1 expression during MI is emerging, very little is known about its altered expression in other forms of cardiac disease. By examining how RUNX1 expression is altered during different forms of cardiac disease, this could provide important insight into the regulatory stimuli of the gene and allow for comparisons between different disease models. Therefore, to further characterise the altered expression of *Runx1* during cardiac disease and compare it with the previous MI model, this involved utilising a rat model of hypertension (SHRSP) and congenic rat models of altered LV mass.

5.1.2 LV mass and hypertension

LV hypertrophy (LVH) is an accepted independent predictor of cardiovascular morbidity and mortality (Devereux *et al.*, 1994; de *et al.*, 2002). LVH occurs in response to injury or elevated load as part of LV remodelling, however while initially compensatory, LVH can eventually lead to HF. The pathophysiological mechanisms underlying the progression of LVH to HF remain poorly understood. Although the most common cause of LVH is an elevated BP, the correlation between the two remains very complex. The intensity of BP load has been found not to always correspond to the degree of LVH observed in humans; for example, it has been documented that individuals with comparable levels of high BP demonstrate largely variable extents of LVH (Nunez *et al.*, 1996). Furthermore, one report

revealed that there was no evidence of LVH in 50% of hypertensive patients (Devereux *et al.*, 1994).

5.1.2.1 Genetic basis for LV mass

These differences are believed to be as a result of the complex polygenic nature of LV mass inheritance. Studies on twin children have revealed that LV mass is genetically determined in childhood (Verhaaren *et al.*, 1991). Body weight, BP, SV, sodium intake and physical activity are all known to be a strong correlate of LV mass in adults (Kupari *et al.*, 1994), with >90% of the correlation between LV mass and body weight as a result of common genes (Verhaaren *et al.*, 1991). Therefore, within a normal adult population LV mass has a significant genetic determination (Swan *et al.*, 2003). One way to study complex genetic factors such as LV mass which could be important for cardiac disease is using inbred animal models.

5.1.3 Rat model of hypertension

Experimental models of hypertension have been developed in the rat over the last forty years including the spontaneously hypertensive rat (SHR) (OKAMOTO & AOKI, 1963), the stroke-prone SHR (SHRSP) (Okamoto *et al.*, 1974), Dahl salt-sensitive (DAHL *et al.*, 1962) and Sabra rats (Lutsky *et al.*, 1984). These models demonstrate many of the clinical features of human hypertension including LV hypertrophy (Yamori *et al.*, 1979), impaired myocardial function (Conrad *et al.*, 1991), increased susceptibility to stroke (Jeffs *et al.*, 1997) and renal failure (Kawabe *et al.*, 1978). Inbred animal models offer the advantage of genetic homogeneity and complete control of environmental factors but most importantly they allow for specific inter-crosses to generate sub-strains which can provide insights into genetic determinants of hypertension which are beyond the scope of human studies. These sub-strains are useful for the study of specific genetic regions important for hypertension such as altered LV mass. This approach involves the identification of quantitative trait loci (QTL), which are regions of a chromosome containing genes for a particular trait. This then makes it possible to narrow down the genes contained within the QTL interval.

5.1.3.1 Congenic strains

In order to dissect out the QTL of interest, this usually involves the construction of a congenic strain whereby a chromosomal segment containing the QTL from a donor strain is introgressed into a recipient strain using a backcrossing breeding scheme. If the QTL of

interest is successfully moved then the resulting congenic strain will be identical to the recipient strain except for the QTL. The congenic strain can then be used to assess the QTL-related phenotype alterations. According to Mendelian laws it can take up to 8-10 crosses to dilute the donor genome to >99% of the recipient. Brother-sister mating can then *fix* the congenic strain as homozygous. This is known as the traditional congenic breeding method. However this method can take up to 3-4 years to produce the desired congenic strain (Frantz *et al.*, 1998). A faster method has been developed which involves selecting male offspring that contain the fewest donor alleles and using these for the breeding; this is called marker-assisted speed breeding (Figure 5.1) and can reduce the time taken to produce the congenic strain by approximately half (~ 2 years) (Jeffs *et al.*, 2000).

5.1.3.2 QTL for LV mass

QTLs for LV mass have been identified using this approach. This is important for the study of LVH because a detailed study by Tanase *et al.* revealed from a study of 23 inbred strains of normotensive and hypertensive rats that an estimated 65-75% of the difference in cardiac mass between strains was genetically linked (Tanase *et al.*, 1982). Therefore, through the use of genetic crosses between normotensive and hypertensive strains numerous linkage studies have revealed the existence of QTL for LV mass, some BP-dependent and others independent of BP in a number of chromosomal regions. For example, BP-independent QTL for LV mass have been mapped along several different regions of chromosome 17 (Deng *et al.*, 1994;Pravenec *et al.*, 1995;Tsujita *et al.*, 2000). QTL for LV mass which are found to be dependent on BP have been identified on chromosomes 2, 4, 19 (Pravenec *et al.*, 1995) and 7 (Tsujita *et al.*, 2000;Garrett *et al.*, 1998).

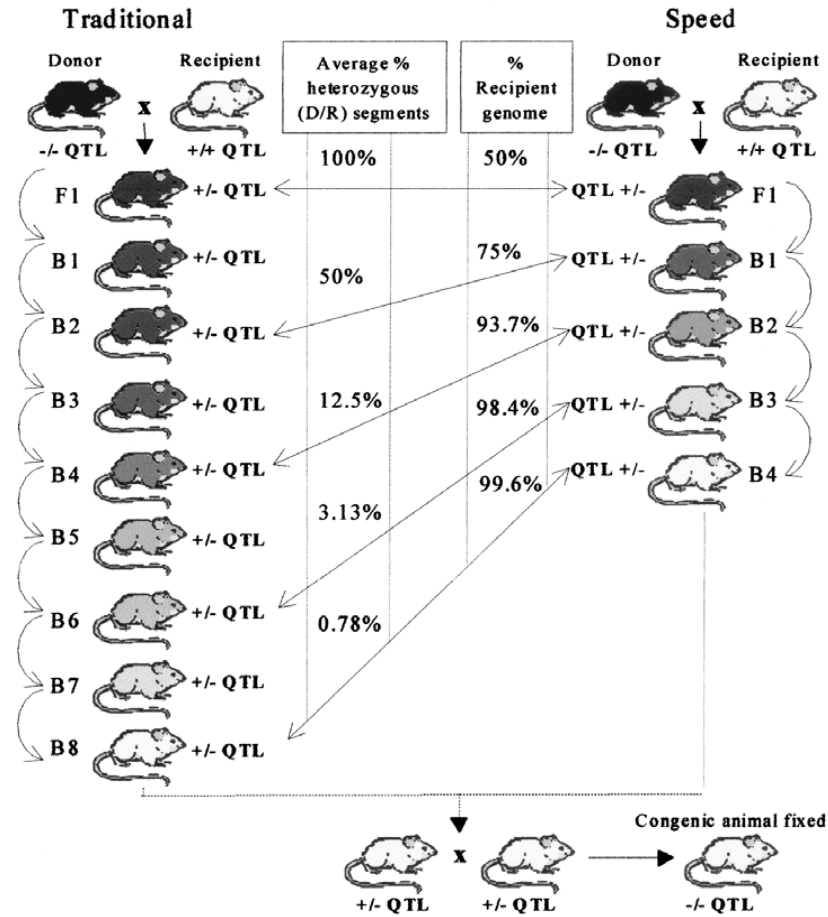


Figure 5.1 Traditional and speed congenic breeding.

Construction of congenic strains showing the differences between traditional and marker-assisted speed breeding.

Arrows indicate the backcross at which the background heterozygosity is theoretically the same. Decreasing shades of grey represent dilution of the donor genome. D=donor strain alleles, R=recipient strain alleles, B=backcross, F1=first filial generation. Taken from (Graham *et al.*, 2005).

5.1.3.3 Chromosome 14 congenic strains

Through the use of genome-wide linkage analysis, groups here at the University of Glasgow previously identified a QTL for LV mass on chromosome 14 of the stroke-prone spontaneously hypertensive rat (SHRSP) (Clark *et al.*, 1996). To explore this, two congenic strains have been produced using SHRSP and its normotensive control strain, Wistar Kyoto (WKY):

- (i) WKY.SP_{Gla14a} in which the QTL on chromosome 14 from SHRSP has been introgressed into WKY rats (denoted WKY-congenic);
- (ii) SP.WKY_{Gla14a} in which the QTL on chromosome 14 from WKY has been introgressed into SHRSP (denoted SHRSP-congenic).

The nomenclature for these strains includes the recipient strain (first abbreviation) followed by the donor strain (second abbreviation); Gla denotes that the strains originate from Glasgow colonies and the number 14 refers to the chromosome number. For simplicity, these strains will be referred throughout the rest of the thesis as **WKY-congenic** and **SHRSP-congenic**.

5.1.4 Functional assessment of the models using PV methodology

These congenic strains can be utilised for the identification of genes within this QTL which could be potential targets for hypertension therapy; however, this model also represents a very effective model for the investigation of *Runx* expression patterns during different cardiac diseases which will be the main focus for this thesis. Previous phenotype measurements (echocardiography and radiotelemetry) of these congenic strains have revealed that they each show alterations in LV mass with little change in their systolic BP. Therefore it is likely that this QTL is being regulated without influence by BP. However the measurements that were performed to measure this were largely dependent on loading conditions. One way to measure LV function without the influence of BP load is using pressure-volume analysis. This allows assessment of LV performance *in vivo* without the influence of load. This method has been widely used in humans and large animals (Kass *et al.*, 1988b; Little & Cheng, 1993), however the recent development of miniature PV catheters has made the technique applicable to smaller animals such as rodents (Pacher *et al.*, 2008).

5.1.5 Cardiac fibrosis can alter normal functioning in these models

LV function in hypertensive heart disease models can be largely influenced by the level of structural remodelling, for example the degree of LVH as previously discussed but also patterns of ECM remodelling which are also characteristic of this model (Weber *et al.*, 1991a; Weber *et al.*, 1991b). The accumulation of fibrillar collagen, representing myocardial fibrosis is a major determinant of the LV diastolic properties: during hypertensive pressure-overload, the ventricles enlarge to accommodate the increased wall stress and this is usually accompanied by disproportionate deposition of collagen around the myocardial arteries and muscle fibres as a means of conferring tensile strength to the myocardium to further support the heart during increased load (Kai *et al.*, 2005). Myocardial fibrosis affects diastolic performance in that it can limit normal diastolic

'suction', impair myocardial compliance and compromise the length-dependent muscle fibre shortening during contraction (Burlew & Weber, 2002).

5.1.6 Aims

The aims of the work presented in this chapter were therefore as follows:

- (i) Characterise systolic and diastolic function at baseline and at different preloads in each strain using the PV catheter system in order to assess load-independent analysis of cardiac function. This would allow a functional characterisation of the different strains to assess the differences in phenotypes, and segregate the strains into different functional models of cardiac disease for the investigation of *Runx* expression levels.
- (ii) Measure *Runx1* expression in these strains and identify whether the different models show different patterns of expression.
- (iii) Assess changes in structural cardiac fibrosis of the heart in these strains to characterise differences between the strains, identify possible links with function and assess possible links with *Runx1* expression.

5.2 Methods

The congenic strains have been bred and maintained at the University of Glasgow since 1991. Genotyping and radiotelemetry probe implantation was performed by Dr. Delyth Graham and arterial BP and LVMI measurements were previously collected by Dr. Delyth Graham and Dr. Kirsten Douglas as described in the General Methods chapter.

5.2.1 Blood pressure determination

Radiotelemetry transmitter probes (*Dataquest IV telemetry system, Data Sciences International*) were surgically implanted into the abdominal aorta when the animals reached 12 weeks of age for the measurement of systolic BP over the subsequent 4 weeks. Measurements were taken for 10 s every 5 min and these measurements were averaged for each hour.

5.2.2 LV mass measurements

LV mass was measured using echocardiography when the animals were 16 weeks of age. Animals were anaesthetised (isoflurane) and short axis 2D M-mode images were taken through the left parasternal window at the papillary muscle level using ACUSON Sequoia C512 echocardiograph. Mean data from six consecutive cardiac cycles from each M-mode image were used to calculate LV mass using the ASE-cube formula with Devereux correction factor as previously published (Devereux *et al.*, 1986):

$$LV\ mass = 0.8 (1.04(EDD + PWT + AWT)^3 - EDD^3) + 0.6 \quad \text{Eq. 20}$$

Where EDD is the end-diastolic dimension (mm), PWT is the posterior wall thickness (mm), AWT is the anterior wall thickness (mm). LV mass was normalised to tibial length (TL).

5.2.3 LV PV Measurements

16 week-old animals were induced and maintained with isoflurane on a face-mask (1.5-2%). Body temperature was maintained at $37^{\circ}\text{C} \pm 0.5$ using a rectal probe connected to a homeothermic heat blanket system (*Harvard Apparatus 507221F*). A 1.9F pressure-volume catheter (*SciSense*) was inserted into the carotid artery and advanced through the aortic valve into the left ventricle guided by changes in pressure. Following a ten-minute stabilisation period, pressure and volume measurements were recorded in steady state and during reduced preloads by temporarily occluding the inferior vena cava. To offset parallel volume (V_p) from surrounding conductive structures, three bolus injections (35 μl each) of 15% hypertonic saline was administered into the left jugular vein at the end of the experiment to allow a mean value for V_p to be taken.

5.2.4 Harvesting of hearts

Animals were sacrificed by cervical dislocation and the heart was removed and washed in ice-cold saline (0.9% sodium chloride w/v). The aorta was cut transversely, mounted on to a 19G cannula attached to a syringe and perfused retrogradely with ice-cold saline to rinse blood out of the coronary vessels. Hearts were blotted dry on tissue paper and weighed using a precision electronic balance. The LV free wall was then dissected free and also weighed. The LV free wall was then cut into small pieces approximately 5mm^2 and each were snap-frozen in liquid nitrogen and stored at -80°C until needed for biochemical experiments.

5.2.5 Preparation of heart sections for Sirius red staining

Harvested hearts were fixed in 10% neutral buffered formalin for a minimum of 24 h to allow sufficient penetration of the tissue. Sectioning and staining of the sections was performed by Mr Andy Carswell. Briefly, the hearts were paraffin-embedded and sectioned using a microtome (3 μ m thick). Sections were deparaffinised and hydrated using a clearing agent (*HistoClear, Fisher Scientific, U.K*) for 2 x washes followed by 100% ethanol, 90% ethanol, 70% ethanol then distilled water for 7 min in each solution. Sections were then stained for 1 h with picrosirius red, which is a collagen-specific dye that stains collagen red, followed by 2 x washes of acidified water and 2 x washes of tap water for 5 min each. Sections were then dehydrated through 70% ethanol, 90% ethanol, 100% ethanol and *HistoClear* (2 x washes) for 7 min each. The dehydrated sections were then coverslip-mounted with a mounting agent (*Histomount, Invitrogen, U.K.*).

5.2.6 Measurement of cardiac fibrosis

Transverse sections of LV apex stained with Sirius red were examined with an *Olympus BX41* microscope (x20 magnification) and images were captured with a *Qimaging Go-3* camera with the use of *QCapturePro* software. Collagen was quantified using *ImageProPlus* software which counted the number of red pixels of a set threshold of red colour using a histogram scale within a fixed area (300 x 300 pixels) for the blood vessels (perivascular fibrosis) and the adjacent interstitial areas (interstitial fibrosis). Perivascular fibrosis was assessed in at least 5 randomly selected vessels per heart. Blood vessels with comparable lumen size were selected for as much as possible and only vessels which could fit into the box were used and any that were <50% the size of the box were not included. Interstitial fibrosis was measured in areas adjacent to the blood vessels; three separate adjacent areas to each blood vessel were used for this and a mean value taken. Interstitial areas contained no obvious blood vessels or other structures. All perivascular and interstitial measurements were then averaged to give a mean value of perivascular and interstitial fibrosis for each heart.

5.2.7 qRT-PCR

RNA extraction, cDNA synthesis and qRT-PCR were performed as described in the General Methods Section 2.12. RNA was extracted using a phenol-chloroform extraction-based method using the miRNeasy RNA Extraction Kit (*Qiagen*) according to the supplier's protocol. Following DNase treatment of the extracted RNA, first-strand cDNA

was synthesised from 2 µg of RNA using the Omniscript Reverse-Transcription Kit (*Qiagen*). *Runx1* gene expression in cDNA samples was measured by qRT-PCR with *Runx1*-specific primers in a SYBR green assay using a thermal cycler with accompanying software (ABI 7500 sequence detection system). GAPDH was used to normalise cDNA levels.

5.2.8 Data recording and statistical analysis

All PV data were recorded on a *Dell* laptop using *LabScribe2.0* software version 2.241 at a sampling rate of 2000 samples.s⁻¹ and analysed offline using *LabScribe2.0* software. All data in the text and figures are expressed as mean ± SEM. Statistical significance was measured using student's paired or unpaired t-test for comparisons between a maximum of two groups, or ANOVA followed by the Bonferroni or Tukey post-hoc test where appropriate for comparing more than two groups. A *P* value of <0.05 was considered statistically significant.

5.3 Results

5.3.1 LV mass and systolic blood pressure

Age, BW, tibial length, LV mass index (LVMI) and systolic blood pressure (SBP) for each strain are shown in Table 5.1. The WKY-congenic, SHRSP and SHRSP-congenic were all significantly smaller in BW ($P<0.05$ for each strain) and had significantly shorter tibial lengths (TL) compared to WKY ($P<0.05$ for each strain). LV mass was estimated using echocardiography and expressed relative to TL. LV mass and SBP measurements were performed by Dr Kirsten Douglas and Dr Delyth Graham. SHRSP demonstrated significantly greater LVMI than WKY (increased by 25.6% of WKY; $P<0.05$). The WKY-congenic showed a significant increase in LVMI compared to WKY (by 17.3%; $P<0.05$) and the SHRSP-congenic demonstrated a significant decrease in LVMI compared to SHRSP (by 16.4%; $P<0.05$). SBP was unchanged between the SHRSP and SHRSP-congenic; both of these strains had significantly elevated SBP compared to WKY and were considered hypertensive as defined by SBP>150 mmHg. The WKY-congenic showed a small but significant increase in SBP (by 6.1%) when compared to WKY; however both of these strains remained normotensive with SBP within the normal range for rats (119-146 mmHg; (Pacher *et al.*, 2008)).

Table 5.1 LVMI and SBP in the congenic and background strains.

Animals	Age (weeks)	BW (g)	Tibial Length (mm)	LVMI (g/mm)	SBP (mmHg)
WKY (n=10)	16	337.70 ± 9.51	47.70 ± 1.25	16.33 ± 0.29	136.46 ± 2.88
WKY-congenic (n=13)	16	319.46 ± 4.79*	44.31 ± 0.40*	19.16 ± 10.34*	144.83 ± 2.45*
SHRSP (n=6)	16	257.83 ± 4.01†	40.00 ± 1.00†	20.51 ± 1.03†	192.06 ± 3.66†
SHRSP-congenic (n=5)	16	247.40 ± 9.45†	39.20 ± 0.49†	17.14 ± 0.42*	181.87 ± 7.16*†

BW = body weight; LVMI = left-ventricular mass index (LV mass normalised to tibial length) measured using echocardiography; SBP = systolic blood pressure, daytime recordings using radiotelemetry. * $P < 0.05$ between the congenic and respective background strain. † $P < 0.05$ when compared to WKY.

5.3.2 Haemodynamic LV function

LV PV measurements were used to assess changes in LV function in each of the four strains. The results of these measurements are presented in Figure 5.2, Figure 5.3 and summarised in Table 5.2.

5.3.2.1 Systolic functional parameters of the heart

Figure 5.2A shows typical pressure traces from each of the four strains and typical PV loops from each strain are shown in Figure 5.2B. Figure 5.3 shows the results of systolic parameters of cardiac function between the groups. Heart rate was the same in all four strains with no statistical differences observed ($P > 0.05$; Figure 5.3A (i)). Both the SHRSP and SHRSP-congenic showed significantly elevated ESP compared to WKY (to 148% and 154% of WKY levels for SHRSP and SHRSP-congenic respectively; $P < 0.05$ for both; Figure 5.2A-B & Figure 5.3A (ii)) and the WKY-congenic (to 133% and 138% of WKY-congenic levels for SHRSP and SHRSP-congenic respectively; $P < 0.05$ for both; Figure 5.2A & Figure 5.3A (ii)). SHRSP and SHRSP-congenic were both hypertensive with $ESP > 150$ mmHg (Figure 5.2A-B & Figure 5.3A (ii)). ESP was not different between the SHRSP and SHRSP-congenic ($P > 0.05$). The WKY-congenic showed a small but significant (to 111% of WKY levels) increase in ESP in the WKY-congenic compared to WKY ($P < 0.05$; Figure 5.3A (ii)) but both WKY and WKY-congenic were normotensive $ESP < 146$ mmHg. There were no differences in the maximal rate of rise in pressure (dP/dt_{max}) between the WKY-congenic and WKY ($P > 0.05$), nor between the SHRSP-congenic and SHRSP ($P > 0.05$; Figure 5.3A (iii)). Both the SHRSP and the SHRSP-congenic showed higher dP/dt_{max} compared to WKY (to 142% and 143% of WKY levels for SHRSP and SHRSP-congenic respectively; $P < 0.05$ for both; Figure 5.3A (iii)) and

WKY-congenic (to 138% and 139% of WKY-congenic for SHRSP and SHRSP-congenic respectively; $P < 0.05$ for both; Figure 5.3A (iii)). CO was significantly reduced in the WKY-congenic compared to WKY (to 71% of WKY; $P < 0.05$; Figure 5.3A (iv)) but conserved between the SHRSP-congenic and SHRSP ($P > 0.05$; Figure 5.3A (iv)).

5.3.2.2 Diastolic functional parameters of the heart

The WKY-congenic showed an increase in EDP to 146% of WKY levels ($P < 0.05$; Figure 5.3B (i)) and the SHRSP-congenic showed a decrease in EDP to 60.7% of SHRSP levels ($P < 0.05$; Figure 5.3B (i)). Compared to WKY, the maximum rate of fall in pressure (dP/dt_{\min}) increased in the SHRSP to 140% of WKY levels ($P < 0.05$; Figure 5.3B (ii)) and in the SHRSP-congenic to 140% greater of WKY ($P < 0.05$; Figure 5.3B (ii)). Similarly, when compared to the WKY-congenic, dP/dt_{\min} was increased in the SHRSP to 137% of WKY-congenic ($P < 0.05$; Figure 5.3B (ii)) and in the SHRSP-congenic to 137% of WKY-congenic ($P < 0.05$; Figure 5.3B (ii)). However, there were no differences in dP/dt_{\min} observed between each congenic and their respective background strains (WKY-congenic vs. WKY $P > 0.05$; SHRSP-congenic vs. SHRSP $P > 0.05$; Figure 5.3B (ii)). No differences in the relaxation time constant Tau (τ) were observed between the four strains ($P > 0.05$; Figure 5.3B (iii)). The EDPVR stiffness constant (β) was found to be significantly higher in the WKY-congenic compared to WKY (3.0-fold higher; $P < 0.05$) and significantly lower in the SHRSP-congenic compared to SHRSP (3.5-fold lower; $P < 0.05$). SHRSP showed significantly greater LV stiffness than WKY (3.0-fold higher; $P < 0.05$; Figure 5.3).

5.3.2.3 Volume parameters

No differences were observed in ESV between the four strains ($P > 0.05$; Figure 5.3C (i)). EDV was significantly reduced in the WKY-congenic compared to WKY (by 26.2% of WKY; $P < 0.05$ Figure 5.3C (ii)). No differences in EDV were observed between the SHRSP-congenic and SHRSP ($P > 0.05$) nor between SHRSP and WKY ($P > 0.05$; Figure 5.3C (ii)). SV was significantly reduced in the WKY-congenic compared to WKY (to 68.8% of WKY levels; $P < 0.05$), however SV was not different in the SHRSP-congenic compared to SHRSP ($P > 0.05$) nor between SHRSP and WKY ($P > 0.05$; Figure 5.3C (iii)). EF was unchanged across all four strains ($P > 0.05$; Figure 5.3C (iv)).

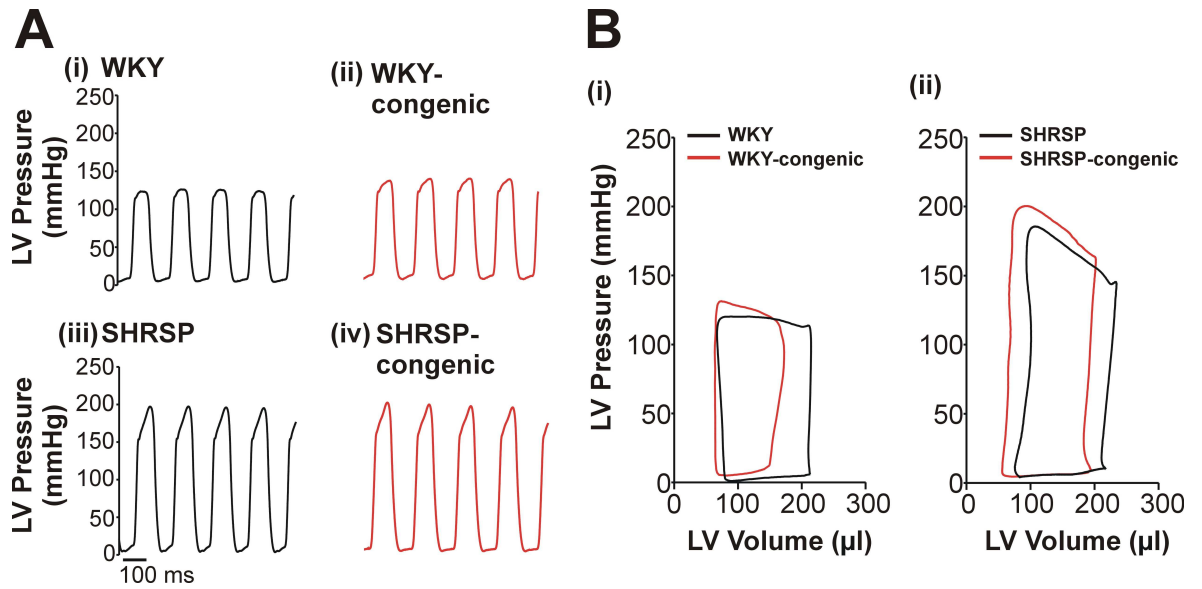


Figure 5.2 Representative LV pressures and PV loops.

A (i-iv). LV intra-ventricular pressures from WKY, WKY-congenic (red), SHRSP and SHRSP-congenic (red). B (i). Typical PV loops from WKY (black) and WKY-congenic (red). B (ii) Typical PV loops from SHRSP (black) and SHRSP-congenic (red).

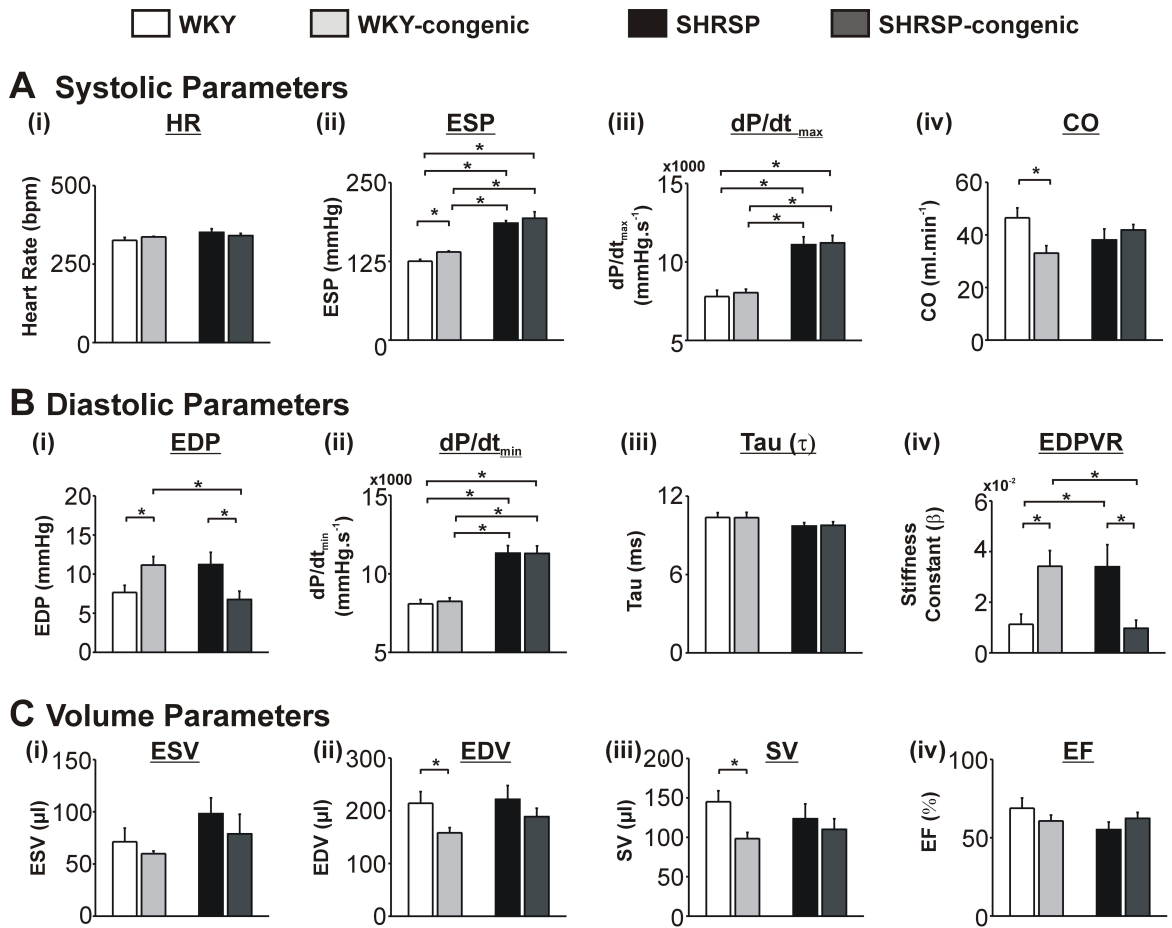


Figure 5.3 Haemodynamic PV indices of LV function.

Systolic functional parameters (A i-iv), diastolic functional parameters (B i-iv) and volume parameters (C i-iii) in WKY ($n=7$; white bar), WKY-congenic ($n=5$; light grey bar), SHRSP ($n=7$; black bar) and SHRSP-congenic ($n=7$; dark grey bar). Data shown are mean \pm SEM * $P < 0.05$.

Table 5.2 Haemodynamic PV data from the congenic and background strains.

	WKY (n=7)	WKY-congenic (n=5)	SHRSP (n=7)	SHRSP- congenic (n=7)
HR (bpm)	325.8 ± 9.0	336.6 ± 1.8	350.9 ± 11.8	340.6 ± 7.2
ESP (mmHg)	125.2 ± 3.1	139.9 ± 1.5*	185.6 ± 4.0†	193.3 ± 10.4†
EDP (mmHg)	7.7 ± 0.9	11.2 ± 1.1*	11.2 ± 1.6	6.8 ± 1.1*
dP/dt_{max} (mmHg.s⁻¹)	7796.4 ± 393.5	8042.9 ± 222.8	11092.7 ± 501.1†	11208.8 ± 477.3†
dP/dt_{min} (mmHg.s⁻¹)	8085.0 ± 272.3	8243.0 ± 222.7	11309.4 ± 479.2 †	11293.7 ± 478.2†
Tau (ms)	10.4 ± 0.4	10.4 ± 0.4	9.7 ± 0.3	9.8 ± 0.3
EDPVR	0.011 ± 0.004	0.034 ± 0.006*	0.034 ± 0.009†	0.010 ± 0.03*
ESV (μl)	71.3 ± 13.1	59.8 ± 2.6	98.2 ± 15.2	78.8 ± 18.8
EDV (μl)	214.2 ± 21.9	158.1 ± 10.0*	221.7 ± 26.2	188.8 ± 15.9
SV (μl)	142.9 ± 16.8	98.3 ± 7.9*	123.5 ± 18.8	122.3 ± 6.7
CO (ml.min⁻¹)	46.5 ± 3.7	33.1 ± 2.8*	38.1 ± 4.2	41.9 ± 2.1
EF (%)	68.8 ± 6.5	60.7 ± 3.7	55.2 ± 4.8	63.5 ± 4.3

HR = heart rate; ESP = end-systolic pressure; EDP = end-diastolic pressure; dP/dt_{max} = maximal rate of rise of pressure; -dP/dt_{min} = maximal rate of fall in pressure; Tau (τ) = relaxation time constant; EDPVR = end-diastolic pressure-volume relationship stiffness constant. ESV = end-systolic volume; EDV = end-diastolic volume; SV = stroke volume; EF = ejection fraction; CO = cardiac output. Values are expressed as mean ± SEM. * *P* < 0.05 vs. time-matched sham control. † *P* < 0.05 compared to WKY.

5.3.3 Collagen content

Collagen levels in the heart were assessed by measuring the positive collagen area from Sirius red histology sections of the heart. When compared to WKY, the WKY-congenic showed significantly higher levels of perivascular collagen levels (13.9 ± 2.6 vs. 5.8 ± 0.4 %; WKY-congenic ($n=5$) vs. WKY ($n=3$); $P<0.05$; Figure 5.4B) and interstitial collagen levels (4.6 ± 0.8 vs. 1.7 ± 0.2 %; WKY-congenic ($n=5$) vs. WKY ($n=3$); $P<0.05$; Figure 5.4C). Compared to SHRSP, the SHRSP-congenic demonstrated significantly reduced levels of interstitial fibrosis (1.9 ± 0.3 vs. 3.3 ± 0.5 %; SHRSP-congenic ($n=4$) vs. SHRSP ($n=4$); $P<0.05$; Figure 5.4B) but had significantly elevated levels of perivascular fibrosis (17.7 ± 2.8 vs. 8.0 ± 1.7 %; SHRSP-congenic ($n=4$) vs. SHRSP ($n=4$); $P<0.05$; Figure 5.4C).

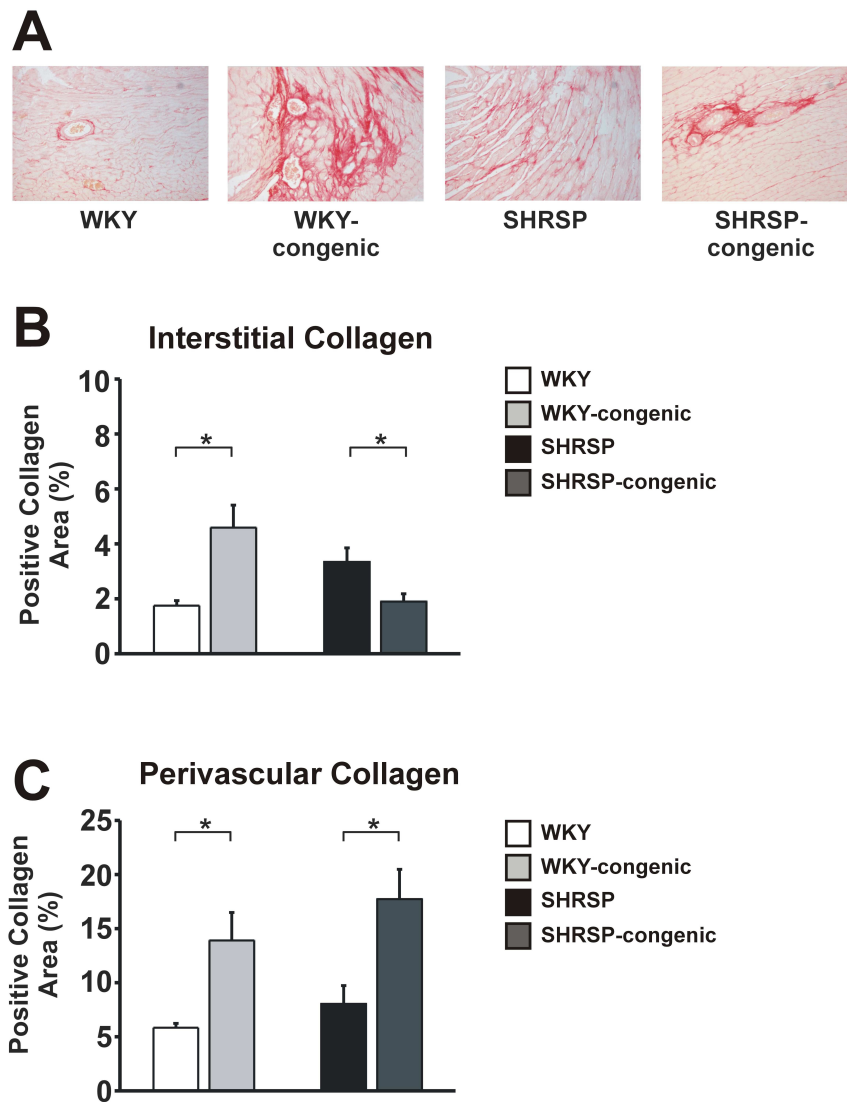


Figure 5.4 Collagen levels in the congenic and background strains.

A. Representative photographs of Sirius red sections showing areas of collagen (red) in WKY, WKY-congenic, SHRSP and SHRSP-congenic. B. Interstitial fibrosis measured from Sirius red sections from WKY ($n=3$), WKY-congenic ($n=5$), SHRSP ($n=4$) and SHRSP-congenic ($n=4$). C. Perivascular fibrosis measured from Sirius red sections from WKY ($n=3$), WKY-congenic ($n=5$), SHRSP ($n=4$) and SHRSP-congenic ($n=4$). Data shown are mean \pm SEM. * $P<0.05$.

5.3.4 *Runx1* gene expression

Runx1 mRNA levels were measured using qRT-PCR on whole LV free wall taken from each of the four strains. The WKY-congenic showed a significant reduction in *Runx1* levels compared to WKY (0.11 ± 0.05 vs. 0.47 ± 0.06 RQ; WKY-congenic ($n=5$) vs. WKY ($n=5$); $P<0.05$; Figure 5.5). There were no differences in *Runx1* expression between the SHRSP-congenic and SHRSP (0.19 ± 0.07 vs. 0.27 ± 0.05 RQ; SHRSP-congenic ($n=5$) vs. SHRSP ($n=5$); $P<0.05$; Figure 5.5). WKY also showed higher levels of *Runx1* compared to the SHRSP-congenic (0.47 ± 0.06 vs. 0.19 ± 0.07 RQ; WKY ($n=5$) vs. SHRSP-congenic

($n=5$); $P<0.05$; Figure 5.5). Although there also appears to be a trend towards lower expression in the SHRSP compared to WKY, this did not reach statistical significance.

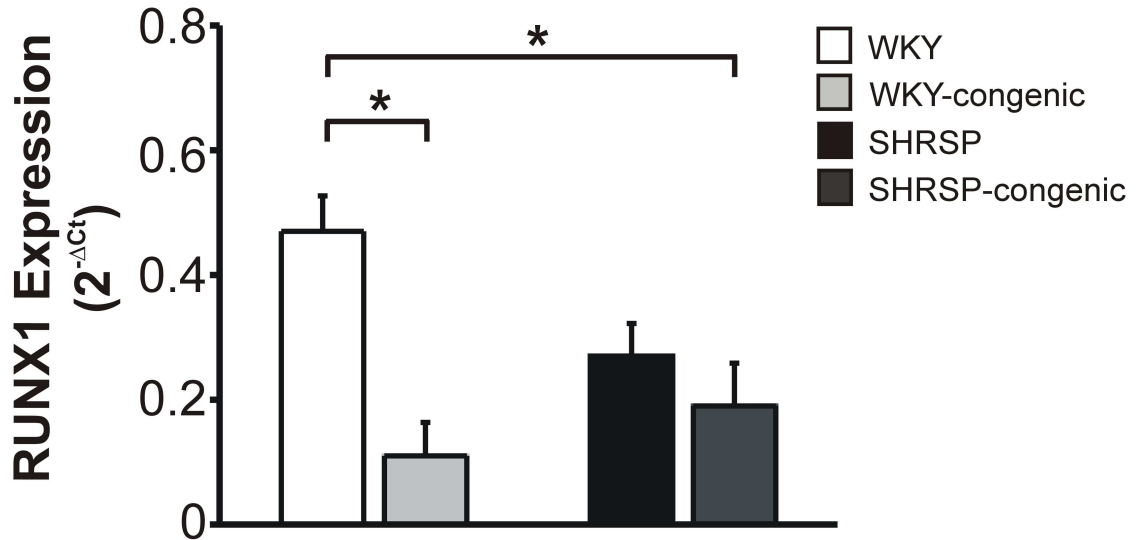


Figure 5.5 *Runx1* expression in the congenic and background strains.

Runx1 expression as measured by qRT-PCR using *Runx1*-specific primers for WKY ($n=5$; white bar), WKY-congenic ($n=5$; light gray bar), SHRSP ($n=5$; black bar) and SHRSP-congenic ($n=5$; dark gray bar). *Runx1* levels are expressed using the $2^{-\Delta Ct}$ method. * $P<0.05$ using ANOVA with the Tukey-Kramer multiple comparison's post-hoc test.

5.3.5 Links with *Runx1* expression and LV function

Regression analysis was performed to assess whether a relationship existed between *Runx1* expression and LV function. The functional parameter used was the relaxation time constant (τ) as it was found to be the most sensitive to small changes in the relationship between function and *Runx* expression. The value for τ was paired with the $2^{-\Delta Ct}$ for the same heart across the different strains. The $2^{-\Delta Ct}$ value was used as this was the method of analysis for the congenic study as a single value for each heart. Unfortunately there were no samples available for the WKY-congenic for this part of the study. The results are shown in Figure 5.6 which revealed that a significant correlation between *Runx1* expression and dysfunction in terms of impaired relaxation: i.e. as τ increased, *Runx1* expression increased ($y=0.13x-1.03$; $R=0.82$; $P<0.05$).

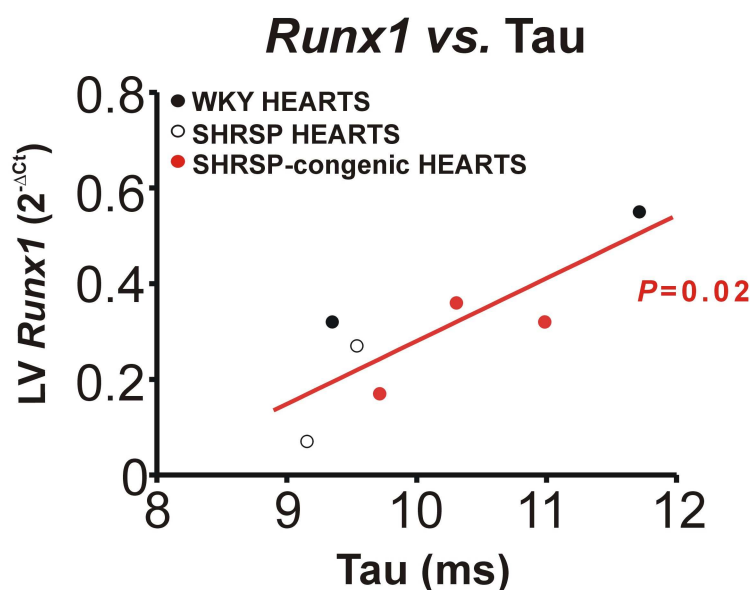


Figure 5.6 Relationship between Tau (τ) and *Runx1* expression in the WKY, SHRSP and SHRSP-congenic strains.

Linear regression analysis of the relationship between the $2^{-\Delta Ct}$ value for *Runx1* expression and the value for τ for each heart. Each point on the graph is an individual heart. WKY hearts ($n=2$; black circles), SHRSP hearts ($n=2$; open circles) and SHRSP-congenic hearts ($n=3$; red circles).

5.4 Discussion

QTLs that regulate LV mass are important for the study of LVH which is known to be an independent predictor of adverse cardiovascular outcome clinically (Devereux *et al.*, 1994; Verdecchia *et al.*, 1995). Previous work at the University of Glasgow has identified a QTL for LVMI on chromosome 14 of the SHRSP (Clark *et al.*, 1996). This QTL is localised between markers D14Mgh3 and R58 which are ≈ 12.3 cM apart (Clark *et al.*, 1996). This has been verified through the construction of congenic strains: (i) WKY.SPGLa_{14a} (denoted WKY congenic) in which the QTL on chromosome 14 of SHRSP has been introgressed into WKY and (ii) SP.WKYGLa_{14a} (denoted SHRSP congenic) in which the QTL from WKY has been introgressed into SHRSP. Both of these congenic strains demonstrate alterations in LV mass; the WKY-congenic shows increased LV mass and the SHRSP-congenic shows decreased LV mass. RUNX1 has been previously shown to have altered expression in the heart during cardiac disease; for example in human MI cardiac tissue (Gattenlohner *et al.*, 2003) and as the work in this thesis has revealed, in a mouse model of MI. The hypertensive rat model (SHRSP) and the associated congenic strains described in this study represent two further animal models of cardiac disease for

which altered *Runx* levels have not been previously reported and offer potential further insight into altered patterns of *Runx* expression in the heart during disease.

5.4.1 Congenic strains demonstrate a separation between LV mass and BP

Changes in LVMI with little change in BP: The chromosome 14 congenic strains demonstrate alterations in LVMI; however these changes occur with little (less than 12%) or no change in SBP. This has been verified through both radio telemetry measurements and LV PV measurements which have independently shown a small but significant increase in SBP in the WKY-congenic (compared to WKY), although the extent of this change does differ between the two methods. One reason for this discrepancy may be the effects of anaesthesia as PV measurements are performed under anaesthesia while radio telemetry measurements are recorded from conscious animals. Isoflurane anaesthesia is known to reduce blood pressure as a direct result of vasodilation and depressed myocardial contractility (Conzen *et al.*, 1992). Indeed the ESPs observed from animals that underwent PV analysis under anaesthesia showed lower ESP than arterial SBP from radio telemetry in conscious animals. Despite this, both sets of measurements have independently shown that although the WKY-congenic showed a small increase in arterial SBP and LVESP it remained normotensive, despite an increased LVMI. Similarly, the SHRSP-congenic showed no differences in arterial SBP or LVESP compared to SHRSP despite having significantly reduced LVMI. Changes in LV mass therefore occurred with no change in the normotensive or hypertensive status of the animal.

Separation between LVMI and BP: QTLs for LV mass can either be BP-dependent or BP-independent. BP-independent QTL for LV mass can increase LVMI in normotensive individuals or reduce LVMI in hypertension (Llamas *et al.*, 2005). This is important for the study of LVH in which there are discrepancies in the correlation between LVH and BP (Nunez *et al.*, 1996). Elevated BP in hypertension is the most common cause of LVH; however the intensity of BP load does not always correspond to the degree of LVH observed in patients (Devereux *et al.*, 1994). In individuals with comparable high BP the level of LVH can be largely continuous (Cohn, 1998). Similarly one report revealed no evidence of LVH in 50% of hypertensive patients (Devereux *et al.*, 1994). Several genetic linkage studies have identified QTL for LV mass, some of which are regulated by BP and others which are regulated independently of BP - for example several groups have identified various BP-independent QTL for LV mass at different locations on chromosome

17 (Deng *et al.*, 1994;Pravenec *et al.*, 1995;Tsujita *et al.*, 2000;Yagil *et al.*, 1998). QTL for LV mass which are dependent on BP have been identified on chromosomes 2, 4, 19 (Pravenec *et al.*, 1995) and 7 (Tsujita *et al.*, 2000;Garrett *et al.*, 1998).

Model of segregated LVMI and BP: In this study, QTL on chromosome 14 for LVMI causes changes in LVMI without alterations to the hypertensive (or normotensive) status of the animal. This is similar to the findings of Pravenec *et al.* (1995) who reported that for the LVMI QTL on chromosome 17, there was a significant correlation with LV mass but no correlations with systolic, diastolic or MAP; furthermore, no correlation was found between BP and LV mass. Furthermore in our study, the changes in LVMI are evident at 5 weeks of age (data not shown) before the onset of hypertension. This would suggest there is a BP-independent element to the regulation of this QTL for LVMI. Therefore utilising these congenic strains represents a model which has segregated LV mass from BP. This could allow for the identification of novel candidate genes for LVMI unaffected by BP in hypertension.

5.4.2 Congenic strains with altered LV mass show BP-independent diastolic dysfunction

It is well-documented from clinical studies and data from animal models that alterations in LV mass can affect the systolic and diastolic functioning of the heart (Lorell & Carabello, 2000a;Cingolani *et al.*, 2003). Both systolic and diastolic function can be influenced by the load on the heart. In order to measure changes in cardiac function independently of load, the PV catheter system was utilised as a method which allows assessment of diastolic LV performance independently from loading conditions.

5.4.2.1 Systolic function

SHRSP-congenic: These measurements confirmed enhanced systolic performance in the hypertensive animals (SHRSP and SHRSP-congenic) which both demonstrated elevated ESP of >150 mmHg confirming that they have high BP consistent with hypertension. These findings were in agreement with arterial SBP measurements which were generated using a separate method, radiotelemetry. This was further supported by elevated dP/dt_{max} in these animals. Both SHRSP and SHRSP-congenic were therefore confirmed as hypertensive with enhanced contractility; however these strains showed no differences in systolic parameters with each other and were hypertensive to the same degree.

WKY-congenic: Despite a small increase in ESP, the WKY-congenic showed normal ESP (119-146 mmHg; (Pacher *et al.*, 2008)) and was therefore considered normotensive like WKY. It is unclear the cause of this slight elevation in BP however the WKY-congenic had normal dP/dt_{\min} not different to WKY. Despite having normotensive properties of systolic function there was an overall decline in CO in the WKY-congenic strain which is likely because the EDV was smaller and despite equivalent EF this led to diminished SV as well as CO (heart rate was unchanged). Reduced EDV indicates a smaller luminal LV which may be due to increased wall thickness consistent with concentric remodelling (Lorell & Carabello, 2000a). Although wall thickness data was not available to confirm this, this finding is consistent with the increased LV mass observed in these animals. As the WKY-congenic was the only strain to show any differences in EDV, it would suggest that introducing the QTL on chromosome 14 can alter LV mass through what is potentially by concentric wall thickening – however, by removing the QTL on chromosome 14 this does reverse the effect as no changes in EDV were observed in the SHRSP-congenic. The reasons for this would require further investigation. EF was unchanged across all four strains which may be as a consequence of compensatory remodelling (increased LVH) which is known to preserve EF (Aurigemma *et al.*, 1995). This finding is not unusual for hypertensive rats at 16-wk as others have shown that EF remains normal in the SHR until 72-wk of age when HF begins to develop (Mirsky *et al.*, 1983). Similarly CO and SV also do not begin to reduce until 90-wk in the SHR (Pfeffer *et al.*, 1979a), consistent with the finding in this present study for SHRSP (and SHRSP-congenic).

5.4.2.2 Diastolic function

SHRSP-congenic: Despite no change in systolic performance between the SHRSP-congenic and SHRSP there were alterations in diastolic function. The SHRSP-congenic demonstrated reduced LV mass, despite equivalent systolic function to SHRSP showed improvements in diastolic function (to control WKY levels for EDP and EDPVR). This was evident from a lower EDP consistent with improved filling and load-independent reduced end-diastolic stiffness. *In vivo* measurements of diastolic dysfunction for the SHRSP in the literature are extremely limited, there are however findings described by others for this in the SHR model: for example 40-wk old SHR function characterised by Millar PV measurements showed increased myocardial stiffness (derived from the EDPVR) and impaired relaxation (Cingolani *et al.*, 2003). These findings were also confirmed by other studies in the SHR (Nishimura *et al.*, 1985;Pfeffer *et al.*, 1979a). In an

ex vivo SHRSP working heart of the same age as the animals in this study (16-wk) there was a significant increase in EDP, consistent with our findings *in vivo* (Chen *et al.*, 2001). Interestingly, the relaxation time constant (τ) was unaltered between all four strains suggesting the time to relax was not different between all strains despite altered filling pressures and myocardial stiffness. This was an unusual finding as τ usually increases in hypertensive heart disease due to increased LVH and fibrosis (Leite-Moreira *et al.*, 1999). This has been demonstrated in the SHR model with prolongation of τ concurrent with increased LVH and fibrosis (Nishimura *et al.*, 1985; Cingolani *et al.*, 2003). However, in both of these studies the animals were at a greater age (28-50 wk and 40-wk of age) than the animals in our study (16-wk old). Therefore it may be that τ is only affected when the animals are older and/or reached a critical threshold of hypertensive heart disease. In dogs, τ is unchanged as hypertension is developing (2-4 wk) and is only increased when the animals reach a stable hypertensive state (>14-wk) (Gelpi *et al.*, 1991). It is therefore possible that it may take longer than 16-wk to see changes in τ in the rat model. An elevated EDP and raised EDPVR with a normal τ is not uncommon as it has been described previously in humans (Maurer *et al.*, 2004). However with reduced rates of relaxation (using dP/dt_{\min}) in the SHRSP in this study it does question the lack of change in the τ – at present the reasons behind this discrepancy are not clear.

WKY-congenic: In contrast, the WKY-congenic which had an increased LV mass and was normotensive like WKY demonstrated reduced diastolic performance with raised EDP and higher LV stiffness. These data show that there were both load-dependent and load-independent alterations in LV diastolic function in both strains. Collectively, other than τ , the diastolic indices revealed diastolic dysfunction in the WKY-congenic with no change in systolic dysfunction. Diastolic dysfunction with preserved systolic function is being increasingly recognised in humans (Redfield *et al.*, 2003); a recent population-based survey revealed that diastolic dysfunction was observed 5 times more than systolic dysfunction (Fischer *et al.*, 2003). Diastolic dysfunction has become an early marker of cardiac damage in hypertension and is well known to precede HF during hypertensive heart disease (Grossman, 2000; Zile & Brutsaert, 2002).

5.4.2.3 Volume data

LV volumes (both ESP and EDP) were not different between SHRSP-congenic and SHRSP suggesting the two strains were operating at equivalent LV volumes. These were also no different to WKY which suggests that, despite increased LV mass in SHRSP this is

not affecting LV luminal volume. This is not uncommon as LV mass can increase with no change in the chamber radius (Lorell & Carabello, 2000b). However in the WKY-congenetic reductions in EDV are present with increased LV mass suggesting that in these animals there is evidence of concentric hypertrophy accompanied by reduced chamber volume. This would suggest that the QTL segment which has been introgressed into these animals may have led to concentric hypertrophy therefore this phenotype could be linked to the specific QTL. When the QTL is removed (SHRSP-congenetic) the effect is lost as EDV is found to be unchanged compared to SHRSP which further supports that there may be genes on the QTL linked to this phenotype observed.

5.4.3 Altered diastolic dysfunction may be linked to altered cardiac fibrosis

Possible triggers for cardiac fibrosis: Myocardial stiffness, although influenced by many factors, is largely believed to be related to myocardial structural components, particularly myocardial fibrosis which is the accumulation of collagen within the myocardium (Brilla *et al.*, 1991a). Increased myocardial fibrosis is common during hypertension as a mechanism to increase tensile strength and support hypertrophied cardiomyocytes to prevent LV deformation during conditions of elevated load (Weber *et al.*, 1987). However, prolonged overloading can lead to excessive and/or disproportionate myocardial fibrosis which can reduce the compliance of the myocardium and be responsible for increased stiffening of the ventricle that can lead to diastolic dysfunction (Brilla *et al.*, 1991a). In early hypertensive heart disease, fibrotic collagen is observed mainly in the perivascular space surrounding the myocardial blood vessels (perivascular fibrosis) usually as a result of overload-induced vascular inflammation. Pressure-overload occurs because the narrowed, stiffened arteries in the vasculature have increased MAP in hypertension (due to reduced arterial diameter) which creates an elevated load on the ventricles of the heart which must work harder to provide adequate circulation to the body's tissues. The increase in arterial pressure and elevated mechanical strain on the coronary vessels are believed to initiate a series of inflammatory changes in the coronary arterial wall including the activation of the chemokine, monocyte chemoattractant protein-1 (MCP-1) which recruits macrophages to the area which produce profibrotic cytokines that stimulate fibrosis in the perivascular space (Nicoletti & Michel, 1999). Perivascular fibrosis can then subsequently spread into the adjacent interstitium (interstitial fibrosis) as part of a "reactive fibrosis" (Brilla *et al.*, 1991a). Increased fibrosis during cardiac remodelling can be classified as either *reactive*, which relates to the progressive spread of collagen in the interstitial space and adventitia of

intramyocardial coronary arteries or *reparative* which occurs when areas of cardiomyocyte loss are replaced by fibrosis (e.g. following necrosis in myocardial infarcts). Presence of interstitial fibrosis is therefore usually secondary to perivascular fibrosis and therefore by examining levels of both perivascular and interstitial fibrosis this allows for assessment of the progression of fibrosis.

Differences in cardiac fibrosis in the congenic models: Cardiac fibrosis was measured in the four strains for this study by quantifying collagen-positive areas in Sirius red sections of the LV. Comparing the background strains, SHRSP shows increased levels of both perivascular and interstitial fibrosis compared to WKY consistent with a hypertensive model - increased cardiac fibrosis (both perivascular and interstitial) is a prominent feature of hypertensive rat models of hypertension as has been shown in SHR (Brilla *et al.*, 1991a; Nishimura *et al.*, 1985) and SHRSP (Sawamura *et al.*, 1990). Additionally, both congenic strains demonstrated alterations in the level of fibrosis compared to their respective background strains. The WKY-congenic showed significantly higher levels of both perivascular and interstitial fibrosis compared to WKY, indicating both an increase in collagen deposition but also to a more advanced stage (as evidenced by high interstitial in addition to high perivascular fibrosis). Higher levels of interstitial fibrosis could be contributing to the increased myocardial stiffness observed in these animals as evidenced by the EDPVR measurements. The SHRSP-congenic demonstrated reduced levels of interstitial fibrosis compared to its respective SHRSP which would also explain the reduced myocardial stiffness in these animals. Interestingly, while there was reduced interstitial fibrosis in the SHRSP-congenic, there was an increase in the level of perivascular fibrosis. Given that perivascular fibrosis can be associated with increased inflammation, it's possible that the SHRSP-congenic, like the WKY-congenic, is sensitive to increased inflammation of the myocardial blood vessels. The cause of this however remains unclear. This finding would support the hypothesis that these animals have more inflamed blood vessels which seems likely given that when fed a salt diet they show a very high incidence of stroke within 24 h compared to SHRSP (personal communication with Dr. Delyth Graham; data not shown). It may also be that the SHRSP-congenic is at an earlier stage of the fibrosis process by the absence of any spread into the interstitial areas or that the fibrosis is more concentrated around the perivascular space. Increased perivascular fibrosis with reduced interstitial collagen has been previously reported in rats, albeit in volume-overload hypertrophy (Hutchinson *et al.*, 2010; Voloshenyuk & Gardner, 2010).

5.4.4 ***Runx1* expression is altered in the congenic strain of increased LV mass**

Genes may be regulated differently under different cardiac disease conditions:

Samples of LV from each of the four strains were tested for the expression of the *Runx1* gene which has been previously shown to have altered expression in the heart during cardiac disease; for example in human MI cardiac tissue (Gattenlohner *et al.*, 2003) and as the work in this thesis has revealed, in a mouse model of MI. It is possible for cardiac genes to be regulated differently under different conditions of disease. Some genes may be altered as a result of specific stimuli only and may not show the same pattern in different models of cardiac diseases. For example, the gene for NCAM (CD56), a neural cellular adhesion molecule, is over-expressed during chronic ischaemic HF which is found to be specific for ischaemic damage compared to other cardiac diseases including congestive cardiomyopathy, hypertrophic obstructive cardiomyopathy, myocarditis and sarcoidosis (Gattenloner *et al.*, 2004). However, another study revealed that NCAM was also up-regulated during remodelling of hypertrophy to HF in a Dahl salt-sensitive rat model (Ventura-Clapier *et al.*, 2004) suggesting that the stimulus may not be ischaemia-specific.

Differences in *Runx1* expression between the congenic models and the MI model:

While there were no differences found in the expression of *Runx1* between the SHRSP-congenic and SHRSP, there was a marked reduction in expression in the WKY-congenic compared to WKY. The two congenic strains both showed lower levels of *Runx1* compared to WKY. *Runx1* expression was decreased within the rat model of increased LV mass and fibrosis compared to an up-regulation observed the in the mouse MI model suggesting there are different triggers in the different models contributing to *Runx1* expression levels. It is possible that like NCAM, *Runx1* could be sensitive to ischaemic insult triggering greater expression levels, and under conditions of overload-induced hypertrophy the *Runx1* gene is repressed. The molecular mechanism by which ischaemic stimuli are converted into intracellular signals are not clear, but one study has shown that ischaemia may preferentially activate specific protein kinase cascades which may be responsible for specific gene activation (Shimizu *et al.*, 1997). Differences in the expression pattern of the same gene have also been reported previously in a similar two models: for example an increase in mRNA for the T-type Ca²⁺ channel occurs in post-MI remodelling rat myocardium (Qin *et al.*, 1995) but not in a rat model of overload hypertrophy (Vassort & Alvarez, 1994).

Reasons for the differences in expression patterns between the models:

(i) One potential reason for the differences in gene expression between an MI-induced injury and a pressure-overload injury may be related to the differences in the hypertrophy response between the models. Hypertrophy is known to be a major cause of altered gene expression in the heart, particularly for transcription factors which are induced by hypertrophic stimuli to orchestrate the synthesis of new contractile sarcomeres for the protection of the heart (Akazawa & Komuro, 2003). MI results in a *regional* hypertrophy, mainly confined to the surviving myocardium which is largely eccentric due to volume overload (Sadoshima *et al.*, 1992). Pressure-overload (like in the case of hypertension) results in a *global* hypertrophy which is largely a concentric hypertrophy (Lorell & Carabello, 2000a). Therefore one possibility is that the differences in mechanical stimuli between the two models could explain the differences in gene expression patterns – the same may also be true for *Runx1*.

(ii) Another major difference in the remodelling between the two models which may contribute to the opposing gene expression patterns may be related to the ECM remodelling pattern – namely cardiac fibrosis. In the MI heart, cardiac fibrosis is primarily *reparative* meaning that the increased collagen levels are intended to replace the lost cardiomyocytes (French & Kramer, 2007), while in the pressure-overload model the fibrosis is predominantly a *reactive* fibrosis whereby collagen accumulates and spreads as part of an inflammatory response (Brilla *et al.*, 1991b). It is possible therefore that the differences in fibrosis patterns could also contribute to the differences in *Runx1* expression between these two models. RUNX1 is known to be expressed in fibroblasts (Wotton *et al.*, 2004); however given that these two models both contain fibroblasts but show opposite effects on *Runx1* expression it would indicate that there are other mechanisms involved than just *Runx1* being present in fibroblast cells.

5.4.5 Potential links with *Runx1* and degree of LV dysfunction

As was observed in the MI model, *Runx1* levels correlated significantly with degree of cardiac dysfunction among the rat strains (in hearts with greatest diastolic dysfunction, *Runx1* levels were highest). Utilising a different animal model of cardiac disease (other than MI) offered another approach to assessing the relationship between *Runx1* expression with cardiac dysfunction without the influence of the infarct associated with MI. Although a single gene may be altered differently in different forms of cardiac disease which is an important consideration, it may also reveal similar patterns between expression levels of

the gene and its relationship with cardiac dysfunction. Unfortunately n numbers were low ($n=2$ or 3) but from these small groups, similar trends to the MI model were observed in the WKY and SHRSP groups in regards to the relationship between *Runx1* mRNA levels and degree of cardiac dysfunction – i.e. lower function (prolonged τ), higher *Runx1* – despite differences in the overall expression pattern of *Runx* between the two models: a lower expression in the diseased state in the rat model, which was the opposite to the MI model (higher expression in the diseased state). The conclusion to make from the comparison with the different models is that the correlation between *Runx1* expression and degree of LV function is identical – reduced function, higher *Runx1* which further supports a link between *Runx1* expression and cardiac function without influence of an infarct size

CHAPTER 6

General Discussion

6.1 Rationale for the study

The main aim of this thesis was to examine the altered expression patterns of the RUNX genes in different experimental models of heart disease. The RUNX family of transcription factors are essential regulators of normal functioning during development but have received increased interest as important markers in human disease. RUNX genes are up-regulated in response to injury or insult which has been observed in striated muscle types. In skeletal muscle, levels of RUNX1 are relatively low but during disrupted electrical activity the expression increases nearly 100-fold and was shown to be a protective mediator in the muscle preventing harmful atrophy and further deterioration (Wang *et al.*, 2005). When the work by Gattenlohner *et al.* in 2003 (Gattenlohner *et al.*, 2003) identified an up-regulation of RUNX1 in the heart of patients with MI this raised a similar idea about the protective potential of RUNX1 over-expression in the heart. The work from this thesis set out to characterise the altered expression in two different experimental models of cardiac disease; MI as had been observed for the human patient study, and a rat model of hypertension with further genetically altered strains with more specific altered LV mass. These different models allowed a more thorough dissection of the expression patterns of the *Runx* genes in heart disease arising from different insults with differing patterns of remodelling and dysfunction. The study therefore aimed to provide novel information on the levels of *Runx* gene expression in heart disease and the potential implications for its role during the disease. Knowledge of the expression of RUNX in the heart even under healthy conditions is at present very limited and the work therefore aimed not only to improve knowledge of *Runx* levels in the normal heart and during disease but inform potential relevance of RUNX in future therapeutic treatments of CVD.

6.2 Major aims and findings

6.2.1 Suitability of animal models

One of the important aspects that the work in this thesis has demonstrated is the value of utilising experimental animal models in research. Each of the animal models used for this study conformed to the main set of criteria considered necessary for their use as disease models in that they mimicked the human phenotype closely, produced symptoms which were predictable and controllable, permitted study in a stable, chronic condition and allowed for relevant cardiac, haemodynamic and biochemical parameters to be measured (Doggrell & Brown, 1998; Houser *et al.*, 2012). In particular the mouse MI model was not

previously available in the laboratory and has since been developed with great success which has been made possible by a capacity building Integrative Mammalian Biology (IMB) award from the BBSRC designed to build and consolidate best practice *in vivo* research. It was therefore mandatory that a significant component of this thesis involved *in vivo* studies.

6.2.2 Development and characterisation of a mouse model of MI

Animal models of disease are highly valuable as they allow study of the disease in a controlled manner. In characterising gene expression changes in animal models for the future of human medicine it is imperative that the animal model mimics the human condition as closely as possible and represents a clinically relevant disease model for these experiments. Therefore one of the initial aims of the thesis was to develop and characterise a model of MI in the mouse which would allow for potential genetic manipulations at a later stage of the project for the extended study of *Runx* genes in MI through knockout transgenic models. Animal models of MI have been widely investigated however it was important to ensure the model developed a sufficient level of dysfunction and structural remodelling associated with this disease for subsequent gene expression studies using the model. It was hypothesised that the model would reproducibly present the clinical features of MI and therefore be a suitable platform for the study of altered *Runx* expression under the conditions of this disease. The mouse model of MI was successfully established in the laboratory using the CAL method producing a model with reproducible infarct sizes and low mortality that demonstrated not only features consistent with other published murine models but most importantly with human MI including LV systolic and diastolic dysfunction, altered electrical activity with increased frequency of VPC arrhythmias, cardiac structural remodelling including hypertrophy, wall thinning, chamber dilation and collagen deposition. The model was therefore considered suitable for subsequent RUNX studies in the context of MI.

6.2.3 Characterisation of congenic rat strains of altered LV mass

The rat hypertensive model (SHRSP) developed enhanced systolic performance with diastolic dysfunction and increased cardiac fibrosis consistent with other published SHRSP models and with human hypertension. The genetically-induced chromosome 14 congenic strains showed a BP-independent diastolic dysfunction or improvement in diastolic function with links with myocardial stiffness believed to be due to the patterns of cardiac

fibrosis observed. These models therefore represented different models for further *Runx* expression studies.

6.2.4 *Runx* and MI

This is the first study to examine changes in *Runx* expression in the heart using an animal model of MI. Present data on *Runx* in the heart was limited, even in the healthy non-diseased heart. *RUNX* expression in the diseased heart was also relatively unknown with studies that had investigated this unable to provide information on quantitative changes, disease progression alterations and in some cases precise cellular locations of the changes in expression in the heart was not available. This work has provided novel information on many of these areas in which previously knowledge was lacking. One of the first key findings was that *Runx* is present in control sham hearts therefore indicating a basal level of *Runx* in the healthy adult mouse heart. Furthermore *RUNX1* has been immunolocalised to cardiomyocytes as well as other cell types such as inflammatory cells and fibroblasts based on structural identification and observations from a qualified pathologist. To our knowledge this is the first study to show the presence of *RUNX1* in adult cardiomyocytes.

Key findings: The study findings have revealed that in hearts from mice post-MI there is a significant increase in the expression of all three *Runx* genes which was consistent with the finding from the human patient study, however work from the mouse model revealed that these changes were confined to the areas within and around the injury i.e. the infarct (all three *Runx* genes) and peri-infarct region (*Runx1* and *Runx3*) with no change in expression within regions remote from the infarct (namely the remote LV and RV). This was true at 4-wk after the initial insult. At 8-wk post-insult, expression levels of *Runx1* were not different to the observations at 4-wk with higher levels of *Runx1* in the infarct and peri-infarct; however with up-regulation in the remote LV region in addition which was not observed at 4-wk. Increased expression of *Runx* genes in the heart post-MI does not solely arise from cardiomyocytes, it is accepted that there are other cell types (such as fibroblasts and inflammatory cells as mentioned above) that are also contributing to the increased expression. It would be an important step to further dissect out the relative contributions from the cell types, which would be of particular relevance to potential altered functioning in cardiomyocytes. This could be done by a means of cell separation utilising filtration techniques or FACS methods on the digested infarcted heart.

Collectively however the results have identified spatial and temporal alterations of *Runx*

expression in the infarcted heart post-MI in a murine model warranting further investigation into the potential functional relevance of this.

Possible implications: These findings indicate that *Runx* expression is altered as a result of MI however the functional significance of this to the heart remains unclear. Data from this thesis have shown there are significant correlations between the level of *Runx* increase with extent of dysfunction in that hearts with the highest level of *Runx* show the greatest dysfunction (for *Runx1* and *Runx3*). However the main problem with interpreting this finding is that there may be potential influence from the infarct size; there is a positive correlation with degree of dysfunction and increasing infarct size and the levels of *Runx* are known to be highest in the infarct region – therefore it became difficult to ascertain whether the degree of dysfunction in the heart was as a result of infarct size or increased *Runx* expression. One thing that became evident was that when the influence from the infarct was removed the trends were the same. This was performed firstly by removing the contribution of *Runx* expression from the infarct from the analysis and the relationships were as before with the infarct included and secondly, in a separate disease model without an infarct the trend also remained further giving weight to a direct link with *Runx* and function. A direct link would be an exciting prospect in the field of cardiac medicine as it may indicate that *Runx* may be an important candidate for potential future biomarkers or a therapeutic target of heart disease. However it is important to emphasise that this area requires a greater deal of further investigation in identifying the precise links but may represent a crucial component for further work.

Further direction: In terms of the functional role of *Runx* in cardiomyocytes this remains at present relatively unknown. Studies have indicated that *Runx2* may contribute to fibrosis and calcification through Notch signalling in atherosclerotic hearts. It was originally hypothesised that RUNX may exhibit a similar role in cardiac muscle as had been shown in skeletal muscle on the basis that both muscle groups share similarities in structure and function and the triggering insult is very similar in the disturbances of electrical activity. Preliminary data from our laboratory has shown that over-expression of RUNX1 in rabbit cardiomyocytes led to significantly reduced Ca^{2+} transient amplitudes and prolonged decay of Ca^{2+} transients versus control cardiomyocytes. Based on these observations it would suggest that the increased expression of RUNX1 led to poorer contraction and impaired relaxation in the cardiomyocytes, which would indicate a detrimental rather than protective effect by RUNX1 meaning that the original point on similar protective features in cardiac muscle was disproved. Given the knowledge that

RUNX1 is an activator of the phospholamban gene in injured skeletal muscle, it is feasible that RUNX1 may regulate Pln in cardiac muscle. Pln is a key player in Ca^{2+} handling during EC coupling and an increased Pln would lead to the changes observed above which has been showed in Pln over-expressing mice. It is however not clear from the data alone that this is the case and this would require the use of transgenic mice and measurements of Pln expression in the RUNX-overexpressing cells, importantly phosphorylated and unphosphorylated states which is essential for making the link with the Ca^{2+} alterations observed.

6.2.5 *Runx* and hypertension/altered LV mass

RUNX1 levels were also assessed in a separate experimental animal model of cardiac disease, in rat strains of genetic hypertension and in strains of altered LV mass. In contrast to the results observed in MI, *Runx1* was down-regulated in the diseased animals in the rat models. Normotensive control WKY rats showed the highest levels of *Runx1* expression in the whole LV where the WKY-congenic and SHRSP-congenic showed significantly reduced levels of *Runx1* LV expression. The functional significance of this has also yet to be investigated. As with the MI model, a significant correlation was observed in with abundance of *Runx1* and level of dysfunction (higher *Runx1* in heart with greatest dysfunction) in this model.

6.2.6 Differences in *Runx* expression between the different models

By assessing how the behaviour of a single gene changes (in terms of its expression) in different cardiac diseases can provide a greater deal of information regarding the triggers for the gene of interest in CVD. The assessment of *Runx* expression in not just a different animal model of CVD i.e. hypertensive rat (SHRSP) but also in specific congenic substrains of this model to further dissect out the significance of *Runx* expression in CVD (in terms of a different phenotype) is highly advantageous and offers more insight into the behaviour of *Runx* in cardiac disease. Neither of the *Runx* genes are located on chromosome 14 therefore the effects on *Runx* expression are likely to be related to the resulting phenotype rather than the manipulations to chromosome 14.

6.3 Future directions

There are several directions for future work that have arisen from this work. (i) The first would be to further explore the functional relevance of altered *Runx* in the heart. This is of crucial importance to achieve a more complete understanding of the potential clinical relevance of *Runx* in the context of heart disease. The functional role of *Runx* in the heart could be addressed by further experimentation on RUNX over-expression in cardiomyocytes or by direct cardiac injection into the heart *in vivo*. It would be important to induce over-expression to similar levels observed that endogenous RUNX was up-regulated to within the disease model to allow for accurate comparisons.

(ii) Another route to further explore RUNX function in the heart would be through the use of a *Runx*-knockout model. Transgenic animals with a cardiac specific knockout (global knockouts of *Runx* would be embryonically fatal) could be assessed for any functional alterations in response to MI. This would involve inducing MI in these transgenic animals and assessing the effects on cardiac function as a result of this. Based on the observations from this thesis the hypothesis is that *Runx*-ablation would lead to a reduced extent of dysfunction post-MI given the preliminary data indicating that RUNX1 over-expression in cardiomyocytes led to greater dysfunction. The next stage from the functional investigation would be to investigate the mechanism of functional improvement. The links with phospholamban have been proposed but a greater deal of work would be needed to fully elucidate this. This could be investigated by assessing expression levels of phospholamban protein in its unphosphorylated and phosphorylated forms using specific antibodies sensitive to the two states in Western blots. Based on the possible link with increased *Runx1* leading to increased *Pln* gene expression and subsequent contractility impairment, it is hypothesised that an increase in Pln protein expression and a reduction in phosphorylated Pln would be observed in RUNX-overexpressing hearts which could contribute to the impairment in systolic function. With knowledge on altered expression, functional role and mechanistic actions this would offer a more completed picture of the clinical relevance of *Runx* in cardiac disease.

(iii) The 1-wk animals which developed a severe MI phenotype and were possibly showing early signs of CHF have shown interesting results in the level of remodelling but also in the levels of *Runx* expression. It is possible that *Runx* levels are greater in HF however this remains to be investigated fully. If it were possible to produce more animals

with this phenotype or extend the MI period to a point where animals entered into CHF it could further assist in the links with *Runx* up-regulation.

(iv) The problem with contaminating cells in the infarcted heart (such as fibroblasts and inflammatory infiltrate) poses problems in identifying the relative contribution from the cardiomyocytes which is relevant for functional implications in these cells. This could also be further assessed using rigorous separation techniques on the infarcted heart cells such as filtration or plating methods to allow gene expression measurements to be performed on pure populations of cardiomyocytes from the infarcted heart.

(v) There could also be future potential to assess *Runx* expression in more disease models such as alternative models of pressure-overload for example (e.g. transverse aortic constriction (TAC) models) and observe the comparisons with the pressure-overload models in this study. Disease models of myocarditis and further work on valvular disease could also be investigated, all giving a fuller picture for triggers of *Runx* expression during heart disease.

(vi) Another avenue to take with this work would be to try and identify the specific stimuli which trigger RUNX over-expression using experiments designed to provide specific conditions that may be possible triggers for example: *ex vivo* preparations (to assess changes independent of neurohormonal influence present *in vivo*) for example use of a Langendorff-perfused heart subjected to various conditions present in MI including: hypoxia (95% N₂/5% CO₂ incubation ± sodium cyanide (NaCN)), oxygen radical production (hydrogen peroxide, H₂O₂), deprivation of energy sources (ATP, glucose), acidosis and osmotic stressors. Furthermore a cultured papillary muscle preparation would allow insight into whether electrical stimulation of the heart influences RUNX1 expression as we can expose the muscle to pacing and non-pacing conditions. Furthermore, we can use cultured papillary muscles to examine the effects of cell necrosis on RUNX1 expression through a cryoinjury approach.

6.4 Final conclusion

Overall the work from this thesis has shown the value of using animal models in the ability to reproduce human heart disease and its many clinically relevant features for cardiac research, and has for the first time shown the relevance of the *Runx* genes in heart disease through use of such animal models. The experimental data shows that in response to MI in

a mouse model there is an up-regulation of *Runx* genes in the heart located predominantly within and around the areas of injury that can extend into remote regions as the MI progresses. In contrast to MI, in response to hypertension in rats and in genetically-altered sub-strains with altered LV mass there is a down-regulation of *Runx1*. In both models the same observation was evident that *Runx* expression correlated positively with deterioration of function. However, future work should aim to: (i) establish whether a direct link exists between *Runx* expression and level of dysfunction, and (ii) explore the functional and mechanistic roles of *Runx* in the heart. Such work would enable us to determine the potential therapeutic value of the *Runx* family in heart disease.

Appendix

Derivation of the $2^{-\Delta\Delta C_t}$ formula:

The derivation for this equation has been published in the *Applied Biosystems User Bulletin No. 2 (P/N 4303859)* (Applied Biosystems, 1997) and can be described as follows:

1. The exponential amplification of a PCR reaction can be described as:

$$X_n = X_0 \times (1 + E_x)^n$$

X_n	Number of target molecules at cycle number n
X_0	Initial number of target molecules
E_x	Efficiency of the amplification
n	Number of cycles

2. The C_t describes the cycle number at which the fluorescence reaches a fixed threshold, therefore (for target gene X and housekeeping gene H):

$$X_T = X_0 \times (1 + E_x)^{C_{T,X}} = K_x$$

X_T	Threshold number of target molecules
$C_{T,X}$	Threshold cycle for target amplification
K_x	Constant

$$H_T = H_0 \times (1 + E_H)^{C_{T,H}} = K_H$$

X_n	Threshold number of housekeeping molecules
X_0	Initial number of housekeeping molecules
E_x	Efficiency of housekeeping reaction
n	Threshold cycle for housekeeping amplification
K_H	Constant

3. To normalise to the housekeeping gene, the target gene (X_T) is divided by the housekeeping gene (H_T):

$$\frac{X_T}{H_T} = \frac{X_0 \times (1 + E_x)^{C_{T,x}}}{H_0 \times (1 + E_H)^{C_{T,H}}} = \frac{K_x}{K_H} \times K$$

X_N	X_0/R_0 normalised amount of target
ΔC_T	$C_{T,X} - C_{T,R}$ difference in threshold cycles for target and

As the $2^{-\Delta\Delta C_T}$ method assumes the same efficiency of the reaction between the target gene and the housekeeping gene, i.e. $E_x = E_H = E$, thus:

$$\frac{X_0}{H_0} \times (1 + E)^{C_{T,x} - C_{T,H}} = K \quad \text{or} \quad X_N \times (1 + E)^{\Delta C_T} = K \quad \text{or} \quad X_N = K \times (1 + E)^{-\Delta C_T}$$

$\Delta\Delta C_T$	$\Delta C_{T,X} - \Delta C_{T,R}$
--------------------	-----------------------------------

The last step is to divide the X_N for any sample Y by the calibrator CL (sample to which other samples are to be expressed relative to), i.e.

$$\frac{X_{N,Y} = K \times (1 + E)^{-\Delta C_{T,Y}}}{X_{N,CL} = K \times (1 + E)^{-\Delta C_{T,CL}}} = (1 + E)^{-\Delta\Delta C_T}$$

Since the efficiency is assumed to be close to 1, the final equation becomes $2^{-\Delta\Delta C_T}$.

References

- Runge MS, Patterson C (2006). *Principles of Molecular Medicine.*, 2nd ed. Humana Press, New Jersey.
- Adams TD, Yanowitz FG, Fisher AG, Ridges JD, Nelson AG, Hagan AD, Williams RR, & Hunt SC (1985). Heritability of cardiac size: an echocardiographic and electrocardiographic study of monozygotic and dizygotic twins. *Circulation* **71**, 39-44.
- Adya N, Stacy T, Speck NA, & Liu PP (1998). The leukemic protein core binding factor beta (CBFbeta)-smooth-muscle myosin heavy chain sequesters CBFalpha2 into cytoskeletal filaments and aggregates. *Mol Cell Biol* **18**, 7432-7443.
- Aihara Y, Kurabayashi M, Saito Y, Ohyama Y, Tanaka T, Takeda S, Tomaru K, Sekiguchi K, Arai M, Nakamura T, & Nagai R (2000). Cardiac ankyrin repeat protein is a novel marker of cardiac hypertrophy: role of M-CAT element within the promoter. *Hypertension* **36**, 48-53.
- Akazawa H & Komuro I (2003). Roles of cardiac transcription factors in cardiac hypertrophy. *Circ Res* **92**, 1079-1088.
- Aljaroudi W, Alraies MC, Halley C, Rodriguez L, Grimm RA, Thomas JD, & Jaber WA (2012). Impact of progression of diastolic dysfunction on mortality in patients with normal ejection fraction. *Circulation* **125**, 782-788.
- Allender S, Peto V, Scarborough P, & Raynor M (2006). British Heart Foundation statistics database: coronary heart disease statistics. London, British Heart Foundation.
- Alliston T, Choy L, Ducy P, Karsenty G, & Derynck R (2001). TGF-beta-induced repression of CBFA1 by Smad3 decreases cbfa1 and osteocalcin expression and inhibits osteoblast differentiation. *EMBO J* **20**, 2254-2272.
- Amann K, Gharehbaghi H, Stephen S, & Mall G (1995). Hypertrophy and hyperplasia of smooth muscle cells of small intramyocardial arteries in spontaneously hypertensive rats. *Hypertension* **25**, 124-131.
- Ambler SK, Hodges YK, Jones GM, Long CS, & Horwitz LD (2008). Prolonged administration of a dithiol antioxidant protects against ventricular remodeling due to ischemia-reperfusion in mice. *Am J Physiol Heart Circ Physiol* **295**, H1303-H1310.
- Anderson PA, Malouf NN, Oakeley AE, Pagani ED, & Allen PD (1992). Troponin T isoform expression in the normal and failing human left ventricle: a correlation with myofibrillar ATPase activity. *Basic Res Cardiol* **87 Suppl 1**, 117-127.
- Anversa P, Beghi C, Kikkawa Y, & Olivetti G (1986a). Myocardial infarction in rats. Infarct size, myocyte hypertrophy, and capillary growth. *Circ Res* **58**, 26-37.
- Anversa P, Palackal T, Sonnenblick EH, Olivetti G, Meggs LG, & Capasso JM (1990). Myocyte cell loss and myocyte cellular hyperplasia in the hypertrophied aging rat heart. *Circ Res* **67**, 871-885.
- Applied Biosystems. User Bulletin No. 2. 1997.
- Arai M, Alpert NR, MacLennan DH, Barton P, & Periasamy M (1993). Alterations in sarcoplasmic reticulum gene expression in human heart failure. A possible mechanism for alterations in systolic and diastolic properties of the failing myocardium. *Circ Res* **72**, 463-469.
- Aronson BD, Fisher AL, Blechman K, Caudy M, & Gergen JP (1997). Groucho-dependent and -independent repression activities of Runt domain proteins. *Mol Cell Biol* **17**, 5581-5587.

- Aurigemma GP, Silver KH, Priest MA, & Gaasch WH (1995). Geometric changes allow normal ejection fraction despite depressed myocardial shortening in hypertensive left ventricular hypertrophy. *J Am Coll Cardiol* **26**, 195-202.
- Ayoubi TA & Van De Ven WJ (1996). Regulation of gene expression by alternative promoters. *FASEB J* **10**, 453-460.
- Baan J, van der Velde ET, de Bruin HG, Smeenk GJ, Koops J, van Dijk AD, Temmerman D, Senden J, & Buis B (1984). Continuous measurement of left ventricular volume in animals and humans by conductance catheter. *Circulation* **70**, 812-823.
- Bae NS, Swanson MJ, Vassilev A, & Howard BH (2004). Human histone deacetylase SIRT2 interacts with the homeobox transcription factor HOXA10. *J Biochem* **135**, 695-700.
- Bae SC & Ito Y (1999). Regulation mechanisms for the heterodimeric transcription factor, PEBP2/CBF. *Histol Histopathol* **14**, 1213-1221.
- Bangsow C, Rubins N, Glusman G, Bernstein Y, Negreanu V, Goldenberg D, Lotem J, Ben-Asher E, Lancet D, Levanon D, & Groner Y (2001). The RUNX3 gene--sequence, structure and regulated expression. *Gene* **279**, 221-232.
- Bartlett JM & Stirling D (2003). A short history of the polymerase chain reaction. *Methods Mol Biol* **226**, 3-6.
- Bartosova D, Chvapil M, Korecky B, Poupa O, Rakusan K, Turek Z, & Vizek M (1969). The growth of the muscular and collagenous parts of the rat heart in various forms of cardiomegaly. *J Physiol* **200**, 285-295.
- Bassani JW, Bassani RA, & Bers DM (1994). Relaxation in rabbit and rat cardiac cells: species-dependent differences in cellular mechanisms. *J Physiol* **476**, 279-293.
- Bayat H, Swaney JS, Ander AN, Dalton N, Kennedy BP, Hammond HK, & Roth DM (2002). Progressive heart failure after myocardial infarction in mice. *Basic Research in Cardiology* **97**, 206-213.
- Beltrami CA, Finato N, Rocco M, Feruglio GA, Puricelli C, Cigola E, Quaini F, Sonnenblick EH, Olivetti G, & Anversa P (1994). Structural basis of end-stage failure in ischemic cardiomyopathy in humans. *Circulation* **89**, 151-163.
- Berardi MJ, Sun C, Zehr M, Abildgaard F, Peng J, Speck NA, & Bushweller JH (1999). The Ig fold of the core binding factor alpha Runt domain is a member of a family of structurally and functionally related Ig-fold DNA-binding domains. *Structure* **7**, 1247-1256.
- Bers DM (2002). Cardiac excitation-contraction coupling. *Nature* **415**, 198-205.
- Bers DM & Perez-Reyes E (1999). Ca channels in cardiac myocytes: structure and function in Ca influx and intracellular Ca release. *Cardiovasc Res* **42**, 339-360.
- Bers DM & Stiffel VM (1993). Ratio of ryanodine to dihydropyridine receptors in cardiac and skeletal muscle and implications for E-C coupling. *Am J Physiol* **264**, C1587-C1593.
- Beuckelmann DJ, Nabauer M, & Erdmann E (1992). Intracellular calcium handling in isolated ventricular myocytes from patients with terminal heart failure. *Circulation* **85**, 1046-1055.
- Bhavsar PK, Dellow KA, Yacoub MH, Brand NJ, & Barton PJ (2000). Identification of cis-acting DNA elements required for expression of the human cardiac troponin I gene promoter. *J Mol Cell Cardiol* **32**, 95-108.

- Bialik S, Geenen DL, Sasson IE, Cheng R, Horner JW, Evans SM, Lord EM, Koch CJ, & Kitsis RN (1997). Myocyte apoptosis during acute myocardial infarction in the mouse localizes to hypoxic regions but occurs independently of p53. *J Clin Invest* **100**, 1363-1372.
- Black BL & Olson EN (1998). Transcriptional control of muscle development by myocyte enhancer factor-2 (MEF2) proteins. *Annu Rev Cell Dev Biol* **14**, 167-196.
- Blaustein MP, Hamlyn JM, & Pallone TL (2007). Sodium pumps: ouabain, ion transport, and signaling in hypertension. *Am J Physiol Renal Physiol* **293**, F438.
- Blaustein MP & Lederer WJ (1999). Sodium/calcium exchange: its physiological implications. *Physiol Rev* **79**, 763-854.
- Blaustein MP, Zhang J, Chen L, & Hamilton BP (2006). How does salt retention raise blood pressure? *Am J Physiol Regul Integr Comp Physiol* **290**, R514-R523.
- Blyth K, Cameron ER, & Neil JC (2005). The RUNX genes: gain or loss of function in cancer. *Nat Rev Cancer* **5**, 376-387.
- Bogousslavsky J (2003). Frontal lobe dysfunction in cerebrovascular disease. *Schweiz Arch Neurol Psychiatr* **59-65**.
- Bogun F, Crawford T, Chalfoun N, Kuhne M, Sarrazin JF, Wells D, Good E, Jongnarangsin K, Oral H, Chugh A, Pelosi F, & Morady F (2008). Relationship of frequent postinfarction premature ventricular complexes to the reentry circuit of scar-related ventricular tachycardia. *Heart Rhythm* **5**, 367-374.
- Bonvini RF, Hendiri T, & Camenzind E (2005). Inflammatory response post-myocardial infarction and reperfusion: a new therapeutic target? *Eur Heart J Suppl* **7**, 127-136.
- Brattelid T, Winer LH, Levy FO, Liestol K, Sejersted OM, & Andersson KB (2010). Reference gene alternatives to Gapdh in rodent and human heart failure gene expression studies. *BMC Mol Biol* **11**, 22.
- Brener SJ & Tschopp D (2009). Complications of Acute Myocardial Infarction. Disease Management Project: Cardiology. Cleveland, OH.
- Brilla CG, Janicki JS, & Weber KT (1991a). Cardioreparative effects of lisinopril in rats with genetic hypertension and left ventricular hypertrophy. *Circulation* **83**, 1771-1779.
- Brilla CG, Janicki JS, & Weber KT (1991b). Impaired diastolic function and coronary reserve in genetic hypertension. Role of interstitial fibrosis and medial thickening of intramyocardial coronary arteries. *Circ Res* **69**, 107-115.
- Brilla CG, Janicki JS, & Weber KT (1991c). Impaired diastolic function and coronary reserve in genetic hypertension. Role of interstitial fibrosis and medial thickening of intramyocardial coronary arteries. *Circ Res* **69**, 107-115.
- Brilla CG, Pick R, Tan LB, Janicki JS, & Weber KT (1990). Remodeling of the rat right and left ventricles in experimental hypertension. *Circ Res* **67**, 1355-1364.
- British Heart Foundation. Coronary Heart Disease Statistics 2010.
- Brivanou AH & Darnell JE (2002). Signal transduction and the control of gene expression. *Science* **295**, 813-818.
- Bruneau BG (2002). Transcriptional regulation of vertebrate cardiac morphogenesis. *Circ Res* **90**, 509-519.

- Bruneau BG, Nemer G, Schmitt JP, Charron F, Robitaille L, Caron S, Conner DA, Gessler M, Nemer M, Seidman CE, & Seidman JG (2001). A murine model of Holt-Oram syndrome defines roles of the T-box transcription factor Tbx5 in cardiogenesis and disease. *Cell* **106**, 709-721.
- Buda AJ, Zotz RJ, & Gallagher KP (1986). Characterization of the functional border zone around regionally ischemic myocardium using circumferential flow-function maps. *J Am Coll Cardiol* **8**, 150-158.
- Buermans HPJ, Redout EM, Schiel AE, Musters RJP, Zuidwijk M, Eijk PP, van Hardeveld C, Kasanmoentalib S, Visser FC, Ylstra B, & Simonides WS (2005). Microarray analysis reveals pivotal divergent mRNA expression profiles early in the development of either compensated ventricular hypertrophy or heart failure. *Physiological Genomics* **21**, 314-323.
- Burkhoff D, Mirsky I, & Suga H (2005). Assessment of systolic and diastolic ventricular properties via pressure-volume analysis: a guide for clinical, translational, and basic researchers. *Am J Physiol Heart Circ Physiol* **289**, H501-H512.
- Burlew BS & Weber KT (2002). Cardiac fibrosis as a cause of diastolic dysfunction. *Herz* **27**, 92-98.
- Burns CE, Traver D, Mayhall E, Shepard JL, & Zon LI (2005a). Hematopoietic stem cell fate is established by the Notch-Runx pathway. *Genes Dev* **19**, 2331-2342.
- Burns MJ, Nixon GJ, Foy CA, & Harris N (2005b). Standardisation of data from real-time quantitative PCR methods - evaluation of outliers and comparison of calibration curves. *BMC Biotechnol* **5**, 31.
- Cai Z, de BM, Ma X, Dortland B, Luteijn T, Downing RJ, & Dzierzak E (2000). Haploinsufficiency of AML1 affects the temporal and spatial generation of hematopoietic stem cells in the mouse embryo. *Immunity* **13**, 423-431.
- Carlsson P & Mahlapuu M (2002). Forkhead transcription factors: key players in development and metabolism. *Dev Biol* **250**, 1-23.
- Caroni P & Carafoli E (1981). The Ca²⁺-pumping ATPase of heart sarcolemma. Characterization, calmodulin dependence, and partial purification. *J Biol Chem* **256**, 3263-3270.
- Carretero OA & Oparil S (2000). Essential hypertension. Part I: definition and etiology. *Circulation* **101**, 329-335.
- Chen CY & Schwartz RJ (1995). Identification of novel DNA binding targets and regulatory domains of a murine tinman homeodomain factor, nkx-2.5. *J Biol Chem* **270**, 15628-15633.
- Chen CY & Schwartz RJ (1996). Recruitment of the tinman homolog Nkx-2.5 by serum response factor activates cardiac alpha-actin gene transcription. *Mol Cell Biol* **16**, 6372-6384.
- Chen H, Higashino H, Maeda K, Zhang Z, Ohta Y, Wang Z, Su DF, & Yuan WJ (2001). Reduction of cardiac norepinephrine improves postischemic heart function in stroke-prone spontaneously hypertensive rats. *J Cardiovasc Pharmacol* **38**, 821-832.
- Chen X, Piacentino V, III, Furukawa S, Goldman B, Margulies KB, & Houser SR (2002). L-type Ca²⁺ channel density and regulation are altered in failing human ventricular myocytes and recover after support with mechanical assist devices. *Circ Res* **91**, 517-524.
- Chien KR & Olsen EN (2002). Converging pathways and principles in heart development and disease. *Cell* **110**, 153-162.

Chiong M, Wang ZV, Pedrozo Z, Cao DJ, Troncoso R, Ibacache M, Criollo A, Nemchenko A, Hill JA, & Lavandro S (2011). Cardiomyocyte death: mechanisms and translational implications. *Cell Death Dis* **2**, e244.

Choi JY, Pratap J, Javed A, Zaidi SK, Xing L, Balint E, Dalamangas S, Boyce B, van Wijnen AJ, Lian JB, Stein JL, Jones SN, & Stein GS (2001). Subnuclear targeting of Runx/Cbfa/AML factors is essential for tissue-specific differentiation during embryonic development. *Proc Natl Acad Sci U S A* **98**, 8650-8655.

Christensen Geal (1997). Physiological assessment of complex cardiac phenotypes in genetically engineered mice. *Am J Physiol Heart Circ Physiol* 1351-1360.

Chu G, Haghghi K, & Kranias EG (2002). From mouse to man: understanding heart failure through genetically altered mouse models. *J Card Fail* **8**, S432-S449.

Chu G & Kranias EG (2006). Phospholamban as a therapeutic modality in heart failure. *Novartis Found Symp* **274**, 156-171.

Cingolani OH, Yang XP, Cavasin MA, & Carretero OA (2003). Increased systolic performance with diastolic dysfunction in adult spontaneously hypertensive rats. *Hypertension* **41**, 249-254.

Ciulla MM, Paliotti R, Ferrero S, Braidotti P, Esposito A, Gianelli U, Busca G, Cioffi U, Bulfamante G, & Magrini F (2004). Left ventricular remodeling after experimental myocardial cryoinjury in rats. *J Surg Res* **116**, 91-97.

Clark JS, Jeffs B, Davidson AO, Lee WK, Anderson NH, Bihoreau MT, Brosnan MJ, Devlin AM, Kelman AW, Lindpaintner K, & Dominiczak AF (1996). Quantitative trait loci in genetically hypertensive rats. Possible sex specificity. *Hypertension* **28**, 898-906.

Coffman JA (2003). Runx transcription factors and the developmental balance between cell proliferation and differentiation. *Cell Biol Int* **27**, 315-324.

Cohen BM & Hasselbring B (2007). *Coronary Heart Disease: a guide to diagnosis and treatment*. Addicus Books.

Cohn JN (1998). Arteries, myocardium, blood pressure and cardiovascular risk: towards a revised definition of hypertension. *J Hypertens* **16**, 2117-2124.

Cohn JN, Ferrari R, & Sharpe N (2000). Cardiac remodeling--concepts and clinical implications: a consensus paper from an international forum on cardiac remodeling. Behalf of an International Forum on Cardiac Remodeling. *J Am Coll Cardiol* **35**, 569-582.

Colucci WS (1997). Molecular and cellular mechanisms of myocardial failure. *American Journal of Cardiology* **80**, L15-L25.

Colucci WS & Braunwald E (2001). *Heart Disease*, pp. 503-528. Philadelphia.

Conrad CH, Brooks WW, Robinson KG, & Bing OH (1991). Impaired myocardial function in spontaneously hypertensive rats with heart failure. *Am J Physiol* **260**, H136-H145.

Conzen PF, Vollmar B, Habazettl H, Frink EJ, Peter K, & Messmer K (1992). Systemic and regional hemodynamics of isoflurane and sevoflurane in rats. *Anesth Analg* **74**, 79-88.

Costandi PN, Frank LR, McCulloch AD, & Omens JH (2006). Role of diastolic properties in the transition to failure in a mouse model of the cardiac dilatation. *Am J Physiol Heart Circ Physiol* **291**, H2971-H2979.

- Crute BE, Lewis AF, Wu Z, Bushweller JH, & Speck NA (1996). Biochemical and biophysical properties of the core-binding factor alpha2 (AML1) DNA-binding domain. *J Biol Chem* **271**, 26251-26260.
- Custodio MR, Koike MK, Neves KR, Dos Reis LM, Gracioli FG, Neves CL, Batista DG, Magalhaes AO, Hawlitschek P, Oliveira IB, Dominguez WV, Moyses RM, & Jorgetti V (2012). Parathyroid hormone and phosphorus overload in uremia: impact on cardiovascular system. *Nephrol Dial Transplant* **27**, 1437-1445.
- Dahl LK, Heine M, & Tassinari L (1962). Role of genetic factors in susceptibility to experimental hypertension due to chronic excess salt ingestion. *Nature* **194**, 480-482.
- Daniels SD, Meyer RA, & Loggie JM (1990). Determinants of cardiac involvement in children and adolescents with essential hypertension. *Circulation* **82**, 1243-1248.
- Davidson AO, Schork N, Jaques BC, Kelman AW, Sutcliffe RG, Reid JL, & Dominiczak AF (1995). Blood pressure in genetically hypertensive rats. Influence of the Y chromosome. *Hypertension* **26**, 452-459.
- de Zwaan C, Daemen MJ, & Hermens WT (2001). Mechanisms of cell death in acute myocardial infarction: pathophysiological implications for treatment. *Neth Heart J* **9**, 30-44.
- de SG, Verdecchia P, Pede S, Gorini M, & Maggioni AP (2002a). Prognosis of inappropriate left ventricular mass in hypertension: the MAVI Study. *Hypertension* **40**, 470-476.
- de SG, Verdecchia P, Pede S, Gorini M, & Maggioni AP (2002b). Prognosis of inappropriate left ventricular mass in hypertension: the MAVI Study. *Hypertension* **40**, 470-476.
- del M, Harding SE, Schmidt U, Matsui T, Kang ZB, Dec GW, Gwathmey JK, Rosenzweig A, & Hajjar RJ (1999). Restoration of contractile function in isolated cardiomyocytes from failing human hearts by gene transfer of SERCA2a. *Circulation* **100**, 2308-2311.
- Deng AY, Dene H, Pravenec M, & Rapp JP (1994). Genetic mapping of two new blood pressure quantitative trait loci in the rat by genotyping endothelin system genes. *J Clin Invest* **93**, 2701-2709.
- Devereux RB, Alonso DR, Lutas EM, Gottlieb GJ, Campo E, Sachs I, & Reichek N (1986). Echocardiographic assessment of left ventricular hypertrophy: comparison to necropsy findings. *Am J Cardiol* **57**, 450-458.
- Devereux RB, de SG, Ganau A, & Roman MJ (1994a). Left ventricular hypertrophy and geometric remodeling in hypertension: stimuli, functional consequences and prognostic implications. *J Hypertens Suppl* **12**, S117-S127.
- Devereux RB, de SG, Ganau A, & Roman MJ (1994b). Left ventricular hypertrophy and geometric remodeling in hypertension: stimuli, functional consequences and prognostic implications. *J Hypertens Suppl* **12**, S117-S127.
- Dewald O, Zymek P, Winkelmann K, Koerting A, Ren G, Abou-Khamis T, Michael LH, Rollins BJ, Entman ML, & Frangogiannis NG (2005). CCL2/Monocyte Chemoattractant Protein-1 regulates inflammatory responses critical to healing myocardial infarcts. *Circ Res* **96**, 881-889.
- Diamond G & Forrester JS (1972). Effect of coronary artery disease and acute myocardial infarction on left ventricular compliance in man. *Circulation* **45**, 11-19.
- Dickinson HO, Mason JM, Nicolson DJ, Campbell F, Beyer FR, Cook JV, Williams B, & Ford GA (2006). Lifestyle interventions to reduce raised blood pressure: a systematic review of randomized controlled trials. *J Hypertens* **24**, 215-233.

- Dixon JA & Spinale FG (2009). Large animal models of heart failure: a critical link in the translation of basic science to clinical practice. *Circ Heart Fail* **2**, 262-271.
- Dodd DA, Atkinson JB, Olson RD, Buck S, Cusack BJ, Fleischer S, & Boucek RJ, Jr. (1993). Doxorubicin cardiomyopathy is associated with a decrease in calcium release channel of the sarcoplasmic reticulum in a chronic rabbit model. *J Clin Invest* **91**, 1697-1705.
- Doggrell SA & Brown L (1998a). Rat models of hypertension, cardiac hypertrophy and failure. *Cardiovasc Res* **39**, 89-105.
- Doggrell SA & Brown L (1998b). Rat models of hypertension, cardiac hypertrophy and failure. *Cardiovasc Res* **39**, 89-105.
- Dominiczak AF, McLaren Y, Kusel JR, Ball DL, Goodfriend TL, Bohr DF, & Reid JL (1993). Lateral diffusion and fatty acid composition in vascular smooth muscle membrane from stroke-prone spontaneously hypertensive rats. *Am J Hypertens* **6**, 1003-1008.
- Doris PA & Fornage M (2005). The transcribed genome and the heritable basis of essential hypertension. *Cardiovasc Toxicol* **5**, 95-108.
- Drissi H, Luc Q, Shakoori R, Chuva De Sousa LS, Choi JY, Terry A, Hu M, Jones S, Neil JC, Lian JB, Stein JL, van Wijnen AJ, & Stein GS (2000). Transcriptional autoregulation of the bone related CBFA1/RUNX2 gene. *J Cell Physiol* **184**, 341-350.
- Ducy P (2000). Cbfa1: a molecular switch in osteoblast biology. *Dev Dyn* **219**, 461-471.
- Duerr GD, Elhafi N, Bostani T, Ellinger J, Swieny L, Kolobara E, Welz A, & Dewald O (2011). Comparison of myocardial remodeling between cryoinfarction and reperfused infarction in mice. *J Biomed Biotechnol* **2011**, 961298.
- Durst KL & Hiebert SW (2004). Role of RUNX family members in transcriptional repression and gene silencing. *Oncogene* **23**, 4220-4224.
- Edelman GM (1986). Cell adhesion molecules in neural histogenesis. *Annu Rev Physiol* **48**, 417-430.
- Egger M & Niggli E (2000). Paradoxical block of the Na⁺-Ca²⁺ exchanger by extracellular protons in guinea-pig ventricular myocytes. *J Physiol* **523 Pt 2**, 353-366.
- Ehrlich M (2003). Expression of various genes is controlled by DNA methylation during mammalian development. *J Cell Biochem* **88**, 899-910.
- Eising GPeal (1994). Force-frequency relations during heart failure in pigs. *Am J Physiol* **267**, H2516-H2522.
- Eisner DA, Trafford AW, Diaz ME, Overend CL, & O'Neill SC (1998). The control of Ca release from the cardiac sarcoplasmic reticulum: regulation versus autoregulation. *Cardiovasc Res* **38**, 589-604.
- Elliott EB, Kelly A, Smith GL, & Loughrey CM (2012). Isolated rabbit working heart function during progressive inhibition of myocardial SERCA activity. *Circ Res* **110**, 1618-1627.
- Ellison GM, Waring CD, Vicinanza C, & Torella D (2012). Physiological cardiac remodelling in response to endurance exercise training: cellular and molecular mechanisms. *Heart* **98**, 5-10.
- Elsevier. Genetic Nomenclature Guide. Trends in Genetics (1998). Cambridge, U.K., Elsevier Science Ltd.

- Elsherif L, Huang MS, Shai SY, Yang Y, Li RY, Chun J, Mekany MA, Chu AL, Kaufman SJ, & Ross RS (2008). Combined deficiency of dystrophin and beta1 integrin in the cardiac myocyte causes myocardial dysfunction, fibrosis and calcification. *Circ Res* **102**, 1109-1117.
- Erbel R & Heusch G (2000). Coronary microembolization. *J Am Coll Cardiol* **36**, 22-24.
- Everaert BR, Boulet GA, Timmermans JP, & Vrints CJ (2011). Importance of suitable reference gene selection for quantitative real-time PCR: special reference to mouse myocardial infarction studies. *PLoS One* **6**, e23793.
- Fabiato A (1983). Calcium-induced release of calcium from the cardiac sarcoplasmic reticulum. *Am J Physiol* **245**, C1-14.
- Fabiato A (1985). Time and calcium dependence of activation and inactivation of calcium-induced release of calcium from the sarcoplasmic reticulum of a skinned canine cardiac Purkinje cell. *J Gen Physiol* **85**, 247-289.
- Fabiato A & Fabiato F (1975). Contractions induced by a calcium-triggered release of calcium from the sarcoplasmic reticulum of single skinned cardiac cells. *J Physiol* **249**, 469-495.
- Fainaru O, Woolf E, Lotem J, Yarmus M, Brenner O, Goldenberg D, Negreanu V, Bernstein Y, Levanon D, Jung S, & Groner Y (2004). Runx3 regulates mouse TGF-beta-mediated dendritic cell function and its absence results in airway inflammation. *EMBO J* **23**, 969-979.
- Fang L, Gao XM, Moore XL, Kiriazis H, Su Y, Ming Z, Lim YL, Dart AM, & Du XJ (2007a). Differences in inflammation, MMP activation and collagen damage account for gender difference in murine cardiac rupture following myocardial infarction. *J Mol Cell Cardiol* **43**, 535-544.
- Fang L, Moore XL, Gao XM, Dart AM, Lim YL, & Du XJ (2007b). Down-regulation of mitofusin-2 expression in cardiac hypertrophy in vitro and in vivo. *Life Sci* **80**, 2154-2160.
- Ferdinandy P, Schulz R, & Baxter GF (2007). Interaction of cardiovascular risk factors with myocardial ischemia/reperfusion injury, preconditioning, and postconditioning. *Pharmacol Rev* **59**, 418-458.
- Fernandez B, Duran AC, Fernandez MC, Fernandez-Gallego T, Icardo JM, & Sans-Coma V (2008). The coronary arteries of the C57BL/6 mouse strains: implications for comparison with mutant models. *J Anat* **212**, 12-18.
- Finsen AV, Woldbaek PR, Li J, Wu J, Lyberg T, Tonnessen T, & Christensen G (2004). Increased syndecan expression following myocardial infarction indicates a role in cardiac remodeling. *Physiol Genomics* **16**, 301-308.
- Fischer M, Baessler A, Hense HW, Hengstenberg C, Muscholl M, Holmer S, Doring A, Broeckel U, Riegger G, & Schunkert H (2003). Prevalence of left ventricular diastolic dysfunction in the community. Results from a Doppler echocardiographic-based survey of a population sample. *Eur Heart J* **24**, 320-328.
- Flaim SF, Weitzel RL, & Zelis R (1981). Mechanism of Action of Nitroglycerin During Exercise in A Rat Model of Heart-Failure - Improvement of Blood-Flow to the Renal, Splanchnic, and Cutaneous Beds. *Circulation Research* **49**, 458-468.
- Fleige S & Pfaffl MW (2006). RNA integrity and the effect on the real-time qRT-PCR performance. *Mol Aspects Med* **27**, 126-139.
- Fomovsky GM & Holmes JW (2010). Evolution of scar structure, mechanics, and ventricular function after myocardial infarction in the rat. *Am J Physiol Heart Circ Physiol* **298**, H221-H228.

- Foote, KK & Loughrey CM (2010). A comparison of left ventricular pressure-volume measurements in adult rats using three different techniques. *J Physiol Proc Physiol Soc* **19**, PC22.
- Forrester JS, Diamond G, Parmley WW, & Swan HJ (1972). Early increase in left ventricular compliance after myocardial infarction. *J Clin Invest* **51**, 598-603.
- Fox JG (2007). *The mouse in biomedical research.*, 2nd ed. Academic Press.
- Frangogiannis NG (2010). Syndecan-1: a critical mediator in cardiac fibrosis. *Hypertension* **55**, 233-235.
- Frangogiannis NG, Ren G, Dewald O, Zymek P, Haudek S, Koerting A, Winkelmann K, Michael LH, Lawler J, & Entman ML (2005). Critical role of endogenous thrombospondin-1 in preventing expansion of healing myocardial infarcts. *Circulation* **111**, 2935-2942.
- Frangogiannis NG, Shimoni S, Chang SM, Ren G, Dewald O, Gersch C, Shan K, Aggeli C, Reardon M, Letsou GV, Espada R, Ramchandani M, Entman ML, & Zoghbi WA (2002a). Active interstitial remodeling: an important process in the hibernating human myocardium. *J Am Coll Cardiol* **39**, 1468-1474.
- Frangogiannis NG, Shimoni S, Chang SM, Ren G, Shan K, Aggeli C, Reardon MJ, Letsou GV, Espada R, Ramchandani M, Entman ML, & Zoghbi WA (2002b). Evidence for an active inflammatory process in the hibernating human myocardium. *Am J Pathol* **160**, 1425-1433.
- Frangogiannis NG, Smith CW, & Entman ML (2002c). The inflammatory response in myocardial infarction. *Cardiovasc Res* **53**, 31-47.
- Frantz SA, Kaiser M, Gardiner SM, Gauguier D, Vincent M, Thompson JR, Bennett T, & Samani NJ (1998). Successful isolation of a rat chromosome 1 blood pressure quantitative trait locus in reciprocal congenic strains. *Hypertension* **32**, 639-646.
- Franzini-Armstrong C (1970). Studies of the Triad: I. Structure of the Junction in Frog Twitch Fibers. *J Cell Biol* **47**, 488-499.
- French BA & Kramer CM (2007). Mechanisms of Post-Infarct Left Ventricular Remodeling. *Drug Discov Today Dis Mech* **4**, 185-196.
- Frey N & Olson EN (2003). Cardiac hypertrophy: the good, the bad, and the ugly. *Annu Rev Physiol* **65**, 45-79.
- Fu Y, Chang AC, Fournier M, Chang L, Niessen K, & Karsan A (2011). RUNX3 maintains the mesenchymal phenotype after termination of the Notch signal. *J Biol Chem* **286**, 11803-11813.
- Fujioka Y, Komeda M, & Matsuoka S (2000). Stoichiometry of Na⁺-Ca²⁺ exchange in inside-out patches excised from guinea-pig ventricular myocytes. *J Physiol* **523 Pt 2**, 339-351.
- Gajarsa JJ & Kloner RA (2011). Left ventricular remodeling in the post-infarction heart: a review of cellular, molecular mechanisms, and therapeutic modalities. *Heart Fail Rev* **16**, 13-21.
- Gao E, Lei YH, Shang X, Huang ZM, Zuo L, Boucher M, Fan Q, Chuprun JK, Ma XL, & Koch WJ (2010a). A novel and efficient model of coronary artery ligation and myocardial infarction in the mouse. *Circ Res* **107**, 1445-1453.
- Gao XM, Dart AM, Dewar E, Jennings G, & Du XJ (2000). Serial echocardiographic assessment of left ventricular dimensions and function after myocardial infarction in mice. *Cardiovasc Res* **45**, 330-338.

Gao XM, Dilley RJ, Samuel CS, Percy E, Fullerton MJ, Dart AM, & Du XJ (2002). Lower risk of postinfarct rupture in mouse heart overexpressing beta(2)-adrenergic receptors: Importance of collagen content. *Journal of Cardiovascular Pharmacology* **40**, 632-640.

Gao XM, Ming ZQ, Su YD, Fang L, Kiriazis H, Xu Q, Dart AM, & Du XJ (2010b). Infarct size and post-infarct inflammation determine the risk of cardiac rupture in mice. *International Journal of Cardiology* **143**, 20-28.

Gao XM (2005). Mouse model of post-infarct ventricular rupture: time course, strain- and gender-dependency, tensile strength, and histopathology. *Cardiovasc Res* **65**, 469-477.

Garg V, Muth AN, Ransom JF, Schluterman MK, Barnes R, King IN, Grossfeld PD, & Srivastava D (2005). Mutations in NOTCH1 cause aortic valve disease. *Nature* **437**, 270-274.

Garrett MR, Dene H, Walder R, Zhang QY, Cicila GT, Assadnia S, Deng AY, & Rapp JP (1998). Genome scan and congenic strains for blood pressure QTL using Dahl salt-sensitive rats. *Genome Res* **8**, 711-723.

Gattenlohner S, Waller C, Ertl G, Bultmann BD, Muller-Hermelink HK, & Marx A (2003). NCAM(CD56) and RUNX1(AML1) are up-regulated in human ischemic cardiomyopathy and a rat model of chronic cardiac ischemia. *American Journal of Pathology* **163**, 1081-1090.

Gattenloner S, Waller C, Ertl G, Bultmann BD, Muller-Hermelink HK, & Marx A (2004). [The overexpression of NCAM (CD56) in human hearts is specific for ischemic damage]. *Verh Dtsch Ges Pathol* **88**, 246-251.

Gavazzi A, De MR, Renosto G, Moro A, Borgia M, Caroli A, Castelli G, Ciaccheri M, Pavan D, De VC, & . (1993). The spectrum of left ventricular size in dilated cardiomyopathy: clinical correlates and prognostic implications. SPIC (Italian Multicenter Cardiomyopathy Study) Group. *Am Heart J* **125**, 410-422.

Gehrmann J, Frantz S, Maguire CT, Vargas M, Ducharme A, Wakimoto H, Lee RT, & Berul CI (2001). Electrophysiological characterization of murine myocardial ischemia and infarction. *Basic Res Cardiol* **96**, 237-250.

Gelpi RJ, Pasipoularides A, Lader AS, Patrick TA, Chase N, Hittinger L, Shannon RP, Bishop SP, & Vatner SF (1991). Changes in diastolic cardiac function in developing and stable perinephritic hypertension in conscious dogs. *Circ Res* **68**, 555-567.

Georgakopoulos D, Mitzner WA, Chen CH, Byrne BJ, Millar HD, Hare JM, & Kass DA (1998). In vivo murine left ventricular pressure-volume relations by miniaturized conductance micromanometry. *Am J Physiol* **274**, H1416-H1422.

Gerdes AM & Capasso JM (1995). Structural remodeling and mechanical dysfunction of cardiac myocytes in heart failure. *J Mol Cell Cardiol* **27**, 849-856.

Gerety M & Watanabe M (1997). Polysialylated NCAM expression on endocardial cells of the chick primary atrial septum. *Anat Rec* **247**, 71-84.

Gergen JP & Butler BA (1988). Isolation of the Drosophila segmentation gene runt and analysis of its expression during embryogenesis. *Genes Dev* **2**, 1179-1193.

Gheorghide M & Bonow RO (1998). Chronic heart failure in the United States: a manifestation of coronary artery disease. *Circulation* **97**, 282-289.

Ghosh G, Subramanian IV, Adhikari N, Zhang X, Joshi HP, Basi D, Chandrashekhar YS, Hall JL, Roy S, Zeng Y, & Ramakrishnan S (2010). Hypoxia-induced microRNA-424 expression in human endothelial cells regulates HIF-alpha isoforms and promotes angiogenesis. *J Clin Invest* **120**, 4141-4154.

- Ghozi MC, Bernstein Y, Negreanu V, Levanon D, & Groner Y (1996). Expression of the human acute myeloid leukemia gene AML1 is regulated by two promoter regions. *Proc Natl Acad Sci U S A* **93**, 1935-1940.
- Ghuran AV & Camm AJ (2001). Ischaemic heart disease presenting as arrhythmias. *Br Med Bull* **59**, 193-210.
- Gidh-Jain M, Huang BY, Jain P, Gick G, & El Sherif N (1998). Alterations in cardiac gene expression during ventricular remodeling following experimental myocardial infarction. *Journal of Molecular and Cellular Cardiology* **30**, 627-637.
- Giles TD, Berk BC, Black HR, Cohn JN, Kostis JB, Izzo JL, Jr., & Weber MA (2005). Expanding the definition and classification of hypertension. *J Clin Hypertens (Greenwich)* **7**, 505-512.
- Glennon PE, Sugden PH, & Poole-Wilson PA (1995). Cellular mechanisms of cardiac hypertrophy. *Br Heart J* **73**, 496-499.
- Gomez AM, Guatimosim S, Dilly KW, Vassort G, & Lederer WJ (2001). Heart failure after myocardial infarction: altered excitation-contraction coupling. *Circulation* **104**, 688-693.
- Goni R, Garcia P, & Foissac S. The qPCR data statistical analysis. 2009. Integromics SL.
- Gonzalez A, Lopez B, & Diez J (2004). Fibrosis in hypertensive heart disease: role of the renin-angiotensin-aldosterone system. *Med Clin North Am* **88**, 83-97.
- Gordon GB, Bush DE, & Weisman HF (1988a). Reduction of atherosclerosis by administration of dehydroepiandrosterone. A study in the hypercholesterolemic New Zealand white rabbit with aortic intimal injury. *J Clin Invest* **82**, 712-720.
- Gordon GB, Bush DE, & Weisman HF (1988b). Reduction of atherosclerosis by administration of dehydroepiandrosterone. A study in the hypercholesterolemic New Zealand white rabbit with aortic intimal injury. *J Clin Invest* **82**, 712-720.
- Gordon L, Wharton J, Moore SE, Flanigan TP, Gulbenkian S, Walsh FS, David-Ferreira JF, Winter RJ, & Polak JM (1990a). Expression of neural cell adhesion molecule immunoreactivity in hypertrophic myocardium. *Life Sci* **47**, 601-609.
- Gordon L, Wharton J, Moore SE, Walsh FS, Moscoso JG, Penketh R, Wallwork J, Taylor KM, Yacoub MH, & Polak JM (1990b). Myocardial localization and isoforms of neural cell adhesion molecule (N-CAM) in the developing and transplanted human heart. *J Clin Invest* **86**, 1293-1300.
- Gorman JH, III, Gorman RC, Plappert T, Jackson BM, Hiramatsu Y, St John-Sutton MG, & Edmunds LH, Jr. (1998). Infarct size and location determine development of mitral regurgitation in the sheep model. *J Thorac Cardiovasc Surg* **115**, 615-622.
- Graf K, Do YS, Ashizawa N, Meehan WP, Giachelli CM, Marboe CC, Fleck E, & Hsueh WA (1997). Myocardial osteopontin expression is associated with left ventricular hypertrophy. *Circulation* **96**, 3063-3071.
- Graham D, McBride MW, Brain NJ, & Dominiczak AF (2005). Congenic/consomic models of hypertension. *Methods Mol Med* **108**, 3-15.
- Gronemeyer H, Gustafsson JA, & Laudet V (2004). Principles for modulation of the nuclear receptor superfamily. *Nat Rev Drug Discov* **3**, 950-964.
- Grossman W (2000). Defining diastolic dysfunction. *Circulation* **101**, 2020-2021.

- Grund F, Sommerschild HT, Lyberg T, Kirkeboen KA, & Ilebekk A (1999). Microembolization in pigs: effects on coronary blood flow and myocardial ischemic tolerance. *Am J Physiol* **277**, H533-H542.
- Gu TL, Goetz TL, Graves BJ, & Speck NA (2000). Auto-inhibition and partner proteins, core-binding factor beta (CBFbeta) and Ets-1, modulate DNA binding by CBFalpha2 (AML1). *Mol Cell Biol* **20**, 91-103.
- Guarda E, Katwa LC, Myers PR, Tyagi SC, & Weber KT (1993). Effects of endothelins on collagen turnover in cardiac fibroblasts. *Cardiovasc Res* **27**, 2130-2134.
- Guccione JM, Moonly SM, Moustakidis P, Costa KD, Moulton MJ, Ratcliffe MB, & Pasque MK (2001). Mechanism underlying mechanical dysfunction in the border zone of left ventricular aneurysm: a finite element model study. *Ann Thorac Surg* **71**, 654-662.
- Gude NA, Emmanuel G, Wu W, Cottage CT, Fischer K, Quijada P, Muraski JA, Alvarez R, Rubio M, Schaefer E, & Sussman MA (2008). Activation of Notch-mediated protective signaling in the myocardium. *Circ Res* **102**, 1025-1035.
- Guerra S, Leri A, Wang X, Finato N, Di LC, Beltrami CA, Kajstura J, & Anversa P (1999). Myocyte death in the failing human heart is gender dependent. *Circ Res* **85**, 856-866.
- Guyton AC & Hall JE (2006). *Textbook of medical physiology.*, 11th ed. Elsevier Saunders.
- Gwathmey JK, Copelas L, MacKinnon R, Schoen FJ, Feldman MD, Grossman W, & Morgan JP (1987). Abnormal intracellular calcium handling in myocardium from patients with end-stage heart failure. *Circ Res* **61**, 70-76.
- Gwathmey JK, Slawsky MT, Hajjar RJ, Briggs GM, & Morgan JP (1990). Role of intracellular calcium handling in force-interval relationships of human ventricular myocardium. *J Clin Invest* **85**, 1599-1613.
- Gwathmey JK, Warren SE, Briggs GM, Copelas L, Feldman MD, Phillips PJ, Callahan M, Jr., Schoen FJ, Grossman W, & Morgan JP (1991). Diastolic dysfunction in hypertrophic cardiomyopathy. Effect on active force generation during systole. *J Clin Invest* **87**, 1023-1031.
- Habtemariam B, Anisimov VM, & MacKerell AD, Jr. (2005). Cooperative binding of DNA and CBFbeta to the Runt domain of the CBFalpha studied via MD simulations. *Nucleic Acids Res* **33**, 4212-4222.
- Hajjar I, Kotchen JM, & Kotchen TA (2006). Hypertension: trends in prevalence, incidence, and control. *Annu Rev Public Health* **27**, 465-490.
- Hamacher J, Arras M, Bootz F, Weiss M, Schramm R, & Moehrlen U (2008). Microscopic wire guide-based orotracheal mouse intubation: description, evaluation and comparison with transillumination. *Lab Anim* **42**, 222-230.
- Hannenhalli S, Putt ME, Gilmore JM, Wang J, Parmacek MS, Epstein JA, Morrisey EE, Margulies KB, & Cappola TP (2006). Transcriptional genomics associates FOX transcription factors with human heart failure. *Circulation* **114**, 1269-1276.
- Hansson GK (2005). Inflammation, atherosclerosis, and coronary artery disease. *N Engl J Med* **352**, 1685-1695.
- Harada K, Grossman W, Friedman M, Edelman ER, Prasad PV, Keighley CS, Manning WJ, Sellke FW, & Simons M (1994). Basic fibroblast growth factor improves myocardial function in chronically ischemic porcine hearts. *J Clin Invest* **94**, 623-630.

- Hasegawa K, Lee SJ, Jobe SM, Markham BE, & Kitsis RN (1997). cis-Acting sequences that mediate induction of beta-myosin heavy chain gene expression during left ventricular hypertrophy due to aortic constriction. *Circulation* **96**, 3943-3953.
- Hasenfuss G (1998). Animal models of human cardiovascular disease, heart failure and hypertrophy. *Cardiovasc Res* **39**, 60-76.
- Hasenfuss G, Meyer M, Schillinger W, Preuss M, Pieske B, & Just H (1997). Calcium handling proteins in the failing human heart. *Basic Res Cardiol* **92 Suppl 1**, 87-93.
- Hasenfuss G, Schillinger W, Lehnart SE, Preuss M, Pieske B, Maier LS, Prestle J, Minami K, & Just H (1999). Relationship between Na⁺-Ca²⁺-exchanger protein levels and diastolic function of failing human myocardium. *Circulation* **99**, 641-648.
- Hautala N, Tokola H, Luodonpaa M, Puhakka J, Romppanen H, Vuolteenaho O, & Ruskoaho H (2001). Pressure overload increases GATA4 binding activity via endothelin-1. *Circulation* **103**, 730-735.
- He FJ & MacGregor GA (2009). A comprehensive review on salt and health and current experience of worldwide salt reduction programmes. *J Hum Hypertens* **23**, 363-384.
- Hermanides R & Ottervanger JP (2008). Treatment of ST-elevation myocardial infarction. *Future Cardiol* **4**, 391-397.
- Herrera M & Garvin JL (2005). A high-salt diet stimulates thick ascending limb eNOS expression by raising medullary osmolality and increasing release of endothelin-1. *Am J Physiol Renal Physiol* **288**, F58-F64.
- Herzig TC, Jobe SM, Aoki H, Molckentin JD, Cowley AW, Jr., Izumo S, & Markham BE (1997). Angiotensin II type 1a receptor gene expression in the heart: AP-1 and GATA-4 participate in the response to pressure overload. *Proc Natl Acad Sci U S A* **94**, 7543-7548.
- Heusch G (1998). Hibernating myocardium. *Physiol Rev* **78**, 1055-1085.
- Heusch G & Schulz R (1996). Myocardial hibernation: adaptation to ischaemia. *Eur Heart J* **17**, 824-828.
- Heusch G & Schulz R (2002a). Hibernating myocardium: new answers, still more questions! *Circ Res* **91**, 863-865.
- Heusch G & Schulz R (2002b). Myocardial hibernation. *Ital Heart J* **3**, 282-284.
- Heymans S, Lutun A, Nuyens D, Theilmeier G, Creemers E, Moons L, Dyspersin GD, Cleutjens JP, Shipley M, Angellilo A, Levi M, Nube O, Baker A, Keshet E, Lupu F, Herbert JM, Smits JF, Shapiro SD, Baes M, Borgers M, Collen D, Daemen MJ, & Carmeliet P (1999). Inhibition of plasminogen activators or matrix metalloproteinases prevents cardiac rupture but impairs therapeutic angiogenesis and causes cardiac failure. *Nat Med* **5**, 1135-1142.
- Himes SR, Cronau S, Mulford C, & Hume DA (2005a). The Runx1 transcription factor controls CSF-1-dependent and -independent growth and survival of macrophages. *Oncogene* **24**, 5278-5286.
- Himes SR, Cronau S, Mulford C, & Hume DA (2005b). The Runx1 transcription factor controls CSF-1-dependent and -independent growth and survival of macrophages. *Oncogene* **24**, 5278-5286.
- Hirota S, Otsu K, Nishida K, Higuchi Y, Morita T, Nakayama H, Yamaguchi O, Mano T, Matsumura Y, Ueno H, Tada M, & Hori M (2002). Involvement of nuclear factor-kappaB and

- apoptosis signal-regulating kinase 1 in G-protein-coupled receptor agonist-induced cardiomyocyte hypertrophy. *Circulation* **105**, 509-515.
- Hoekman MF, Jacobs FM, Smidt MP, & Burbach JP (2006). Spatial and temporal expression of FoxO transcription factors in the developing and adult murine brain. *Gene Expr Patterns* **6**, 134-140.
- Holtz J (1998). Role of ACE inhibition or AT(1) blockade in the remodeling following myocardial infarction. *Basic Research in Cardiology* **93**, 92-100.
- Hood WB, Jr., Bianco JA, Kumar R, & Whiting RB (1970). Experimental myocardial infarction. IV. Reduction of left ventricular compliance in the healing phase. *J Clin Invest* **49**, 1316-1323.
- Hood WB, Jr., McCarthy B, & Lown B (1967). Myocardial infarction following coronary ligation in dogs. Hemodynamic effects of isoproterenol and acetylstrophanthidin. *Circ Res* **21**, 191-199.
- Hoogenkamp M, Lichtinger M, Krysinska H, Lancrin C, Clarke D, Williamson A, Mazzarella L, Ingram R, Jorgensen H, Fisher A, Tenen DG, Kouskoff V, Lacaud G, & Bonifer C (2009). Early chromatin unfolding by RUNX1: a molecular explanation for differential requirements during specification versus maintenance of the hematopoietic gene expression program. *Blood* **114**, 299-309.
- Horan MJ & Kennedy HL (1984). Ventricular ectopy. History, epidemiology, and clinical implications. *JAMA* **251**, 380-386.
- Horton RA, Moren LA, Scrimgeour G, & Rawn D (2006). *Principles of Biochemistry* Pearson Prentice Hall.
- Houser SR, Margulies KB, Murphy AM, Spinale FG, Francis GS, Prabhu SD, Rockman HA, Kass DA, Molkentin JD, Sussman MA, & Koch W (2012). Animal Models of Heart Failure: A Scientific Statement From the American Heart Association. *Circ Res*.
- Hove-Madsen L & Bers DM (1993). Sarcoplasmic reticulum Ca²⁺ uptake and thapsigargin sensitivity in permeabilized rabbit and rat ventricular myocytes. *Circ Res* **73**, 820-828.
- Huang B, Wang S, Qin D, Boutjdir M, & El-Sherif N (1999). Diminished basal phosphorylation level of phospholamban in the postinfarction remodeled rat ventricle: role of beta-adrenergic pathway, G(i) protein, phosphodiesterase, and phosphatases. *Circ Res* **85**, 848-855.
- Huang NF, Sievers RE, Park JS, Fang Q, Li S, & Lee RJ (2006). A rodent model of myocardial infarction for testing the efficacy of cells and polymers for myocardial reconstruction. *Nat Protoc* **1**, 1596-1609.
- Hutchinson KR, Stewart JA, Jr., & Lucchesi PA (2010). Extracellular matrix remodeling during the progression of volume overload-induced heart failure. *J Mol Cell Cardiol* **48**, 564-569.
- Huysman JA, Vliegen HW, Van der Laarse A, & Eulderink F (1989). Changes in nonmyocyte tissue composition associated with pressure overload of hypertrophic human hearts. *Pathol Res Pract* **184**, 577-581.
- Ihara Y, Suzuki YJ, Kitta K, Jones LR, & Ikeda T (2002). Modulation of gene expression in transgenic mouse hearts overexpressing calsequestrin. *Cell Calcium* **32**, 21-29.
- Inoue K, Ozaki S, Shiga T, Ito K, Masuda T, Okado N, Iseda T, Kawaguchi S, Ogawa M, Bae SC, Yamashita N, Itohara S, Kudo N, & Ito Y (2002). Runx3 controls the axonal projection of proprioceptive dorsal root ganglion neurons. *Nat Neurosci* **5**, 946-954.
- Intengan HD & Schiffrin EL (2001). Vascular remodeling in hypertension: roles of apoptosis, inflammation, and fibrosis. *Hypertension* **38**, 581-587.

- Isaaz K, Ethevenot G, Admant P, Brembilla B, & Pernot C (1989). A new Doppler method of assessing left ventricular ejection force in chronic congestive heart failure. *Am J Cardiol* **64**, 81-87.
- Ito K, Liu Q, Salto-Tellez M, Yano T, Tada K, Ida H, Huang C, Shah N, Inoue M, Rajnakova A, Hiong KC, Peh BK, Han HC, Ito T, Teh M, Yeoh KG, & Ito Y (2005). RUNX3, a novel tumor suppressor, is frequently inactivated in gastric cancer by protein mislocalization. *Cancer Res* **65**, 7743-7750.
- Ito Y (1999). Molecular basis of tissue-specific gene expression mediated by the runt domain transcription factor PEBP2/CBF. *Genes Cells* **4**, 685-696.
- Iwamura N, Nagao K, Toyama J, Yamada K, & Shibata S (1977). Effects of A Polypeptide Anthopleurin-A on Transmembrane Action Potentials of Canine Cardiac Fibers. *Journal of Molecular and Cellular Cardiology* **9**, 41.
- Iwanaga K, Takano H, Ohtsuka M, Hasegawa H, Zou Y, Qin Y, Odaka K, Hiroshima K, Tadokoro H, & Komuro I (2004). Effects of G-CSF on cardiac remodeling after acute myocardial infarction in swine. *Biochem Biophys Res Commun* **325**, 1353-1359.
- Izzo JL, Jr. & Shykoff BE (2001). Arterial stiffness: clinical relevance, measurement, and treatment. *Rev Cardiovasc Med* **2**, 29-40.
- Jackson BM, Gorman JH, Moainie SL, Guy TS, Narula N, Narula J, John-Sutton MG, Edmunds LH, Jr., & Gorman RC (2002). Extension of borderzone myocardium in postinfarction dilated cardiomyopathy. *J Am Coll Cardiol* **40**, 1160-1167.
- Jackson BM, Gorman JH, III, Salgo IS, Moainie SL, Plappert T, St John-Sutton M, Edmunds LH, Jr., & Gorman RC (2003). Border zone geometry increases wall stress after myocardial infarction: contrast echocardiographic assessment. *Am J Physiol Heart Circ Physiol* **284**, H475-H479.
- Jalil JE, Janicki JS, Pick R, & Weber KT (1991). Coronary vascular remodeling and myocardial fibrosis in the rat with renovascular hypertension. Response to captopril. *Am J Hypertens* **4**, 51-55.
- James P, Inui M, Tada M, Chiesi M, & Carafoli E (1989). Nature and site of phospholamban regulation of the Ca²⁺ pump of sarcoplasmic reticulum. *Nature* **342**, 90-92.
- Jameson JN, Kasper DL, Harrison TR, Braunwald E, Fauci AS, Hauser SL, & Longo DL (2005). *Harrison's Principles of Internal Medicine.*, 16th ed. McGraw-Hill Medical Publishing Division, New York.
- Jeffs B, Clark JS, Anderson NH, Gratton J, Brosnan MJ, Gauguier D, Reid JL, Macrae IM, & Dominiczak AF (1997). Sensitivity to cerebral ischaemic insult in a rat model of stroke is determined by a single genetic locus. *Nat Genet* **16**, 364-367.
- Jeffs B, Negrin CD, Graham D, Clark JS, Anderson NH, Gauguier D, & Dominiczak AF (2000). Applicability of a "speed" congenic strategy to dissect blood pressure quantitative trait loci on rat chromosome 2. *Hypertension* **35**, 179-187.
- Jeyaseelan R, Poizat C, Baker RK, Abdishoo S, Isterabadi LB, Lyons GE, & Kedes L (1997). A novel cardiac-restricted target for doxorubicin. CARP, a nuclear modulator of gene expression in cardiac progenitor cells and cardiomyocytes. *J Biol Chem* **272**, 22800-22808.
- Jiang H, Zhang F, Kurosu T, & Peterlin BM (2005a). Runx1 binds positive transcription elongation factor b and represses transcriptional elongation by RNA polymerase II: possible mechanism of CD4 silencing. *Mol Cell Biol* **25**, 10675-10683.
- Jiang H, Zhang F, Kurosu T, & Peterlin BM (2005b). Runx1 binds positive transcription elongation factor b and represses transcriptional elongation by RNA polymerase II: possible mechanism of CD4 silencing. *Mol Cell Biol* **25**, 10675-10683.

- Joho S, Ishizaka S, Sievers R, Foster E, Simpson PC, & Grossman W (2007). Left ventricular pressure-volume relationship in conscious mice. *Am J Physiol Heart Circ Physiol* **292**, H369-H377.
- Jugdutt BI (2003). Ventricular remodeling after infarction and the extracellular collagen matrix: when is enough enough? *Circulation* **108**, 1395-1403.
- Kaab S, Barth AS, Margerie D, Dugas M, Gebauer M, Zwermann L, Merk S, Pfeufer A, Steinmeyer K, Bleich M, Kreuzer E, Steinbeck G, & Nabauer M (2004). Global gene expression in human myocardium-oligonucleotide microarray analysis of regional diversity and transcriptional regulation in heart failure. *Journal of Molecular Medicine-Jmm* **82**, 308-316.
- Kadambi VJ, Ponniah S, Harrer JM, Hoit BD, Dorn GW, Walsh RA, & Kranias EG (1996). Cardiac-specific overexpression of phospholamban alters calcium kinetics and resultant cardiomyocyte mechanics in transgenic mice. *J Clin Invest* **97**, 533-539.
- Kadambi VJ (1998). Genetically engineered mice: model systems for left ventricular failure. *J Card Fail* **4**, 263-270.
- Kagoshima H, Shigesada K, & Kohara Y (2007). RUNX regulates stem cell proliferation and differentiation: insights from studies of *C. elegans*. *J Cell Biochem* **100**, 1119-1130.
- Kagoshima H, Shigesada K, Satake M, Ito Y, Miyoshi H, Ohki M, Pepling M, & Gergen P (1993). The Runt domain identifies a new family of heteromeric transcriptional regulators. *Trends Genet* **9**, 338-341.
- Kahan T & Bergfeldt L (2005). Left ventricular hypertrophy in hypertension: its arrhythmogenic potential. *Heart* **91**, 250-256.
- Kai H, Kuwahara F, Tokuda K, & Imaizumi T (2005). Diastolic dysfunction in hypertensive hearts: roles of perivascular inflammation and reactive myocardial fibrosis. *Hypertens Res* **28**, 483-490.
- Kajstura J, Zhang X, Reiss K, Szoke E, Li P, Lagrasta C, Cheng W, Darzynkiewicz Z, Olivetti G, & Anversa P (1994). Myocyte cellular hyperplasia and myocyte cellular hypertrophy contribute to chronic ventricular remodeling in coronary artery narrowing-induced cardiomyopathy in rats. *Circ Res* **74**, 383-400.
- Kakinuma Y, Miyauchi T, Yuki K, Murakoshi N, Goto K, & Yamaguchi I (2001). Novel molecular mechanism of increased myocardial endothelin-1 expression in the failing heart involving the transcriptional factor hypoxia-inducible factor-1 α induced for impaired myocardial energy metabolism. *Circulation* **103**, 2387-2394.
- Kamachi Y, Ogawa E, Asano M, Ishida S, Murakami Y, Satake M, Ito Y, & Shigesada K (1990). Purification of a mouse nuclear factor that binds to both the A and B cores of the polyomavirus enhancer. *J Virol* **64**, 4808-4819.
- Kamekura S, Kawasaki Y, Hoshi K, Shimoaka T, Chikuda H, Maruyama Z, Komori T, Sato S, Takeda S, Karsenty G, Nakamura K, Chung UI, & Kawaguchi H (2006). Contribution of runt-related transcription factor 2 to the pathogenesis of osteoarthritis in mice after induction of knee joint instability. *Arthritis Rheum* **54**, 2462-2470.
- Kasahara H, Bartunkova S, Schinke M, Tanaka M, & Izumo S (1998). Cardiac and extracardiac expression of Csx/Nkx2.5 homeodomain protein. *Circ Res* **82**, 936-946.
- Kass DA, Maughan WL, Ciuffo A, Graves W, Healy B, & Weisfeldt ML (1988a). Disproportionate Epicardial Dilation After Transmural Infarction of the Canine Left-Ventricle - Acute and Chronic Differences. *Journal of the American College of Cardiology* **11**, 177-185.

- Kass DA, Maughan WL, Guo ZM, Kono A, Sunagawa K, & Sagawa K (1987). Comparative influence of load versus inotropic states on indexes of ventricular contractility: experimental and theoretical analysis based on pressure-volume relationships. *Circulation* **76**, 1422-1436.
- Kass DA, Midei M, Graves W, Brinker JA, & Maughan WL (1988b). Use of a conductance (volume) catheter and transient inferior vena caval occlusion for rapid determination of pressure-volume relationships in man. *Cathet Cardiovasc Diagn* **15**, 192-202.
- Kass DA, Yamazaki T, Burkhoff D, Maughan WL, & Sagawa K (1986). Determination of left ventricular end-systolic pressure-volume relationships by the conductance (volume) catheter technique. *Circulation* **73**, 586-595.
- Kawabe K, Watanabe TX, Shiono K, & Sokabe H (1978). Influence on blood pressure of renal isografts between spontaneously hypertensive and normotensive rats, utilizing the F1 hybrids. *Jpn Heart J* **19**, 886-894.
- Kehat I & Molkentin JD (2010). Molecular pathways underlying cardiac remodeling during pathophysiological stimulation. *Circulation* **122**, 2727-2735.
- Kelly A, Elliott EB, Matsuda R, Kaneko N, Smith GL, & Loughrey CM (2012). The effect of K201 on isolated working rabbit heart mechanical function during pharmacologically induced Ca²⁺ overload. *Br J Pharmacol* **165**, 1068-1083.
- Kido M, Du L, Sullivan CC, Li X, Deutsch R, Jamieson SW, & Thistlethwaite PA (2005). Hypoxia-inducible factor 1-alpha reduces infarction and attenuates progression of cardiac dysfunction after myocardial infarction in the mouse. *J Am Coll Cardiol* **46**, 2116-2124.
- Kilbey A, Blyth K, Wotton S, Terry A, Jenkins A, Bell M, Hanlon L, Cameron ER, & Neil JC (2007). Runx2 disruption promotes immortalization and confers resistance to oncogene-induced senescence in primary murine fibroblasts. *Cancer Res* **67**, 11263-11271.
- Kim WY, Sieweke M, Ogawa E, Wee HJ, Englmeier U, Graf T, & Ito Y (1999). Mutual activation of Ets-1 and AML1 DNA binding by direct interaction of their autoinhibitory domains. *EMBO J* **18**, 1609-1620.
- Kirichok Y, Krapivinsky G, & Clapham DE (2004). The mitochondrial calcium uniporter is a highly selective ion channel. *Nature* **427**, 360-364.
- Kiss E, Ball NA, Kranias EG, & Walsh RA (1995). Differential changes in cardiac phospholamban and sarcoplasmic reticular Ca(2+)-ATPase protein levels. Effects on Ca²⁺ transport and mechanics in compensated pressure-overload hypertrophy and congestive heart failure. *Circ Res* **77**, 759-764.
- Kitabayashi I, Aikawa Y, Nguyen LA, Yokoyama A, & Ohki M (2001). Activation of AML1-mediated transcription by MOZ and inhibition by the MOZ-CBP fusion protein. *EMBO J* **20**, 7184-7196.
- Kittleson MM, Minhas KM, Irizarry RA, Ye SQ, Edness G, Breton E, Conte JV, Tomaselli G, Garcia JG, & Hare JM (2005). Gene expression analysis of ischemic and nonischemic cardiomyopathy: shared and distinct genes in the development of heart failure. *Physiol Genomics* **21**, 299-307.
- Klocke R, Tian W, Kuhlmann MT, & Nikol S (2007). Surgical animal models of heart failure related to coronary heart disease. *Cardiovasc Res* **74**, 29-38.
- Kloner RA & Jennings RB (2001). Consequences of brief ischemia: stunning, preconditioning, and their clinical implications: part 1. *Circulation* **104**, 2981-2989.
- Klug WS & Cummings MR (2005). *Essentials of Genetics.*, 5th ed. Pearson Prentice Hall.

- Komori T, Yagi H, Nomura S, Yamaguchi A, Sasaki K, Deguchi K, Shimizu Y, Bronson RT, Gao YH, Inada M, Sato M, Okamoto R, Kitamura Y, Yoshiki S, & Kishimoto T (1997). Targeted disruption of *Cbfa1* results in a complete lack of bone formation owing to maturational arrest of osteoblasts. *Cell* **89**, 755-764.
- Komuro I & Izumo S (1993). *Csx*: a murine homeobox-containing gene specifically expressed in the developing heart. *Proc Natl Acad Sci U S A* **90**, 8145-8149.
- Kosloski LM, Bales IK, Allen KB, Walker BL, Borkon AM, Stuart RS, Pak AF, & Wacker MJ (2009). Purification of cardiac myocytes from human heart biopsies for gene expression analysis. *Am J Physiol Heart Circ Physiol* **297**, H1163-H1169.
- Koss KL, Grupp IL, & Kranias EG (1997). The relative phospholamban and SERCA2 ratio: a critical determinant of myocardial contractility. *Basic Res Cardiol* **92 Suppl 1**, 17-24.
- Koutsourakis M, Langeveld A, Patient R, Beddington R, & Grosveld F (1999). The transcription factor GATA6 is essential for early extraembryonic development. *Development* **126**, 723-732.
- Kramer CM, Lima JA, Reichek N, Ferrari VA, Llaneras MR, Palmon LC, Yeh IT, Tallant B, & Axel L (1993). Regional differences in function within noninfarcted myocardium during left ventricular remodeling. *Circulation* **88**, 1279-1288.
- Kramer CM, Rogers WJ, Park CS, Seibel PS, Shaffer A, Theobald TM, Reichek N, Onodera T, & Gerdes AM (1998). Regional myocyte hypertrophy parallels regional myocardial dysfunction during post-infarct remodeling. *J Mol Cell Cardiol* **30**, 1773-1778.
- Kuhlmann MT, Kirchof P, Klocke R, Hasib L, Stypmann J, Fabritz L, Stelljes M, Tian W, Zwiener M, Mueller M, Kienast J, Breithardt G, & Nikol S (2006). G-CSF/SCF reduces inducible arrhythmias in the infarcted heart potentially via increased connexin43 expression and arteriogenesis. *J Exp Med* **203**, 87-97.
- Kumar D, Hacker TA, Buck J, Whitesell LF, Kaji EH, Douglas PS, & Kamp TJ (2005). Distinct mouse coronary anatomy and myocardial infarction consequent to ligation. *Coron Artery Dis* **16**, 41-44.
- Kupari M, Koskinen P, & Virolainen J (1994). Correlates of left ventricular mass in a population sample aged 36 to 37 years. Focus on lifestyle and salt intake. *Circulation* **89**, 1041-1050.
- Lackie PM, Zuber C, & Roth J (1991). Expression of polysialylated N-CAM during rat heart development. *Differentiation* **47**, 85-98.
- LaFramboise WA, Bombach KL, Dhir RJ, Muha N, Cullen RF, Pogozelski AR, Turk D, George JD, Guthrie RD, & Magovern JA (2005). Molecular dynamics of the compensatory response to myocardial infarct. *Journal of Molecular and Cellular Cardiology* **38**, 103-117.
- Laidlaw DW, Houmoud MK, Weinstock NA, Estes M, & Link MS. Prognosis and treatment of ventricular arrhythmias following myocardial infarction. *Current Cardiology Reviews* **3**, 23-33. 2007.
- Latchman DS (1997). Transcription factors: an overview. *Int J Biochem Cell Biol* **29**, 1305-1312.
- Layland J, Solaro RJ, & Shah AM (2005). Regulation of cardiac contractile function by troponin I phosphorylation. *Cardiovasc Res* **66**, 12-21.
- Lederman RJ (2005). Cardiovascular interventional magnetic resonance imaging. *Circulation* **112**, 3009-3017.
- Lee KS, Kim HJ, Li QL, Chi XZ, Ueta C, Komori T, Wozney JM, Kim EG, Choi JY, Ryoo HM, & Bae SC (2000). *Runx2* is a common target of transforming growth factor beta1 and bone

morphogenetic protein 2, and cooperation between Runx2 and Smad5 induces osteoblast-specific gene expression in the pluripotent mesenchymal precursor cell line C2C12. *Mol Cell Biol* **20**, 8783-8792.

Lee SH, Che X, Jeong JH, Choi JY, Lee YJ, Lee YH, Bae SC, & Lee YM (2012). Runx2 Protein Stabilizes Hypoxia-inducible Factor-1alpha through Competition with von Hippel-Lindau Protein (pVHL) and Stimulates Angiogenesis in Growth Plate Hypertrophic Chondrocytes. *J Biol Chem* **287**, 14760-14771.

Lee SH, Kim J, Kim WH, & Lee YM (2009). Hypoxic silencing of tumor suppressor RUNX3 by histone modification in gastric cancer cells. *Oncogene* **28**, 184-194.

Lee TI & Young RA (2000). Transcription of eukaryotic protein-coding genes. *Annu Rev Genet* **34**, 77-137.

Leite-Moreira AF, Correia-Pinto J, & Gillebert TC (1999). Afterload induced changes in myocardial relaxation: a mechanism for diastolic dysfunction. *Cardiovasc Res* **43**, 344-353.

Lensch MW & Daley GQ (2004). Origins of mammalian hematopoiesis: in vivo paradigms and in vitro models. *Curr Top Dev Biol* **60**, 127-196.

Levanon D, Bettoun D, Harris-Cerruti C, Woolf E, Negreanu V, Eilam R, Bernstein Y, Goldenberg D, Xiao C, Fliegau M, Kremer E, Otto F, Brenner O, Lev-Tov A, & Groner Y (2002). The Runx3 transcription factor regulates development and survival of TrkC dorsal root ganglia neurons. *EMBO J* **21**, 3454-3463.

Levanon D, Brenner O, Negreanu V, Bettoun D, Woolf E, Eilam R, Lotem J, Gat U, Otto F, Speck N, & Groner Y (2001a). Spatial and temporal expression pattern of Runx3 (Aml2) and Runx1 (Aml1) indicates non-redundant functions during mouse embryogenesis. *Mech Dev* **109**, 413-417.

Levanon D, Brenner O, Otto F, & Groner Y (2003a). Runx3 knockouts and stomach cancer. *EMBO Rep* **4**, 560-564.

Levanon D, Glusman G, Bangsow T, Ben-Asher E, Male DA, Avidan N, Bangsow C, Hattori M, Taylor TD, Taudien S, Blechschmidt K, Shimizu N, Rosenthal A, Sakaki Y, Lancet D, & Groner Y (2001b). Architecture and anatomy of the genomic locus encoding the human leukemia-associated transcription factor RUNX1/AML1. *Gene* **262**, 23-33.

Levanon D, Glusman G, Bettoun D, Ben-Asher E, Negreanu V, Bernstein Y, Harris-Cerruti C, Brenner O, Eilam R, Lotem J, Fainaru O, Goldenberg D, Pozner A, Woolf E, Xiao C, Yarmus M, & Groner Y (2003b). Phylogenesis and regulated expression of the RUNT domain transcription factors RUNX1 and RUNX3. *Blood Cells Mol Dis* **30**, 161-163.

Levanon D, Glusman G, Bettoun D, Ben-Asher E, Negreanu V, Bernstein Y, Harris-Cerruti C, Brenner O, Eilam R, Lotem J, Fainaru O, Goldenberg D, Pozner A, Woolf E, Xiao C, Yarmus M, & Groner Y (2003c). Phylogenesis and regulated expression of the RUNT domain transcription factors RUNX1 and RUNX3. *Blood Cells Mol Dis* **30**, 161-163.

Levanon D, Goldstein RE, Bernstein Y, Tang H, Goldenberg D, Stifani S, Paroush Z, & Groner Y (1998). Transcriptional repression by AML1 and LEF-1 is mediated by the TLE/Groucho corepressors. *Proc Natl Acad Sci U S A* **95**, 11590-11595.

Levanon D & Groner Y (2004). Structure and regulated expression of mammalian RUNX genes. *Oncogene* **23**, 4211-4219.

Levick RJ (2010). *An Introduction to Cardiovascular Physiology*, 5th ed. Butterworth Heinemann, Great Britain.

- Levy D, Garrison RJ, Savage DD, Kannel WB, & Castelli WP (1990). Prognostic implications of echocardiographically determined left ventricular mass in the Framingham Heart Study. *N Engl J Med* **322**, 1561-1566.
- Levy D, Larson MG, Vasan RS, Kannel WB, & Ho KK (1996). The progression from hypertension to congestive heart failure. *JAMA* **275**, 1557-1562.
- Li B, Li Q, Wang X, Jana KP, Redaelli G, Kajstura J, & Anversa P (1997). Coronary constriction impairs cardiac function and induces myocardial damage and ventricular remodeling in mice. *Am J Physiol* **273**, H2508-H2519.
- Li L, Chu G, Kranias EG, & Bers DM (1998). Cardiac myocyte calcium transport in phospholamban knockout mouse: relaxation and endogenous CaMKII effects. *Am J Physiol* **274**, H1335-H1347.
- Li L, Desantiago J, Chu G, Kranias EG, & Bers DM (2000). Phosphorylation of phospholamban and troponin I in beta-adrenergic-induced acceleration of cardiac relaxation. *Am J Physiol Heart Circ Physiol* **278**, H769-H779.
- Li QL, Ito K, Sakakura C, Fukamachi H, Inoue K, Chi XZ, Lee KY, Nomura S, Lee CW, Han SB, Kim HM, Kim WJ, Yamamoto H, Yamashita N, Yano T, Ikeda T, Itohara S, Inazawa J, Abe T, Hagiwara A, Yamagishi H, Ooe A, Kaneda A, Sugimura T, Ushijima T, Bae SC, & Ito Y (2002). Causal relationship between the loss of RUNX3 expression and gastric cancer. *Cell* **109**, 113-124.
- Liang Q & Molkenin JD (2002). Divergent signaling pathways converge on GATA4 to regulate cardiac hypertrophic gene expression. *J Mol Cell Cardiol* **34**, 611-616.
- Libby P (2001). Current concepts of the pathogenesis of the acute coronary syndromes. *Circulation* **104**, 365-372.
- Licata A, Aggarwal R, Robinson RB, & Boyden P (1997). Frequency dependent effects on Cai transients and cell shortening in myocytes that survive in the infarcted heart. *Cardiovasc Res* **33**, 341-350.
- Lin MC, Rockman HA, & Chien KR (1995). Heart and lung disease in engineered mice. *Nat Med* **1**, 749-751.
- Linck B, Boknik P, Eschenhagen T, Muller FU, Neumann J, Nose M, Jones LR, Schmitz W, & Scholz H (1996). Messenger RNA expression and immunological quantification of phospholamban and SR-Ca(2+)-ATPase in failing and nonfailing human hearts. *Cardiovasc Res* **31**, 625-632.
- Lips DJ, van der Nagel T, Steendijk P, Palmem M, Janssen BJ, van Dantzig JM, de Windt LJ, & Doevendans PA (2004). Left ventricular pressure-volume measurements in mice: comparison of closed-chest versus open-chest approach. *Basic Res Cardiol* **99**, 351-359.
- Little WC & Cheng CP (1993). Effect of exercise on left ventricular-arterial coupling assessed in the pressure-volume plane. *Am J Physiol* **264**, H1629-H1633.
- Litwin SE, Raya TE, Anderson PG, Litwin CM, Bressler R, & Goldman S (1991). Induction of myocardial hypertrophy after coronary ligation in rats decreases ventricular dilatation and improves systolic function. *Circulation* **84**, 1819-1827.
- Liu J, Yan Y, Liu L, Xie Z, Malhotra D, Joe B, & Shapiro JJ (2011). Impairment of Na/K-ATPase signaling in renal proximal tubule contributes to Dahl salt-sensitive hypertension. *J Biol Chem* **286**, 22806-22813.
- Liu JLY, Maniadakis N, Gray A, & Rayner M (2002). The economic burden of coronary heart disease in the UK. *Heart* **88**, 597-603.

- Liu PP, Hajra A, Wijmenga C, & Collins FS (1995). Molecular pathogenesis of the chromosome 16 inversion in the M4Eo subtype of acute myeloid leukemia. *Blood* **85**, 2289-2302.
- Llamas B, Jiang Z, Rainville ML, Picard S, & Deschepper CF (2005). Distinct QTLs are linked to cardiac left ventricular mass in a sex-specific manner in a normotensive inbred rat inter-cross. *Mamm Genome* **16**, 700-711.
- Look AT (1997). Oncogenic transcription factors in the human acute leukemias. *Science* **278**, 1059-1064.
- Lopez B, Gonzalez A, Varo N, Laviades C, Querejeta R, & Diez J (2001). Biochemical assessment of myocardial fibrosis in hypertensive heart disease. *Hypertension* **38**, 1222-1226.
- Lopez-Sendon J, Gonzalez A, Lopez de SE, Coma-Canella I, Roldan I, Dominguez F, Maqueda I, & Martin JL (1992). Diagnosis of subacute ventricular wall rupture after acute myocardial infarction: sensitivity and specificity of clinical, hemodynamic and echocardiographic criteria. *J Am Coll Cardiol* **19**, 1145-1153.
- Lorell BH & Carabello BA (2000a). Left ventricular hypertrophy: pathogenesis, detection, and prognosis. *Circulation* **102**, 470-479.
- Lorell BH & Carabello BA (2000b). Left ventricular hypertrophy: pathogenesis, detection, and prognosis. *Circulation* **102**, 470-479.
- Lorsbach RB, Moore J, Ang SO, Sun W, Lenny N, & Downing JR (2004). Role of RUNX1 in adult hematopoiesis: analysis of RUNX1-IRES-GFP knock-in mice reveals differential lineage expression. *Blood* **103**, 2522-2529.
- Lu J, Maruyama M, Satake M, Bae SC, Ogawa E, Kagoshima H, Shigesada K, & Ito Y (1995). Subcellular localization of the alpha and beta subunits of the acute myeloid leukemia-linked transcription factor PEBP2/CBF. *Mol Cell Biol* **15**, 1651-1661.
- Lukasik SM, Zhang L, Corpora T, Tomanicek S, Li Y, Kundu M, Hartman K, Liu PP, Laue TM, Biltonen RL, Speck NA, & Bushweller JH (2002). Altered affinity of CBF beta-SMMHC for Runx1 explains its role in leukemogenesis. *Nat Struct Biol* **9**, 674-679.
- Lund AH & van LM (2002). RUNX: a trilogy of cancer genes. *Cancer Cell* **1**, 213-215.
- Lutgens E, Daemen MJAP, de Muinck ED, Debets J, Leenders P, & Smits JFM (1999). Chronic myocardial infarction in the mouse: cardiac structural and functional changes. *Cardiovascular Research* **41**, 586-593.
- Lutsky I, Aizer F, & Mor N (1984). The Sabra rat: definition of a laboratory animal. *Isr J Med Sci* **20**, 603-612.
- Lutterbach B, Westendorf JJ, Linggi B, Isaac S, Seto E, & Hiebert SW (2000). A mechanism of repression by acute myeloid leukemia-1, the target of multiple chromosomal translocations in acute leukemia. *J Biol Chem* **275**, 651-656.
- Lyon H (1991). *Theory and strategy in histochemistry*. Springer-Verlag, Berlin.
- Lyons I, Parsons LM, Hartley L, Li R, Andrews JE, Robb L, & Harvey RP (1995). Myogenic and morphogenetic defects in the heart tubes of murine embryos lacking the homeo box gene Nkx2-5. *Genes Dev* **9**, 1654-1666.
- Magovern JA, Christlieb IY, Badylak SF, Lantz GC, & Kao RL (1992). A model of left ventricular dysfunction caused by intracoronary adriamycin. *Ann Thorac Surg* **53**, 861-863.

- Maiese K, Chong ZZ, & Shang YC (2008). OutFOXing disease and disability: the therapeutic potential of targeting FoxO proteins. *Trends Mol Med* **14**, 219-227.
- Mane VP, Heuer MA, Hillyer P, Navarro MB, & Rabin RL (2008). Systematic method for determining an ideal housekeeping gene for real-time PCR analysis. *J Biomol Tech* **19**, 342-347.
- Mani K & Kitsis RN (2003). Myocyte apoptosis: programming ventricular remodeling. *J Am Coll Cardiol* **41**, 761-764.
- Marambio P, Toro B, Sanhueza C, Troncoso R, Parra V, Verdejo H, Garcia L, Quiroga C, Munafó D, Diaz-Elizondo J, Bravo R, Gonzalez MJ, Diaz-Araya G, Pedrozo Z, Chiong M, Colombo MI, & Lavandero S (2010). Glucose deprivation causes oxidative stress and stimulates aggresome formation and autophagy in cultured cardiac myocytes. *Biochim Biophys Acta* **1802**, 509-518.
- Marino TA, Kent RL, Uboh CE, Fernandez E, Thompson EW, & Cooper G (1985). Structural analysis of pressure versus volume overload hypertrophy of cat right ventricle. *Am J Physiol* **249**, H371-H379.
- Marx SO, Reiken S, Hisamatsu Y, Jayaraman T, Burkhoff D, Rosemlit N, & Marks AR (2000a). PKA phosphorylation dissociates FKBP12.6 from the calcium release channel (ryanodine receptor): defective regulation in failing hearts. *Cell* **101**, 365-376.
- Marx SO, Reiken S, Hisamatsu Y, Jayaraman T, Burkhoff D, Rosemlit N, & Marks AR (2000b). PKA phosphorylation dissociates FKBP12.6 from the calcium release channel (ryanodine receptor): defective regulation in failing hearts. *Cell* **101**, 365-376.
- Masaki H, Imaizumi T, Ando S, Hirooka Y, Harada S, Momohara M, Nagano M, & Takeshita A (1993). Production of Chronic Congestive-Heart-Failure by Rapid Ventricular Pacing in the Rabbit. *Cardiovascular Research* **27**, 828-831.
- Masci PG, Ganame J, Francone M, Desmet W, Lorenzoni V, Iacucci I, Barison A, Carbone I, Lombardi M, Agati L, Janssens S, & Bogaert J (2011). Relationship between location and size of myocardial infarction and their reciprocal influences on post-infarction left ventricular remodelling. *Eur Heart J* **32**, 1640-1648.
- Matsumura S, Iwanaga S, Mochizuki S, Okamoto H, Ogawa S, & Okada Y (2005). Targeted deletion or pharmacological inhibition of MMP-2 prevents cardiac rupture after myocardial infarction in mice. *J Clin Invest* **115**, 599-609.
- Maurer MS, Spevack D, Burkhoff D, & Kronzon I (2004). Diastolic dysfunction: can it be diagnosed by Doppler echocardiography? *J Am Coll Cardiol* **44**, 1543-1549.
- McBride MW, Charchar FJ, Graham D, Miller WH, Strahorn P, Carr FJ, & Dominiczak AF (2004). Functional genomics in rodent models of hypertension. *J Physiol* **554**, 56-63.
- McCormick RJ, Musch TI, Bergman BC, & Thomas DP (1994). Regional differences in LV collagen accumulation and mature cross-linking after myocardial infarction in rats. *Am J Physiol* **266**, H354-H359.
- McCullagh WH, Covell JW, & Ross J, Jr. (1972). Left ventricular dilatation and diastolic compliance changes during chronic volume overloading. *Circulation* **45**, 943-951.
- McCully JD, Wakiyama H, Hsieh YJ, Jones M, & Levitsky S (2004). Differential contribution of necrosis and apoptosis in myocardial ischemia-reperfusion injury. *Am J Physiol Heart Circ Physiol* **286**, H1923-H1935.
- McMurray JJ & Pfeffer MA (2005). Heart failure. *Lancet* **365**, 1877-1889.

Melle C, Camacho JA, Surber R, Betge S, Von Eggeling F, & Zimmer T (2006). Region-specific alterations of global protein expression in the remodelled rat myocardium. *International Journal of Molecular Medicine* **18**, 1207-1215.

Meyer M, Schillinger W, Pieske B, Holubarsch C, Heilmann C, Posival H, Kuwajima G, Mikoshiba K, Just H, Hasenfuss G, & . (1995). Alterations of sarcoplasmic reticulum proteins in failing human dilated cardiomyopathy. *Circulation* **92**, 778-784.

Michael LH, Ballantyne CM, Zachariah JP, Gould KE, Pocius JS, Taffet GE, Hartley CJ, Pham TT, Daniel SL, Funk E, & Entman ML (1999). Myocardial infarction and remodeling in mice: effect of reperfusion. *Am J Physiol* **277**, H660-H668.

Michael LH, Entman ML, Hartley CJ, Youker KA, Zhu J, Hall SR, Hawkins HK, Berens K, & Ballantyne CM (1995). Myocardial ischemia and reperfusion: a murine model. *Am J Physiol* **269**, H2147-H2154.

Michaud J, Wu F, Osato M, Cotties GM, Yanagida M, Asou N, Shigesada K, Ito Y, Benson KF, Raskind WH, Rossier C, Antonarakis SE, Israels S, McNicol A, Weiss H, Horwitz M, & Scott HS (2002). In vitro analyses of known and novel RUNX1/AML1 mutations in dominant familial platelet disorder with predisposition to acute myelogenous leukemia: implications for mechanisms of pathogenesis. *Blood* **99**, 1364-1372.

Mirsky I, Pfeffer JM, Pfeffer MA, & Braunwald E (1983). The contractile state as the major determinant in the evolution of left ventricular dysfunction in the spontaneously hypertensive rat. *Circ Res* **53**, 767-778.

Mitchell PJ & Tjian R (1989). Transcriptional regulation in mammalian cells by sequence-specific DNA binding proteins. *Science* **245**, 371-378.

Miyoshi H, Ohira M, Shimizu K, Mitani K, Hirai H, Imai T, Yokoyama K, Soeda E, & Ohki M (1995). Alternative splicing and genomic structure of the AML1 gene involved in acute myeloid leukemia. *Nucleic Acids Res* **23**, 2762-2769.

Miyoshi H, Shimizu K, Kozu T, Maseki N, Kaneko Y, & Ohki M (1991). t(8;21) breakpoints on chromosome 21 in acute myeloid leukemia are clustered within a limited region of a single gene, AML1. *Proc Natl Acad Sci U S A* **88**, 10431-10434.

Moldestad O, Karlsen P, Molden S, & Storm JF (2009). Tracheotomy improves experiment success rate in mice during urethane anesthesia and stereotaxic surgery. *J Neurosci Methods* **176**, 57-62.

Molkentin JD (2000). The zinc finger-containing transcription factors GATA-4, -5, and -6. Ubiquitously expressed regulators of tissue-specific gene expression. *J Biol Chem* **275**, 38949-38952.

Molkentin JD & Markham BE (1993). Myocyte-specific enhancer-binding factor (MEF-2) regulates alpha-cardiac myosin heavy chain gene expression in vitro and in vivo. *J Biol Chem* **268**, 19512-19520.

Molkentin JD & Olsen EN (1996). Defining the regulatory networks for muscle development. *Curr Opin Genet Dev* **6**, 445-453.

Moniotte S, Vaerman JL, Kockx MM, Larrouy D, Langin D, Noirhomme P, & Balligand JL (2001). Real-time RT-PCR for the detection of beta-adrenoceptor messenger RNAs in small human endomyocardial biopsies. *J Mol Cell Cardiol* **33**, 2121-2133.

Monnet E & Chachques JC (2005). Animal models of heart failure: what is new? *Ann Thorac Surg* **79**, 1445-1453.

- Moore XL, Tan SL, Lo CY, Fang L, Su YD, Gao XM, Woodcock EA, Summers RJ, Tregear GW, Bathgate RA, & Du XJ (2007). Relaxin antagonizes hypertrophy and apoptosis in neonatal rat cardiomyocytes. *Endocrinology* **148**, 1582-1589.
- Moreo A, Ambrosio G, De CB, Pu M, Tran T, Mauri F, & Raman SV (2009). Influence of myocardial fibrosis on left ventricular diastolic function: noninvasive assessment by cardiac magnetic resonance and echo. *Circ Cardiovasc Imaging* **2**, 437-443.
- Morgan JP (1991a). Abnormal intracellular modulation of calcium as a major cause of cardiac contractile dysfunction. *N Engl J Med* **325**, 625-632.
- Morgan JP (1991b). Abnormal intracellular modulation of calcium as a major cause of cardiac contractile dysfunction. *New Engl J Med* **325**, 625-632.
- Mork HK, Sjaastad I, Sejersted OM, & Louch WE (2009). Slowing of cardiomyocyte Ca²⁺ release and contraction during heart failure progression in postinfarction mice. *Am J Physiol Heart Circ Physiol* **296**, H1069-H1079.
- Morrissey EE, Ip HS, Tang Z, Lu MM, & Parmacek MS (1997). GATA-5: a transcriptional activator expressed in a novel temporally and spatially-restricted pattern during embryonic development. *Dev Biol* **183**, 21-36.
- Moss AJ, Davis HT, DeCamilla J, & Bayer LW (1979). Ventricular ectopic beats and their relation to sudden and nonsudden cardiac death after myocardial infarction. *Circulation* **60**, 998-1003.
- Movsesian MA, Bristow MR, & Krall J (1989). Ca²⁺ uptake by cardiac sarcoplasmic reticulum from patients with idiopathic dilated cardiomyopathy. *Circ Res* **65**, 1141-1144.
- Mukouyama Y, Chiba N, Hara T, Okada H, Ito Y, Kanamaru R, Miyajima A, Satake M, & Watanabe T (2000). The AML1 transcription factor functions to develop and maintain hematogenic precursor cells in the embryonic aorta-gonad-mesonephros region. *Dev Biol* **220**, 27-36.
- Mulieri LA, Hasenfuss G, Leavitt B, Allen PD, & Alpert NR (1992). Altered myocardial force-frequency relation in human heart failure. *Circulation* **85**, 1743-1750.
- Muller JG, Thompson JT, Edmonson AM, Rackley MS, Kasahara H, Izumo S, McQuinn TC, Menick DR, & O'Brien TX (2002). Differential regulation of the cardiac sodium calcium exchanger promoter in adult and neonatal cardiomyocytes by Nkx2.5 and serum response factor. *J Mol Cell Cardiol* **34**, 807-821.
- Muller-Ehmsen J, Nickel J, Zobel C, Hirsch I, Bolck B, Brixius K, & Schwinger RH (2003). Longer term effects of ouabain on the contractility of rat isolated cardiomyocytes and on the expression of Ca and Na regulating proteins. *Basic Res Cardiol* **98**, 90-96.
- Nabauer M & Kaab S (1998). Potassium channel down-regulation in heart failure. *Cardiovasc Res* **37**, 324-334.
- Nagamachi A, Htun PW, Ma F, Miyazaki K, Yamasaki N, Kanno M, Inaba T, Honda Z, Okuda T, Oda H, Tsuji K, & Honda H (2010). A 5' untranslated region containing the IRES element in the Runx1 gene is required for angiogenesis, hematopoiesis and leukemogenesis in a knock-in mouse model. *Dev Biol* **345**, 226-236.
- Nagao K, Ono K, Iwanaga Y, Tamaki Y, Kojima Y, Horie T, Nishi H, Kinoshita M, Kuwabara Y, Hasegawa K, Kita T, & Kimura T (2010). Neural cell adhesion molecule is a cardioprotective factor up-regulated by metabolic stress. *J Mol Cell Cardiol* **48**, 1157-1168.
- Nahrendorf M, Wiesmann F, Hiller KH, Han H, Hu K, Waller C, Ruff J, Haase A, Ertl G, & Bauer WR (2000). In vivo assessment of cardiac remodeling after myocardial infarction in rats by cine-magnetic resonance imaging. *J Cardiovasc Magn Reson* **2**, 171-180.

- Nakahara T, Shimizu T, Kawai-Kowase K, Tancha T, Iso T, Arai M, & Kurabayashi M (2008). Osteogenic Transcription Factor Runx2 Suppresses Atrial and B-Type Natriuretic Peptide Gene Expression in Rat Cardiacmyocytes: Possible Role of Runx2 in Cardiac Fibrosis. *Circulation*, 118:S_1026.
- Nam S, Jin YH, Li QL, Lee KY, Jeong GB, Ito Y, Lee J, & Bae SC (2002). Expression pattern, regulation, and biological role of runt domain transcription factor, run, in *Caenorhabditis elegans*. *Mol Cell Biol* 22, 547-554.
- Narula J, Dawson MS, Singh BK, Amanullah A, Acio ER, Chaudhry FA, Arani RB, & Iskandrian AE (2000). Noninvasive characterization of stunned, hibernating, remodeled and nonviable myocardium in ischemic cardiomyopathy. *J Am Coll Cardiol* 36, 1913-1919.
- Natarajan A, Yamagishi H, Ahmad F, Li D, Roberts R, Matsuoka R, Hill S, & Srivastava D (2001). Human eHAND, but not dHAND, is down-regulated in cardiomyopathies. *J Mol Cell Cardiol* 33, 1607-1614.
- Negoro S, Oh H, Tone E, Kunisada K, Fujio Y, Walsh K, Kishimoto T, & Yamauchi-Takahara K (2001). Glycoprotein 130 regulates cardiac myocyte survival in doxorubicin-induced apoptosis through phosphatidylinositol 3-kinase/Akt phosphorylation and Bcl-xL/caspase-3 interaction. *Circulation* 103, 555-561.
- Nevadunsky NS, Barbieri JS, Kwong J, Merritt MA, Welch WR, Berkowitz RS, & Mok SC (2009). RUNX3 protein is overexpressed in human epithelial ovarian cancer. *Gynecol Oncol* 112, 325-330.
- NHS Executive. Burdens of disease: a discussion document. 1996. Wetherby, Department of Health.
- NHS Information Centre. Health Survey for England 2009: Trend Tables. 2010. The NHS Information Centre for Health and Social Care.
- Nian M, Lee P, Khaper N, & Liu P (2004). Inflammatory cytokines and postmyocardial infarction remodeling. *Circ Res* 94, 1543-1553.
- Nicoletti A & Michel JB (1999). Cardiac fibrosis and inflammation: interaction with hemodynamic and hormonal factors. *Cardiovasc Res* 41, 532-543.
- Nigam V & Srivastava D (2009). Notch1 represses osteogenic pathways in aortic valve cells. *J Mol Cell Cardiol* 47, 828-834.
- Nishimura H, Kubo S, Nishioka A, Imamura K, Kawamura K, & Hasegawa M (1985). Left ventricular diastolic function of spontaneously hypertensive rats and its relationship to structural components of the left ventricle. *Clin Sci (Lond)* 69, 571-579.
- Nolan SE, Mannisi JA, Bush DE, Healy B, & Weisman HF (1988a). Increased afterload aggravates infarct expansion after acute myocardial infarction. *J Am Coll Cardiol* 12, 1318-1325.
- Nolan SE, Mannisi JA, Bush DE, Healy B, & Weisman HF (1988b). Increased afterload aggravates infarct expansion after acute myocardial infarction. *J Am Coll Cardiol* 12, 1318-1325.
- North T, Gu TL, Stacy T, Wang Q, Howard L, Binder M, Marin-Padilla M, & Speck NA (1999). Cbfa2 is required for the formation of intra-aortic hematopoietic clusters. *Development* 126, 2563-2575.
- Nunez DJ, Clifford CP, al-Mahdawi S, & Dutka D (1996). Hypertensive cardiac hypertrophy--is genetic variance the missing link? *Br J Clin Pharmacol* 42, 107-117.
- O'Brien E, Beevers DG, & Gregory YH (2007). *ABC of hypertension*. BMJ Books, London.

- Ogawa E, Inuzuka M, Maruyama M, Satake M, Naito-Fujimoto M, Ito Y, & Shigesada K (1993). Molecular cloning and characterization of PEBP2 beta, the heterodimeric partner of a novel *Drosophila* runt-related DNA binding protein PEBP2 alpha. *Virology* **194**, 314-331.
- Ogawa S, Satake M, & Ikuta K (2008). Physical and functional interactions between STAT5 and Runx transcription factors. *J Biochem* **143**, 695-709.
- Ohler A & Ravens U (1994). Effects of E-4031, almokalant and tedisamil on postrest action potential duration of human papillary muscles. *J Pharmacol Exp Ther* **270**, 460-465.
- Okamoto K, Yamori Y, & Nagaoka A (1974). Establishment of the stroke-prone spontaneously hypertensive rat. *Circ Res* 34-35 (suppl I) I143-153.
- Okamoto K & Aoki K (1963). Development of a strain of spontaneously hypertensive rats. *Jpn Circ J* **27**, 282-293.
- Okuda T, Nishimura M, Nakao M, & Fujita Y (2001). RUNX1/AML1: A central player in hematopoiesis. *International Journal of Hematology* **74**, 252-257.
- Okuda T, vanDeursen J, Hiebert SW, Grosveld G, & Downing JR (1996). AML1, the target of multiple chromosomal translocations in human leukemia, is essential for normal fetal liver hematopoiesis. *Cell* **84**, 321-330.
- Olivetti G, Abbi R, Quaini F, Kajstura J, Cheng W, Nitahara JA, Quaini E, Di LC, Beltrami CA, Krajewski S, Reed JC, & Anversa P (1997). Apoptosis in the failing human heart. *N Engl J Med* **336**, 1131-1141.
- Olivetti G, Capasso JM, Sonnenblick EH, & Anversa P (1990). Side-to-side slippage of myocytes participates in ventricular wall remodeling acutely after myocardial infarction in rats. *Circ Res* **67**, 23-34.
- Otto F, Lubbert M, & Stock M (2003). Upstream and downstream targets of RUNX proteins. *J Cell Biochem* **89**, 9-18.
- Otto F, Thornell AP, Crompton T, Denzel A, Gilmour KC, Rosewell IR, Stamp GW, Beddington RS, Mundlos S, Olsen BR, Selby PB, & Owen MJ (1997). *Cbfa1*, a candidate gene for cleidocranial dysplasia syndrome, is essential for osteoblast differentiation and bone development. *Cell* **89**, 765-771.
- Overington JP, Al-Lazikani B, & Hopkins AL (2006). How many drug targets are there? *Nat Rev Drug Discov* **5**, 993-996.
- Pacher P, Nagayama T, Mukhopadhyay P, Batkai S, & Kass DA (2008). Measurement of cardiac function using pressure-volume conductance catheter technique in mice and rats. *Nature Protocols* **3**, 1422-1434.
- Paoni NF & Lowe DG (2001). Expression profiling techniques for cardiac molecular phenotyping. *Trends Cardiovasc Med* **11**, 218-221.
- Park MH, Shin HI, Choi JY, Nam SH, Kim YJ, Kim HJ, & Ryoo HM (2001). Differential expression patterns of Runx2 isoforms in cranial suture morphogenesis. *J Bone Miner Res* **16**, 885-892.
- Passier R, Zeng H, Frey N, Naya FJ, Nicol RL, McKinsey TA, Overbeek P, Richardson JA, Grant SR, & Olson EN (2000). CaM kinase signaling induces cardiac hypertrophy and activates the MEF2 transcription factor in vivo. *J Clin Invest* **105**, 1395-1406.
- Patient RK & McGhee JD (2002). The GATA family (vertebrates and invertebrates). *Curr Opin Genet Dev* **12**, 416-422.

- Patten RD & Hall-Porter MR (2009). Small animal models of heart failure: development of novel therapies, past and present. *Circ Heart Fail* **2**, 138-144.
- Patten RDeal (1998). Ventricular remodeling in a mouse model of myocardial infarction. *Am J Physiol Heart Circ Physiol* **274**, H1812-H1820.
- Pearlman ES, Weber KT, Janicki JS, Pietra GG, & Fishman AP (1982). Muscle fiber orientation and connective tissue content in the hypertrophied human heart. *Lab Invest* **46**, 158-164.
- Pelletier N, Champagne N, Stifani S, & Yang XJ (2002). MOZ and MORF histone acetyltransferases interact with the Runt-domain transcription factor Runx2. *Oncogene* **21**, 2729-2740.
- Perez NG, Hashimoto K, McCune S, Altschuld RA, & Marban E (1999). Origin of contractile dysfunction in heart failure: calcium cycling versus myofilaments. *Circulation* **99**, 1077-1083.
- Perez S, Royo LJ, Astudillo A, Escudero D, Alvarez F, Rodriguez A, Gomez E, & Otero J (2007). Identifying the most suitable endogenous control for determining gene expression in hearts from organ donors. *BMC Mol Biol* **8**, 114.
- Perrino C & Rockman HA (2006). GATA4 and the two sides of gene expression reprogramming. *Circ Res* **98**, 715-716.
- Peters NS (1995). Myocardial gap junction organization in ischemia and infarction. *Microsc Res Tech* **31**, 375-386.
- Petersen S, Peto V, Rayner M, Leal J, Luengo-Fernandez R, & Gray A. European cardiovascular disease statistics 2005. 2005. London, British Heart Foundation.
- Petrich BG, Gong X, Lerner DL, Wang X, Brown JH, Saffitz JE, & Wang Y (2002). c-Jun N-terminal kinase activation mediates downregulation of connexin43 in cardiomyocytes. *Circ Res* **91**, 640-647.
- Pfeffer JM, Pfeffer MA, Fishbein MC, & Frohlich ED (1979a). Cardiac function and morphology with aging in the spontaneously hypertensive rat. *Am J Physiol* **237**, H461-H468.
- Pfeffer JM, Pfeffer MA, Fletcher PJ, & Braunwald E (1991a). Progressive ventricular remodeling in rat with myocardial infarction. *Am J Physiol* **260**, H1406-H1414.
- Pfeffer JM, Pfeffer MA, Fletcher PJ, & Braunwald E (1991b). Progressive ventricular remodeling in rat with myocardial infarction. *Am J Physiol* **260**, H1406-H1414.
- Pfeffer MA & Braunwald E (1990). Ventricular remodeling after myocardial infarction. Experimental observations and clinical implications. *Circulation* **81**, 1161-1172.
- Pfeffer MA, Pfeffer JM, Fishbein MC, Fletcher PJ, Spadaro J, Kloner RA, & Braunwald E (1979b). Myocardial infarct size and ventricular function in rats. *Circ Res* **44**, 503-512.
- Philip-Couderc P, Tavares NI, Roatti A, Lerch R, Montessuit C, & Baertschi AJ (2008). Forkhead transcription factors coordinate expression of myocardial KATP channel subunits and energy metabolism. *Circ Res* **102**, e20-e35.
- Pimanda JE, Donaldson IJ, de Bruijn MF, Kinston S, Knezevic K, Huckle L, Piltz S, Landry JR, Green AR, Tannahill D, & Gottgens B (2007a). The SCL transcriptional network and BMP signaling pathway interact to regulate RUNX1 activity. *Proc Natl Acad Sci U S A* **104**, 840-845.
- Pimanda JE, Donaldson IJ, de Bruijn MF, Kinston S, Knezevic K, Huckle L, Piltz S, Landry JR, Green AR, Tannahill D, & Gottgens B (2007b). The SCL transcriptional network and BMP signaling pathway interact to regulate RUNX1 activity. *Proc Natl Acad Sci U S A* **104**, 840-845.

- Pinto JM & Boyden PA (1999). Electrical remodeling in ischemia and infarction. *Cardiovasc Res* **42**, 284-297.
- Planaguma J, Diaz-Fuertes M, Gil-Moreno A, Abal M, Monge M, Garcia A, Baro T, Thomson TM, Xercavins J, Alameda F, & Reventos J (2004a). A differential gene expression profile reveals overexpression of RUNX1/AML1 in invasive endometrioid carcinoma. *Cancer Research* **64**, 8846-8853.
- Planaguma J, Diaz-Fuertes M, Gil-Moreno A, Abal M, Monge M, Garcia A, Baro T, Thomson TM, Xercavins J, Alameda F, & Reventos J (2004b). A differential gene expression profile reveals overexpression of RUNX1/AML1 in invasive endometrioid carcinoma. *Cancer Res* **64**, 8846-8853.
- Pogwizd SM, Schlotthauer K, Li L, Yuan W, & Bers DM (2001). Arrhythmogenesis and contractile dysfunction in heart failure: Roles of sodium-calcium exchange, inward rectifier potassium current, and residual beta-adrenergic responsiveness. *Circ Res* **88**, 1159-1167.
- Pons S, Fornes P, Hagege AA, Heudes D, Giudicelli JF, & Richer C (2003). Survival, haemodynamics and cardiac remodelling follow up in mice after myocardial infarction. *Clin Exp Pharmacol Physiol* **30**, 25-31.
- Post WS, Larson MG, Myers RH, Galderisi M, & Levy D (1997). Heritability of left ventricular mass: the Framingham Heart Study. *Hypertension* **30**, 1025-1028.
- Pozner A, Goldenberg D, Negreanu V, Le SY, Elroy-Stein O, Levanon D, & Groner Y (2000). Transcription-coupled translation control of AML1/RUNX1 is mediated by cap- and internal ribosome entry site-dependent mechanisms. *Mol Cell Biol* **20**, 2297-2307.
- Pravenec M, Gauguier D, Schott JJ, Buard J, Kren V, Bila V, Szpirer C, Szpirer J, Wang JM, Huang H, & . (1995). Mapping of quantitative trait loci for blood pressure and cardiac mass in the rat by genome scanning of recombinant inbred strains. *J Clin Invest* **96**, 1973-1978.
- Primatesta P, Bost L, & Poulter NR (2000). Blood pressure levels and hypertension status among ethnic groups in England. *J Hum Hypertens* **14**, 143-148.
- Pu J, Robinson RB, & Boyden PA (2000). Abnormalities in Ca(i)handling in myocytes that survive in the infarcted heart are not just due to alterations in repolarization. *J Mol Cell Cardiol* **32**, 1509-1523.
- Qi M, Shannon TR, Euler DE, Bers DM, & Samarel AM (1997). Downregulation of sarcoplasmic reticulum Ca(2+)-ATPase during progression of left ventricular hypertrophy. *Am J Physiol* **272**, H2416-H2424.
- Qin D, Jain P, Boutjdir M, & El-Sherif N. Expression of T-type calcium current in remodeled hypertrophied left ventricle from adult rat following myocardial infarction. *Circulation* **92**, I-587. 1995.
- Raya TE, Gay RG, Lancaster L, Aguirre M, Moffett C, & Goldman S (1988). Serial changes in left ventricular relaxation and chamber stiffness after large myocardial infarction in rats. *Circulation* **77**, 1424-1431.
- Redfield MM, Jacobsen SJ, Burnett JC, Jr., Mahoney DW, Bailey KR, & Rodeheffer RJ (2003). Burden of systolic and diastolic ventricular dysfunction in the community: appreciating the scope of the heart failure epidemic. *JAMA* **289**, 194-202.
- Rennett J, Coffman JA, Mushegian AR, & Robertson AJ (2003). The evolution of Runx genes I. A comparative study of sequences from phylogenetically diverse model organisms. *BMC Evol Biol* **3**, 4.

- Rettig R (1993). Does the kidney play a role in the aetiology of primary hypertension? Evidence from renal transplantation studies in rats and humans. *J Hum Hypertens* **7**, 177-180.
- Richardson CA & Flecknell PA (2005). Anaesthesia and post-operative analgesia following experimental surgery in laboratory rodents: are we making progress? *Altern Lab Anim* **33**, 119-127.
- Ringer S (1882a). Concerning the Influence exerted by each of the Constituents of the Blood on the Contraction of the Ventricle. *J Physiol* **3**, 380-393.
- Ringer S (1882b). Regarding the Action of Hydrate of Soda, Hydrate of Ammonia, and Hydrate of Potash on the Ventricle of the Frog's Heart. *J Physiol* **3**, 195-202.
- Ringer S (1883a). A further Contribution regarding the influence of the different Constituents of the Blood on the Contraction of the Heart. *J Physiol* **4**, 29-42.
- Ringer S (1883b). A third contribution regarding the Influence of the Inorganic Constituents of the Blood on the Ventricular Contraction. *J Physiol* **4**, 222-225.
- Robertson AJ, Dickey CE, McCarthy JJ, & Coffman JA (2002). The expression of SpRunt during sea urchin embryogenesis. *Mech Dev* **117**, 327-330.
- Rockman HA, Ono S, Ross RS, Jones LR, Karimi M, Bhargava V, Ross J, Jr., & Chien KR (1994). Molecular and physiological alterations in murine ventricular dysfunction. *Proc Natl Acad Sci U S A* **91**, 2694-2698.
- Roger VL, Go AS, Lloyd-Jones DM, Adams RJ, Berry JD, Brown TM, Carnethon MR, Dai S, de SG, Ford ES, Fox CS, Fullerton HJ, Gillespie C, Greenlund KJ, Hailpern SM, Heit JA, Ho PM, Howard VJ, Kissela BM, Kittner SJ, Lackland DT, Lichtman JH, Lisabeth LD, Makuc DM, Marcus GM, Marelli A, Matchar DB, McDermott MM, Meigs JB, Moy CS, Mozaffarian D, Mussolino ME, Nichol G, Paynter NP, Rosamond WD, Sorlie PD, Stafford RS, Turan TN, Turner MB, Wong ND, & Wylie-Rosett J (2011). Heart disease and stroke statistics--2011 update: a report from the American Heart Association. *Circulation* **123**, e18-e209.
- Rohde LE, Ducharme A, Arroyo LH, Aikawa M, Sukhova GH, Lopez-Anaya A, McClure KF, Mitchell PG, Libby P, & Lee RT (1999). Matrix metalloproteinase inhibition attenuates early left ventricular enlargement after experimental myocardial infarction in mice. *Circulation* **99**, 3063-3070.
- Roth DM, White FC, Mathieu-Costello O, Guth BD, Heusch G, Bloor CM, & Longhurst JC (1987). Effects of left circumflex Ameroid constrictor placement on adrenergic innervation of myocardium. *Am J Physiol* **253**, H1425-H1434.
- Runge MS & Patterson CP (2006a). *Principles of Molecular Medicine.*, 2nd ed. Humana Press, New Jersey.
- Runge MS & Patterson CP (2006b). *Principles of Molecular Medicine.*, 2nd ed. Humana Press, New Jersey.
- Saadane N, Alpert L, & Chalifour LE (1999). Expression of immediate early genes, GATA-4, and Nkx-2.5 in adrenergic-induced cardiac hypertrophy and during regression in adult mice. *Br J Pharmacol* **127**, 1165-1176.
- Sabbah HN, Stein PD, Kono T, Gheorghiane M, Levine TB, Jafri S, Hawkins ET, & Goldstein S (1991). A canine model of chronic heart failure produced by multiple sequential coronary microembolizations. *Am J Physiol* **260**, H1379-H1384.
- Sadoshima J & Izumo S (1993). Molecular characterization of angiotensin II--induced hypertrophy of cardiac myocytes and hyperplasia of cardiac fibroblasts. Critical role of the AT1 receptor subtype. *Circ Res* **73**, 413-423.

- Sadoshima J, Takahashi T, Jahn L, & Izumo S (1992). Roles of mechano-sensitive ion channels, cytoskeleton, and contractile activity in stretch-induced immediate-early gene expression and hypertrophy of cardiac myocytes. *Proc Natl Acad Sci U S A* **89**, 9905-9909.
- Sadoshima J, Xu Y, Slayter HS, & Izumo S (1993). Autocrine release of angiotensin II mediates stretch-induced hypertrophy of cardiac myocytes in vitro. *Cell* **75**, 977-984.
- Saito A, Inui M, Radermacher M, Frank J, & Fleischer S (1988). Ultrastructure of the calcium release channel of sarcoplasmic reticulum. *J Cell Biol* **107**, 211-219.
- Saito Y, Yoshizawa T, Takizawa F, Ikegame M, Ishibashi O, Okuda K, Hara K, Ishibashi K, Obinata M, & Kawashima H (2002). A cell line with characteristics of the periodontal ligament fibroblasts is negatively regulated for mineralization and Runx2/Cbfa1/Osf2 activity, part of which can be overcome by bone morphogenetic protein-2. *J Cell Sci* **115**, 4191-4200.
- Sakakura C, Hagiwara A, Mivagawa K, Nakashima S, Yoshikawa T, Kin S, Nakase Y, Ito K, Yamagishi H, Yazumi S, Chiba T, & Ito Y (2005a). Frequent downregulation of the runt domain transcription factors RUNX1, RUNX3 and their cofactor CBFβ in gastric cancer. *International Journal of Cancer* **113**, 221-228.
- Sakakura C, Hagiwara A, Miyagawa K, Nakashima S, Yoshikawa T, Kin S, Nakase Y, Ito K, Yamagishi H, Yazumi S, Chiba T, & Ito Y (2005b). Frequent downregulation of the runt domain transcription factors RUNX1, RUNX3 and their cofactor CBFβ in gastric cancer. *Int J Cancer* **113**, 221-228.
- Salto-Tellez M, Yung LS, El-Oakley RM, Tang TP, Almsherqi ZA, & Lim SK (2004). Myocardial infarction in the C57BL/6J mouse: a quantifiable and highly reproducible experimental model. *Cardiovasc Pathol* **13**, 91-97.
- Salzmann JL, Michel JB, Bruneval P, Ossondo NM, Barres DR, & Camilleri JP (1986). Automated image analysis of myocardial collagen pattern in pressure and volume overload in rat cardiac hypertrophy. *Anal Quant Cytol Histol* **8**, 326-332.
- Sam F, Sawyer DB, Chang DL, Eberli FR, Ngoy S, Jain M, Amin J, Apstein CS, & Colucci WS (2000). Progressive left ventricular remodeling and apoptosis late after myocardial infarction in mouse heart. *Am J Physiol Heart Circ Physiol* **279**, H422-H428.
- Sane DC, Mozingo WS, & Becker RC (2009). Cardiac Rupture After Myocardial Infarction New Insights From Murine Models. *Cardiology in Review* **17**, 293-299.
- Sanoudou D, Vafiadaki E, Arvanitis DA, Kranias E, & Kontrogianni-Konstantopoulos A (2005). Array lessons from the heart: focus on the genome and transcriptome of cardiomyopathies. *Physiol Genomics* **21**, 131-143.
- Saraste A, Pulkki K, Kallajoki M, Heikkilä P, Laine P, Mattila S, Nieminen MS, Parvinen M, & Voipio-Pulkki LM (1999). Cardiomyocyte apoptosis and progression of heart failure to transplantation. *Eur J Clin Invest* **29**, 380-386.
- Satake M, Nomura S, Yamaguchi-Iwai Y, Takahama Y, Hashimoto Y, Niki M, Kitamura Y, & Ito Y (1995). Expression of the Runt domain-encoding PEBP2 alpha genes in T cells during thymic development. *Mol Cell Biol* **15**, 1662-1670.
- Sawamura I, Hazama F, & Kinoshita M (1990). Histological and histometrical study of myocardial fibrosis in spontaneously hypertensive rats of the stroke-prone strain. *Jpn Circ J* **54**, 1274-1282.
- Scarborough P, Wickramasinghe K, Bhatnagar P, & Rayner M (2011). Trends in Coronary Artery Disease 1961-2011. London, British Heart Foundation.

- Scarborough P, Bhatnagar P, Wickramasinghe K, Smolina K, Mitchell C & Rayner M (2010). Coronary heart statistics 2010. British Heart Foundation. London.
- Scherrer-Crosbie M, Ullrich R, Bloch KD, Nakajima H, Nasser B, Aretz HT, Lindsey ML, Vancon AC, Huang PL, Lee RT, Zapol WM, & Picard MH (2001). Endothelial nitric oxide synthase limits left ventricular remodeling after myocardial infarction in mice. *Circulation* **104**, 1286-1291.
- Schmidt U, Hajjar RJ, Kim CS, Lebeche D, Doye AA, & Gwathmey JK (1999). Human heart failure: cAMP stimulation of SR Ca(2+)-ATPase activity and phosphorylation level of phospholamban. *Am J Physiol* **277**, H474-H480.
- Schmittgen TD & Livak KJ (2008). Analyzing real-time PCR data by the comparative C(T) method. *Nat Protoc* **3**, 1101-1108.
- Schneider M, Kostin S, Strom CC, Aplin M, Lyngbaek S, Theilade J, Grigorian M, Andersen CB, Lukanidin E, Hansen JL, & Sheikh SP (2007). S100A4 is upregulated in injured myocardium and promotes growth and survival of cardiac myocytes. *Cardiovascular Research* **75**, 40-50.
- Schocken DD, Benjamin EJ, Fonarow GC, Krumholz HM, Levy D, Mensah GA, Narula J, Shor ES, Young JB, & Hong Y (2008). Prevention of heart failure: a scientific statement from the American Heart Association Councils on Epidemiology and Prevention, Clinical Cardiology, Cardiovascular Nursing, and High Blood Pressure Research; Quality of Care and Outcomes Research Interdisciplinary Working Group; and Functional Genomics and Translational Biology Interdisciplinary Working Group. *Circulation* **117**, 2544-2565.
- Schroeder A, Mueller O, Stocker S, Salowsky R, Leiber M, Gassmann M, Lightfoot S, Menzel W, Granzow M, & Ragg T (2006). The RIN: an RNA integrity number for assigning integrity values to RNA measurements. *BMC Mol Biol* **7**, 3.
- Schuster EH & Bulkley BH (1979). Expansion of transmural myocardial infarction: a pathophysiological factor in cardiac rupture. *Circulation* **60**, 1532-1538.
- Schwarte LA, Zurbier CJ, & Ince C (2000). Mechanical ventilation of mice. *Basic Res Cardiol* **95**, 510-520.
- Schwinger RH, Bohm M, & Erdmann E (1992). Inotropic and lusitropic dysfunction in myocardium from patients with dilated cardiomyopathy. *Am Heart J* **123**, 116-128.
- Schwinger RH, Bohm M, Schmidt U, Karczewski P, Bavendiek U, Flesch M, Krause EG, & Erdmann E (1995). Unchanged protein levels of SERCA II and phospholamban but reduced Ca²⁺ uptake and Ca(2+)-ATPase activity of cardiac sarcoplasmic reticulum from dilated cardiomyopathy patients compared with patients with nonfailing hearts. *Circulation* **92**, 3220-3228.
- Scobioala S, Klocke R, Kuhlmann M, Tian W, Hasib L, Milting H, Koenig S, Stelljes M, El-Banayosy A, Tenderich G, Michel G, Breithardt G, & Nikol S (2008). Up-regulation of nestin in the infarcted myocardium potentially indicates differentiation of resident cardiac stem cells into various lineages including cardiomyocytes. *FASEB J* **22**, 1021-1031.
- Semenza GL (1996). Transcriptional regulation by hypoxia-inducible factor 1 molecular mechanisms of oxygen homeostasis. *Trends Cardiovasc Med* **6**, 151-157.
- Semenza GL (1999). *Transcription Factors and Human Disease*. Oxford University Press, Oxford.
- Semenza GL, Roth PH, Fang HM, & Wang GL (1994). Transcriptional regulation of genes encoding glycolytic enzymes by hypoxia-inducible factor 1. *J Biol Chem* **269**, 23757-23763.

Sengupta A, Molkentin JD, Paik JH, DePinho RA, & Yutzey KE (2011). FoxO transcription factors promote cardiomyocyte survival upon induction of oxidative stress. *J Biol Chem* **286**, 7468-7478.

Sengupta A, Molkentin JD, & Yutzey KE (2009). FoxO transcription factors promote autophagy in cardiomyocytes. *J Biol Chem* **284**, 28319-28331.

Sezaki S, Hirohata S, Iwabu A, Nakamura K, Toeda K, Miyoshi T, Yamawaki H, Demircan K, Kusachi S, Shiratori Y, & Ninomiya Y (2005). Thrombospondin-1 is induced in rat myocardial infarction and its induction is accelerated by ischemia/reperfusion. *Exp Biol Med (Maywood)* **230**, 621-630.

Shannon TR, Ginsburg KS, & Bers DM (2000). Potentiation of fractional sarcoplasmic reticulum calcium release by total and free intra-sarcoplasmic reticulum calcium concentration. *Biophys J* **78**, 334-343.

Shih PA & O'Connor DT (2008). Hereditary determinants of human hypertension: strategies in the setting of genetic complexity. *Hypertension* **51**, 1456-1464.

Shimizu N, Omura T, Hanatani A, Kim S, Iwao H, & Yoshiyama M. The time course of MAP kinase and transcription factor DNA binding activities in myocardial infarcted rats. *Circulation* **96**, I-197. 1997.

Shiojima I, Komuro I, Oka T, Hiroi Y, Mizuno T, Takimoto E, Monzen K, Aikawa R, Akazawa H, Yamazaki T, Kudoh S, & Yazaki Y (1999). Context-dependent transcriptional cooperation mediated by cardiac transcription factors Csx/Nkx-2.5 and GATA-4. *J Biol Chem* **274**, 8231-8239.

Shiomi T, Tsutsui H, Matsusaka H, Murakami K, Hayashidani S, Ikeuchi M, Wen J, Kubota T, Utsumi H, & Takeshita A (2004). Overexpression of glutathione peroxidase prevents left ventricular remodeling and failure after myocardial infarction in mice. *Circulation* **109**, 544-549.

Shioura KM, Geenen DL, & Goldspink PH (2007). Assessment of cardiac function with the pressure-volume conductance system following myocardial infarction in mice. *Am J Physiol Heart Circ Physiol* **293**, H2870-H2877.

Shubeita HE, McDonough PM, Harris AN, Knowlton KU, Glembotski CC, Brown JH, & Chien KR (1990). Endothelin induction of inositol phospholipid hydrolysis, sarcomere assembly, and cardiac gene expression in ventricular myocytes. A paracrine mechanism for myocardial cell hypertrophy. *J Biol Chem* **265**, 20555-20562.

Sigma Aldrich. Technical Guide Notes: Optimizing qPCR. 2010.

Silver MA, Pick R, Brilla CG, Jalil JE, Janicki JS, & Weber KT (1990). Reactive and reparative fibrillar collagen remodelling in the hypertrophied rat left ventricle: two experimental models of myocardial fibrosis. *Cardiovasc Res* **24**, 741-747.

Singh M, Foster CR, Dalal S, & Singh K (2010). Osteopontin: role in extracellular matrix deposition and myocardial remodeling post-MI. *J Mol Cell Cardiol* **48**, 538-543.

Sipido KR, Volders PG, Vos MA, & Verdonck F (2002). Altered Na/Ca exchange activity in cardiac hypertrophy and heart failure: a new target for therapy? *Cardiovasc Res* **53**, 782-805.

Siwik DA & Colucci WS (2004). Regulation of matrix metalloproteinases by cytokines and reactive oxygen/nitrogen species in the myocardium. *Heart Fail Rev* **9**, 43-51.

Smith GL, Elliott EE, Kettlewell S, Currie S, & Quinn FR (2006). Na(+)/Ca(2+) exchanger expression and function in a rabbit model of myocardial infarction. *J Cardiovasc Electrophysiol* **17 Suppl 1**, S57-S63.

- Solaro RJ & Rarick HM (1998). Troponin and tropomyosin: proteins that switch on and tune in the activity of cardiac myofilaments. *Circ Res* **83**, 471-480.
- Soonpaa MH & Field LJ (1998). Survey of studies examining mammalian cardiomyocyte DNA synthesis. *Circ Res* **83**, 15-26.
- Spoelstra EN, Ince C, Koeman A, Emons VM, Brouwer LA, van Luyn MJ, Westerink BH, & Remie R (2007). A novel and simple method for endotracheal intubation of mice. *Lab Anim* **41**, 128-135.
- Srivastava D (1999). HAND proteins: molecular mediators of cardiac development and congenital heart disease. *Trends Cardiovasc Med* **9**, 11-18.
- St Louis JD, Hughes GC, Kypson AP, DeGrado TR, Donovan CL, Coleman RE, Yin B, Steenbergen C, Landolfo KP, & Lowe JE (2000). An experimental model of chronic myocardial hibernation. *Ann Thorac Surg* **69**, 1351-1357.
- Stanton LW, Garrard LJ, Damm D, Garrick BL, Lam A, Kapoun AM, Zheng Q, Protter AA, Schreiner GF, & White RT (2000). Altered patterns of gene expression in response to myocardial infarction. *Circulation Research* **86**, 939-945.
- Stawowy P, Blaschke F, Pfautsch P, Goetze S, Lippek F, Wollert-Wulf B, Fleck E, & Graf K (2002). Increased myocardial expression of osteopontin in patients with advanced heart failure. *Eur J Heart Fail* **4**, 139-146.
- Subramaniam MM, Chan JY, Yeoh KG, Quek T, Ito K, & Salto-Tellez M (2009). Molecular pathology of RUNX3 in human carcinogenesis. *Biochim Biophys Acta* **1796**, 315-331.
- Sudhakar S, Li Y, Katz MS, & Elango N (2001). Translational regulation is a control point in RUNX2/Cbfa1 gene expression. *Biochem Biophys Res Commun* **289**, 616-622.
- Sun Y (2009). Myocardial repair/remodelling following infarction: roles of local factors. *Cardiovasc Res* **81**, 482-490.
- Sun Y & Weber KT (2000). Infarct scar: a dynamic tissue. *Cardiovasc Res* **46**, 250-256.
- Sutton MG & Sharpe N (2000). Left ventricular remodeling after myocardial infarction: pathophysiology and therapy. *Circulation* **101**, 2981-2988.
- Svenson KL, Bogue MA, & Peters LL (2003). Invited review: Identifying new mouse models of cardiovascular disease: a review of high-throughput screens of mutagenized and inbred strains. *J Appl Physiol* **94**, 1650-1659.
- Swan L, Birnie DH, Padmanabhan S, Inglis G, Connell JM, & Hillis WS (2003). The genetic determination of left ventricular mass in healthy adults. *Eur Heart J* **24**, 577-582.
- Swynghedauw B (1991). Remodeling of the Heart in Chronic Pressure Overload. *Basic Research in Cardiology* **86**, 99-105.
- Swynghedauw B (1999). Molecular mechanisms of myocardial remodeling. *Physiol Rev* **79**, 215-262.
- Takagawa J, Zhang Y, Wong ML, Sievers RE, Kapasi NK, Wang Y, Yeghiazarians Y, Lee RJ, Grossman W, & Springer ML (2007). Myocardial infarct size measurement in the mouse chronic infarction model: comparison of area- and length-based approaches. *J Appl Physiol* **102**, 2104-2111.

- Takahashi T, Allen PD, & Izumo S (1992). Expression of A-, B-, and C-type natriuretic peptide genes in failing and developing human ventricles. Correlation with expression of the Ca(2+)-ATPase gene. *Circ Res* **71**, 9-17.
- Tanaka Y, Watanabe T, Chiba N, Niki M, Kuroiwa Y, Nishihira T, Satomi S, Ito Y, & Satake M (1997). The protooncogene product, PEBP2 beta/CBF beta, is mainly located in the cytoplasm and has an affinity with cytoskeletal structures. *Oncogene* **15**, 677-683.
- Tanase H, Yamori Y, Hansen CT, & Lovenberg W (1982). Heart size in inbred strains of rats. Part 1. Genetic determination of the development of cardiovascular enlargement in rats. *Hypertension* **4**, 864-872.
- Tang L, Guo B, Javed A, Choi JY, Hiebert S, Lian JB, van Wijnen AJ, Stein JL, Stein GS, & Zhou GW (1999). Crystal structure of the nuclear matrix targeting signal of the transcription factor acute myelogenous leukemia-1/polyoma enhancer-binding protein 2alphaB/core binding factor alpha2. *J Biol Chem* **274**, 33580-33586.
- Tarnavski O, McMullen JR, Schinke M, Nie Q, Kong S, & Izumo S (2004). Mouse cardiac surgery: comprehensive techniques for the generation of mouse models of human diseases and their application for genomic studies. *Physiol Genomics* **16**, 349-360.
- Tatematsu K, Yoshimoto N, Koyanagi T, Tokunaga C, Tachibana T, Yoneda Y, Yoshida M, Okajima T, Tanizawa K, & Kuroda S (2005). Nuclear-cytoplasmic shuttling of a RING-IBR protein RBCK1 and its functional interaction with nuclear body proteins. *J Biol Chem* **280**, 22937-22944.
- Telfer JC & Rothenberg EV (2001). Expression and function of a stem cell promoter for the murine CBFalpha2 gene: distinct roles and regulation in natural killer and T cell development. *Dev Biol* **229**, 363-382.
- Terracciano CM, Philipson KD, & MacLeod KT (2001). Overexpression of the Na(+)/Ca(2+) exchanger and inhibition of the sarcoplasmic reticulum Ca(2+)-ATPase in ventricular myocytes from transgenic mice. *Cardiovasc Res* **49**, 38-47.
- Thaik CM, Calderone A, Takahashi N, & Colucci WS (1995). Interleukin-1 beta modulates the growth and phenotype of neonatal rat cardiac myocytes. *J Clin Invest* **96**, 1093-1099.
- Thattaliyath BD, Livi CB, Steinhilber ME, Toney GM, & Firulli AB (2002). HAND1 and HAND2 are expressed in the adult-rodent heart and are modulated during cardiac hypertrophy. *Biochem Biophys Res Commun* **297**, 870-875.
- Thirunavukkarasu K, Mahajan M, McLarren KW, Stifani S, & Karsenty G (1998a). Two domains unique to osteoblast-specific transcription factor Osf2/Cbfa1 contribute to its transactivation function and its inability to heterodimerize with Cbfbeta. *Mol Cell Biol* **18**, 4197-4208.
- Thirunavukkarasu K, Mahajan M, McLarren KW, Stifani S, & Karsenty G (1998b). Two domains unique to osteoblast-specific transcription factor Osf2/Cbfa1 contribute to its transactivation function and its inability to heterodimerize with Cbfbeta. *Mol Cell Biol* **18**, 4197-4208.
- Thom T, Haase N, Rosamond W, Howard VJ, Rumsfield J, & Manolio T (2006). Heart disease and stroke statistics - 2006 update: a report from the American Heart Association Statistics Committee and Stroke Statistics Subcommittee. *Circulation* e85-e151.
- Thomas SA, Chapa DW, Friedmann E, Durden C, Ross A, Lee MC, & Lee HJ (2008). Depression in patients with heart failure: prevalence, pathophysiological mechanisms, and treatment. *Crit Care Nurse* **28**, 40-55.
- Thompson JT, Rackley MS, & O'Brien TX (1998). Upregulation of the cardiac homeobox gene Nkx2-5 (CSX) in feline right ventricular pressure overload. *Am J Physiol* **274**, H1569-H1573.

- Thygesen K, Alpert JS, White HD, Jaffe AS, Apple FS, Galvani M, Katus HA, Newby LK, Ravkilde J, Chaitman B, Clemmensen PM, Dellborg M, Hod H, Porela P, Underwood R, Bax JJ, Beller GA, Bonow R, Van der Wall EE, Bassand JP, Wijns W, Ferguson TB, Steg PG, Uretsky BF, Williams DO, Armstrong PW, Antman EM, Fox KA, Hamm CW, Ohman EM, Simoons ML, Poole-Wilson PA, Gurfinkel EP, Lopez-Sendon JL, Pais P, Mendis S, Zhu JR, Wallentin LC, Fernandez-Aviles F, Fox KM, Parkhomenko AN, Priori SG, Tendera M, Voipio-Pulkki LM, Vahanian A, Camm AJ, De CR, Dean V, Dickstein K, Filippatos G, Funck-Brentano C, Hellemans I, Kristensen SD, McGregor K, Sechtem U, Silber S, Tendera M, Widimsky P, Zamorano JL, Morais J, Brener S, Harrington R, Morrow D, Lim M, Martinez-Rios MA, Steinhubl S, Levine GN, Gibler WB, Goff D, Tubaro M, Dudek D, & Al-Attar N (2007). Universal definition of myocardial infarction. *Circulation* **116**, 2634-2653.
- Tkatchenko TV, Moreno-Rodriguez RA, Conway SJ, Molkenkin JD, Markwald RR, & Tkatchenko AV (2009). Lack of periostin leads to suppression of Notch1 signaling and calcific aortic valve disease. *Physiol Genomics* **39**, 160-168.
- Togi K, Kawamoto T, Yamauchi R, Yoshida Y, Kita T, & Tanaka M (2004). Role of Hand1/eHAND in the dorso-ventral patterning and interventricular septum formation in the embryonic heart. *Mol Cell Biol* **24**, 4627-4635.
- Toko H, Zhu W, Takimoto E, Shiojima I, Hiroi Y, Zou Y, Oka T, Akazawa H, Mizukami M, Sakamoto M, Terasaki F, Kitaura Y, Takano H, Nagai T, Nagai R, & Komuro I (2002). Csx/Nkx2-5 is required for homeostasis and survival of cardiac myocytes in the adult heart. *J Biol Chem* **277**, 24735-24743.
- Topol EJ & Yadav JS (2000). Recognition of the importance of embolization in atherosclerotic vascular disease. *Circulation* **101**, 570-580.
- Trafford AW, Diaz ME, Negretti N, & Eisner DA (1997). Enhanced Ca²⁺ current and decreased Ca²⁺ efflux restore sarcoplasmic reticulum Ca²⁺ content after depletion. *Circ Res* **81**, 477-484.
- Trueblood NA, Xie Z, Communal C, Sam F, Ngoy S, Liaw L, Jenkins AW, Wang J, Sawyer DB, Bing OH, Apstein CS, Colucci WS, & Singh K (2001). Exaggerated left ventricular dilation and reduced collagen deposition after myocardial infarction in mice lacking osteopontin. *Circ Res* **88**, 1080-1087.
- Tsuda T, Wu J, Gao E, Joyce J, Markova D, Dong H, Liu Y, Zhang H, Zou Y, Gao F, Miller T, Koch W, Ma X, & Chu ML (2012). Loss of fibulin-2 protects against progressive ventricular dysfunction after myocardial infarction. *J Mol Cell Cardiol* **52**, 273-282.
- Tsujita Y, Iwai N, Tamaki S, Nakamura Y, Nishimura M, & Kinoshita M (2000). Genetic mapping of quantitative trait loci influencing left ventricular mass in rats. *Am J Physiol Heart Circ Physiol* **279**, H2062-H2067.
- Tsunoda T, Takashima Y, Tanaka Y, Fujimoto T, Doi K, Hirose Y, Koyanagi M, Yoshida Y, Okamura T, Kuroki M, Sasazuki T, & Shirasawa S (2010). Immune-related zinc finger gene ZFAT is an essential transcriptional regulator for hematopoietic differentiation in blood islands. *Proc Natl Acad Sci U S A* **107**, 14199-14204.
- Tyson KL, Reynolds JL, McNair R, Zhang Q, Weissberg PL, & Shanahan CM (2003). Osteo/chondrocytic transcription factors and their target genes exhibit distinct patterns of expression in human arterial calcification. *Arterioscler Thromb Vasc Biol* **23**, 489-494.
- Vacher E, Richer C, & Giudicelli JF (1996). Effects of losartan on cerebral arteries in stroke-prone spontaneously hypertensive rats. *J Hypertens* **14**, 1341-1348.
- van den Bos EJ, Mees BM, de Waard MC, de CR, & Duncker DJ (2005). A novel model of cryoinjury-induced myocardial infarction in the mouse: a comparison with coronary artery ligation. *Am J Physiol Heart Circ Physiol* **289**, H1291-H1300.

- van der Borne SWMeal (2009). Mouse strain determines the outcome of wound healing after myocardial infarction. *Cardiovascular Research* **84**, 273-282.
- van Empel VP, Bertrand AT, Hofstra L, Crijns HJ, Doevendans PA, & de Windt LJ (2005). Myocyte apoptosis in heart failure. *Cardiovasc Res* **67**, 21-29.
- van Laake LW, Passier R, Monshouwer-Kloots J, Nederhoff MG, Ward-van OD, Field LJ, van Echteld CJ, Doevendans PA, & Mummery CL (2007). Monitoring of cell therapy and assessment of cardiac function using magnetic resonance imaging in a mouse model of myocardial infarction. *Nat Protoc* **2**, 2551-2567.
- Van KR, Kalkman EA, Saxena PR, & Schoemaker RG (2000). Altered cardiac collagen and associated changes in diastolic function of infarcted rat hearts. *Cardiovasc Res* **46**, 316-323.
- Vandervelde S, van Luyn MJ, Rozenbaum MH, Petersen AH, Tio RA, & Harmsen MC (2007). Stem cell-related cardiac gene expression early after murine myocardial infarction. *Cardiovasc Res* **73**, 783-793.
- Vasilyev N, Williams T, Brennan ML, Unzek S, Zhou X, Heinecke JW, Spitz DR, Topol EJ, Hazen SL, & Penn MS (2005). Myeloperoxidase-generated oxidants modulate left ventricular remodeling but not infarct size after myocardial infarction. *Circulation* **112**, 2812-2820.
- Vassort G & Alvarez J (1994). Cardiac T-type calcium current: pharmacology and roles in cardiac tissues. *J Cardiovasc Electrophysiol* **5**, 376-393.
- Ventura-Clapier R, Garnier A, & Veksler V (2004). Energy metabolism in heart failure. *J Physiol* **555**, 1-13.
- Verdecchia P, Schillaci G, Borgioni C, Ciucci A, Battistelli M, Bartoccini C, Santucci A, Santucci C, Reboldi G, & Porcellati C (1995). Adverse prognostic significance of concentric remodeling of the left ventricle in hypertensive patients with normal left ventricular mass. *J Am Coll Cardiol* **25**, 871-878.
- Verhaaren HA, Schieken RM, Mosteller M, Hewitt JK, Eaves LJ, & Nance WE (1991). Bivariate genetic analysis of left ventricular mass and weight in pubertal twins (the Medical College of Virginia twin study). *Am J Cardiol* **68**, 661-668.
- Voloshenyuk TG & Gardner JD (2010). Estrogen improves TIMP-MMP balance and collagen distribution in volume-overloaded hearts of ovariectomized females. *Am J Physiol Regul Integr Comp Physiol* **299**, R683-R693.
- Voss J, Jones LR, & Thomas DD (1994a). The physical mechanism of calcium pump regulation in the heart. *Biophys J* **67**, 190-196.
- Voss J, Jones LR, & Thomas DD (1994b). The physical mechanism of calcium pump regulation in the heart. *Biophys J* **67**, 190-196.
- Walker JC, Ratcliffe MB, Zhang P, Wallace AW, Fata B, Hsu EW, Saloner D, & Guccione JM (2005). MRI-based finite-element analysis of left ventricular aneurysm. *Am J Physiol Heart Circ Physiol* **289**, H692-H700.
- Wang J, Bo H, Meng X, Wu Y, Bao Y, & Li Y (2006). A simple and fast experimental model of myocardial infarction in the mouse. *Tex Heart Inst J* **33**, 290-293.
- Wang J, Panakova D, Kikuchi K, Holdway JE, Gemberling M, Burris JS, Singh SP, Dickson AL, Lin YF, Sabeh MK, Werdich AA, Yelon D, Macrae CA, & Poss KD (2011). The regenerative capacity of zebrafish reverses cardiac failure caused by genetic cardiomyocyte depletion. *Development* **138**, 3421-3430.

- Wang XH, Zhang GP, Jin HM, & Chen SF (2007). Dynamic changes in the expression of growth factor receptors in the myocardium microvascular endothelium after murine myocardial infarction. *Chin Med J (Engl)* **120**, 485-490.
- Wang XX, Blagden C, Fan JH, Nowak SJ, Taniuchi I, Littman DR, & Burden SJ (2005). Runx1 prevents wasting, myofibrillar disorganization, and autophagy of skeletal muscle. *Genes & Development* **19**, 1715-1722.
- Watanabe M, Timm M, & Fallah-Najmabadi H (1992). Cardiac expression of polysialylated NCAM in the chicken embryo: correlation with the ventricular conduction system. *Dev Dyn* **194**, 128-141.
- Weber KT (1997). Extracellular matrix remodeling in heart failure - A role for de novo angiotensin II generation. *Circulation* **96**, 4065-4082.
- Weber KT & Brilla CG (1991). Pathological hypertrophy and cardiac interstitium. Fibrosis and renin-angiotensin-aldosterone system. *Circulation* **83**, 1849-1865.
- Weber KT, Brilla CG, & Janicki JS (1991a). Cardioreparation with lisinopril in the management of hypertension and heart failure. *Cardiology* **79 Suppl 1**, 62-73.
- Weber KT, Brilla CG, & Janicki JS (1991b). Myocardial remodeling and pathologic hypertrophy. *Hosp Pract (Off Ed)* **26**, 73-80.
- Weber KT, Brilla CG, & Janicki JS (1991c). Signals for the remodeling of the cardiac interstitium in systemic hypertension. *J Cardiovasc Pharmacol* **17 Suppl 2**, S14-S19.
- Weber KT, Brilla CG, Janicki JS, Reddy HK, & Campbell SE (1991d). Myocardial fibrosis: role of ventricular systolic pressure, arterial hypertension, and circulating hormones. *Basic Res Cardiol* **86 Suppl 3**, 25-31.
- Weber KT, Janicki JS, Pick R, Abrahams C, Shroff SG, Bashey RI, & Chen RM (1987). Collagen in the hypertrophied, pressure-overloaded myocardium. *Circulation* **75**, I40-I47.
- Wehrens XHT, Kirchhoff S, & Doevendans PA (2000). Mouse electrocardiography: An interval of thirty years. *Cardiovascular Research* **45**, 231-237.
- Weisman HF, Bush DE, Mannisi JA, Weisfeldt ML, & Healy B (1988a). Cellular mechanisms of myocardial infarct expansion. *Circulation* **78**, 186-201.
- Weisman HF, Bush DE, Mannisi JA, Weisfeldt ML, & Healy B (1988b). Cellular mechanisms of myocardial infarct expansion. *Circulation* **78**, 186-201.
- Weisman HF & Healy B (1987). Myocardial infarct expansion, infarct extension, and reinfarction: pathophysiologic concepts. *Prog Cardiovasc Dis* **30**, 73-110.
- Wencker D, Chandra M, Nguyen K, Miao W, Garantziotis S, Factor SM, Shirani J, Armstrong RC, & Kitsis RN (2003). A mechanistic role for cardiac myocyte apoptosis in heart failure. *J Clin Invest* **111**, 1497-1504.
- Westendorf JJ & Hiebert SW (1999). Mammalian runt-domain proteins and their roles in hematopoiesis, osteogenesis, and leukemia. *J Cell Biochem Suppl* **32-33**, 51-58.
- Whittaker P, Boughner DR, & Kloner RA (1991a). Role of collagen in acute myocardial infarct expansion. *Circulation* **84**, 2123-2134.
- Whittaker P, Boughner DR, & Kloner RA (1991b). Role of collagen in acute myocardial infarct expansion. *Circulation* **84**, 2123-2134.

- Whittaker P, Boughner DR, Kloner RA, & Przyklenk K (1991c). Stunned myocardium and myocardial collagen damage: differential effects of single and repeated occlusions. *Am Heart J* **121**, 434-441.
- WHO. Global Atlas on Cardiovascular Disease Prevention and Control. Mendis, S., Puska, P., and Norrving, B. World Health Organisation. 2011.
- Williams GH (1982). The renin-angiotensin system and hypertension. *Clin Exp Pharmacol Physiol Suppl* **7**, 31-40.
- Wilson RB & Hartroft WS (1970). Pathogenesis of myocardial infarcts in rats fed a thrombogenic diet. *Arch Pathol* **89**, 457-469.
- Winegrad S (1965). Autoradiographic studies of intracellular calcium in frog skeletal muscle. *J Gen Physiol* **48**, 455-479.
- Woolf E, Xiao C, Fainaru O, Lotem J, Rosen D, Negreanu V, Bernstein Y, Goldenberg D, Brenner O, Berke G, Levanon D, & Groner Y (2003). Runx3 and Runx1 are required for CD8 T cell development during thymopoiesis. *Proc Natl Acad Sci U S A* **100**, 7731-7736.
- Wotton SF, Blyth K, Kilbey A, Jenkins A, Terry A, Bernardin-Fried F, Friedman AD, Baxter EW, Neil JC, & Cameron ER (2004). RUNX1 transformation of primary embryonic fibroblasts is revealed in the absence of p53. *Oncogene* **23**, 5476-5486.
- Xiao G, Jiang D, Gopalakrishnan R, & Franceschi RT (2002). Fibroblast growth factor 2 induction of the osteocalcin gene requires MAPK activity and phosphorylation of the osteoblast transcription factor, Cbfa1/Runx2. *J Biol Chem* **277**, 36181-36187.
- Xiao ZS, Simpson LG, & Quarles LD (2003). IRES-dependent translational control of Cbfa1/Runx2 expression. *J Cell Biochem* **88**, 493-505.
- Xu YJ, Chapman D, Dixon IMC, Sethi R, Guo X, & Dhalla NS (2004). Differential gene expression in infarct scar and viable myocardium from rat heart following coronary ligation. *Journal of Cellular and Molecular Medicine* **8**, 85-92.
- Yagil C, Sapojnikov M, Kreutz R, Katni G, Lindpaintner K, Ganten D, & Yagil Y (1998). Salt susceptibility maps to chromosomes 1 and 17 with sex specificity in the Sabra rat model of hypertension. *Hypertension* **31**, 119-124.
- Yamagishi H, Olson EN, & Srivastava D (2000). The basic helix-loop-helix transcription factor, dHAND, is required for vascular development. *J Clin Invest* **105**, 261-270.
- Yamori Y, Mori C, Nishio T, Ooshima A, Horie R, Ohtaka M, Soeda T, Saito M, Abe K, Nara Y, Nakao Y, & Kihara M (1979). Cardiac hypertrophy in early hypertension. *Am J Cardiol* **44**, 964-969.
- Yan X, Zhang J, Pan L, Wang P, Xue H, Zhang L, Gao X, Zhao X, Ning Y, & Chen YG (2011). TSC-22 promotes transforming growth factor beta-mediated cardiac myofibroblast differentiation by antagonizing Smad7 activity. *Mol Cell Biol* **31**, 3700-3709.
- Yang F, Liu YH, Yang XP, Xu J, Kapke A, & Carretero OA (2002). Myocardial infarction and cardiac remodelling in mice. *Exp Physiol* **87**, 547-555.
- Yang Y, Ma Y, Han W, Li J, Xiang Y, Liu F, Ma X, Zhang J, Fu Z, Su YD, Du XJ, & Gao XM (2008). Age-related differences in postinfarct left ventricular rupture and remodeling. *Am J Physiol Heart Circ Physiol* **294**, H1815-H1822.

- Yue P, Long CS, Austin R, Chang KC, Simpson PC, & Massie BM (1998). Post-infarction heart failure in the rat is associated with distinct alterations in cardiac myocyte molecular phenotype. *Journal of Molecular and Cellular Cardiology* **30**, 1615-1630.
- Zamurovic N, Cappellen D, Rohner D, & Susa M (2004). Coordinated activation of notch, Wnt, and transforming growth factor-beta signaling pathways in bone morphogenic protein 2-induced osteogenesis. Notch target gene Hey1 inhibits mineralization and Runx2 transcriptional activity. *J Biol Chem* **279**, 37704-37715.
- Zarain-Herzberg A, Afzal N, Elimban V, & Dhalla NS (1996). Decreased expression of cardiac sarcoplasmic reticulum Ca(2+)-pump ATPase in congestive heart failure due to myocardial infarction. *Mol Cell Biochem* **163-164**, 285-290.
- Zeman RJ, Zhao J, Zhang Y, Zhao W, Wen X, Wu Y, Pan J, Bauman WA, & Cardozo C (2009a). Differential skeletal muscle gene expression after upper or lower motor neuron transection. *Pflugers Arch* **458**, 525-535.
- Zeman RJ, Zhao J, Zhang Y, Zhao W, Wen X, Wu Y, Pan J, Bauman WA, & Cardozo C (2009b). Differential skeletal muscle gene expression after upper or lower motor neuron transection. *Pflugers Arch* **458**, 525-535.
- Zhang H, Chen X, Gao E, MacDonnell SM, Wang W, Kolpakov M, Nakayama H, Zhang X, Jaleel N, Harris DM, Li Y, Tang M, Berretta R, Leri A, Kajstura J, Sabri A, Koch WJ, Molkentin JD, & Houser SR (2010). Increasing cardiac contractility after myocardial infarction exacerbates cardiac injury and pump dysfunction. *Circ Res* **107**, 800-809.
- Zhang J, Lee MY, Cavalli M, Chen L, Berra-Romani R, Balke CW, Bianchi G, Ferrari P, Hamlyn JM, Iwamoto T, Lingrel JB, Matteson DR, Wier WG, & Blaustein MP (2005). Sodium pump alpha2 subunits control myogenic tone and blood pressure in mice. *J Physiol* **569**, 243-256.
- Zhang JF, Huang D, Yang YN, Gao XM, & Ma YT (2008a). Percutaneous transcatheter closure of patent ductus arteriosus with an amplatzer duct occluder using retrograde guidewire-established femoral arteriovenous loop. *Clin Exp Pharmacol Physiol* **35**, 606-610.
- Zhang JF, Ma YT, Yang YN, Gao XM, Liu F, Chen BD, Li XM, & Xiang Y (2008b). [Effects of ischemia postconditioning on ischemia-reperfusion injury and reperfusion injury salvage kinase signal transduction pathways in isolated mouse hearts]. *Zhonghua Xin Xue Guan Bing Za Zhi* **36**, 161-166.
- Zhang T, Yong SL, Tian XL, & Wang QK (2007). Cardiac-specific overexpression of SCN5A gene leads to shorter P wave duration and PR interval in transgenic mice. *Biochem Biophys Res Commun* **355**, 444-450.
- Zhang XQ, Ng YC, Musch TI, Moore RL, Zelis R, & Cheung JY (1998). Sprint training attenuates myocyte hypertrophy and improves Ca²⁺ homeostasis in postinfarction myocytes. *J Appl Physiol* **84**, 544-552.
- Zhao C, Zha Y, Wu X, Chen L, Shi J, & Cui L (2011). The quantification of ADAMTS4 and 8 expression and selection of reference genes for quantitative real-time PCR analysis in myocardial infarction. *Biomed Pharmacother* **65**, 555-559.
- Zhao D, Seth DM, & Navar LG (2009). Enhanced distal nephron sodium reabsorption in chronic angiotensin II-infused mice. *Hypertension* **54**, 120-126.
- Zhou YX, Xu X, Chen L, Li C, Brodie SG, & Deng CX (2000). A Pro250Arg substitution in mouse Fgfr1 causes increased expression of Cbfa1 and premature fusion of calvarial sutures. *Hum Mol Genet* **9**, 2001-2008.

Zhu H, Garcia AV, Ross RS, Evans SM, & Chien KR (1991). A conserved 28-base-pair element (HF-1) in the rat cardiac myosin light-chain-2 gene confers cardiac-specific and alpha-adrenergic-inducible expression in cultured neonatal rat myocardial cells. *Mol Cell Biol* **11**, 2273-2281.

Zhu W, Shiojima I, Hiroi Y, Zou Y, Akazawa H, Mizukami M, Toko H, Yazaki Y, Nagai R, & Komuro I (2000). Functional analyses of three Csx/Nkx-2.5 mutations that cause human congenital heart disease. *J Biol Chem* **275**, 35291-35296.

Zhu XJ, Yeadon JE, & Burden SJ (1995). Aml1 Is Expressed in Skeletal-Muscle and Is Regulated by Innervation (Vol 14, Pg 8056, 1994). *Molecular and Cellular Biology* **15**, 1136.

Zile MR & Brutsaert DL (2002). New concepts in diastolic dysfunction and diastolic heart failure: Part I: diagnosis, prognosis, and measurements of diastolic function. *Circulation* **105**, 1387-1393.

Zimmer HG, Gerdes AM, Lortet S, & Mall G (1990). Changes in heart function and cardiac cell size in rats with chronic myocardial infarction. *J Mol Cell Cardiol* **22**, 1231-1243.

Zolk O, Frohme M, Maurer A, Kluxen FW, Hentsch B, Zubakov D, Hoheisel JD, Zucker IH, Pepe S, & Eschenhagen T (2002). Cardiac ankyrin repeat protein, a negative regulator of cardiac gene expression, is augmented in human heart failure. *Biochem Biophys Res Commun* **293**, 1377-1382.

Zolotareva AG & Kogan ME (1978). Production of experimental occlusive myocardial infarction in mice. *Cor Vasa* **20**, 308-314.